UNIVERSIDADE DE LISBOA
FACULDADE DE CIÊNCIAS

Electrosynthesis of biocompatible polycatecholamine films – Evaluation of their performance in biosensing

" Documento Definitivo"

Doutoramento em Química

Especialidade em Química Física

Luís Miguel Camacho Caldeira de Almeida

Tese orientada por:
Doutora Ana Pimenta da Gama Silveira Viana Semedo
Doutor Jorge Manuel Palma Correia

Documento especialmente elaborado para a obtenção do grau de doutor

2024

UNIVERSIDADE DE LISBOA
FACULDADE DE CIÊNCIAS

Electrosynthesis of biocompatible polycatecholamine films – Evaluation of their performance in biosensing

Doutoramento em Química

Especialidade em Química Física

Luís Miguel Camacho Caldeira de Almeida

Tese orientada por:

Doutora Ana Pimenta da Gama Silveira Viana Semedo

Doutor Jorge Manuel Palma Correia

Júri:
Presidente:

- Doutor João Manuel Pires da Silva, Professor Catedrático da Faculdade de Ciências da Universidade de Lisboa.

Vogais:

- Doutor Christopher Michael Ashton Brett, Professor Catedrático da Faculdade de Ciências e Tecnologia da Universidade de Coimbra;
- Doutor Carlos Manuel Melo Pereira, Professor Associado com Agregação da Faculdade de Ciências da Universidade do Porto;
- Doutora Maria Cristina Fialho Oliveira, Professora Auxiliar da Escola de Ciências da Vida e do Ambiente da Universidade de Trás-os-Montes e Alto Douro;
- Doutora Ana Paula Pereira Paiva, Professora Associada com Agregação da Faculdade de Ciências da Universidade de Lisboa;
- Doutora Ana Pimenta da Gama da Silveira Viana Semedo, Professora Associada da Faculdade de Ciências da Universidade de Lisboa (orientadora).

Documento especialmente elaborado para a obtenção do grau de doutor

Doutoramento financiado pela Fundação para Ciência e a Tecnologia através da bolsa SFRH/BD/129566/2017 e respetiva extensão COVID/BD/152149/2022

2024

Tudo fará sentido acreditando no disparate.

Agradecimentos

Começo por agradecer à minha orientadora, a Dra. Ana Viana, por todos os conselhos científicos, mas também pessoais, por toda a motivação e resiliência que me transmitiu e por sempre se preocupar com o sucesso do meu percurso académico. Foram muitos ensinamentos que não esquecerei.

Agradeço ao meu co-orientador, o Dr. Jorge Correia, por me acolher no Laboratório de Eletroquímica Interfacial, por todos os concelhos e ensinamentos científicos e por me incutir o espírito da coerência, da prudência e do rigor. São memórias que guardarei com estima, admiração e diversão.

Agradeço ao Mestre Rui Correia, por todo o companheirismo e sede pela descoberta. Foi alguém me mostrou como a imaginação nos pode levar de facto a descobrir coisas surpreendentes.

Agradeço a todos os membros do Grupo de Eletroquímica Interfacial, Dra. Olinda Monteiro, Dra. Virgínia Ferreira, e também à Beatriz, à Luísa, ao Daniel, ao Jorge, …, a lista não termina, por todo o ambiente de interajuda que enriquece o nosso laboratório. Agradeço também à Dra. Tânia Frade por toda a simpatia e animação que trouxe ao laboratório e pelo trabalho que realizámos juntos.

Agradeço a um grupinho muito especial do piso de cima, a Laura, a Rebeca e a Violeta, pelas rizadas, cafés e almoços que passámos juntos, e por serem as cobaias perfeitas para degustar marmeladas chinesas (achamos nós que são marmeladas).

I thank the great team of scientists at the Institute of Mechanics of the Chinese Academy of Sciences, Dr. Gang Jin, Dr. Yu Niu, and Dr. Liu Wei for warmly receiving me in Beijing, for all the fruitful collaboration and enlightening teachings on advanced optics.

I thank Dr. Barbara Pałys, from the Faculty of Chemistry at the University of Warsaw, for promptly taking on the task of Raman characterization and for making me feel kindly welcomed in her laboratory.

I thank to the exceptional team of scientists at the Research Institute on Terrestrial Ecosystems, National Research Council of Italy, Dr. Alessandra Morana, Dr. Francesco La Cara, and Dr Guiseppe Squillaci, for their insightful collaboration and unwavering dedication in our joint endeavor to develop functional phenolic biosensors.

Agradeço à Fundação para a Ciência e Tecnologia por ter aceitado financiar este projeto científico e por continuar a apoiar a ciência e os cientistas portugueses a alcançarem novos horizontes. Somos uma comunidade científica à escala global que continuará a dar frutos para

o desenvolvimento das sociedades, mas que apenas continuará a funcionar se a sua importância for reconhecida.

Agradeço ao atual Centro de Química Estrutural, em particular ao seu Polo Científico localizado na Faculdade de Ciências da Universidade de Lisboa, por me ter acolhido, ainda com a antiga designação de Centro de Química e Bioquímica e me facultar as suas instalações, equipamentos e recursos imprescindíveis ao sucesso deste trabalho doutoral. Queria também agradecer ao exemplar apoio científico e educativo de várias professoras da casa que acompanharam o desenrolar do meu percurso pela FCUL: à Dra. Ana Paula Paiva, à Dra. Maria Estrela Jorge e à Dra. Filomena Martins, um sincero e respeitoso obrigado.

Agradeço à Joana Martins, não por ensinamentos científicos, mas por me mostrar como animar a vida e como ultrapassar as mais diversas dificuldades; dificuldades essas que vão desde a limpeza de bolores, passando pelas logísticas culinárias e terminando na importantíssima regulação da nossa sanidade mental. Foram grandes aventuras, as que se viveram na Penha, e onde o desenrascanço, que te caracteriza, e o *amangueitamento* não faltaram.

Finalizo agradecendo aos meus pais, por estarem sempre dispostos a apoiar-me incondicionalmente, por torcerem pelo meu bem-estar e pelo carinho depositado ao longo dos anos. Espero ter sido sempre um motivo de orgulho para vocês.

Obrigado a todos!

Thank you everyone!

Abstract

The combined role of catechol and amine groups in determining the adhesive properties of biomimetic adhesives and promoting favorable interactions for protein immobilization in bio-inspired polymers is a current topic of discussion with great potential to advance the development of biosensing technologies. This doctoral work explores the electrochemical synthesis of polycatecholamines and polycatechol providing fast, efficient, and reproducible coating of carbon and gold electrodes while delivering fine-tuning of the physicochemical properties of the deposited nanometric-thin films. Surface characterization is extensively employed by electrochemical techniques, ellipsometry, quartz crystal microbalance, contact angle goniometry, atomic force microscopy, reflectance infrared spectroscopy, and X-ray photoelectron spectroscopy.

Electrosynthesized polydopamine shows superior electroactivity and electron transfer properties regarding its chemically synthesized counterpart, which is attributed to a more organized polymeric structure comprising non-cyclized dopamine monomeric units and less incorporation of the indoline- and indole-type cyclized species.

During electropolymerization of catecholamines, the amine group accelerates deposition resulting in compact polydopamine and polynorepinephrine films. The presence of carboxyl groups inhibit deposition leading to slow growth and originating very thin and porous films of poly(3,4-dihydroxyphenylalanine) and poly(caffeic acid). Polycatechol and polynorepinephrine display the most regular growths and superior electroactivities.

A one-step potentiostatic method is proposed to co-immobilize fungal laccase and polydopamine on cheap and disposable graphite electrodes, as demonstrated by the very reproducible and highly catalytic responses, at pH 4.6, of several phenolic compounds (caffeic, rosmarinic and gallic acid), allowing the quantification of the phenol content of a chestnut shell extract from agro-industrial wastes. A bacterial laccase was successfully immobilized on graphite/polynorepinephrine modified electrodes, obtaining enhanced catalytic responses with respect to polydopamine modified electrodes, shifting the optimal working pH to neutral values.

A successful one-step modification strategy with ethanolamine allowed the synthesis of ready-to-use polydopamine-based immunosensing platforms that prevent non-specific adsorption without the need for additional chemical coupling reactions or blocking steps throughout the affinity assay. The use of polyDOPA did not improve the detection of anti-human immunoglobulin G with respect to polydopamine films, whereas polynorepinephrine,

and especially polycatechol, greatly improved the optical sensitivity of the immunologic affinity assay.

Keywords:

- Catechol chemistry;
- Polycatecholamine thin films;
- Electropolymerization;
- Electrochemical enzymatic biosensors;
- Optical immunosensors.

Resumo

A identificação dos grupos catecol e amina como funções químicas determinantes das propriedades adesivas das proteínas de mexilhões marinhos inspira, atualmente, o desenvolvimento de adesivos e revestimentos biomiméticos. Pelo que se entende de momento, os mexilhões regulam as forças de adesão e coesão das suas proteínas bissais principalmente através do estado de protonação e oxidação do catecol. Este grupo pode estabelecer uma multitude de interações reversíveis (não covalentes: pontes de hidrogénio, ligações de coordenação, interações π-π e π-catião) ou irreversíveis (covalentes: através de adições do tipo Michael e formação de base de Schiff), compatibilizando-o com superfícies poliméricas, cerâmicas e metálicas. Um exemplo notável de um material inspirado pela versatilidade do grupo catecol é a polidopamina (PDA): um revestimento sintético que exibe um carácter adesivo universal e ainda a capacidade de imobilizar, à superfície, diversos péptidos, proteínas, iões, nanomateriais e polinucleótidos. Esta combinação de características é extremamente desejável para desenvolver superfícies biossensoras, cujo desempenho depende fortemente da imobilização robusta de biomoléculas sem prejudicar a sua atividade catalítica. São reportadas diversas aplicações que beneficiam da química superficial de polidopamina: cultura celular, administração de fármacos, revestimentos anti-incrustantes, baterias, proteção contra a corrosão, membranas de separação, fotocatálise, entre outros. No entanto, as sínteses químicas em meio homogéneo comumente utilizadas para produzir polidopamina, são, de modo geral, ineficientes e não proporcionam um controlo rigoroso das propriedades físico-químicas do filme nanométrico depositado. É o caso do método de revestimento por imersão em condições alcalinas, que apesar de se ter tornado popular na literatura científica, é caracterizado por velocidades de espessamento baixas e pela perda de material no meio reacional. Várias estratégias têm sido usadas para acelerar a polimerização oxidativa da dopamina, nomeadamente, através da ação de tirosinase, iões metálicos, e outros oxidantes mais agressivos, como o persulfato de amónio e o periodato de sódio. Apesar destes oxidantes promoverem modificações mais rápidas quando comparadas ao uso de oxigénio dissolvido em solução, os filmes de polidopamina formados sofrem alterações na sua composição, seja pela incorporação dos reagentes, seja pela degradação do anel benzénico do grupo catecol, tornando-se pouco aderentes. Torna-se por isso importante desenvolver melhores métodos sintéticos que permitam controlar a estrutura química do filme depositado, juntando as suas propriedades à aplicação tecnológica pretendida. Atendendo a esse propósito, neste trabalho doutoral explorou-se um método que ainda à data de hoje é muitíssimo menos estudado, a eletropolimerização, pretendendo-se promover uma modificação mais rápida, controlada e

eficiente da superfície, em relação às modificações químicas supramencionadas. Com o método eletroquímico, em vez da polimerização ser promovida no seio da solução, a oxidação da molécula que contem o grupo catecol ocorre perto da superfície de um material condutor e a sua velocidade pode ser regulada com grande precisão pelo controlo de corrente ou potencial, produzindo um filme aderente em segundos ou minutos. Foram eletropolimerizadas várias catecolaminas, nomeadamente, a dopamina, a norepinefrina, e a DOPA (3,4-dihidroxifenilalanina), e também o catecol e o ácido cafeico, recorrendo a materiais tipicamente usados em elétrodos (carbono e ouro) como substratos. Selecionando este conjunto de moléculas foi possível avaliar os efeitos dos diversos grupos químicos adicionais ao catecol (amina, hidroxilo e carboxilo) no processo de eletropolimerização e, consequentemente, nas propriedades físico-químicas dos filmes poliméricos resultantes. Parâmetros como morfologia e forças de adesão, avaliadas por microscopia de força atómica (AFM), não foram significativamente afetados pelos grupos químicos adicionais, uma vez que todos os polímeros apresentaram uma superfície lisa, uniforme e granular com forças de adesão semelhantes em relação a uma ponta de AFM funcionalizada com amina.

A proximidade entre os grupos amina e catecol nas catecolaminas leva à formação de espécies ciclizadas, aumentando a complexidade do processo de eletropolimerização e a composição química das policatecolaminas resultantes. Combinando gravimetria *in situ* (por microbalança eletroquímica de cristal de quartzo) e ellipsometria *ex situ*, é possível inferir que o grupo amina, nos monómeros de dopamina e norepinefrina, acelera o espessamento do polímero, embora os filmes resultantes sejam mais compactos e menos eletroativos em comparação ao policatecol. Em contraste, o catecol, o ácido cafeico e a DOPA geram filmes muito porosos, uma vez que mais de metade da variação de massa durante a eletropolimerização provem do aprisionamento de eletrólito. Além disso, o grupo carboxilo é claramente identificado como um inibidor do crescimento da poli(3,4-dihidroxifenilalanina) (ePDOPA) e do poli(ácido cafeico), como se confirma pelas velocidades de deposição e espessuras baixas. Em contraste, o grupo hidroxilo não teve nenhum efeito drástico na velocidade de deposição ou porosidade da polinorepinefrina (ePNE).

As conversões redox quinona/hidroquinona das policatecolaminas indicam que as principais unidades poliméricas são monómeros não ciclizados, incorporando uma menor quantidade de unidades monoméricas cíclicas indolínicas e indólicas, relativamente às primeiras. Entendeu-se ainda que a síntese eletroquímica favorece de modo geral a menor incorporação de espécies ciclizadas em comparação a métodos químicos. De entre as policatecolaminas estudadas, a polinorepinefrina é o polímero mais eletroativo e possui a menor

fração de espécies ciclizadas. No policatecol, as principais unidades oligoméricas deverão derivar do acoplamento C-C, no entanto a polimerização através do acoplamento C-O-C é uma hipótese a considerar. A análise por espectroscopia de fotoeletrões por raio-X (XPS), por espectroscopia de infravermelho de refletância e por goniometria de ângulos de contacto comprovam a preservação dos grupos químicos adicionais, hidroxilo e carboxilo, na estrutura da ePDOPA e ePNE. Para explicar as caracterizações eletroquímicas e espectroscópicas observadas, tornou-se imperativa uma reconsideração do mecanismo de polimerização proposto. A descrição convencional na literatura de uma via de reação unidirecional, assumindo um homopolímero de unidades de dihidroxi-indole, entra em conflito com a multiplicidade de processos redox evidentes no revestimento de polidopamina. Em vez disso, a presença de uma via reacional ramificada proporciona uma representação mais precisa da (eletro)polimerização de catecolaminas, mantendo o esquema Raper-Manson, anteriormente proposto, como a principal causa da heterogeneidade química dos polímeros. Assim, um modelo co-polimérico mostra-se mais vantajoso para elucidar a origem dos diversos processos redox superficiais quinona/hidroquinona, e também para explicar as variações na estrutura química, hidrofilicidade, morfologia e espessuras dos filmes de policatecol e policatecolaminas.

É proposto um método potentiostático, rápido e reprodutível que resultou numa imobilização robusta de lacase fungal na matriz de ePDA, recorrendo a apenas um só passo de modificação. A incorporação do enzima na ePDA não afeta grandemente o comportamento redox, propriedades óticas e morfologia do filme, sugerindo interações não covalentes entre a lacase e a ePDA, bem como uma boa distribuição superficial do enzima. O método foi aplicado com sucesso a elétrodos descartáveis de grafite, permitindo alcançar respostas muito reprodutíveis e altamente catalíticas a vários compostos fenólicos: ácido cafeico, rosmarínico e gálico. Além disso, o biossensor foi utilizado para medir e determinar o conteúdo fenólico de um extrato aquoso de resíduos de casca de castanha (proveniente de resíduos agroindustriais), produzindo uma quantificação semelhante à obtida por cromatografia líquida de alta eficiência. Uma lacase de origem bacteriana foi também imobilizada com sucesso em elétrodos modificados de grafite por polinorepinefrina, obtendo respostas catalíticas melhoradas em relação aos elétrodos modificados com polidopamina, proporcionando ainda desviar o pH ideal de trabalho para valores neutros.

Uma estratégia eletroquímica de uma só etapa foi também aplicada com sucesso ao desenvolvimento de superfícies imunossensoras com base num filme híbrido de polidopamina-etanolamina. A eletropolimerização da dopamina na presença de etanolamina permite uma modificação expedita e reprodutível de superfícies de ouro, resultando numa plataforma capaz

de evitar a adsorção não específica, sem a necessidade de recorrer a reações adicionais de acoplamento químico, ou longos passos de bloqueio superficial com tampões à base de proteínas. A voltametria cíclica, espectroscopia de infravermelho de refletância especular e XPS confirmam a formação de ligações covalentes entre a etanolamina e a estrutura química da polidopamina. Os ensaios de afinidade realizados pela técnica de ressonância de plasmão de superfície e as medições elipsométricas permitem concluir com clareza que o filme híbrido de polidopamina-etanolamina levou a um melhoramento drástico da deteção ótica da imunoglobulina G anti-humana. Não se verificaram melhoramentos analíticos utilizando a ePDOPA em substituição pela ePDA. No entanto, a ePNE destaca-se por ter melhorado o rácio de deteção anticorpo-antigénio, e o policatecol por melhorar a sensibilidade ótica destas superfícies.

Realizou-se um estudo *in situ* elipsométrico e gravimétrico detalhado focado em melhorar as propriedades condutoras e de permeabilidade da polidopamina. Aumentando o limite de crescimento anódico tipicamente utilizado no crescimento potentiostático da polidopamina (de 0,8 para 1,1 V *vs.* SCE), foi possível obter matrizes poliméricas com maior espessura, rugosidade, porosidade, eletroatividade e permeabilidade iónica em comparação com aqueles sintetizados usando limites anódicos mais baixos. Os filmes mais espessos de polidopamina abrem portas para potenciais melhorias na otimização da quantidade de enzima imobilizada sem comprometer a transdução eletroquímica tão crucial no desempenho analítico de um biossensor.

Por fim, importa referir que os filmes finos de policatecol e policatecolaminas eletrossintetizadas provaram ser materiais quimicamente versáteis para lidar com a intrincada tarefa de criar e otimizar superfícies biossensoras. Com esta tese, a compreensão científica de base sobre como as catecolaminas geram matrizes compatíveis à imobilização de biomoléculas é significativamente melhorada através da elucidação das relações estrutura-propriedade aqui apresentadas. O uso de policatecol e policatecolaminas para a biofuncionalização de superfícies aplicadas a biossensores, sejam de transdução ótica ou eletroquímica, é inequivocamente demonstrado.

Palavras-chave:

- Química do grupo catecol;
- Filmes finos de policatecolaminas;
- Eletropolimerização;
- Biossensores enzimáticos eletroquímicos;
- Imunossensores óticos.

Contents

Papers and personal contribution

Most of the scientific data and discussion presented in this doctoral document is already published. For organizational purposes, the page separators of chapters IV, V, VI and VII identify the papers with shared content. Here lies a list of the papers and my personal contribution by the chronological order of their publication:

1 – L. C. Almeida, R. D. Correia, A. Marta, G. Squillaci, A. Morana, F. La Cara, J. P. Correia, A. S. Viana, "Electrosynthesis of polydopamine films - tailored matrices for laccase-based biosensors", Applied Surface Science 480 (2019) 979-989, DOI: 10.1016/j.apsusc.2019.03.015.

This work is discussed in **chapter IV**.

Contribution: I wrote the original manuscript and conducted all the experiments, including electrochemical assays, absorbance ultraviolet-visible spectroscopy (UV-Vis), specular reflectance Fourier-transformed infrared spectroscopy (FTIR) and atomic force microscopy (AFM); conceptualized the UV-Vis spectroscopic assays to monitor electrosynthesis of polydopamine; proposed the electropolymerization mechanism with collaboration of the other authors; wrote computational code for the nonlinear fitting of ellipsometric data; used proprietary software to analyze data from X-ray photoelectron spectroscopy (XPS), FTIR, and AFM.

2 – L.C. Almeida, R.D. Correia, G. Squillaci, A. Morana, F. La Cara, J.P. Correia, A.S. Viana, Electrochemical deposition of bio-inspired laccase-polydopamine films for phenolic sensors, Electrochimica Acta. 319 (2019) 462-471, doi:10.1016/j.electacta.2019.06.180.

This work is discussed in **chapter VI**.

Contribution: First-authorship is equally shared with R.D. Correia. I wrote the first draft of the manuscript; conducted the majority of the experiments, except for the catalytic assays of graphite/ePDA-Lac electrodes and the Bradford assay; performed nonlinear fitting of the ellipsometric data using the personally developed software; performed AFM image treatment.

3 – L.C. Almeida, T. Frade, R.D. Correia, Y. Niu, G. Jin, J.P. Correia, A.S. Viana, Electrosynthesis of polydopamine-ethanolamine films for the development of immunosensing interfaces, Scientific Reports. 11 (2021) 1–12, doi:10.1038/s41598-021-81816-1.

This work is discussed in **chapter VII**.

Contribution: I designed, conducted and interpreted the electrochemical synthesis of dopamine in the presence of ethanolamine; and analyzed the FTIR and XPS spectra. I partially conducted the surface plasmon resonance assays and ellipsometric experiments, and participated in the ellipsometric calculations. I wrote the discussion section and participated in the revision of the manuscript.

4 – L.C. Almeida, R.D. Correia, B. Palys, J.P. Correia, A.S. Viana, Comprehensive study of the electrochemical growth and physicochemical properties of polycatecholamines and polycatechol, Electrochimica Acta. 386 (2021) 138515, doi:10.1016/j.electacta.2021.138515.

This work is discussed in **chapter V**.

Contribution: I conceptualized the work, wrote the original manuscript, designed and conducted all of the experiments, and performed the calculations/fittings to analyze the data from the ellipsometry, electrochemical impedance spectroscopy and XPS data.

5 – L.C. Almeida, R.D. Correia, J.P. Correia, A.S. Viana, Combined Electrochemical, Ellipsometric and Microgravimetric Study of Ion Permeable Polydopamine Films, J. Electrochem. Soc. 169 (2022) 046503, doi: 10.1149/1945-7111/ac60f0.

This work is discussed in **chapter V**.

Contribution: First-authorship is equally shared with R.D. Correia; I wrote the original manuscript, interpreted and analyzed all the data; R.D. Correia conceptualized, designed and conducted the *in situ* ellipsometric assays and the electrochemical characterizations.

6 – L.C. Almeida, J.F. Zeferino, C. Branco, A. Morana, G. Squillaci, R. Santos, P. Ihalainen, L. Sobhana, J.P. Correia, A.S. Viana, Polynorepinephrine and polydopamine-bacterial laccase coatings for phenolic amperometric biosensors, *submitted manuscript*.

This work is discussed in **chapter VI**.

Contribution: I conceptualize the work and wrote the original draft of the manuscript; performed the nonlinear fitting of the ellipsometric data; carried out preliminary assays; supervised the experimental work and participated in all the data analysis of electroanalytic assays, UV-Vis, and AFM imaging.

List of abbreviations

ABTS	2,2'-Azino-bis(3-ethylbenzothiazoline-6-sulfonic acid)
AFM	Atomic force microscopy
Anti-IgG	Anti-human immunoglobulin G
ATR	Attenuated total reflection
BSA	Bovine serum albumin
ca.	*circa* (about)
cf.	*confer* (compare)
CA	Catechol
CAF	Caffeic acid
CPB	Citrate-phosphate buffer
CPE	Constant-phase element
CV	Cyclic voltammetry
DA	Dopamine
DAC	Dopaminochrome
DHI	Dihydroxyindole
DMP	Dimethylphenol
DMSO	Dimethylsulfoxide
DMT	Derjaguin-Muller-Toporov (model)
DOPA	Dihydroxyphenylalanine
e.g.	*exempli gratia* (for example)
etc.	*et cetera* (and so forth)
et al.	*et alia* (and others)
EIS	Electrochemical impedance spectroscopy
ELISA	Enzyme-linked immunosorbent assay
ePCA	Electrosynthesized polycatechol
ePCAF	Electrosynthesized poly(caffeic acid)
ePDA	Electrosynthesized polydopamine
ePDOPA	Electrosynthesized poly(3,4-dihydroxyphenylalanine)
ePNE	Electrosynthesized polynorepinephrine
EQCM	Electrochemical quartz crystal microbalance
ETA	Ethanolamine

FTIR	Fourier Transform Infrared Spectroscopy
GAE	Gallic acid equivalents
GC	Glassy carbon
HOPG	Highly oriented pyrolytic graphite
HPLC	High-performance liquid chromatography
HQ	Hydroquinone
IgG	Immunoglobulin G
IQ	Indolequinone
IR	Infrared
JKR	Johnson-Kendall-Roberts (model)
Lac	Laccase
LacMG	Laccase from MetGen
LacNZ	Laccase from Novozymes
LDAC	Leucodopaminechrome
LOD	Limit of detection
MSE	Mean squared error
Mfp	Mussel foot protein
NE	Norepinephrine
NMR	Nuclear magnetic resonance
OCP	Open circuit potential
PBS	Phosphate buffered saline
PBST	Phosphate buffered saline with Tween®
PCSA	Polarizer-compensator-sample-analyzer (configuration)
PDA	Polydopamine
PDOPA	Poly(3,4-dihydroxyphenylalanine)
PNE	Polynorepinephrine
Q	Quinone
QCM	Quartz crystal microbalance
RIU	Refractive index units
RU	Resonance units or Response units
SAMs	Self-assembled monolayers
SCE	Saturated calomel electrode
SPM	Scanning Probe Microscopy

SPR	Surface plasmon resonance
STM	Scanning Tunneling Microscopy
TIR	Total internal reflection
T1	Type 1 (copper center)
T2/T3	Type 2 and type 3 (copper center)
Tris	Tris(hydroxymethyl)aminomethane
UV-Vis	Ultraviolet-visible
vs.	*versus* (against)
XPS	X-ray photoelectron spectroscopy

List of symbols

A Area (cm^2)

c Light of speed in vacuum (299 792 458 m s^{-1})

C Concentration (mol dm^{-3} or M)

C^* Bulk concentration

C_d Double layer capacitance (F)

C_f Integrated QCM sensitivity constant (Hz g^{-1})

d Density (g cm^{-3})

d_q Density of quartz (2.648 g cm^{-3})

D Diffusion coefficient (cm^2 s^{-1})

E Electric field magnitude (V m^{-1})

E_{rp} Parallel electric field component of reflected light

E_{rs} Perpendicular electric field component of reflected light

E_{ip} Parallel electric field component of incident light

E_{is} Perpendicular electric field component of incident light

E Electric potential (V)

$E^{0'}$ Formal potential

$E_{1/2}$ Half-wave potential

E_p^a Anodic peak potential

E_p^c Cathodic peak potential

E_λ Potential of inversion in cyclic voltammetry

f Frequency (Hz)

f_0 Fundamental resonant frequency

F Faraday constant (96 485.3399 C mol^{-1})

i Imaginary unit ($\sqrt{-1}$)

i Current (A)

i_p^a Anodic peak current

i_p^c Cathodic peak current

i_0 Apparent exchange current

j Imaginary unit ($\sqrt{-1}$)

j Densidade de corrente (A cm^{-2})

j_p^a Anodic peak current density

j_p^c Cathodic peak current density

j_b	Background current density
j_{max}	Maximum catalytic current density
L	Thickness (nm)
k	Extinction coefficient
K_M	Michaelis-Menten constant (mol dm^{-3} or M)
m	Mass (g)
n	Number of electrons
n	Real refractive index
N	Number of points
$\hat{n}$	Complex refractive index
R	Gas constant (8.314 472 J K^{-1} mol^{-1})
R	Resistance (Ω)
R_{ct}	Charge transfer resistance
R_{Ω}	Resistance of solution
R_q	Root mean square roughness (nm)
t	Time (s)
T	Temperature (K)
Z	Impedance (Ω)
Z_0	Impedance magnitude
Z'	Real part of the impedance (resistance)
Z''	Imaginary part of the impedance (reactance)
Z_W	Warburg impedance
Z_{CPE}	Impedance of a constant-phase element

α	Absorptivity (m^{-1})
Γ	Surface coverage (mol cm^{-2})
δ	Bending vibrational mode in IR spectroscopy
Δ	Phase difference (°)
ε	Electric permittivity
θ_{WCA}	Water contact angle (°)
θ_{SPR}	Resonance angle (°)
λ	Wavelength (m)
λ	Time of inversion in cyclic voltammetry

μ_q	Shear modulus of an AT-cut quartz (2.947×10^{11} g cm^{-1} s^{-2})
v	Scan rate (V s^{-1})
ν	Stretching vibrational mode in IR spectroscopy
ρ	Complex reflection coefficient
σ	Standard deviation
φ	Phase angle in electrochemical impedance spectroscopy
φ_0	Incident angle (°)
χ_{ie}	Fraction of incorporated electrolyte solution
χ^2	Figure of merit of nonlinear fitting
Ψ	Azimuthal angle (°)

List of figures

List of tables

Chapter I

Introduction

1. Introduction

1.1. Mussel-inspired chemistry: biomimicking to solve wet adhesion

Adhesion is the interfacial phenomenon responsible for keeping different materials assembled together through the attractive interactions of their atoms [1,2]. Without a doubt, adhesive forces are ubiquitous: they are necessary to explain natural phenomena and also to manufacture any man-made object or infrastructure. For adhesion to be strong and long-lasting, intimate contact between the two materials surfaces must occur, simply because the interaction between atoms is mediated by short-range forces [1,3]. This fact becomes an evident problem in solid interfaces that have inherent roughness, never touching each other perfectly. To solve this problem, a viscous material – the adhesive – can be introduced between the two solids, establishing a bonded joint where effective contact holds the materials together for a useful period of time [2]. Common names given to adhesive materials are glue, cement, paste, and mucilage. Although the adhesive viscosity allows a better interlocking towards the adherent surface, the adhesion phenomena may not occur if the surfaces are not clean and dry. For instance, water (or moisture) is usually pointed out as a surface contaminant that prevents adhesion, deteriorating the performance of most synthetic adhesive polymers [4,5]. In contrast, nature seems to have solved the problem of wet adhesion by the trial and error of many generations. A clear example of successful adhesion is found amongst marine organisms that were adapted to live in the intertidal zone, such as mussels [6] and barnacles [7], attaching to the surface of rocks or ship hulls in wet conditions. Great attention has been given to the study of the natural adhesives secreted by these and other marine organisms [8,9], with the prospect of mimicking their composition and mode of action. Mussels and barnacles are interesting model organisms since their adhesive proteins have specifically evolved to allow permanent adhesion in wet conditions. Permanent adhesion implies meaningful adhesion and cohesion strengths to counteract tidal forces, however, from the technological point of view, natural adhesives may not match the high performance required for certain applications. For instance, the adhesion strength values of mussels byssus (1 – 5 MPa) are not regarded as impressive, compared to synthetic adhesives in dry conditions (*e.g.* polyimides, 50 MPa) [4,6,10]. The technological interest in studying natural adhesives relies on mimicking their composition, and subsequently mimicking their ability to adhere to any surface (chemical versatility), overcoming the hydration layer of the substrate (proper wetting), and achieving adequate modulus matching during curing (controlled phase transition). Understanding and translating

these properties to a biomimetic adhesive is therefore challenging, due to the complex composition and chemistry of natural adhesives. However, if some underlying rules are understood, the synthesis of a new generation of wet adhesives for single or multipurpose becomes possible. The adhesive proteins secreted by marine organisms also display another set of interesting properties, namely, non-toxicity, low immunogenicity, and biodegradability [7,11], making this natural material pertinent for developments in medicine, dentistry, and biotechnological applications – areas that require adhesion of soft tissues or bones in wet conditions. Highlighted applications in the literature include: regeneration of injured skin, wound closure, surgical repair, hemostatic sealing, and securing biodevices to biological tissue [5,12,13].

The work of J. H. Waite and colleagues lead the way to the identification of the catechol group as a key chemical function responsible for the adhesive properties of mussel foot proteins (mfp) [14,15]. The speculation of the role of catechol in the adhesion of several *Mytilus* species emerges from the unusual number of post-translational modifications of their mfps, which leads to a high content of the amino acid DOPA (3,4-dihydroxyphenyl-*L*-alanine) in proteins located at the tip of mussels byssal threads (**Figure 1.1**). Two particular proteins of low molecular weight, the mfp-3f and the mfp-5, display the highest DOPA molar fraction of around 20–30 % and the highest works of adhesion[1] towards mica surface amongst the known mfps [4]. In fact, the concentration of DOPA was proven to influence the adhesion strengths of synthetic polypeptides in surface force apparatus experiments, offering some explanation for the adhesion behaviors of the natural mfps with different DOPA contents [16]. However, synthetic polypeptides comprising only DOPA moieties represent a failed attempt to mimic the mfp adhesive behavior, since such polypeptides display problems of solubility and chemical stability which impart their use as successful wet adhesives [17,18]. The excessive content of catechol groups is also known to exert excessive cohesion interactions within different organic polymeric structures (besides polypeptides) [19], disrupting the fluidity required for successful adhesion. Another important result that unveils the complex role of DOPA in adhesive behaviors, concerns the complete loss of mfp-3 adhesion towards mica surface after chemical oxidation of the catechol groups to quinone groups by sodium periodate [20]. Thus, a basic understanding of the adhesion properties of mfps starts by acknowledging an optimal content of DOPA and its oxidation susceptibility.

[1] Work of adhesion is defined as the reversible thermodynamic work required to separate the surfaces of two distinct phases from their equilibrium state [21].

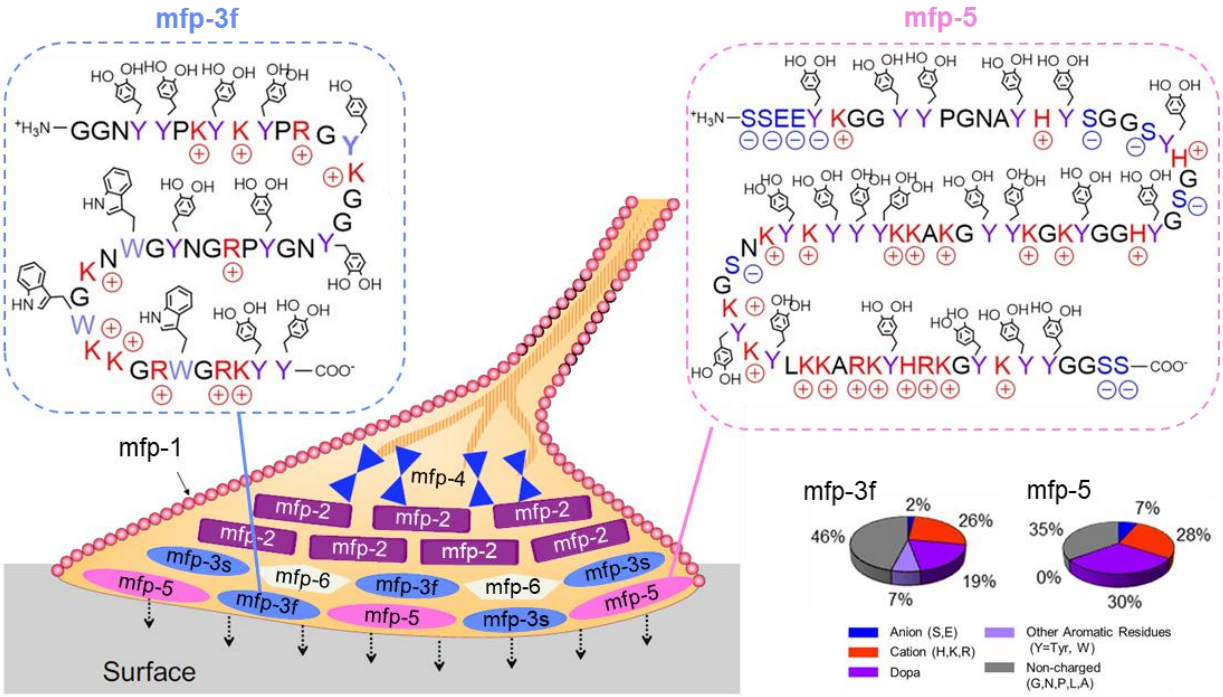

Figure 1.1: Graphical scheme of the six types of mussel foot proteins distribution in the adhesive byssal plaque; Sequences of the surface proteins mfp-3f (a fast variant of *Mytilus californianus*) and mfp-5 (from *Mytilus edulis*), and respective pie charts of their amino acids molar fractions. Capital letters are used to represent amino acids as follows: tyrosine or DOPA (Y), tryptophan (W), lysine (K), arginine (R), histidine (H), glycine (G), asparagine (N), proline (P), leucine (L), alanine (A), serine (S), glutamic acid (E) – adapted from [22,23].

In order to better clarify the role of the catechol group in the adhesive properties of mfps, further studies, using modified atomic force microscopy tips [24,25], were carried out and revealed the formation of reversible (non-covalent) or irreversible (covalent) interactions with surfaces, depending on its oxidation and protonation state (**Figure 1.2**). When protected from oxidation, at lower pH (~ 3) or in the presence of anti-oxidant agents, the reduced catechol group is fully protonated and uncharged (*o*-diphenol), interacting preferably by reversible interactions such as mono or bidentate hydrogen bonds, π-π stacking and π-cation interactions (**Figure 1.2**). At a slightly higher pH (> 4.5), the partial deprotonation of an adsorbed catechol group allows the formation of monodentate coordination bonds with the metal atoms present in some ceramics and metallic surfaces [22,26]. At neutral or alkaline conditions, bidentate coordination bonds have also been postulated to occur, considering the surfaces of titania, magnetite, and other semiconductors [27–30] (**Figure 1.2**). The multitude of possible reversible interactions identified for the catechol group in the reduced state explains, partially, the ability of mussels to adhere to a wide range of materials. These include polymers with low free energy, such as polystyrene and polymethylmethacrylate [15,31], and high free energy ceramics or metals, such as mica, hydroxyapatite, silica [15], titania [32], titanium [24] and steel [15].

Nonetheless, it is important to state that the adhesive behavior of natural mfps (when isolated) is highly dependent on the medium pH. In fact, during the secretion of the adhesive proteins, the mussel foot imposes an acidic and reductive medium, in order to maximize its adhesion to the surface and to control the phase transition to a solid adhesive plaque [22].

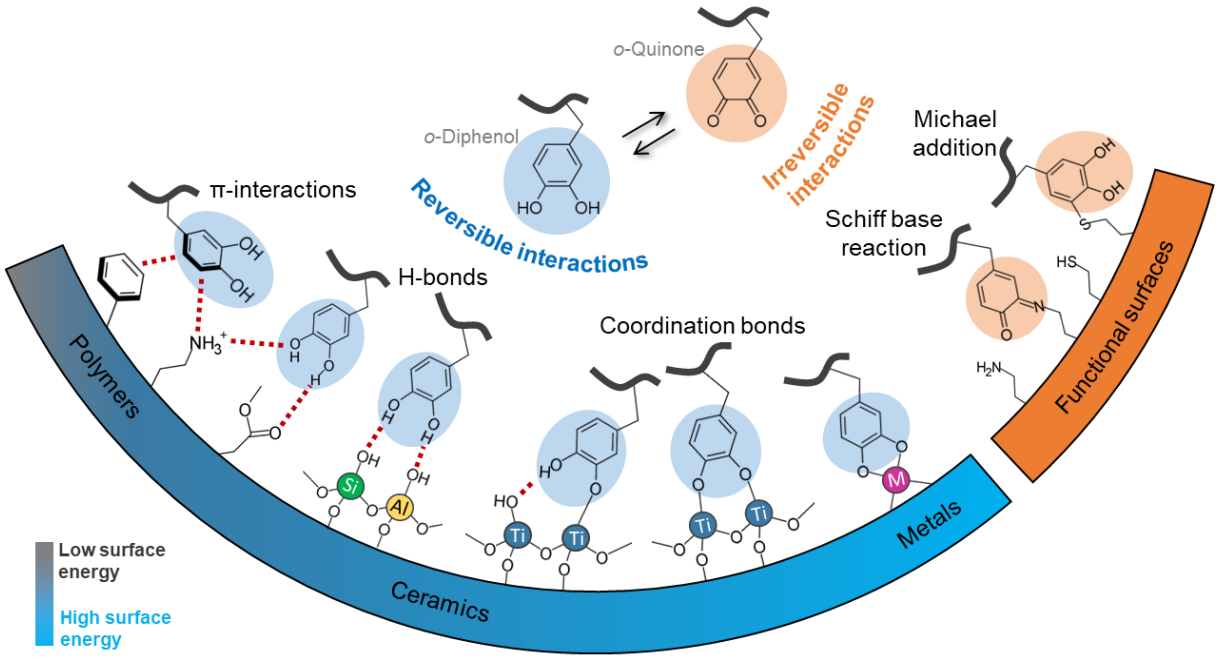

Figure 1.2: Reversible and irreversible surface interactions involved in the adhesion phenomenon promoted by the catechol group in the reduced and protonated state (*o*-diphenol) and in the oxidized and deprotonated state (*o*-quinone).

Besides the reversible interactions identified for the catechol group in the reduced state, a different behavior is noticed when catechol is in its fully oxidized and deprotonated form, *o*-quinone (**Figure 1.2**). The quinone form, usually obtained at basic conditions, is a reactive species that will preferably interact by covalent bonds in the presence of nucleophilic groups such as amines, thiols, and imidazoles, through Michael-type addition or Schiff's base formation [33,34]. Thiols are soft nucleophiles that will preferably attack the α or β carbons of the Michael system, resulting in a thio-catechol adduct represented in **Figure 1.2**. Amines can similarly undergo a Michael-type addition or attack the carbonyl carbon, leading to the formation of an iminoquinone adduct. Due to the covalent nature of such interactions, the measured force of quinone groups towards amine-rich surfaces is around 3 times stronger than the interaction force of catechol groups coordinated to titanium surfaces [24]. However, in the absence of superficial nucleophilic groups, the available interactions of quinones are reported to be weak; for instance, the adhesion force of quinone towards titanium [24] and titania [35] is 4 times weaker than the catechol group in its reduced and protonated state. The

aforementioned interaction forces, measured by AFM, were found to display similar intensities to the interactions of the phenyl groups with these surfaces. Beyond the interactions between quinones and surface groups of an adherent material, quinones can also interact with functional groups within the polymeric material (cross-linking) they compose, thus greatly affecting cohesion forces. From the adhesive formulation point of view, the presence of quinones can therefore represent a facile curing mechanism upon oxidation of the catechol groups, which was tested successfully in synthetic polymers bearing catechol groups [19,36]. Surprisingly, the adhesion enhancement by crosslinking was observed to occur towards plastics, metals, and wood, achieving, in some cases, the equivalent adhesion forces of cyanoacrylate glues [37,38]. It is not clearly stated in the reported cases if adhesion forces are maintained by non-oxidized catechol groups (from an incomplete oxidation) nor what is the role of other chemical structures in the overall adhesion of an oxidized polymer. Due to the lack of this compositional information, the adhesion enhancement by crosslinking could not be generalized to all types of organic polymers: in fact, adhesion enhancement by crosslinking promoted by oxidation is not always achieved, as seen by the examples of synthetic polymers [39] and the previously mentioned example of natural mfp-3 [20]. The simplest but non-consensual justification for the observed results is that oxidation of the catechol group leads to “less adhesive” quinone groups, limiting the overall adhesion forces between polymer and surface. The apparently contradictory results regarding different oxidized polymers show the importance of a more in-depth understanding of the balance between adhesion and cohesion forces caused by the quinone/catechol equilibria. Another important factor pointed out for the unpredictability of adhesive behaviors is polymers molecular weight, as evaluated for different organic polymers backbones [19,40]. As a general trend, longer polymeric chains provide better adhesion than their shorter versions, as long as the polymeric material is able to properly wet the surface. It is thus clear that chemical structures other than catechol cannot be disregarded in order to explain the adhesion of natural or synthetic polymers.

As expected from a complex composition, the adhesive behavior of mfp-3 and mfp-5 does not depend solely on its DOPA content. As seen in the pie charts of **Figure 1.1**, roughly one-third of the amino acid composition consists of cationic residues, and an even larger fraction is due to non-charged and non-aromatic amino acids. For this reason, efforts have been made to understand the combined role of the several types of amino acids [41]. For instance, co-polymers of DOPA and lysine are water soluble and display improved adhesion towards metallic surfaces compared to both respective homopolymers [17,36], exposing a hidden role of the cationic amino acids in mfp properties. More recently, the combination of DOPA and

lysine was further investigated in surface force apparatus assays [42,43], revealing that the presence of the protonated amine group of lysine residues next to DOPA is responsible for aiding water and salt displacement from the adherent surface, improving adhesion in a synergistic manner. The absence or substitution of the cationic amine by a non-charged group led to the removal of the adhesive behavior, even though catechol groups were present. Identical conclusions about the effect of amine on the adhesive behavior of materials could be drawn from the interaction forces between atomic force microscopy tips modified with catechol and amine groups and the surfaces of mica [44] and silica [45]. In the later study, the cationic amine groups are also seen as responsible for the adhesion of the modified tip with the surface of the ceramic materials, inferring that the role of amines goes beyond salt and water displacement, providing a cooperative electrostatic binding to silica. Since a complete understanding of the mussels adhesion phenomenon is not yet fully achieved, mimicking the composition and properties of the natural mfps to create biomimetic adhesives continues to be an active area of research. More importantly, the recognition of catechol as a tunable chemical function in natural systems provides inspiration for the design of new synthetic materials with desirable properties.

1.2. Polydopamine dip-coating: a surface-independent method

The chemical versatility of the catechol group has not only inspired the development of biomimetic adhesives in the problematic context of wet adhesion [46], but also, the development of bio-inspired coatings in order to tackle other technological challenges of surface chemistry [47,48]. From the chemical point of view, synthetic catechol-based polymers can be envisaged to display the necessary adhesion of an effective coating and display useful complementary properties that may or may not intercept the properties of mussel foot proteins. For example, superhydrophobicity, self-healing, biocompatibility, biofunctionalization, and nanoconjugation, are common desired coating features. To access potential new properties, the incorporation of catechol groups into macromolecular structures of polymers can be achieved, stepwise, by (i) the post-modification of a functional polymer, or directly, by (ii) the polymerization of a catechol-containing precursor (**Figure 1.3**). Strategy (i) bypasses the reactivity of the catechol group, eliminating completely the influence of this group as an active center in chain propagation. As so, a higher degree of control over polymers composition and chain topology may be achieved (using controlled/living polymerization methods), although complex multi-step procedures must be employed to introduce the catechol group as a side-chain moiety. Several examples include the protection and deprotection of catechol before and

after polymer growth [37,49], the oxidation of a phenol-containing polymer [50], or the attachment of catechol-containing molecules by click chemistry [51,52].

To avoid complicated synthetic procedures, strategy (ii) can be used alternatively, where catechol participates in the chain growth as an active center, propagating coupling reactions by its semiquinone and quinone intermediates under alkaline conditions [53,54]. If the catechol precursor has only one active polymerization center (the catechol group), then, its oxidative polymerization will essentially result in the direct incorporation of catechol groups in the main polymeric chain as illustrated in **Figure 1.3**. Although this is the only expected incorporation process in some catechol derivatives with inert lateral groups [55,56], reactive lateral groups are common in catechol-containing molecules, leading to a mixture of main and side-chain catechol groups and to more complex polymerization mechanisms [47].

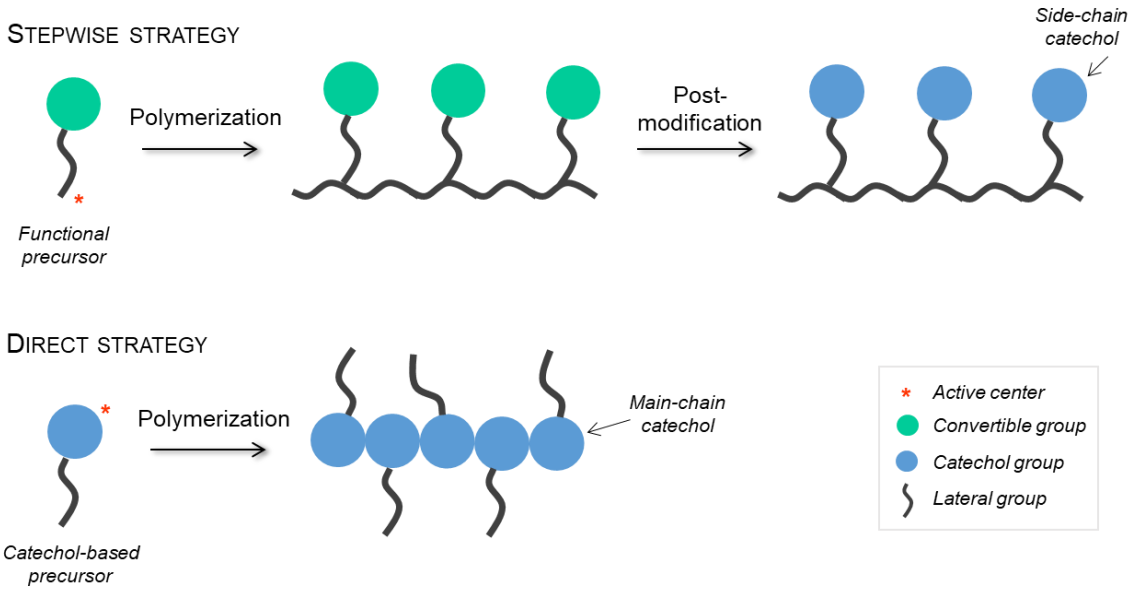

Figure 1.3: Schematic representation of the two main synthetic strategies for catechol group incorporation into polymeric structures.

A notable example of a catechol-containing coating for surface modification purposes appeared in the literature in 2007 [57], utilizing the bio-inspired monomer dopamine – a simple organic molecule comprising a catechol group and an aliphatic amine group (**Figure 1.4**). In an alkaline medium and in the presence of an oxidant, such as molecular oxygen, dopamine undergoes spontaneous oxidative polymerization, coating virtually any type of surface such as metals, ceramics, and polymers, including noble metals, steel, semiconductors, glasses, and plastics [57,58], with an adherent film of nanometric thickness denominated polydopamine (PDA) – **Figure 1.4a**. The universal adhesion character of PDA coatings is a surprising

phenomenon, considering its different composition regarding mfps, and thus it is still vaguely understood. Although the adhesion and cohesion forces in PDA are commonly linked to the chemical versatility of the catechol group [48], details regarding the influence of main or side-chain catechol groups are scarce due to structural complexity. Nonetheless, there is a growing consensus about the combined role of catechol and cationic amine groups in explaining adhesion [59] and cohesion forces in PDA [60,61].

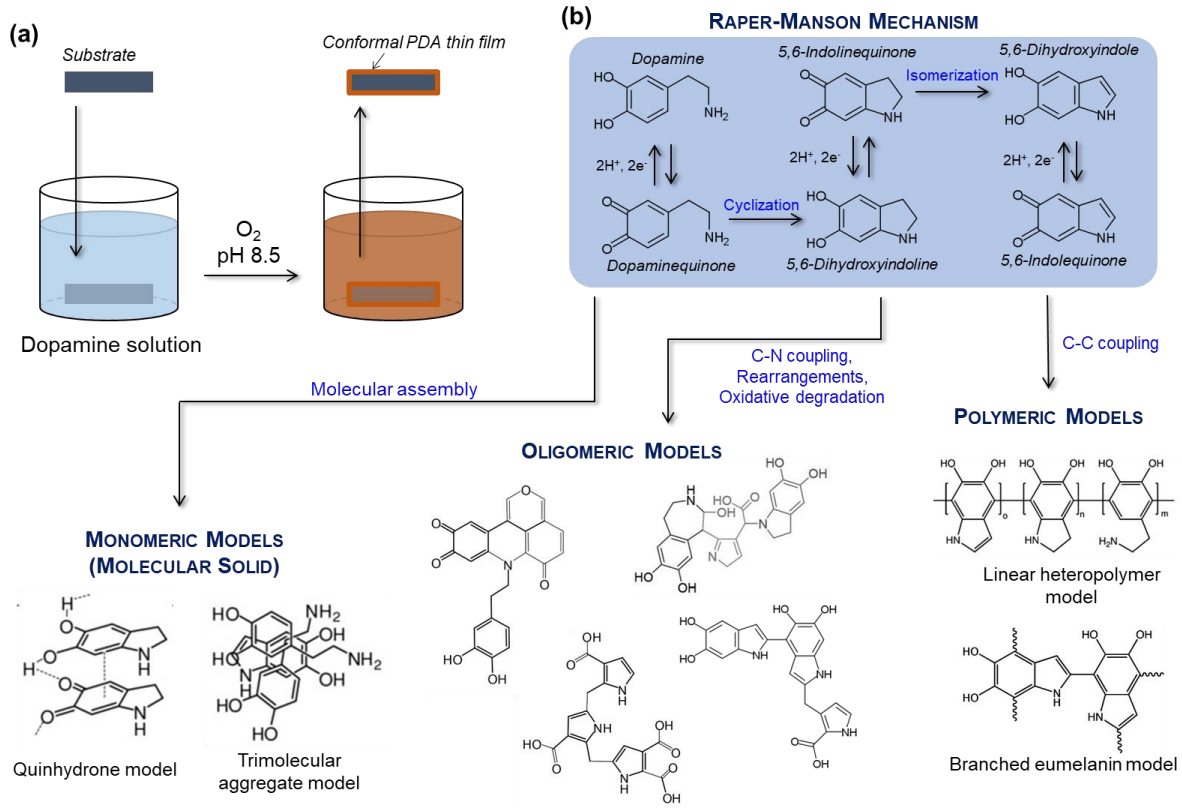

Figure 1.4: Schematic representation of the polydopamine (PDA) dip-coating method **(a)**; Raper-Manson mechanism and consequent models proposed for PDA structure **(b)**.

The simplicity of the dip-coating method in mild conditions combined with the universal adhesion properties of PDA, led to a growing interest over the last decade, as evidenced by its appearance in a large number of scientific reviews on the topic of material science [48,58]. Traditional self-assembly surface modification methods also offer controllable thickness and adjustable functionality of the final coating, however, the PDA modification method differs in its wider substrate compatibility and higher mechanical robustness of the prepared coating. For instance, the formation of self-assembled monolayers using thiolated compounds is restricted to noble metals, whereas monolayers of silanes and phosphonates are limited to metal and metalloid oxides [62]. Mono or multilayers deposited by the Langmuir-Blodgett method are

typically adsorbed onto surfaces by weak non-covalent bonds [63] and require dedicated equipment. Electrostatic multilayer assembly of polyelectrolytes (layer-by-layer deposition) is problematic on hydrophobic surfaces [64]. In contrast to these surface modification methods, the initially proposed PDA dip-coating method does not demand elaborated synthesis prior polymerization to achieve further incorporation of other chemical entities, since dopamine, its oligomers, and the final PDA, are prone to nucleophilic and electrophilic additions [34], metal ions chelation [65], and radical grafting [66]. The immense possibilities offered by this reminiscent mussel-inspired chemistry have thus been extensively explored to further modify a PDA primer coating or to co-deposit a composite coating, incorporating desired chemical groups, ions, biomolecules, nanomaterials, and polymers [58]. A large number of applications can benefit from this unique surface chemistry and capable method, namely, cell culture, drug delivery, antifouling, biosensing, battery development, corrosion protection, separation membranes, photocatalysis, among others [58].

The formation of a conformal thin film from a dopamine solution is a complex deposition phenomenon without a consensual explanation regarding the nature of the molecular aggregation process (physical assembly *versus* polymerization), and without a consensual definition of the chemical structure of the thin solid deposit denominated PDA. Fundamentally, the complexity arises from the variety of repeating units and the multitude of possible reaction paths. Furthermore, PDA chemical characterizations found in the literature may concern thin solid deposits [67,68], dispersed particles in the reaction medium [69], or thin films created in air-liquid interfaces [70,71], hindering a clear definition of PDA chemical nature. Nonetheless, it is generally accepted that the repeating unit heterogeneity comes from the Raper-Mason reaction scheme, proposed in 1948 to explain melanogenesis [72], leading to three types of starting monomers: dopamine, 5,6-dihydroxyindoline and 5,6-dihydroxyindole (**Figure 1.4b**). In this reaction scheme, dopamine is firstly oxidized to dopaminequinone by the dissolved molecular oxygen, following an intramolecular cyclization. The resulting indoline-type entity, 5,6-dihydroxyindoline, can further oxidize and originate its quinone counterpart, 5,6-indolinequinone (also referred to as dopaminechrome). A subsequent isomerization of 5,6-indolinequinone produces the aromatic indole-type compound, 5,6-dihydroxyindole, which can be oxidized to 5,6-indolequinone. The presence of all three types of Raper-Manson monomers (aminocatecholic, indolinic, and indolic) in PDA structure is consistent with its physicochemical characterization, although more simplistic models of monotonous units have been proposed: the quinhydrone model [69] and the eumelanin model [73] (**Figure 1.4b**). In the quinhydrone model, PDA is viewed as a molecular solid of alternating 5,6-

dihydroxyindoline and 5,6-indolinequinone units, held by hydrogen bonds and π-π interactions, excluding any possibility of covalent bonds. This model offers explanation for the ^{15}N and ^{13}C NMR spectra of the PDA particles collected from the reaction medium, however, conflicts with PDA insolubility in water and other solvents. In the case of the eumelanin model, 5,6-dihydroxyindole is considered to be the repeating unit of the PDA structure. The use of a poly(5,6-dihydroxyindole) model (**Figure 1.4b**) comprising only indole-type monomers arises from the same assumption made for the structure of eumelanins: the oxidation of a catecholamine leads to an indole-type precursor which, in turn, polymerizes to form a supramolecular aggregate of branched oligomers [73]. Thus, large attention has been given to the oligomerization of 5,6-dihydroxyindoles, allowing to derive some explanation for the observed optical and semiconducting properties of eumelanins and PDA [74,75]. Although eumelanin and PDA formation share similar initial reaction (Raper-Manson) schemes, eumelanins biosynthesis is known to be enzymatically driven by, at least, an oxidase, a tautomerase, and a decarboxylase, as identified in the late 1990s [76], rendering the structural comparisons between the two materials a difficult task. Furthermore, two independent laboratories have reported that the simple dip-coating method in alkaline conditions does not form an adherent conformal film over quartz substrates if the starting molecule is 5,6-dihydroxyindole instead of dopamine [77,78].

The realization that PDA is inevitably an heterogeneous material – not a homomolecular solid or a homopolymer derived from a single molecule – led to the proposal of more complex models (see **Figure 1.4b**): either i) PDA is a collection of different Raper-Manson monomers held by non-covalent (trimolecular aggregate models [79]) or covalent interactions (heteropolymer model [80]) or ii) PDA is a supramolecular aggregate of more complex trimers [77,81–83]. Although the release of some monomeric units from PDA to solution has been reported [79], molecular solid models are somewhat unrealistic since, over the years, several trimers, tetramers, and octamers have been identified in mass spectroscopy characterizations of PDA. Thus, the oligomeric or polymeric models are commonly used to describe PDA structure, assuming C-C couplings between the Raper-Manson monomers. Chemical changes after chain formation, such as cyclization within dopamine residues, or oxidative degradation that leads to pyrrolecarboxylic acids residues [83] are also suggested to contribute to PDA heterogeneity. In fact, the aforementioned degradations do have an impact on PDA structure, particularly when more aggressive oxidizing agents are used (*e.g.* sodium periodate) [84]. Covalent coupling between Raper-Manson monomers other than the C-C type is also considered to happen in the case of two oligomeric proposed models, namely, the nucleophilic additions of the dopamine

primary amine to other monomers [77,81]. The occurrence of the C-N coupling in the PDA structure is consistent with the mass spectroscopy data of the already mentioned studies, although this type of coupling is not often considered. Another type of interaction worth noting is the π-cation interaction between catechol and primary amine groups. Although π-π stacking was first proposed as the main driven force of molecular assembly in PDA [69,79], π-cation interactions gained more attention in the following years to explain the absence of adherent film formation in the absence of catechol or primary amines, and to explain the delamination behavior of PDA in strong alkaline conditions [60,85].

Discussion about the oligomeric or polymeric nature of PDA is still under debate since the molecular weight distribution characterizations are still lacking. H. Lee *et al.* performed a gel permeation chromatography analysis, pointing to a broad molecular weight distribution, ranging from millions to thousands of dalton [57]. Twelve years later, in 2019, a publication of the same author stated that gel permeation chromatography is unsuitable for molecular weight determination, rendering the preliminary characterization dubious [86]. Using statistical analysis of the adhesion events of atomic force microscopy tips modified with PDA, the authors presented a new estimation for the molecular weight distribution of PDA, averaging at 11.2 kDa. More evidence is still necessary to classify the structure of PDA coatings as oligomeric or polymeric aggregates.

The use of other catecholamine molecules beyond dopamine, that carry additional chemical groups, is also an alternative way of altering the thin coating properties [47,58], although it is not known which molecules may produce an adherent and conformal coating via alkaline dip-coating. The resulting polycatecholamine coatings are not as thoroughly studied as polydopamine, although some examples are worth noting. For instance, DOPA, the original mussel-inspired monomer, does polymerize in alkaline conditions, yielding a very thin coating that is more resilient to strong acid and basic rising compared to PDA [87]; however polyDOPA deposition is much slower than PDA, and the adherence to titania is weaker [88]. PolyDOPA is therefore a case where a material-independent chemistry is not attributed. In contrast, norepinephrine, an hydroxylated derivative of dopamine, was previously demonstrated to create smooth coatings of nanoparticles [89], allowing for chemical post-functionalization [90] and displaying superior hydrophilicity, advantageous in cell adhesion and molecular imprinting applications [91,92]. Polynorepinephrine is a potential alternative to PDA able to coat poly(dimethylsiloxane), poly(tetrafluoroethylene), polystyrene, glass, silicon, gold, amongst other surfaces [89,90,93], thus its formation is also considered to follow a material-independent chemistry. The development of bio-inspired coatings based on a simple dip-coating method

(relying on the direct synthetic strategy of **Figure 1.3**) is still an active area of research, broadening the chemical knowledge about the catechol group.

1.3. Polydopamine electrochemical deposition: an efficient coating solution

Despite the success of the PDA dip-coating method, one of the disadvantages mentioned in the literature that may counteract its facile technological application is the low rate of film growth [94]. Increasing dopamine concentration [95,96], agitation [97], or oxygen concentration [94,98] does not improve much the polymerization rate, still requiring long polymerization hours to achieve thicknesses above 20 nm. Several strategies have been employed to accelerate polydopamine deposition, namely, promoting dopamine oxidation by tyrosinase [99,9100], metal ions [101], and other strong oxidants such as ammonium persulfate, sodium periodate [84,102], allowing quicker modifications. Nonetheless, these strategies limit the application of the formed polydopamine films, due to the contamination with the participating compounds or, in the particular case of periodate usage, the degradation of catechol ring groups to form carboxylic groups. The fast coating of several materials with polydopamine, within minutes range, was already demonstrated using microwave [103], micro-plasma [104], chemical vapor deposition [105], or strong stirring combined with heating at 60 °C [97], however, these methods are not surface specific, yielding a large amount of black precipitate that is not useful to coat the desired surface. Although in the laboratory scale the loss of material in the reaction vessel may not be critical, the inefficiency of the dip-coating becomes obvious when the total area of the target surface (or surfaces) is large. A spray method was proposed by H. Lee *et al.* to mitigate this problem, however, it requires very high concentrations of dopamine [106]. Electrochemical methods can be a solution to provide surface-specific, rapid, and efficient polymerization of dopamine regarding the currently employed polydopamine-based surface modifications. Instead of using an oxidizing agent (such as molecular oxygen or periodate anions) that promotes homogeneous oxidation in bulk solution, the rate of dopamine oxidation (near the surface of a conducting material) can be finely regulated by a current- or potential-controlled electrochemical technique, yielding a polydopamine film within seconds or minutes [107–109] hereafter denominated ePDA (electrosynthesized polydopamine). Analogously to the dip-coating chemical methods, electrochemical methods can also produce adherent, nanometric, and semiconducting coatings, but unlock new advantageous properties that will be further reviewed in the text. Another important advantage of electrochemical methods resides in the possibility of using lower

dopamine concentrations and a wider pH range (above 4 [107,110]) during ePDA synthesis, compared to chemical methods, without losing the nanometric precision over the coating thickness.

In similarity with the chemically driven polymerization of dopamine, monomer oxidation is the first necessary step for the coating formation. Identically to other hydroquinones, dopamine can be electrochemically oxidized to its corresponding quinone pair by a proton-coupled electron transfer process occurring near the surface of a conducting material. In aqueous media this process behaves as an apparent single-step reaction involving the exchange of two electrons and two protons per dopamine molecule, however, quinone/hydroquinone redox systems follow a multi-step reaction scheme involving several redox and protonation states – see **Figure 1.5**. Since the 1970s decade [111,112], the scheme-of-squares has been used to model and interpret the electrochemical behavior of these organic molecules at a microscopic level, where electron and proton transfers are deconstructed into horizontal and vertical transformations, respectively, allowing better visualization of all the possible intermediaries and reaction routes. The predominant step-by-step reaction path of dopamine oxidation to its corresponding quinone at neutral pH is not clearly defined in the literature [113–117]. This difficulty arises from the instability of some intermediates that preclude the estimation of the formal potentials and acid dissociation constants associated with all the steps presented in the scheme-of-squares. Consensually, the dicationic quinone QH_2^{2+} and dianionic catecholate Q^{2-} are usually discarded because of the lack of contribution in explaining the overall process. The major discussion relies on determining reliable kinetic data of the single electron and proton transfers of the semiquinone intermediate ($QH^{\bullet}$), which will determine the order by which electrons and protons are exchanged as a function of working pH.

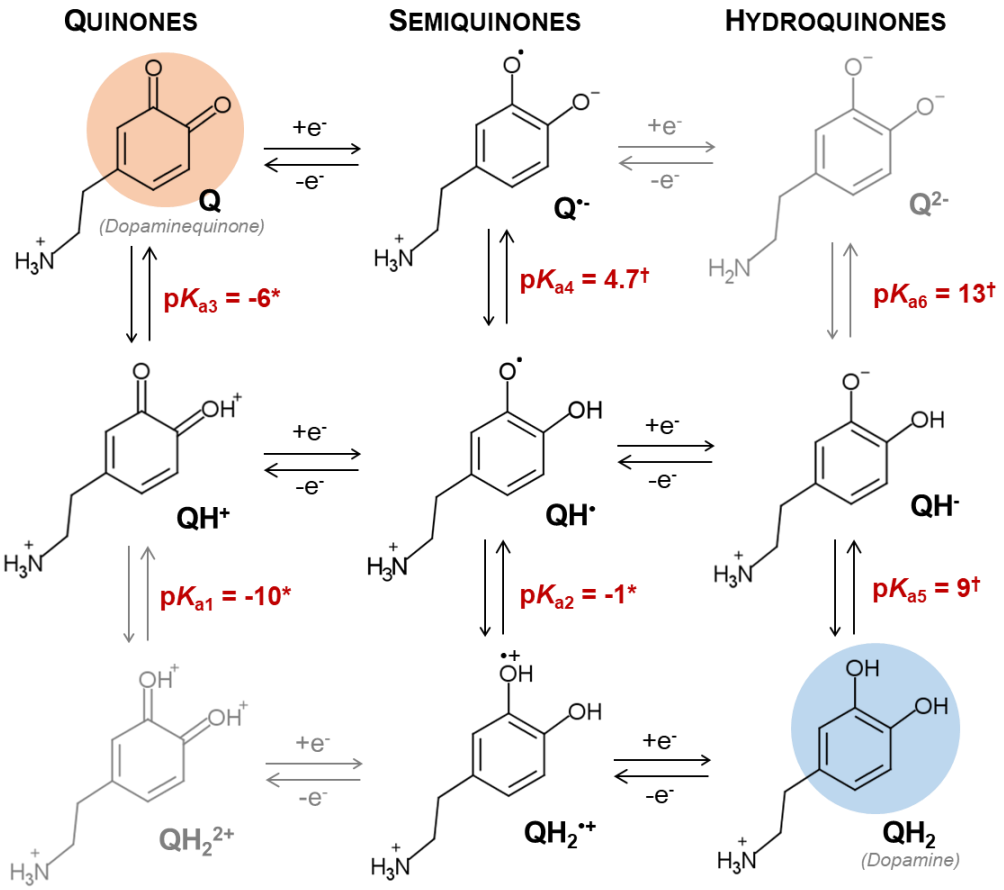

Figure 1.5: Scheme-of-squares of the redox pair dopaminequinone/dopamine. The acid dissociation constants, pK_{a1} to pK_{a3} **(*)** are rough estimates presented in the literature for catechol-containing molecules [114,118], whereas pK_{a4} to pK_{a6} **(†)** were experimentally determined for the dopamine molecule [119–122].

The right column can be viewed as the starting solution of dopamine (**Figure 1.5, QH_2, blue**) before any oxidative process began, and where hydroquinones (in the reduced state) co-exist according to their acid dissociation constants, previously determined [121,122]. At acid or neutral pH, the full protonated form of dopamine (QH_2) is undoubtedly the most representative species in solution. It follows that special attention must be given to the fractions of mono and divalent catecholates (QH^-, Q^{2-}) when studying processes occurring at alkaline conditions, such as oxygen-driven processes [115,123]. Removing one electron from a hydroquinone results in the formation of a semiquinone radical, presented in the central column of the scheme-of-squares (**Figure 1.5**). In aqueous media, the subsequent removal of a second electron from the semiquinone is known to be faster and thermodynamically easier than the first electron, which classifies this redox system as *potential inverted* [112]. The phenomenon of potential inversion is not uncommon in a number of aromatic species [124] and it explains the appearance of single oxidation and reduction peaks in the cyclic voltammograms of multi-electron processes [125]. In the case of Q/QH_2 systems, two reasons that cause potential

inversion may be pointed out: i) the rapid deprotonation of the semiquinone $QH_2^{\bullet+}$, due to its acidic nature, avoids the electron removal from a positively charged ion (thermodynamically more difficult than removing an electron from the neutral species QH_2 or $QH^{\bullet}$); ii) the disproportionation reaction of two $QH^{\bullet}$ semiquinones yields Q and QH_2, accelerating the second electron removal [126]. As a result of potential inversion, the voltammetric behavior of dopamine and catechol-containing molecules behave as an apparent single-step redox system, with a higher potential peak separation than well-behaved single-step charge transfer processes.

Although the behavior of the dopaminequinone/dopamine redox pair is fairly studied, the exact mechanism of polydopamine formation from dopamine electro-oxidation is not established. Several electrochemical studies from 1967 to 1983 elucidate, nonetheless, that the electrogenerated dopaminequinone suffers fast intramolecular cyclization [107,127–129], yielding the indoline-type species predicted by the Raper-Manson scheme (*cf.* **Figure 1.4b**). This first crucial identification of electroactive species in solution is easily accomplished by several authors through the use of cyclic voltammetry. **Figure 1.6** shows typical cyclic voltammograms obtained during the repetitive potential sweep of a gold electrode in dopamine solution, aiming for ePDA coating formation.

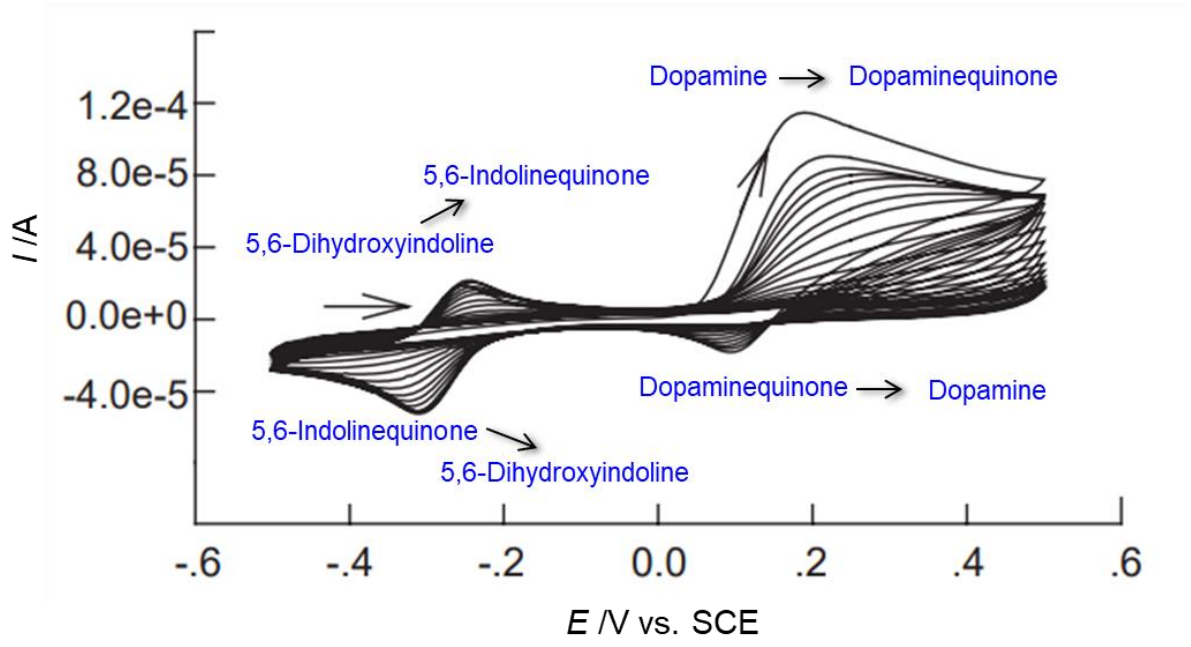

Figure 1.6: Cyclic voltammetry of 2 mM dopamine aqueous solution, in phosphate-buffered saline (pH 7.4), performed at 20 mV s^{-1} using a gold working electrode – adapted from [107]. Confront the Raper-Manson mechanism of **Figure 1.4b** for clarifying the chemical structures of the indicated redox species (blue words).

Besides species identification, the cyclic voltammograms also lead to the attribution of a low conductive nature to the ePDA coating [107,108], since peak currents decrease along potential cycling. In analogy to the chemically driven PDA synthesis, the Raper-Manson scheme is used to explain the appearance of the two redox pairs observed in the cyclic voltammograms during polymer growth, and the poly(5,6-dihydroxyindole) model is assumed to explain ePDA structure [107,108] – a problematic situation is reached: how to reconcile the evident multitude of Q/QH_2 species in the electrolyte solution with the formation of a homopolymer, and why to consider an undetected monomer in the cyclic voltammograms (5,6-dihydroxyindole) as the main polymeric motif. Clearly, a coupling or aggregation mechanism of the Raper-Manson monomers is necessary to clarify the electrosynthesis of ePDA, which may be accomplished by further studying ePDA films. At the moment, electrochemical characterization of ePDA films revealed improved behaviors regarding chemically synthesized PDA, namely, better permeability to ionic species [108] and better electroactivity [130]. The distinct properties of the two film coatings imply structural and/or morphological differences between the materials, which is still under discussion. Understanding the structure-properties relationship in PDA and ePDA coatings is crucial to amplify the technological application of such materials and to better adjust their properties to specific applications. Important reported examples of properties control in chemical PDA include: thermal oxidation to increase the number of reactive quinones [131], the use of different oxidation agents to increase hydrophilicity [84], and chemical vapor deposition methods to improve film conductivity [105]. Nonetheless, due to the lack of a polymeric organized structure [132], such fine control over PDA chemistry is still far from ideal. Electrochemical synthesis is a less explored strategy in the literature and opens the possibility for better tuning the chemical and physical properties of polydopamine.

1.4. Challenges in biosensing: immunosensors and laccase-based sensors

A particular area of research that undoubtedly benefits from surface science insights, namely, the capability to modify surface composition and properties, is the biosensing field. Biosensors are powerful analytical devices of utmost importance in biomedicine, food safety, environmental monitoring, among others [133], with the prospect of avoiding expensive equipment, highly trained personnel and time-consuming steps usually required for (bio)chemical analysis [134]. In contrast to conventional analytical techniques, biosensing technology can easily adapt to miniaturization, and portability and can speed the analysis at the

sampling site, while maintaining sensitivity and selectivity to the target analyte [135]. Taking advantage of the intrinsic specificity of certain biochemical reactions, biosensors are part of a flexible technology with the potential to perform selective, continuous, real-time, and direct analyses, using little or no sample preparation[136,137].

As illustrated in **Figure 1.7**, the biosensor comprises three main parts (bioreceptor, transducer, and detector) that allow the conversion of a biochemical event (catalytic reaction or affinity binding) into a measurable physical signal (electric, magnetic, optical, thermal, *etc.*) [137,138]. The bioreceptor is the biological component responsible for interacting specifically with the analyte (enzymatic substrate, antigen, nucleic acid), producing a physicochemical change in the vicinity of the transducer surface where it is immobilized or confined. The bioreceptor can be an enzyme, antibody, nucleic acid, or even, an organelle, cell, or tissue slice. After the biorecognition event, the signal is transmitted to the detector, which amplifies and processes it to obtain the final quantitative readout. According to the type of the bioreceptor, biosensors can be classified as enzymatic sensors, immunosensors, genosensors, cellular sensors, microbial sensors, *etc.*; or according to the type of transduction phenomenon as electrochemical, optical, piezoelectric, magnetoelastic, thermal or calorimetric sensors. Biomolecule-based biosensors stand out from cell-based biosensors essentially by their fast response and simplicity. In particular, the coupling of glucose oxidase and an electrode surface was a breakthrough in the ’60s, leading the way to the development of the first commercially available glucose biosensor for glycemia monitoring in 1972 [137]. This small and simple to use instrument had an enormous impact on patients with diabetes mellitus, since regular self-monitoring was possible, at home, without the assistance of a medical professional. Glucose biosensors still dominate the market accounting for 85% of the global biosensors market, encompassing point-of-care devices, continuous glucose monitoring systems, and noninvasive glucose monitoring systems [140–141]. Other analytes such as lactate, creatinine, cortisol, urea, and cholesterol are also being targeted in the most recent investigations in the biosensing field due to their health relevance; in fact, wearable biosensors for noninvasive biofluids monitoring is a promising technology in current development [142].

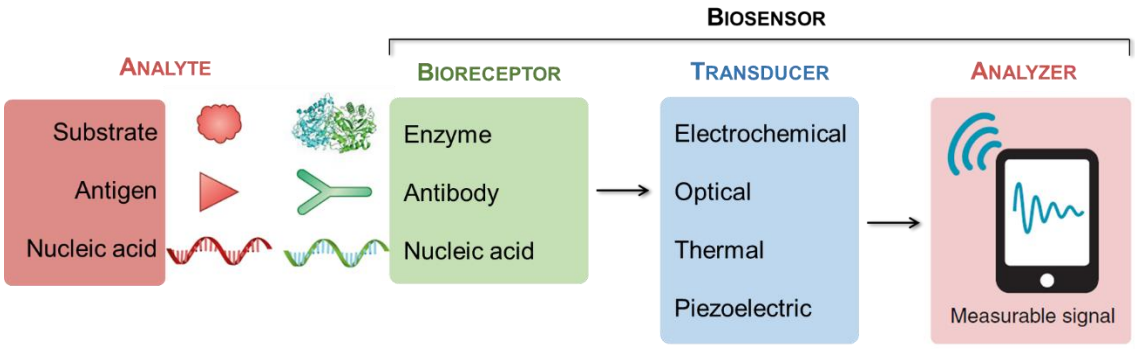

Figure 1.7: Basic components of a biosensor – adapted from [142].

To compete with established analytical techniques, effective biofunctionalization strategies and biomimetic materials are required, which ensure the maintenance of the biorecognition performance under real operational conditions. In modern biosensing research there is a large focus on mimicking the natural environment of biomolecules, or even their recognition sites, to avoid conformational changes and to achieve the high sensitivity and selectivity of the analyte detection [143,144]. Entrapment in polymeric matrices is one of the simplest methodologies that do not induce structural changes in the biomolecule, however, this physical confinement strategy is characterized by low surface loading and by imposing mass transfer limitations. Encapsulation using polymeric particles (instead of a continuous solid matrix) is also a strategy that avoids biomolecules conformational changes, suffering, nonetheless, from identical mass transfer limitations despite improvements in surface loading. Adsorption of biomolecules to surfaces mediated by Van der Walls, hydrogen bonds, or electrostatic interactions usually results in temporary biofunctionalizations since the established interactions are sensitive to pH variations and to the ionic strength of the medium. As so, in general terms, covalent binding provides the most stable immobilization between a biomolecule and an insoluble support; in fact, optimal stability can be achieved if multiple points of the biomolecule are attached to the support, albeit the chemical groups involved in the binding are not important in the catalytic function [145]. Any of the aforementioned types of immobilization require the optimization of surface loading, biomolecule conformation, and orientation, thus concerning a complicated task.

1.4.1. Immunosensors and interfacial immunoassays

Immunosensing is an analytical technology that has witnessed increasing development in the last decades since it provides qualitative or quantitative information regarding the presence of toxins, hormones, proteins, or pathogens, crucial in clinical diagnostics, food quality, and

environmental control [146,147]. A currently employed immunoassay for determining antigens concentrations in a given sample is the enzyme-linked immunosorbent assay (ELISA), developed in the 1960s, in succession to the radioimmunoassay [148]. Instead of utilizing radioactive iodine to label the detection antibody, the ELISA protocols use enzyme-labeled antibodies which allow the detection of an affinity biorecognition event by measuring the absorbance spectra of a chromophoric enzymatic product. As schematically presented in **Figure 1.8**, three major types of ELISA can be distinguished: direct, indirect, and sandwich. In the direct assay, the antigen is firstly adsorbed onto the plastic surface of the microplate well (polystyrene, polyvinyl chloride, or polypropylene), with its subsequent interaction with a specific labeled antibody, denominated primary antibody. Between antigen adsorption and antibody interaction, a blocking step is performed with an animal protein (*e.g.* bovine serum albumin, ovalbumin, aprotinin), to prevent the adsorption of the primary antibody into the uncovered surface of the testing well (limiting non-specific binding and avoiding false positives). In the indirect assay, the primary antibody is not labeled and the detection is made through the use of a labeled secondary antibody that should enhance the sensitivity by multiple binding sites to the primary antibody. To increase the specificity in the attachment of the antigen to the surface, the sandwich assay may be used, where the wells are firstly covered by a capture antibody, thus allowing the use of more complex samples without the need for purification steps. Nonetheless, for the sandwich assay to work, the antigen should display multiple binding sites which is not always the case for low molecular weight antigens.

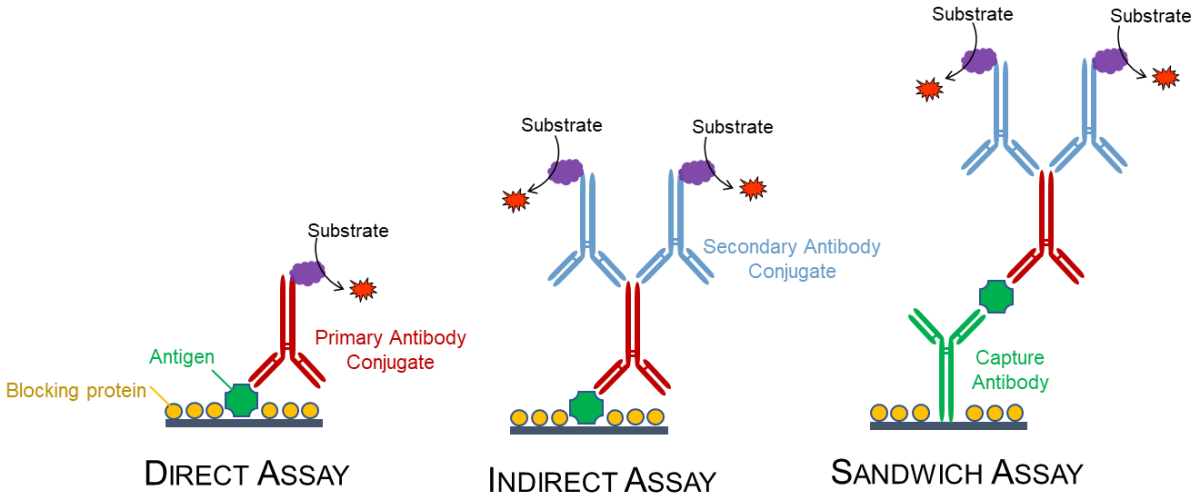

Figure 1.8: Basic types of interfacial immunoassays using labeled antibodies – adapted from [149].

Despite its success, ELISA is a labeled immunologic technology that requires sophisticated synthesis of the immunoglobulin conjugates and expensive cell culture media to

acquire specific antibodies. Furthermore, miniaturization is challenging due to a relatively high sample volume requirement for optical density measurements, and the multistep protocols are inherently time-consuming [150]. The high possibility of false positive or negative results is also pointed out as the result of incomplete blocking of the surface [151]. In contrast, immunosensors may offer miniaturized devices, simpler operation (lower number of operational steps), lower concentration of reagents, and can operate without labeled antibodies. The construction of a label-free immunosensor is still challenging since the immunochemical reaction must be directly detected by measuring physical changes upon complex formation, which is influenced by non-specific adsorption. Commonly reported physical changes for direct immunosensing comprise changes in the interfacial refractive index by total internal reflection techniques (optical); changes in the adsorbed mass by piezoelectric techniques, and changes in the resistive and capacitive behaviors by impedimetric techniques [152]. Despite the overwhelming number of papers in the immunosensing field, there are still unresolved fundamental questions related to immobilization, orientation, and specific properties of the antibodies on the transducer surface.

1.4.2. Laccase-based electrochemical biosensors

In recent decades, the monitoring of phenolic compounds using portable, cheap, and fast-response devices has been growing as an area of scientific investigation [153,154]. The interest in detecting, quantifying, or eliminating compounds that have one, or multiple, hydroxyl groups attached to a benzene ring lies in their involvement and importance in multiple human activities, namely food quality assessment, agro-industrial waste processing, drugs delivery and disposal, and environmental remediation. Essentially, two large classes of phenolic compounds with technological or environmental relevance can be distinguished: polyphenols and phenolic pollutants. Polyphenols are a large group of natural compounds originated from the secondary metabolism of plants [154,155], ending up in plant-based food products and agro-industrial residues. Polyphenols display diverse biological activities and can be classified as hydroxybenzoic and hydroxycinnamic acids (of low molecular weight), flavonoids (of intermediate molecular weight), and tannins (of high molecular weight) [156]. From the point of view of the food industry, polyphenols are relevant for determining the organoleptic properties (color, flavor, texture) and oxidative stability of some foods such as wines [157], olive oils [158], beers, and cocoa [155]. In addition, its presence in agroforestry residues allows for valuing large amounts of biomass for pharmaceutical purposes [159] and food improvement [160], since antioxidant properties [161], anti-inflammatory [162], antiviral [163], and

anticancer [164] properties are attributed to these compounds. In contrast, from the environmental perspective, some phenols are considered as pollutants, namely those coming from the pharmaceutical industry, and from the production of resins, paints, textiles, petrochemicals, and paper [154]. The presence of alkylphenols, halogenated phenolic compounds [165], and synthetic estrogenic hormones in the environment are just a few examples of classes of substances that have alarmed European and North American environmental protection agencies, due to their wide dissemination and potential adverse effects on humans and wild animals.

The performance of several enzymes as biorecognition elements for the construction of a phenolic sensor have been evaluated before, namely, tyrosinase, horseradish peroxidase, and laccase [154]. Tyrosinase proved to be somewhat stable yet very sensitive to inhibitors, while peroxidase depends on the presence of hydrogen peroxide in order to complete its catalytic function [166]. Laccases, on the other hand, exhibit stable catalytic activity after immobilization with a wide range of oxidizable substrates. It is an oxidoreductase found in fungi, bacteria, plants, and insects [167], which catalyzes the oxidation of monophenols, ortho- and para-diphenols, polyphenols, lignins, aminophenols, methoxyphenols, and aromatic amines, with the simultaneous reduction of molecular oxygen to water. Common substrates used to evaluate the catalytic activity of laccases by spectroscopic techniques include the aromatic azo compounds 2,2'-azino-bis(3-ethylbenzothiazoline-6-sulfonic acid) (ABTS), syringaldazine, and also the methoxylated phenols 2-methoxyphenol (guaiacol) and syringol (2,6-dimethoxyphenol) [168,169]. The versatility in converting a variety of substrates by means of redox reactions gives laccase great technological potential in the development of phenolic sensors with amperometric transduction. **Figure 1.9** shows a simplified reaction scheme of the laccase catalytic cycle, highlighting the two copper active centers: T1 and T2/T3. In the catalytic center of T1 copper, the hydroxyl group of the phenolic substrate is oxidized, losing an electron and a proton, and being converted into a phenoxy radical. If the original substrate is a diphenol, this substrate can be re-oxidized in the second available hydroxyl group or it can undergo dismutation ending up, in one way or another, in a quinone product [170]. During the laccase catalytic cycle, 4 electrons are transferred intramolecularly from the T1 center to the T2/T3 trinuclear center, which are separated by the tripeptide histidine-cysteine-histidine (His-Cys-His) at a distance of 13 – 14 Å, allowing the complete reduction of molecular oxygen to water.

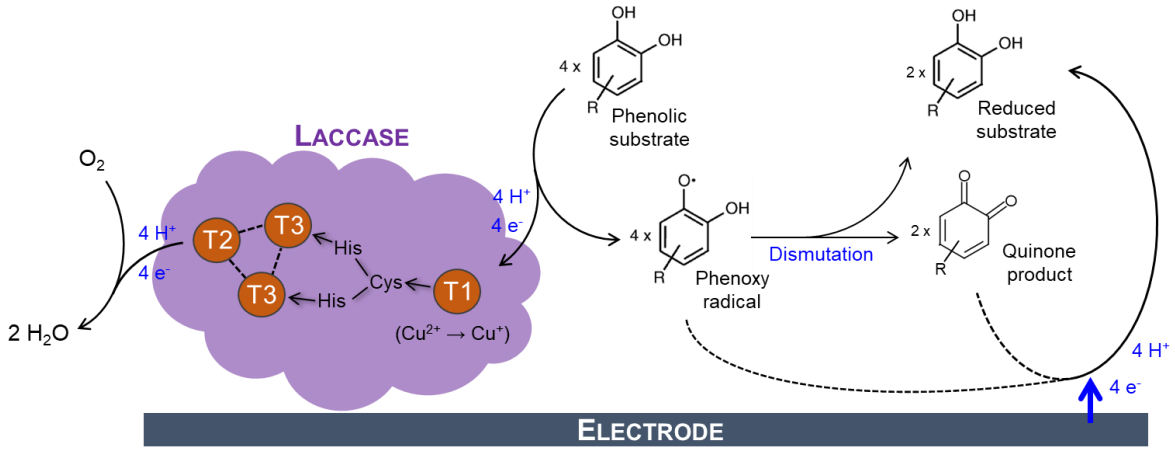

Figure 1.9: Reaction scheme of the catalytic oxidation of diphenols to phenoxy radicals promoted by laccase, with the simultaneous reduction of molecular oxygen to water, and amperometric detection of phenoxy or quinone products at the electrode surface – adapted from [171,172].

The catalytic performance of laccases is recognized as being constrained by the rate of electron transfer between the substrate and the T1 site, which differs amongst laccases from different origins (*e.g.* bacteria, fungi, plants) due to different coordination geometries of the copper center. The rate of substrate oxidation is thus greatly influenced by the redox potential of the aforementioned active center, but also by the substrate-laccase affinity. Due to this fact, higher potential laccases (0.7 – 0.8 V *vs.* NHE) are, in general terms, better suited for catalytic oxidation of phenols, although low potential laccases (0.4 – 0.5 V *vs.* NHE) must not be disregarded [154,173]. For instance, bacterial laccases (prokaryotic) are a typical example of low redox potential laccases that display very interesting properties from the technological point of view; these are: a wide range of working pH and great thermal stability. [174] Nonetheless, since fungal and plant laccases typically display higher redox potential, these are commonly selected for electrochemical applications.

Amperometric biosensors constructed with oxidoreductases can be classified into three generations depending on the mechanism of electron transfer from the enzyme to the electrode material. In the first generation, the co-substrate (*e.g.* oxygen) functions as the electron mediator between the oxidoreductase and the electrode, allowing the indirect quantification of substrate concentration by oxygen consumption or hydrogen peroxide production. In the second generation, electron mediation is achieved by an artificial co-substrate (*e.g.* iron complex) decreasing the oxygen dependency and lowering the working potential for substrate detection. Lastly, a third generation of biosensors can be considered when the electron transfer from the enzyme redox center to the electrode does not involve diffusion-limited mediators, rather, it occurs directly by tunneling or even through a "molecular wire" [175,176]. Although third-

generation biosensors may display improved selectivity and faster electron transfer rates due to the absence of mediators, direct electron transfer is still difficult to attain for many enzymes and electrode configurations. Furthermore, the advantage of lowering the working potential of a biosensor by the implementation of a third-generation architecture is only achieved for oxidoreductases with co-substrate sites with a low potential – a typical example is glucose oxidase. In the case of laccases, the most used architecture is thus based on the direct detection of the electroactive products of phenols oxidation (**Figure 1.9**), namely, quinone or semiquinone species [171,172] without the need for adding a redox mediator. This architecture does not fit in the three classical biosensors generations classification, since the electron transfer from the enzyme to the electrode is mediated by the products, having similar advantages to second-generation biosensors. In similarity to other biosensors with electrochemical transduction, the signal optimization of laccase-based biosensors should involve the maximization of the electrode surface area, the electrical conductivity of intervenient interfacial materials, and the rate of electron transfer across the interface, allowing to achieve the highest sensitivity and lowest detection limits possible.

1.4.3. Polydopamine-based strategies applied to biosensors design

A key feature that makes polydopamine a suitable coating material for biosensing applications is that it modifies the surface with anchoring groups allowing the attachment of biomolecules. From an ideal point of view, a successful confinement of biochemically active proteins to an electrode surface vicinity will suffice to create an analytically powerful biosensor. However, the inclusion of nanomaterials into the biosensing interfaces design is a common choice in the design of enzymatic biosensors, immunosensors, and genosensors, as seen in reviews about the subject [177–179]. Soon after the announcement of polydopamine as a new functional and universal coating in 2007 [57], several publications revealed the successful use of polydopamine-based drop-casting methods to immobilize glucose oxidases and laccases together with several nanomaterials (carbon nanotubes, graphene, magnetite nanoparticles) at electrode surfaces [180–182]. Drop-casting refers to the deposition of a solid film onto a surface during the evaporation of the solvent of a sessile drop, forcing surface adsorption of the non-volatile components. In the particular case of polydopamine-based drop-casts, the biomolecules and nanomaterials deposition implicitly occurs through their entrapment in polydopamine, while adsorption and covalent immobilization should also happen during dopamine polymerization. The contribution of covalent and non-covalent interactions between biomolecules, nanomaterials and polydopamine after film deposition remains ambiguous in

most cases since the experimental evidence is scarce. If the nature of interactions is still poorly understood, the advantage of using a polydopamine matrix becomes meaningless, since other organic polymers could be used instead. The particular case of amperometric glucose biosensors is useful to clarify this point: sensing interfaces prepared with polydopamine and nanomaterials display competing analytical performances against interfaces prepared with other organic polymers (*e.g.* poly(3,4-ethylenedioxythiophene), polyaniline, polyamidoamine), also hybridized with a variety of nanomaterials [183,184]. Looking at the consulted literature, it is not clear if the entrapment of biomolecules in polydopamine renders a better performance than other organic polymers (as a general rule), since nanomaterials are present in these cases. The use of nanomaterials is undoubtedly useful to improve electrodes surface area, enhance catalysis or affinity reactions, and ultimately increase the analytical performance of a biosensing interface [185], and the aforementioned works are important to validate polydopamine as an efficient adhesive agent for nanomaterials and biomolecules. The crucial feature of polydopamine for its biosensing adequacy, namely, providing stable bonds while maintaining or improving the biochemical activity of proteins, is not commonly highlighted nor unapologetically investigated in such multi-component drop-casting strategies.

In addition to one-step drop-casting, multi-step strategies have also been described to construct biosensing interfaces, where one of the steps consists of the conjugation of biomolecules and nanomaterials into hybrid particles, assisted by polydopamines adhesiveness. The reported formulations of protein-polydopamine-nanomaterial particles include not only enzymes, such as laccase [181], glucose oxidase [186,187], galactose oxidase [186], and horseradish peroxidase [188] but also other proteins such as bovine albumin, anti-human immunoglobulin G [187,189] and anti-leptin [190]. The nanoconjugation strategy has been applied in the design of enzymatic sensors and immunosensors for a variety of purposes. In enzymatic sensors, the hybrid nanoparticles should carry and permanently immobilize the enzymes at the surface, while in immunosensors the particles are envisaged to interact specifically with the capture antibodies and amplify the detection signal by a size effect [189], by labeling [187,188] or by magnetic attraction [190]. Although the authors do not focus on assessing the type of chemical bonds between proteins and polydopamine, the stability of the dispersions in several aqueous mediums and the performance of the biosensors are strong indicators of stable bonds between the used proteins and the polydopamine matrix within the prepared particles.

Simpler biosensing interfaces designs without the incorporation of nanomaterials or labeling molecules are less common, albeit they may provide quicker, cheaper, and

straightforward surface modifications compared to more complex strategies. The simple dipping of a pre-modified surface with polydopamine with a protein solution is one example of a simple two-step strategy successfully tested using some enzymes [184,191–193] and capture antibodies [188,194,195], although the exact type of bond between proteins and polydopamine is not known. Some examples of proteins immobilization in one step during the chemical polymerization of dopamine are also reported [193,196], although not in sufficient numbers to establish general best conditions, proteins compatibility with the method, and what are the main factors affecting the immobilization success. The work of A. Nijhuis *et al.* indicates that higher protein concentrations may lead to higher protein deposition in the one-step strategy, while lower protein concentrations are better suited to two-step strategies [193], however, different proteins at different concentrations were utilized in this study. Another immobilization strategy mentioned in the literature is the electrochemical co-deposition of polydopamine and proteins, tested by S. Yao and coworkers towards bovine hemoglobulin [197], anti-human immunoglobulin G [198], glucose oxidase [199,200] and lysozyme [198,199]. These studies reveal that immobilization of active proteins is possible during the potentiodynamic deposition of polydopamine from pH 6 to 9, except for the case of lysozyme which displays the highest isoelectric point (pI = 11) amongst the studied proteins. The authors suggest that immobilization is mainly dictated by electrostatic interactions and favored when proteins are positively charged.

Further clarification of the type of protein-polydopamine interactions is needed, allowing to maximize the stability of the established bonds, maximize proteins biochemical activity, and to even tune polymers structure/composition and choose the adequate immobilization strategy accordingly. An in-depth understanding of polydopamine-based interfaces has the great possibility of allowing innovations in other bio-inspired catechol-based coatings, bringing new powerful biosensing interfaces that can tackle complex analytical problems.

1.5. Objectives and structure of the thesis

The main objective of the thesis concerns the development of biomolecule-compatible coatings through the electropolymerization of catechol derivatives, envisaging biosensing applications with electrochemical or optical transduction. Identification of crucial gaps in the current scientific knowledge motivated the three research topics of the present work:

i) Study of the electrochemically driven reaction pathways in the catecholamines aggregation process, that lead to the surface deposition of the corresponding polycatecholamines coatings, and their physicochemical characterization regarding composition and structural organization, useful for structure-properties analysis.

ii) Evaluate the suitability of potentiodynamic and potentiostatic techniques in the synthesis control of critical coating properties for biosensors signal transduction, namely, thickness, porosity, charge transfer resistance, and optical properties.

iii) Assessment of polycatecholamines biomolecule-compatibility and immobilization effectiveness through measurements of laccases and immunoglobulin biological activities upon surface binding.

To contextualize the present scientific work, Chapter I provides an introduction to the currently known role of catechol and amine groups in the properties of natural and synthetic adhesives; the translation of this property to the success of polydopamine dip-coating method; the opportunity for better control over the synthesis of adherent coatings brought by electrochemical techniques; and finally, the scientific and technological challenges of biosensors development.

Chapter II briefly summarizes the physicochemical principles of the used material characterization techniques, while Chapter III describes the starting materials, experimental conditions, and procedures employed in the preparation and characterization of the modified carbon and gold surfaces.

Chapters IV to VII compile the results and scientific discussion of the doctoral work, not necessarily in chronological order. Firstly, in Chapter IV, structural analysis of polydopamine films prepared by chemical and electrochemical methods reveals key differences that justify their physicochemical properties and the suitability of electrosynthetic methods to prepare amperometric and optical transduction matrices. In addition, the combination of electrochemical and spectroscopic data allowed a refinement of the electropolymerization

mechanism of dopamine. In-depth studies of other catechol derivatives electropolymerization are presented in Chapter V, contributing to the basal structure-property relationships for the subsequent application in the biosensing interfaces described in Chapters VI and VII. Amperometric laccase-based biosensing interfaces are developed in Chapter VI, through one-step potentiostatic co-deposition methodologies or by separating polymer and laccase depositions in two distinct steps, offering biofunctionalization solutions for fungal and bacterial laccases (from Novozymes and MetGen companies). Chapter VII is dedicated to the development of label-free immunosensing platforms, presenting a fast electrochemical modification to avoid non-specific adsorption, and exploring the performance of different polycatecholamines in the optical detection of immunochemical reactions.

1.6. References

[1] K. Kendall, Theoretical aspects of solid-solid adhesion, Science Progress. 72 (1988) 155–171. https://www.jstor.org/stable/43420715.

[2] S.J. Marshall, S.C. Bayne, R. Baier, A.P. Tomsia, G.W. Marshall, A review of adhesion science, Dental Materials. 26 (2010) e11-e16. doi:10.1016/j.dental.2009.11.157.

[3] R.E. Baier, E.G. Shafrin, W.A. Zisman, Adhesion: Mechanisms That Assist or Impede It, Science. 162 (1968) 1360–1368. doi:10.1126/science.162.3860.1360.

[4] B.P. Lee, P.B. Messersmith, J.N. Israelachvili, J.H. Waite, Mussel-Inspired Adhesives and Coatings, Annual Review of Materials Research. 41 (2011) 99–132. doi:10.1146/annurev-matsci-062910-100429.

[5] C. Cui, W. Liu, Recent advances in wet adhesives: Adhesion mechanism, design principle and applications, Progress in Polymer Science. 116 (2021) 101388. doi:10.1016/j.progpolymsci.2021.101388.

[6] J.H. Waite, N.H. Andersen, S. Jewhurst, C. Sun, Mussel adhesion: Finding the tricks worth mimicking, Journal of Adhesion. 81 (2005) 297–317. doi:10.1080/00218460590944602.

[7] L. Khandeparker, A.C. Anil, Underwater adhesion: The barnacle way, International Journal of Adhesion and Adhesives. 27 (2007) 165–172. doi:10.1016/j.ijadhadh.2006.03.004.

[8] E. Hennebert, B. Maldonado, P. Ladurner, P. Flammang, R. Santos, Experimental strategies for the identification and characterization of adhesive proteins in animals: a review, Interface Focus. 5 (2015) 20140064. doi:10.1098/rsfs.2014.0064.

[9] J. Wunderer, B. Lengerer, R. Pjeta, P. Bertemes, L. Kremser, H. Lindner, T. Ederth, M.W. Hess, D. Stock, W. Salvenmoser, P. Ladurner, A mechanism for temporary bioadhesion, Proceedings of the National Academy of Sciences. 116 (2019) 4297–4306. doi:10.1073/pnas.1814230116.

[10] B. Cheng, J. Yu, T. Arisawa, K. Hayashi, J.J. Richardson, Y. Shibuta, H. Ejima, Ultrastrong underwater adhesion on diverse substrates using non-canonical phenolic groups, Nature Communications. 13 (2022) 1892. doi:10.1038/s41467-022-29427-w.

[11] H.J. Cha, D.S. Hwang, S. Lim, Development of bioadhesives from marine mussels, Biotechnology Journal. 3 (2008) 631–638. doi:10.1002/biot.200700258.

[12] S. Baik, H.J. Lee, D.W. Kim, J.W. Kim, Y. Lee, C. Pang, Bioinspired Adhesive Architectures: From Skin Patch to Integrated Bioelectronics, Advanced Materials. 31 (2019) 1803309. doi:10.1002/adma.201803309.

[13] S. Khanlari, M.A. Dubé, Bioadhesives: A Review, Macromolecular Reaction Engineering. 7 (2013) 573–587. doi:10.1002/mren.201300114.

[14] J.H. Waite, M.L. Tanzer, Polyphenolic Substance of Mytilus edulis: Novel Adhesive Containing L-Dopa and Hydroxyproline, Science. 212 (1981) 1038–1040. doi:10.1126/science.212.4498.1038.

[15] R.Y. Floriolli, J. Von Langen, J.H. Waite, Marine surfaces and the expression of specific byssal adhesive protein variants in Mytilus, Marine Biotechnology. 2 (2000) 352–363. doi:10.1007/s101269900032.

[16] T.H. Anderson, J. Yu, A. Estrada, M.U. Hammer, J.H. Waite, J.N. Israelachvili, The contribution of DOPA to substrate-peptide adhesion and internal cohesion of mussel-inspired synthetic peptide films, Advanced Functional Materials. 20 (2010) 4196–4205. doi:10.1002/adfm.201000932.

[17] J. Wang, C. Liu, X. Lu, M. Yin, Co-polypeptides of 3,4-dihydroxyphenylalanine and l-lysine to mimic marine adhesive protein, Biomaterials. 28 (2007) 3456–3468. doi:10.1016/j.biomaterials.2007.04.009.

[18] M.J. Sever, J.J. Wilker, Synthesis of peptides containing DOPA (3,4-dihydroxyphenylalanine), Tetrahedron. 57 (2001) 6139–6146. doi:10.1016/S0040-4020(01)00601-9.

[19] J. Saiz-Poseu, J. Mancebo-Aracil, F. Nador, F. Busqué, D. Ruiz-Molina, The Chemistry behind Catechol-Based Adhesion, Angewandte Chemie International Edition. 58 (2019) 696–714. doi:10.1002/anie.201801063.

[20] J. Yu, W. Wei, E. Danner, J.N. Israelachvili, J.H. Waite, Effects of Interfacial Redox in Mussel Adhesive Protein Films on Mica, Advanced Materials. 23 (2011) 2362–2366. doi:10.1002/adma.201003580.

[21] K.L. Johnson, Mechanics of adhesion, Tribology International. 31 (1998) 413–418. doi:10.1016/S0301-679X(98)00060-7.

[22] J.H. Waite, Mussel adhesion – essential footwork, The Journal of Experimental Biology. 220 (2017) 517–530. doi:10.1242/jeb.134056.

[23] P. Kord Forooshani, B.P. Lee, Recent approaches in designing bioadhesive materials inspired by mussel adhesive protein, Journal of Polymer Science Part A: Polymer Chemistry. 55 (2017) 9–33. doi:10.1002/pola.28368.

[24] H. Lee, N.F. Scherer, P.B. Messersmith, Single-molecule mechanics of mussel adhesion, Proceedings of the National Academy of Sciences. 103 (2006) 12999–13003. doi:10.1073/pnas.0605552103.

[25] T. Utzig, P. Stock, M. Valtiner, Resolving Non-Specific and Specific Adhesive Interactions of Catechols at Solid/Liquid Interfaces at the Molecular Scale, Angewandte Chemie International Edition. 55 (2016) 9524–9528. doi:10.1002/anie.201601881.

[26] S. Bahri, C.M. Jonsson, C.L. Jonsson, D. Azzolini, D.A. Sverjensky, R.M. Hazen, Adsorption and Surface Complexation Study of L-DOPA on Rutile (α-TiO_2) in NaCl Solutions, Environmental Science & Technology. 45 (2011) 3959–3966. doi:10.1021/es1042832.

[27] K.L. Syres, A.G. Thomas, W.R. Flavell, B.F. Spencer, F. Bondino, M. Malvestuto, A. Preobrajenski, M. Grätzel, Adsorbate-Induced Modification of Surface Electronic Structure: Pyrocatechol Adsorption on the Anatase TiO_2 (101) and Rutile TiO_2 (110) Surfaces, The Journal of Physical Chemistry C. 116 (2012) 23515–23525. doi:10.1021/jp308614k.

[28] F. Schwarz, S. Pomp, P. Seidel, X. Li, J. Paier, M. Sterrer, Hydrogen-bond-stabilized high density catechol monolayer on magnetite Fe3O4(111), Surface Science. 719 (2022) 122027. doi:10.1016/j.susc.2022.122027.

[29] A. Calzolari, A. Ruini, A. Catellani, Surface Effects on Catechol/Semiconductor Interfaces, The Journal of Physical Chemistry C. 116 (2012) 17158–17163. doi:10.1021/jp307117h.

[30] J.E. Heckler, G.R. Neher, F. Mehmood, D.B. Lioi, R. Pachter, R. Vaia, W.J. Kennedy, D. Nepal, Surface Functionalization of Ti3C2Tx MXene Nanosheets with Catechols:

Implication for Colloidal Processing, Langmuir. 37 (2021) 5447–5456. doi:10.1021/acs.langmuir.0c03078.

[31] Q. Lu, E. Danner, J.H. Waite, J.N. Israelachvili, H. Zeng, D.S. Hwang, Adhesion of mussel foot proteins to different substrate surfaces, Journal of The Royal Society Interface. 10 (2013) 20120759. doi:10.1098/rsif.2012.0759.

[32] J.L. Dalsin, L. Lin, S. Tosatti, J. Vörös, M. Textor, P.B. Messersmith, Protein Resistance of Titanium Oxide Surfaces Modified by Biologically Inspired mPEG−DOPA, Langmuir. 21 (2005) 640–646. doi:10.1021/la048626g.

[33] E. Faure, C. Falentin-Daudré, C. Jérôme, J. Lyskawa, D. Fournier, P. Woisel, C. Detrembleur, Catechols as versatile platforms in polymer chemistry, Progress in Polymer Science. 38 (2013) 236–270. doi:10.1016/j.progpolymsci.2012.06.004.

[34] J. Liebscher, Chemistry of Polydopamine – Scope, Variation, and Limitation, European Journal of Organic Chemistry. 2019 (2019) 4976–4994. doi:10.1002/ejoc.201900445.

[35] P. Das, M. Reches, Revealing the role of catechol moieties in the interactions between peptides and inorganic surfaces, Nanoscale. 8 (2016) 15309–15316. doi:10.1039/c6nr04550b.

[36] M. Yu, T.J. Deming, Synthetic Polypeptide Mimics of Marine Adhesives, Macromolecules. 31 (1998) 4739–4745. doi:10.1021/ma980268z.

[37] C.R. Matos-Pérez, J.D. White, J.J. Wilker, Polymer Composition and Substrate Influences on the Adhesive Bonding of a Biomimetic, Cross-Linking Polymer, Journal of the American Chemical Society. 134 (2012) 9498–9505. doi:10.1021/ja303369p.

[38] H.J. Meredith, C.L. Jenkins, J.J. Wilker, Enhancing the Adhesion of a Biomimetic Polymer Yields Performance Rivaling Commercial Glues, Advanced Functional Materials. 24 (2014) 3259–3267. doi:10.1002/adfm.201303536.

[39] J. Yang, J. Keijsers, M. van Heek, A. Stuiver, M.A. Cohen Stuart, M. Kamperman, The effect of molecular composition and crosslinking on adhesion of a bio-inspired adhesive, Polymer Chemistry. 6 (2015) 3121–3130. doi:10.1039/C4PY01790K.

[40] H.M. Siebert, J.J. Wilker, Improving the molecular weight and synthesis of a renewable biomimetic adhesive polymer, European Polymer Journal. 113 (2019) 321–327. doi:10.1016/j.eurpolymj.2019.01.063.

[41] H. Chang, V. Adibnia, W. Qi, R. Su, X. Banquy, Ternary Synergy of Lys, Dopa, and Phe Results in Strong Cohesion of Peptide Films, ACS Applied Bio Materials. 6 (2023) 865–873. doi:10.1021/acsabm.2c01009.

[42] G.P. Maier, M. V. Rapp, J.H. Waite, J.N. Israelachvili, A. Butler, Adaptive synergy between catechol and lysine promotes wet adhesion by surface salt displacement, Science. 349 (2015) 628–632. doi:10.1126/science.aab0556.

[43] M. Shin, J.Y. Shin, K. Kim, B. Yang, J.W. Han, N.-K. Kim, H.J. Cha, The position of lysine controls the catechol-mediated surface adhesion and cohesion in underwater mussel adhesion, Journal of Colloid and Interface Science. 563 (2020) 168–176. doi:10.1016/j.jcis.2019.12.082.

[44] Y. Mu, P. Mu, X. Wu, X. Wan, The two facets of the synergic effect of amine cation and catechol on the adhesion of catechol in underwater conditions, Applied Surface Science. 530 (2020) 146973. doi:10.1016/j.apsusc.2020.146973.

[45] Y. Li, C. Liang, L. Gao, S. Li, Y. Zhang, J. Zhang, Y. Cao, Hidden complexity of synergistic roles of Dopa and lysine for strong wet adhesion, Materials Chemistry Frontiers. 1 (2017) 2664–2668. doi:10.1039/C7QM00402H.

[46] W. Zhang, R. Wang, Z. Sun, X. Zhu, Q. Zhao, T. Zhang, A. Cholewinski, F. (Kuo) Yang, B. Zhao, R. Pinnaratip, P.K. Forooshani, B.P. Lee, Catechol-functionalized hydrogels: biomimetic design, adhesion mechanism, and biomedical applications, Chemical Society Reviews. 49 (2020) 433–464. doi:10.1039/C9CS00285E.

[47] H.A. Lee, E. Park, H. Lee, Polydopamine and Its Derivative Surface Chemistry in Material Science: A Focused Review for Studies at KAIST, Advanced Materials. 32 (2020) 1907505. doi:10.1002/adma.201907505.

[48] Y. Liu, K. Ai, L. Lu, Polydopamine and its derivative materials: Synthesis and promising applications in energy, environmental, and biomedical fields, Chemical Reviews. 114 (2014) 5057–5115. doi:10.1021/cr400407a.

[49] C.L. Jenkins, H.M. Siebert, J.J. Wilker, Integrating Mussel Chemistry into a Bio-Based Polymer to Create Degradable Adhesives, Macromolecules. 50 (2017) 561–568. doi:10.1021/acs.macromol.6b02213.

[50] Y. Kuboe, H. Tonegawa, K. Ohkawa, H. Yamamoto, Quinone Cross-Linked Polysaccharide Hybrid Fiber, Biomacromolecules. 5 (2004) 348–357. doi:10.1021/bm034363d.

[51] M. Jia, A. Li, Y. Mu, W. Jiang, X. Wan, Synthesis and adhesive property study of polyoxetanes grafted with catechols via Cu(I)-catalyzed click chemistry, Polymer. 55 (2014) 1160–1166. doi:10.1016/j.polymer.2014.01.028.

[52] M. Ye, R. Jiang, J. Zhao, J. Zhang, X. Yuan, X. Yuan, In situ formation of adhesive hydrogels based on PL with laterally grafted catechol groups and their bonding efficacy

to wet organic substrates, Journal of Materials Science: Materials in Medicine. 26 (2015). doi:10.1007/s10856-015-5608-y.

[53] E. Faure, C. Falentin-Daudré, C. Jérôme, J. Lyskawa, D. Fournier, P. Woisel, C. Detrembleur, Catechols as versatile platforms in polymer chemistry, Progress in Polymer Science. 38 (2013) 236–270. doi:10.1016/j.progpolymsci.2012.06.004.

[54] Q. Lyu, N. Hsueh, C.L.L. Chai, The chemistry of bioinspired catechol(amine)-based coatings, ACS Biomaterials Science & Engineering. 5 (2019) 2708–2724. doi:10.1021/acsbiomaterials.9b00281.

[55] M.A. Rahman, H.A. Al-Abadleh, Surface Water Structure and Hygroscopic Properties of Light Absorbing Secondary Organic Polymers of Atmospheric Relevance, ACS Omega. 3 (2018) 15519–15529. doi:10.1021/acsomega.8b02066.

[56] G.P. Maier, C.M. Bernt, A. Butler, Catechol oxidation: considerations in the design of wet adhesive materials, Biomaterials Science. 6 (2018) 332–339. doi:10.1039/C7BM00884H.

[57] H. Lee, S.M. Dellatore, W.M. Miller, P.B. Messersmith, Mussel-inspired surface chemistry for multifunctional coatings, Science. 318 (2007) 426–430. doi:10.1126/science.1147241.

[58] J.H. Ryu, P.B. Messersmith, H. Lee, Polydopamine surface chemistry: a decade of discovery, ACS Applied Materials and Interfaces. 10 (2018) 7523–7540. doi:10.1021/acsami.7b19865.

[59] H. Hu, J.C. Dyke, B.A. Bowman, C.-C. Ko, W. You, Investigation of Dopamine Analogues: Synthesis, Mechanistic Understanding, and Structure–Property Relationship, Langmuir. 32 (2016) 9873–9882. doi:10.1021/acs.langmuir.6b02141.

[60] S. Hong, Y. Wang, S.Y. Park, H. Lee, Progressive fuzzy cation-π assembly of biological catecholamines, Science Advances. 4 (2018) eaat7457. doi:10.1126/sciadv.aat7457.

[61] C. Lim, J. Huang, S. Kim, H. Lee, H. Zeng, D.S. Hwang, Nanomechanics of Poly(catecholamine) Coatings in Aqueous Solutions, Angewandte Chemie International Edition. 55 (2016) 3342–3346. doi:10.1002/anie.201510319.

[62] S.P. Pujari, L. Scheres, A.T.M. Marcelis, H. Zuilhof, Covalent Surface Modification of Oxide Surfaces, Angewandte Chemie International Edition. 53 (2014) 6322–6356. doi:10.1002/anie.201306709.

[63] O.N. Oliveira, L. Caseli, K. Ariga, The Past and the Future of Langmuir and Langmuir–Blodgett Films, Chemical Reviews. 122 (2022) 6459–6513. doi:10.1021/acs.chemrev.1c00754.

[64] H. Lee, Y. Lee, A.R. Statz, J. Rho, T.G. Park, P.B. Messersmith, Substrate-Independent Layer-by-Layer Assembly by Using Mussel-Adhesive-Inspired Polymers, Advanced Materials. 20 (2008) 1619–1623. doi:10.1002/adma.200702378.

[65] J. Zhu, M.T. Tsehaye, J. Wang, A. Uliana, M. Tian, S. Yuan, J. Li, Y. Zhang, A. Volodin, B. Van der Bruggen, A rapid deposition of polydopamine coatings induced by iron (III) chloride/hydrogen peroxide for loose nanofiltration, Journal of Colloid and Interface Science. 523 (2018) 86–97. doi:10.1016/j.jcis.2018.03.072.

[66] M.D. Nothling, C.G. Bailey, L.L. Fillbrook, G. Wang, Y. Gao, D.R. McCamey, M. Monfared, S. Wong, J.E. Beves, M.H. Stenzel, Polymer Grafting to Polydopamine Free Radicals for Universal Surface Functionalization, Journal of the American Chemical Society. 144 (2022) 6992–7000. doi:10.1021/jacs.2c02073.

[67] R.A. Zangmeister, T.A. Morris, M.J. Tarlov, Characterization of Polydopamine Thin Films Deposited at Short Times by Autoxidation of Dopamine, Langmuir 29 (2013) 8619-8628.pdf, Langmuir. 29 (2013) 8619–8628. doi:10.1021/la400587j.

[68] S. Rella, E. Mazzotta, A. Caroli, M. De Luca, C. Bucci, C. Malitesta, Investigation of polydopamine coatings by X-ray Photoelectron Spectroscopy as an effective tool for improving biomolecule conjugation, Applied Surface Science. 447 (2018) 31–39. doi:10.1016/j.apsusc.2018.03.057.

[69] D.R. Dreyer, D.J. Miller, B.D. Freeman, D.R. Paul, C.W. Bielawski, Elucidating the Structure of Poly(dopamine), Langmuir. 28 (2012) 6428–6435. doi:10.1021/la204831b.

[70] E. Coy, I. Iatsunskyi, J.C. Colmenares, Y. Kim, R. Mrówczyński, Polydopamine Films with 2D-like Layered Structure and High Mechanical Resilience, ACS Applied Materials & Interfaces. 13 (2021) 23113–23120. doi:10.1021/acsami.1c02483.

[71] F. Ponzio, V. Ball, Polydopamine deposition at fluid interfaces, Polymer International. 65 (2016) 1251–1257. doi:10.1002/pi.5124.

[72] H.S. Mason, The chemistry of melanin; mechanism of the oxidation of dihydroxyphenylalanine by tyrosinase, The Journal of Biological Chemistry. 172 (1948) 83–99. PMDI:18920770.

[73] M. d'Ischia, A. Napolitano, A. Pezzella, P. Meredith, M. Buehler, Melanin Biopolymers: Tailoring Chemical Complexity for Materials Design, Angewandte Chemie International Edition. 59 (2020) 11196–11205. doi:10.1002/anie.201914276.

[74] M. d'Ischia, A. Napolitano, A. Pezzella, 5,6-Dihydroxyindole Chemistry: Unexplored Opportunities Beyond Eumelanin, European Journal of Organic Chemistry. 2011 (2011) 5501–5516. doi:10.1002/ejoc.201100796.

[75] C.-T. Chen, F.J. Martin-Martinez, G.S. Jung, M.J. Buehler, Polydopamine and eumelanin molecular structures investigated with ab initio calculations, Chemical Science. 8 (2017) 1631–1641. doi:10.1039/C6SC04692D.

[76] M. Sugumaran, Reactivities of quinone methides versus o-Quinones in catecholamine metabolism and eumelanin biosynthesis, International Journal of Molecular Sciences. 17 (2016) 1–23. doi:10.3390/ijms17091576.

[77] M.L. Alfieri, R. Micillo, L. Panzella, O. Crescenzi, S.L. Oscurato, P. Maddalena, A. Napolitano, V. Ball, M. D'Ischia, Structural Basis of Polydopamine Film Formation: Probing 5,6-Dihydroxyindole-Based Eumelanin Type Units and the Porphyrin Issue, ACS Applied Materials & Interfaces. 10 (2018) 7670–7680. doi:10.1021/acsami.7b09662.

[78] Q. Lyu, N. Hsueh, C.L.L. Chai, Direct Evidence for the Critical Role of 5,6-Dihydroxyindole in Polydopamine Deposition and Aggregation, Langmuir. 35 (2019) 5191–5201. doi:10.1021/acs.langmuir.9b00392.

[79] S. Hong, Y.S. Na, S. Choi, I.T. Song, W.Y. Kim, H. Lee, Non-Covalent Self-Assembly and Covalent Polymerization Co-Contribute to Polydopamine Formation, Advanced Functional Materials. 22 (2012) 4711–4717. doi:10.1002/adfm.201201156.

[80] J. Liebscher, R. Mrówczyński, H.A. Scheidt, C. Filip, N.D. Haìdade, R. Turcu, A. Bende, S. Beck, Structure of polydopamine: A never-ending story?, Langmuir. 29 (2013) 10539–10548. doi:10.1021/la4020288.

[81] Q. Lyu, N. Hsueh, C.L.L. Chai, Unravelling the polydopamine mystery: Is the end in sight?, Polymer Chemistry. 10 (2019) 5771–5777. doi:10.1039/c9py01372e.

[82] Y. Ding, L.-T. Weng, M. Yang, Z. Yang, X. Lu, N. Huang, Y. Leng, Insights into the Aggregation/Deposition and Structure of a Polydopamine Film, Langmuir. 30 (2014) 12258–12269. doi:10.1021/la5026608.

[83] N.F. Della Vecchia, R. Avolio, M. Alfè, M.E. Errico, A. Napolitano, M. D'Ischia, Building-block diversity in polydopamine underpins a multifunctional eumelanin-type platform tunable through a quinone control point, Advanced Functional Materials. 23 (2013) 1331–1340. doi:10.1002/adfm.201202127.

[84] F. Ponzio, J. Barthès, J. Bour, M. Michel, P. Bertani, J. Hemmerlé, M. D'Ischia, V. Ball, Oxidant Control of Polydopamine Surface Chemistry in Acids: A Mechanism-Based Entry to Superhydrophilic-Superoleophobic Coatings, Chemistry of Materials. 28 (2016) 4697–4705. doi:10.1021/acs.chemmater.6b01587.

[85] T.G. Barclay, H.M. Hegab, S.R. Clarke, M. Ginic-Markovic, M. Ginic-Markovic, Versatile Surface Modification Using Polydopamine and Related Polycatecholamines: Chemistry, Structure, and Applications, Advanced Materials Interfaces. 4 (2017) 1601192. doi:10.1002/admi.201601192.

[86] P. Delparastan, K.G. Malollari, H. Lee, P.B. Messersmith, Direct Evidence for the Polymeric Nature of Polydopamine, Angewandte Chemie International Edition. 58 (2019) 1077–1082. doi:10.1002/anie.201811763.

[87] H. Wei, J. Ren, B. Han, L. Xu, L. Han, L. Jia, Stability of polydopamine and poly(DOPA) melanin-like films on the surface of polymer membranes under strongly acidic and alkaline conditions, Colloids and Surfaces B: Biointerfaces. 110 (2013) 22–28. doi:10.1016/j.colsurfb.2013.04.008.

[88] J. Kuang, J.L. Guo, P.B. Messersmith, High ionic strength formation of DOPA-melanin coating for loading and release of cationic antimicrobial compounds, Advanced Materials Interfaces. 1 (2014) 1400145. doi:10.1002/admi.201400145.

[89] S. Hong, J. Kim, Y.S. Na, J. Park, S. Kim, K. Singha, G. Il Im, D.K. Han, W.J. Kim, H. Lee, Poly(norepinephrine): Ultrasmooth material-independent surface chemistry and nanodepot for nitric oxide, Angewandte Chemie - International Edition. 52 (2013) 9187–9191. doi:10.1002/anie.201301646.

[90] S.M. Kang, J. Rho, I.S. Choi, P.B. Messersmith, H. Lee, Norepinephrine: material-independent, multifunctional surface modification reagent, Journal of the American Chemical Society. 131 (2009) 13224–13225. doi:10.1021/ja905183k.

[91] V. Baldoneschi, P. Palladino, S. Scarano, M. Minunni, Polynorepinephrine: state-of-the-art and perspective applications in biosensing and molecular recognition, Analytical and Bioanalytical Chemistry. 412 (2020) 5945–5954. doi:10.1007/s00216-020-02578-9.

[92] P. Palladino, F. Bettazzi, S. Scarano, Polydopamine: surface coating, molecular imprinting, and electrochemistry—successful applications and future perspectives in (bio)analysis, Analytical and Bioanalytical Chemistry. 411 (2019) 4327–4338. doi:10.1007/s00216-019-01665-w.

[93] M. Park, M. Shin, E. Kim, S. Lee, K.I. Park, H. Lee, J.-H. Jang, The Promotion of Human Neural Stem Cells Adhesion Using Bioinspired Poly(norepinephrine) Nanoscale Coating, Journal of Nanomaterials. 2014 (2014) 1–10. doi:10.1155/2014/793052.

[94] H.-C. Yang, Q.-Y. Wu, L.-S. Wan, Z.-K. Xu, Polydopamine gradients by oxygen diffusion controlled autoxidation, Chemical Communications. 49 (2013) 10522. doi:10.1039/c3cc46127k.

[95] V. Ball, D. Del Frari, V. Toniazzo, D. Ruch, Kinetics of polydopamine film deposition as a function of pH and dopamine concentration: Insights in the polydopamine deposition mechanism, Journal of Colloid and Interface Science. 386 (2012) 366–372. doi:10.1016/j.jcis.2012.07.030.

[96] S. Kasemset, L. Wang, Z. He, D.J. Miller, A. Kirschner, B.D. Freeman, M.M. Sharma, Influence of polydopamine deposition conditions on hydraulic permeability, sieving coefficients, pore size and pore size distribution for a polysulfone ultrafiltration membrane, Journal of Membrane Science. 522 (2017) 100–115. doi:10.1016/j.memsci.2016.07.016.

[97] P. Zhou, Y. Deng, B. Lyu, R. Zhang, H. Zhang, H. Ma, Y. Lyu, S. Wei, Rapidly-deposited polydopamine coating via high temperature and vigorous stirring: formation, characterization and biofunctional evaluation, PLOS ONE. 9 (2014) e113087. doi:10.1371/journal.pone.0113087.

[98] H.W. Kim, B.D. McCloskey, T.H. Choi, C. Lee, M.-J. Kim, B.D. Freeman, H.B. Park, Oxygen concentration control of dopamine-induced high uniformity surface coating chemistry, ACS Applied Materials & Interfaces. 5 (2013) 233–238. doi:10.1021/am302439g.

[99] J.Y. Kim, W. Il Kim, W. Youn, J. Seo, B.J. Kim, J.K. Lee, I.S. Choi, Enzymatic film formation of nature-derived phenolic amines, Nanoscale. 10 (2018) 13351–13355. doi:10.1039/c8nr04312d.

[100] M.L. Alfieri, L. Panzella, Y. Arntz, A. Napolitano, V. Ball, M. D'ischia, A clean and tunable mussel-inspired coating technology by enzymatic deposition of pseudo-polydopamine (ψ-pda) thin films from tyramine, International Journal of Molecular Sciences. 21 (2020) 1–14. doi:10.3390/ijms21144873.

[101] F. Bernsmann, V. Ball, F. Addiego, A. Ponche, M. Michel, J.J.D.A. Gracio, V. Toniazzo, D. Ruch, Dopamine-melanin film deposition depends on the used oxidant and buffer solution, Langmuir. 27 (2011) 2819–2825. doi:10.1021/la104981s.

[102] S. El Yakhlifi, M.-L. Alfieri, Y. Arntz, M. Eredia, A. Ciesielski, P. Samorì, M. D'Ischia, V. Ball, Oxidant-dependent antioxidant activity of polydopamine films: The chemistry-morphology interplay, Colloids and Surfaces A: Physicochemical and Engineering Aspects. 614 (2021) 126134. doi:10.1016/j.colsurfa.2021.126134.

[103] M. Lee, S.-H. Lee, I.-K. Oh, H. Lee, Microwave-accelerated rapid, chemical oxidant-free, material-independent surface chemistry of poly(dopamine), Small. 13 (2017) 1600443. doi:10.1002/smll.201600443.

[104] Z. Wang, C. Xu, Y. Lu, G. Wei, G. Ye, T. Sun, J. Chen, Microplasma-assisted rapid, chemical oxidant-free and controllable polymerization of dopamine for surface modification, Polymer Chemistry. 8 (2017) 4388–4392. doi:10.1039/c7py00805h.

[105] H. Coskun, A. Aljabour, L. Uiberlacker, M. Strobel, S. Hild, C. Cobet, D. Farka, P. Stadler, N.S. Sariciftci, Chemical vapor deposition - based synthesis of conductive polydopamine thin-films, Thin Solid Films. 645 (2018) 320–325. doi:10.1016/j.tsf.2017.10.063.

[106] S.H. Hong, S. Hong, M.-H. Ryou, J.W. Choi, S.M. Kang, H. Lee, Sprayable ultrafast polydopamine surface modifications, Advanced Materials Interfaces. 3 (2016) 1500857. doi:10.1002/admi.201500857.

[107] Y. Li, M. Liu, C. Xiang, Q. Xie, S. Yao, Electrochemical quartz crystal microbalance study on growth and property of the polymer deposit at gold electrodes during oxidation of dopamine in aqueous solutions, Thin Solid Films. 497 (2006) 270–278. doi:10.1016/j.tsf.2005.10.048.

[108] F. Bernsmann, J.C. Voegel, V. Ball, Different synthesis methods allow to tune the permeability and permselectivity of dopamine-melanin films to electrochemical probes, Electrochimica Acta. 56 (2011) 3914–3919. doi:10.1016/j.electacta.2011.02.028.

[109] J.L. Wang, B.C. Li, Z.J. Li, K.F. Ren, L.J. Jin, S.M. Zhang, H. Chang, Y.X. Sun, J. Ji, Electropolymerization of dopamine for surface modification of complex-shaped cardiovascular stents, Biomaterials. 35 (2014) 7679–7689. doi:10.1016/j.biomaterials.2014.05.047.

[110] M. Amiri, E. Amali, A. Nematollahzadeh, Poly-dopamine thin film for voltammetric sensing of atenolol, Sensors and Actuators, B: Chemical. 216 (2015) 551–557. doi:10.1016/j.snb.2015.04.082.

[111] S. Patai, Z. Rappoport, The Chemistry of the Quinonoid Compounds, Vol. I, John Wiley & Sons, Ltd., Chichester, UK, 1974. doi:10.1002/9780470771303.

[112] S. Patai, Z. Rappoport, The Chemistry of the Quinonoid Compounds, Vol. II, John Wiley & Sons, Inc., Chichester, UK, 1988. doi:10.1002/9780470772119.

[113] R.P. Bacil, L. Chen, S.H.P. Serrano, R.G. Compton, Dopamine oxidation at gold electrodes: mechanism and kinetics near neutral pH, Physical Chemistry Chemical Physics. 22 (2020) 607–614. doi:10.1039/C9CP05527D.

[114] M.R. Deakin, P.M. Kovach, K.J. Stutts, R.M. Wightman, Heterogeneous Mechanisms of the Oxidation of Catechols and Ascorbic Acid at Carbon Electrodes, Analytical Chemistry. 58 (1986) 1474–1480. doi:10.1021/ac00298a046.

[115] N.M. Contento, P.W. Bohn, Tunable electrochemical pH modulation in a microchannel monitored via the proton-coupled electro-oxidation of hydroquinone, Biomicrofluidics. 8 (2014). doi:10.1063/1.4894275.

[116] M. Sterby, R. Emanuelsson, F. Mamedov, M. Strømme, M. Sjödin, Investigating electron transport in a PEDOT/Quinone conducting redox polymer with in situ methods, Electrochimica Acta. 308 (2019) 277–284. doi:10.1016/j.electacta.2019.03.207.

[117] E. Laviron, Electrochemical reactions with protonations at equilibrium, Journal of Electroanalytical Chemistry and Interfacial Electrochemistry. 164 (1984) 213–227. doi:10.1016/S0022-0728(84)80207-7.

[118] C. Lin, L. Chen, E.E.L. Tanner, R.G. Compton, Electroanalytical study of dopamine oxidation on carbon electrodes: from the macro- to the micro-scale, Physical Chemistry Chemical Physics. 20 (2018) 148–157. doi:10.1039/C7CP07450F.

[119] H.W. Richter, W.H. Waddell, Mechanism of the oxidation of dopamine by the hydroxyl radical in aqueous solution, Journal of the American Chemical Society. 105 (1983) 5434–5440. doi:10.1021/ja00354a041.

[120] A.N. Pham, T.D. Waite, Cu(II)-catalyzed oxidation of dopamine in aqueous solutions: Mechanism and kinetics, Journal of Inorganic Biochemistry. 137 (2014) 74–84. doi:10.1016/j.jinorgbio.2014.03.018.

[121] M.T.I.W. Schüsler-Van Hees, G.M.J.B. Van Henegouwen, M.F.J. Driever, Ionization constants of catechols and catecholamines, Pharmaceutisch Weekblad Scientific Edition. 5 (1983) 102–108. doi:10.1007/BF01960985.

[122] S. Corona-Avendaño, G. Alarcón-Angeles, G.A. Rosquete-Pina, A. Rojas-Hernández, A. Gutierrez, M.T. Ramírez-Silva, M. Romero-Romo, M. Palomar-Pardavé, New Insights on the Nature of the Chemical Species Involved during the Process of Dopamine Deprotonation in Aqueous Solution: Theoretical and Experimental Study, The Journal of Physical Chemistry B. 111 (2007) 1640–1647. doi:10.1021/jp0637227.

[123] M. Salomäki, L. Marttila, H. Kivelä, T. Ouvinen, J. Lukkari, Effects of pH and oxidants on the first steps of polydopamine formation: a thermodynamic approach, The Journal of Physical Chemistry B. 122 (2018) 6314–6327. doi:10.1021/acs.jpcb.8b02304.

[124] D.H. Evans, K. Hu, Inverted potentials in two-electron processes in organic electrochemistry, Journal of the Chemical Society, Faraday Transactions. 92 (1996) 3983. doi:10.1039/ft9969203983.

[125] C. Batchelor-McAuley, R.G. Compton, Voltammetry of multi-electron electrode processes of organic species, Journal of Electroanalytical Chemistry. 669 (2012) 73–81. doi:10.1016/j.jelechem.2012.01.016.

[126] Q. Lin, Q. Li, C. Batchelor-McAuley, R.G. Compton, Two-Electron, Two-Proton Oxidation of Catechol: Kinetics and Apparent Catalysis, The Journal of Physical Chemistry C. 119 (2015) 1489–1495. doi:10.1021/jp511414b.

[127] M.D. Hawley, S. V. Tatawawadi, S. Piekarski, R.N. Adams, Electrochemical Studies of the Oxidation Pathways of Catecholamines, Journal of the American Chemical Society. 89 (1967) 447–450. doi:10.1021/ja00978a051.

[128] C.G. Chavdarian, D. Karashima, N. Castagnoli, H.K. Hundley, Oxidative and Cardiovascular Studies on Natural and Synthetic Catecholamines, Journal of Medicinal Chemistry. 21 (1978) 548–554. doi:10.1021/jm00204a009.

[129] T.E. Young, B.W. Babbitt, Electrochemical Study of the Oxidation of α-Methyldopamine, α-Methylnoradrenaline, and Dopamine, Journal of Organic Chemistry. 48 (1983) 562–566. doi:10.1021/jo00152a029.

[130] J. Yang, L. Niu, Z. Zhang, J. Zhao, L. Chou, Electrochemical Behavior of a Polydopamine Nanofilm, Analytical Letters. 48 (2015) 2031–2039. doi:10.1080/00032719.2015.1010120.

[131] R. Luo, L. Tang, J. Wang, Y. Zhao, Q. Tu, Y. Weng, R. Shen, N. Huang, Improved immobilization of biomolecules to quinone-rich polydopamine for efficient surface functionalization, Colloids and Surfaces B: Biointerfaces. 106 (2013) 66–73. doi:10.1016/j.colsurfb.2013.01.033.

[132] M.E. Lynge, R. van der Westen, A. Postma, B. Städler, Polydopamine—a nature-inspired polymer coating for biomedical science, Nanoscale. 3 (2011) 4916–4928. doi:10.1039/c1nr10969c.

[133] F.S. Felix, L. Angnes, Electrochemical immunosensors – A powerful tool for analytical applications, Biosensors and Bioelectronics. 102 (2018) 470–478. doi:10.1016/j.bios.2017.11.029.

[134] X. Zhang, H. Ju, J. Wang, Electrochemical Sensors, Biosensors and their Biomedical Applications, 1st ed., Elsevier, 2008. doi:10.1016/B978-0-12-373738-0.X5001-6.

[135] J. Davis, D. Huw Vaughan, M.F. Cardosi, Elements of biosensor construction, Enzyme and Microbial Technology. 17 (1995) 1030–1035. doi:10.1016/0141-0229(95)00013-5.

[136] M.P. Marco, D. Barceló, Environmental applications of analytical biosensors, Measurement Science and Technology. 7 (1996) 1547–1562. doi:10.1088/0957-0233/7/11/002.

[137] R.F. Taylor, J.S. Schultz, Handbook of Chemical and Biological Sensors, CRC Press, 1996. doi:10.1201/9780367802516.

[138] C. Adley, Past, Present and Future of Sensors in Food Production, Foods. 3 (2014) 491–510. doi:10.3390/foods3030491.

[139] J.D. Newman, A.P.F. Turner, Home blood glucose biosensors: A commercial perspective, Biosensors and Bioelectronics. 20 (2005) 2435–2453. doi:10.1016/j.bios.2004.11.012.

[140] E.H. Yoo, S.Y. Lee, Glucose biosensors: An overview of use in clinical practice, Sensors. 10 (2010) 4558–4576. doi:10.3390/s100504558.

[141] M.H. Hassan, C. Vyas, B. Grieve, P. Bartolo, Recent Advances in Enzymatic and Non-Enzymatic Electrochemical Glucose Sensing, Sensors. 21 (2021) 4672. doi:10.3390/s21144672.

[142] J. Kim, A.S. Campbell, B.E.F. de Ávila, J. Wang, Wearable biosensors for healthcare monitoring, Nature Biotechnology. 37 (2019) 389–406. doi:10.1038/s41587-019-0045-y.

[143] P.O. Saboe, E. Conte, M. Farell, G.C. Bazan, M. Kumar, Biomimetic and bioinspired approaches for wiring enzymes to electrode interfaces, Energy Environ. Sci. 10 (2017) 14–42. doi:10.1039/C6EE02801B.

[144] M. Hussain, J. Wackerlig, P.A. Lieberzeit, Biomimetic strategies for sensing biological species, Biosensors. 3 (2013) 89–107. doi:10.3390/bios3010089.

[145] S. V. Rao, K.W. Anderson, L.G. Bachas, Oriented Immobilization of Proteins, Mikrochimica Acta. 128 (1998) 127–143. doi:10.1007/bf01243043.

[146] X. Pei, B. Zhang, J. Tang, B. Liu, W. Lai, D. Tang, Sandwich-type immunosensors and immunoassays exploiting nanostructure labels: A review, Analytica Chimica Acta. 758 (2013) 1–18. doi:10.1016/j.aca.2012.10.060.

[147] B. Lu, M.R. Smyth, R. O'Kennedy, Oriented immobilization of antibodies and its applications in immunoassays and immunosensors, The Analyst. 121 (1996) 29R. doi:10.1039/an996210029r.

[148] R.M. Lequin, Enzyme Immunoassay (EIA)/Enzyme-Linked Immunosorbent Assay (ELISA), Clinical Chemistry. 51 (2005) 2415–2418. doi:10.1373/clinchem.2005.051532.

[149] K. Shah, P. Maghsoudlou, Enzyme-linked immunosorbent assay (ELISA): The basics, British Journal of Hospital Medicine. 77 (2016) C98–C101. doi:10.12968/hmed.2016.77.7.C98.

[150] S. Hosseini, P. Vázquez-Villegas, M. Rito-Palomares, S.O. Martinez-Chapa, Advantages, Disadvantages and Modifications of Conventional ELISA, in: SpringerBriefs in Applied Sciences and Technology, 2018: pp. 67–115. doi:10.1007/978-981-10-6766-2_5.

[151] S. Sakamoto, W. Putalun, S. Vimolmangkang, W. Phoolcharoen, Y. Shoyama, H. Tanaka, S. Morimoto, Enzyme-linked immunosorbent assay for the quantitative/qualitative analysis of plant secondary metabolites, Journal of Natural Medicines. 72 (2018) 32–42. doi:10.1007/s11418-017-1144-z.

[152] E. Gizeli, C.R. Lowe, Immunosensors, Current Opinion in Biotechnology. 7 (1996) 66–71. doi:10.1016/S0958-1669(96)80097-8.

[153] S. Alegret, A. Merkoci, Comprehensive Analytical Chemistry: Electrochemical Sensor Analysis, Elsevier, Netherlands, 2007.

[154] M.M. Rodríguez-Delgado, G.S. Alemán-Nava, J.M. Rodríguez-Delgado, G. Dieck-Assad, S.O. Martínez-Chapa, D. Barceló, R. Parra, Laccase-based biosensors for detection of phenolic compounds, TrAC - Trends in Analytical Chemistry. 74 (2015) 21–45. doi:10.1016/j.trac.2015.05.008.

[155] A. Soto-Vaca, A. Gutierrez, J.N. Losso, Z. Xu, J.W. Finley, Evolution of phenolic compounds from color and flavor problems to health benefits, Journal of Agricultural and Food Chemistry. 60 (2012) 6658–6677. doi:10.1021/jf300861c.

[156] A. Escarpa, M.C. Gonzalez, An overview of analytical chemistry of phenolic compounds in foods, Critical Reviews in Analytical Chemistry. 31 (2001) 57–139. doi:10.1080/20014091076695.

[157] J.S. Jensen, S. Demiray, M. Egebo, A.S. Meyer, Prediction of wine color attributes from the phenolic profiles of red grapes (*Vitis vinifera*), Journal of Agricultural and Food Chemistry. 56 (2008) 1105–1115. doi:10.1021/jf072541e.

[158] F. Paiva-Martins, R. Correia, S. Félix, P. Ferreira, M.H. Gordon, Effects of enrichment of refined olive oil with phenolic compounds from olive leaves, Journal of Agricultural and Food Chemistry. 55 (2007) 4139–4143. doi:10.1021/jf063093y.

[159] P. Ambigaipalan, A.C. De Camargo, F. Shahidi, Phenolic Compounds of Pomegranate Byproducts (Outer Skin, Mesocarp, Divider Membrane) and Their Antioxidant Activities, Journal of Agricultural and Food Chemistry. 64 (2016) 6584–6604. doi:10.1021/acs.jafc.6b02950.

[160] M. Sanz, E. Cadahía, E. Esteruelas, Á.M. Muñoz, B. Fernández De Simón, T. Hernández, I. Estrella, Phenolic compounds in chestnut (Castanea sativa Mill.) heartwood. Effect of toasting at cooperage, Journal of Agricultural and Food Chemistry. 58 (2010) 9631–9640. doi:10.1021/jf102718t.

[161] W. Zheng, S.Y. Wang, Antioxidant Activity and Phenolic Compounds in Selected Herbs, J. Agric. Food Chem. 49 (2001) 5165–5170. doi:10.1021/jf010697n.

[162] T.D. Cuong, T.M. Hung, J.C. Kim, E.H. Kim, M.H. Woo, J.S. Choi, J.H. Lee, B.S. Min, Phenolic compounds from caesalpinia sappan heartwood and their anti-inflammatory activity, Journal of Natural Products. 75 (2012) 2069–2075. doi:10.1021/np3003673.

[163] Q.F. Hu, B. Zhou, J.M. Huang, X.M. Gao, L.D. Shu, G.Y. Yang, C.T. Che, Antiviral phenolic compounds from Arundina gramnifolia, Journal of Natural Products. 76 (2013) 292–296. doi:10.1021/np300727f.

[164] V. Kuete, A.T. Mbaveng, E.C.N. Nono, C.C. Simo, M. Zeino, A.E. Nkengfack, T. Efferth, Cytotoxicity of seven naturally occurring phenolic compounds towards multi-factorial drug-resistant cancer cells, Phytomedicine. 23 (2016) 856–863. doi:10.1016/j.phymed.2016.04.007.

[165] M. Montaño, A.C. Gutleb, A.J. Murk, Persistent toxic burdens of halogenated phenolic compounds in humans and wildlife, Environmental Science and Technology. 47 (2013) 6071–6081. doi:10.1021/es400478k.

[166] R.S. Freire, N. Duran, L.T. Kubota, Development of a laccase-based flow injection electrochemical biosensor for the determination of phenolic compounds and its application for monitoring remediation of Kraft E1 paper mill effluent, Analytica Chimica Acta. 463 (2002) 229–238. doi:10.1016/S0003-2670(02)00417-8.

[167] P. Baldrian, Fungal laccases-occurrence and properties, FEMS Microbiology Reviews. 30 (2006) 215–242. doi:10.1111/j.1574-4976.2005.00010.x.

[168] J. Ihssen, R. Reiss, R. Luchsinger, L. Thöny-Meyer, M. Richter, Biochemical properties and yields of diverse bacterial laccase-like multicopper oxidases expressed in Escherichia coli, Scientific Reports. 5 (2015) 1–13. doi:10.1038/srep10465.

[169] S. Brander, J.D. Mikkelsen, K.P. Kepp, Characterization of an alkali- and halide-resistant laccase expressed in E. coli: CotA from Bacillus clausii, PLoS ONE. 9 (2014). doi:10.1371/journal.pone.0099402.

[170] L. Pourcel, J.M. Routaboul, V. Cheynier, L. Lepiniec, I. Debeaujon, Flavonoid oxidation in plants: from biochemical properties to physiological functions, Trends in Plant Science. 12 (2007) 29–36. doi:10.1016/j.tplants.2006.11.006.

[171] A. Jarosz-Wilkołazka, T. Ruzgas, L. Gorton, Amperometric detection of mono- and diphenols at Cerrena unicolor laccase-modified graphite electrode: Correlation between sensitivity and substrate structure, Talanta. 66 (2005) 1219–1224. doi:10.1016/j.talanta.2005.01.026.

[172] M. Di Fusco, C. Tortolini, D. Deriu, F. Mazzei, Laccase-based biosensor for the determination of polyphenol index in wine, Talanta. 81 (2010) 235–240. doi:10.1016/j.talanta.2009.11.063.

[173] Y. Zhang, Z. Lv, J. Zhou, F. Xin, J. Ma, H. Wu, Y. Fang, M. Jiang, W. Dong, Application of eukaryotic and prokaryotic laccases in biosensor and biofuel cells: recent advances and electrochemical aspects, Applied Microbiology and Biotechnology. 102 (2018) 10409–10423. doi:10.1007/s00253-018-9421-7.

[174] P.S. Chauhan, B. Goradia, A. Saxena, Bacterial laccase: recent update on production, properties and industrial applications, 3 Biotech. 7 (2017) 1–20. doi:10.1007/s13205-017-0955-7.

[175] J. Wang, Electrochemical Glucose Biosensors, Chemical Reviews. 108 (2008) 814–825. doi:10.1021/cr068123a.

[176] C. Tan, E.M. Robbins, B. Wu, X.T. Cui, Recent advances in in vivo neurochemical monitoring, Micromachines. 12 (2021). doi:10.3390/mi12020208.

[177] H. Musarurwa, N. Tawanda Tavengwa, Extraction and electrochemical sensing of pesticides in food and environmental samples by use of polydopamine-based materials, Chemosphere. 266 (2021) 129222. doi:10.1016/j.chemosphere.2020.129222.

[178] J.F. Rocha, L.H. Hasimoto, M. Santhiago, Recent progress and future perspectives of polydopamine nanofilms toward functional electrochemical sensors, Analytical and Bioanalytical Chemistry. 415 (2023) 3799–3816. doi:10.1007/s00216-023-04522-z.

[179] P. Salazar, M. Martín, J.L. González-Mora, Polydopamine-modified surfaces in biosensor applications, Polymer Science: Research Advances, Pratical Applications and Educational Aspects. 1 (2007) 385–396.

[180] Y. Tan, W. Deng, Y. Li, Z. Huang, Y. Meng, Q. Xie, M. Ma, S. Yao, Polymeric bionanocomposite cast thin films with in situ laccase-catalyzed polymerization of dopamine for biosensing and biofuel cell applications, Journal of Physical Chemistry B. 114 (2010) 5016–5024. doi:10.1021/jp100922t.

[181] Y. Li, C. Qin, C. Chen, Y. Fu, M. Ma, Q. Xie, Highly sensitive phenolic biosensor based on magnetic polydopamine-laccase- Fe 3O 4 bionanocomposite, Sensors and Actuators, B: Chemical. 168 (2012) 46–53. doi:10.1016/j.snb.2012.01.013.

[182] C. Ruan, W. Shi, H. Jiang, Y. Sun, X. Liu, X. Zhang, Z. Sun, L. Dai, D. Ge, One-pot preparation of glucose biosensor based on polydopamine-graphene composite film modified enzyme electrode, Sensors and Actuators, B: Chemical. 177 (2013) 826–832. doi:10.1016/j.snb.2012.12.010.

[183] C. Chen, Q. Xie, D. Yang, H. Xiao, Y. Fu, Y. Tan, S. Yao, Recent advances in electrochemical glucose biosensors: A review, RSC Advances. 3 (2013) 4473–4491. doi:10.1039/c2ra22351a.

[184] Y. Wei, N. Zhang, Y. Li, G. Shi, L. Jin, Glucose Biosensor Based on the Fabrication of Glucose Oxidase in the Bio-Inspired Polydopamine-Gold Nanoparticle Composite Film, Chinese Journal of Chemistry. 28 (2010) 2489–2493. doi:10.1002/cjoc.201190027.

[185] R. Ahmad, O.S. Wolfbeis, Y.-B. Hahn, H.N. Alshareef, L. Torsi, K.N. Salama, Deposition of nanomaterials: A crucial step in biosensor fabrication, Materials Today Communications. 17 (2018) 289–321. doi:10.1016/j.mtcomm.2018.09.024.

[186] Y. Fu, P. Li, Q. Xie, X. Xu, L. Lei, C. Chen, C. Zou, W. Deng, S. Yao, One-pot preparation of polymer-enzyme-metallic nanoparticle composite films for high-performance biosensing of glucose and galactose, Advanced Functional Materials. 19 (2009) 1784–1791. doi:10.1002/adfm.200801576.

[187] Y. Fu, P. Li, L. Bu, T. Wang, Q. Xie, X. Xu, L. Lei, C. Zou, S. Yao, Chemical/Biochemical Preparation of New Polymeric Bionanocomposites with Enzyme Labels Immobilized at High Load and Activity for High-Performance Electrochemical Immunoassay, The Journal of Physical Chemistry C. 114 (2010) 1472–1480. doi:10.1021/jp9092767.

[188] G. Wang, H. Huang, G. Zhang, X. Zhang, B. Fang, L. Wang, Dual Amplification Strategy for the Fabrication of Highly Sensitive Interleukin-6 Amperometric Immunosensor Based on Poly-Dopamine, Langmuir. 27 (2011) 1224–1231. doi:10.1021/la1033433.

[189] Y. Fu, P. Li, T. Wang, L. Bu, Q. Xie, X. Xu, L. Lei, C. Zou, J. Chen, S. Yao, Novel polymeric bionanocomposites with catalytic Pt nanoparticles label immobilized for high performance amperometric immunoassay, Biosensors and Bioelectronics. 25 (2010) 1699–1704. doi:10.1016/j.bios.2009.12.010.

[190] Y. He, J. Sun, X. Wang, L. Wang, Detection of human leptin in serum using chemiluminescence immunosensor: Signal amplification by hemin/G-quadruplex DNAzymes and protein carriers by Fe_3O_4/polydopamine/Au nanocomposites, Sensors and Actuators B: Chemical. 221 (2015) 792–798. doi:10.1016/j.snb.2015.07.022.

[191] H. Lee, J. Rho, P.B. Messersmith, Facile conjugation of biomolecules onto surfaces via mussel adhesive protein inspired coatings, Advanced Materials. 21 (2009) 431–434. doi:10.1002/adma.200801222.

[192] L.P. Zhu, J.H. Jiang, B.K. Zhu, Y.Y. Xu, Immobilization of bovine serum albumin onto porous polyethylene membranes using strongly attached polydopamine as a spacer, Colloids and Surfaces B: Biointerfaces. 86 (2011) 111–118. doi:10.1016/j.colsurfb.2011.03.027.

[193] A.W.G. Nijhuis, J.J.J.P. van den Beucken, O.C. Boerman, J.A. Jansen, S.C.G. Leeuwenburgh, 1-Step Versus 2-Step Immobilization of Alkaline Phosphatase and Bone Morphogenetic Protein-2 onto Implant Surfaces Using Polydopamine, Tissue Engineering Part C: Methods. 19 (2013) 610–619. doi:10.1089/ten.tec.2012.0313.

[194] Y. Wan, D. Zhang, Y. Wang, P. Qi, B. Hou, Direct immobilisation of antibodies on a bioinspired architecture as a sensing platform, Biosensors and Bioelectronics. 26 (2011) 2595–2600. doi:10.1016/j.bios.2010.11.013.

[195] H.-P. Peng, Y. Hu, A.-L. Liu, W. Chen, X.-H. Lin, X.-B. Yu, Label-free electrochemical immunosensor based on multi-functional gold nanoparticles–polydopamine–thionine–graphene oxide nanocomposites film for determination of alpha-fetoprotein, Journal of Electroanalytical Chemistry. 712 (2014) 89–95. doi:10.1016/j.jelechem.2013.10.013.

[196] J. Mulinari, A. Ambrosi, Y. Feng, Z. He, X. Huang, Q. Li, M. Di Luccio, D. Hotza, J.V. Oliveira, Polydopamine-assisted one-step immobilization of lipase on α-alumina membrane for fouling control in the treatment of oily wastewater, Chemical Engineering Journal. 459 (2023) 141516. doi:10.1016/j.cej.2023.141516.

[197] M. Li, C. Deng, C. Chen, L. Peng, G. Ning, Q. Xie, S. Yao, An Amperometric Hydrogen Peroxide Biosensor Based on a Hemoglobin-Immobilized Dopamine-Oxidation Polymer/Prussian Blue/Au Electrode, Electroanalysis. 18 (2006) 2210–2217. doi:10.1002/elan.200603649.

[198] H. He, Q. Xie, S. Yao, An electrochemical quartz crystal impedance study on anti-human immunoglobulin G immobilization in the polymer grown during dopamine oxidation at an Au electrode, Journal of Colloid and Interface Science. 289 (2005) 446–454. doi:10.1016/j.jcis.2005.03.085.

[199] M. Li, C. Deng, Q. Xie, Y. Yang, S. Yao, Electrochemical quartz crystal impedance study on immobilization of glucose oxidase in a polymer grown from dopamine oxidation at an Au electrode for glucose sensing, Electrochimica Acta. 51 (2006) 5478–5486. doi:10.1016/j.electacta.2006.02.023.

[200] C. Chen, Y. Fu, C. Xiang, Q. Xie, Q. Zhang, Y. Su, L. Wang, S. Yao, Electropolymerization of preoxidized catecholamines on Prussian blue matrix to immobilize glucose oxidase for sensitive amperometric biosensing, Biosensors and Bioelectronics. 24 (2009) 2726–2729. doi:10.1016/j.bios.2008.12.016.

Chapter II

Physicochemical characterization techniques

2. Physicochemical characterization techniques

This chapter intends to briefly summarize the principles of the main electrochemical, optical, gravimetric, spectroscopic and microscopy techniques utilized throughout this work to study the interfacial phenomena, to access the physicochemical properties of materials and to evaluate the analytical performance of the prepared biosensors.

2.1. Chronoamperometry and cyclic voltammetry

To promote and study a variety of chemical reactions occurring at electrodes surface, two potential-controlled electrochemical techniques were used in this work: cyclic voltammetry and chronoamperometry. Chronoamperometry is a potentiostatic technique where the current response of the working electrode to a potential step perturbation is measured over time [1,2]. A single potential step (**Figure 2.1a**) is defined by an initial (E_i) and final (E_f) potential values, starting usually from a value at which no faradaic current occurs to a value at which anodic or cathodic currents develop. An example of the concentration profiles of an electroactive species (at E_f) is represented in **Figure 2.1b**, depicting the evolution of the concentration gradient over time as the result of its immediate depletion at the electrode surface (x = 0).

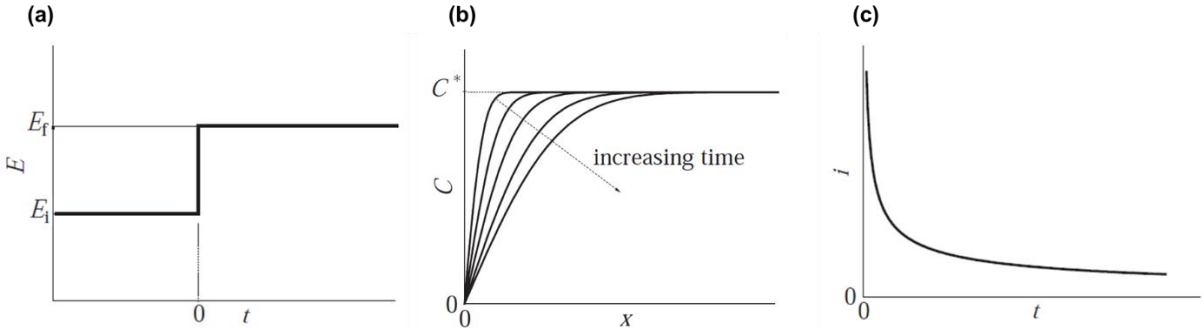

Figure 2.1: Chronoamperogrametric experiment on a planar and stationary electrode: (a) potential step; (b) concentration profiles over time; (c) current transient response – adapted from [2].

In 1903 [3], Frederick Gardner Cottrell deduced the mathematical description of the current response expected in a chronoamperometric experiment (**Equation 2.1**), considering that the mass transport is only dependent of the linear diffusion of the electroactive species, and that the electrode is both stationary and planar (convection and migration are excluded). Nowadays, this equation is simply known as Cottrell equation, and it describes current transients as the one represented in **Figure 2.1c**, from which bulk concentration values and diffusion coefficients can be derived plotting current density against $t^{-1/2}$. Chronoamperometric technique is therefore useful to study the diffusion of species towards the electrode surface,

gathering analytical information directly from analytes or indirectly using redox probes. In addition, since oxidation or reduction reactions are promoted at the electrode surface, the chronoamperometry technique is also used to promote the electrodeposition of a wide variety of coatings, namely, metals, conducting polymers and semiconductors, thus representing an important technique for electrodes modification.

$$j = \frac{nFC^* D^{1/2}}{\pi^{1/2}\, t^{1/2}} \qquad \textbf{(Equation 2.1)}$$

Where:

- j is the current density in A cm^{-2};
- n is the number of electrons involved in the electrochemical reaction;
- F is the Faraday constant (96485.3399 C mol^{-1}) [4];
- D is the diffusion coefficient of the electroactive species in $cm^2\ s^{-1}$;
- C^* is the electroactive species bulk concentration in mol cm^{-3};
- t is the time in s.

Cyclic voltammetry is a linear potential sweeping technique, where the potential applied to the working electrode varies between two fixed values at a constant scan rate (**Figure 2.2a**). Each potential cycle consists of an anodic and cathodic segment, usually corresponding to an oxidation current segment and a reduction current segment in the voltammogram (**Figure 2.2b**). Different thermodynamic, kinetic and analytical information can be extracted from voltammetric assays such as redox potentials, reversibility, kinetic limitations and even enzymatic activity.

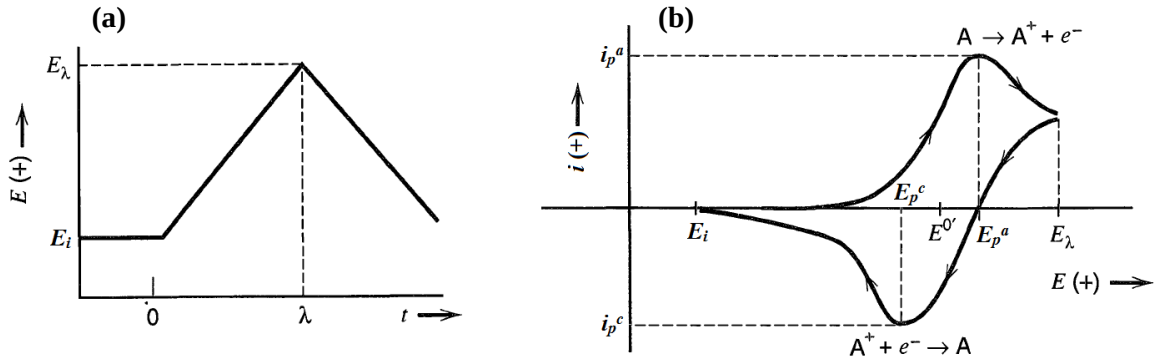

Figure 2.2: Cyclic potential sweep with scan direction inversion at λ **(a)**; typical cyclic voltammogram of a reversible electron transfer **(b)** – adapted from [5].

In the case of the reversible redox conversion $A \rightleftharpoons A^+ + e^-$, two current peaks of equal intensity are expected, corresponding to the anodic (i_p^a, oxidation) and cathodic (i_p^c, reduction) process, occurring at the respective anodic (E_p^a) and cathodic (E_p^c) peak potentials. The formal potential ($E^{0'}$), that characterizes the redox pair in thermodynamic terms, can be estimated

through the average of the two peak potentials ($E^{0'} \approx E_{1/2} = (E_p^c + E_p^a)/2$), assuming similar diffusion coefficients of the species involved in the redox process. In addition to this ideal behavior, there are also quasi-reversible and irreversible behaviors. Empirical confirmation of these behaviors is made by deviations of the $|i_p^a/i_p^c|$ ratio from unity, by a peak potential separation greater than 59/n mV, and by the dependence between peak potentials and scan rate.

The possibility of sweeping the potential at various scan rates, makes cyclic voltammetry an ease tool to assess whether an electrode reaction is diffusion controlled or charge transfer controlled. For diffusion-controlled processes, peak current density (j_p) is expected to correlate linearly with the scan rate square root ($v^{1/2}$), as predicted, for instance, by the Randles-Ševčík equation (**Equation 2.2**)[5]. For charge transfer controlled processes, peak current is expected to correlate linearly with the scan rate (v). This is the case of redox species adsorbed or in very close proximity to the electrode surface, rendering symmetric voltammetric peaks with no potential separation ($\Delta E_p = 0$). Knowing the number of electrons involved in the reaction, the surface coverage (Γ) of these species can even be estimated by the **Equation 2.3** [2]. For instance, acquiring multiple cyclic voltammograms of a modified electrode at different scan rates is one simple way to confirm the presence of attached chemical groups with redox activity, identified them by means of their redox potentials, and even estimate their surface coverage.

$$j_p = 0.4463\, C^* \left(\frac{n^3 F^3 D v}{RT}\right)^{1/2} \qquad \textbf{(Equation 2.2)}$$

$$j_p = \frac{n^2 F^2 \Gamma}{4RT} v \qquad \textbf{(Equation 2.3)}$$

Where:

- j is the current density in A cm^{-2};
- C^* is the electroactive species bulk concentration in mol cm^{-3};
- n is the number of electrons involved in the electrochemical reaction;
- F is the Faraday constant (96485.3399 C mol^{-1}) [4];
- D is the diffusion coefficient of the electroactive species in cm^2 s^{-1};
- v is the potential scan rate in V s^{-1};
- R is the gas constant (8.314 472 J K^{-1} mol^{-1}) [4];
- T is the temperature in K.
- Γ is the surface coverage in mol cm^{-2};

2.2. Electrochemical impedance spectroscopy

Traditional electrochemical experiments involve large perturbation signals, driving the electrode far from the equilibrium. Electrochemical impedance spectroscopy (EIS) is an alternative way to study an electrochemical system using an alternating perturbation signal of small amplitude to retrieve useful physicochemical properties of the system [6,7]. **Figure 2.3a** shows the linear region where typical EIS experiments are performed. In this region, a sinusoidal potential perturbation to the system will result in sinusoidal current response with the same frequency but shifted in phase (φ). The response signal can be better interpreted by the concept of impedance, that is defined as the ratio between the sinusoidal potential and current (**Equation 2.4**), thus presenting the same units as resistance (Ω). More precisely, the signals of potential and current are Fourier transformed, eliminating their time-dependency while keeping the information about their intensities, frequencies and phases. After this mathematical operation, potential and current are now complex valued and placed in the frequency domain. The impedance of an electrochemical cell is therefore a frequency-dependent function fully described by a magnitude (Z_0), that quantifies the total opposition to the current flow, and by a phase angle (φ), that may be interpreted as a balance between resistive (0º) and capacitive (90º) behaviors. Alternatively, these components of impedance can be visualized by its real (Z') and imaginary (Z'') parts, also denominated resistance and reactance, respectively.

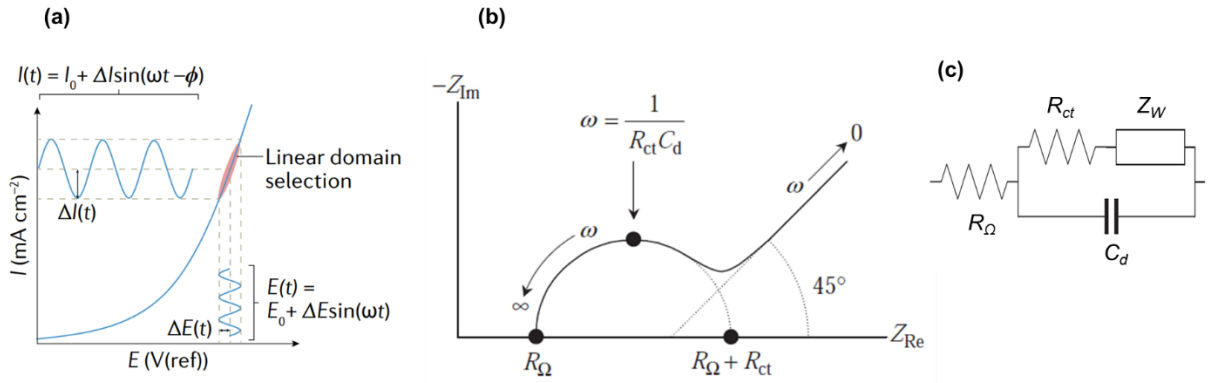

Figure 2.3: Linear domain of a ESI experiment **(a)**; Nyquist plot of the Randles circuit with highlighted key points **(b)**; Randles circuit **(c)** – adapted from [2,8]

To represent the impedance spectra obtained in a range of perturbation frequencies, two useful representations are usually employed: a Bode or a Nyquist plot. In Bode plots, the magnitude and phase shift of the impedance are visualized against the frequency values, requiring the interpretation of two curves. The Nyquist representation simplifies the

visualization of the complex impedance into the cartesian plot of the real and imaginary parts, resulting in a single curve (**Figure 2.3b**). Although the frequency dependency of impedance becomes harder to grasp in the Nyquist plot, this type of data representation is especially useful to recognize a possible equivalent circuit that better describes the electrochemical system in study [9]. The Randles circuit presented in **Figure 2.3c** is a typical equivalent circuit use to describe the electrochemical interface, comprising the ohmic resistance of the solution (R_Ω), the capacitance of the double layer (C_d), and the faradaic impedance that is further divided into the charge transfer resistance (R_{ct}) and the Warburg impedance (Z_W). In terms of physical meaning, the R_Ω value is related with the solutions conductivity and cell geometry. C_d depends on the electrolyte ionic strength and permittivity. R_{ct} describes the difficulty of the charge transfer of the redox probe and it is thus inversely proportional to the apparent exchange current (i_0) near the equilibrium potential ($R_{ct} = RT/nFi_0$). The apparent exchange current is not only a function of the redox probe concentration, but also, sensitive to features of structure and composition of the electrodes surface that may influence the apparent rate constant, for example, the presence of thin polymeric layers, their thickness, porosity, and conductivity. Distinctly from the other circuit elements, Z_W is a complex number that depends on the frequency ($\omega^{-1/2}$) and the diffusion coefficients [5,7], thus describing the mass transfer region in the Nyquist plot. It is a special case of a circuit element with a constant phase angle of 45º [10], predicting the straight line of the Nyquist plot at lower frequency values (**Figure 2.3b**). Through the complex nonlinear least squares fitting of the impedance data, the four elements of the Randles circuit are usually estimated and used to describe an electrochemical system. Although the elements of an equivalent circuit do not physically exist in the electrochemical cell, they are essential in understanding and interpreting impedance spectra. In addition, most of real systems may suffer from rough and inhomogeneous surfaces, thus the impedance spectra may be distorted from an ideal equivalent circuit. To compensate such distortions, the circuit capacitors can be substituted by a constant-phase element (CPE) that is especially useful to fit broadened semi-circles in the Nyquist plot [11,12]. Due to the mathematical definition of the CPE impedance, $Z_{CPE} = Q^{-1}(j\omega)^{-n}$, its pre-factor Q exhibits units of F cm^{-2} s^{n-1} which precludes the direct comparison with pure capacitance values. Nonetheless, using a CPE that behaves closely to a capacitance element ($0.8 < n < 1$) is a useful way to maintain the equivalent circuit simplicity and derive physical meaning from the other circuit components.

$$Z_{cell}(\omega) = \frac{\mathcal{F}\{E_{cell}(\omega t)\}}{\mathcal{F}\{I_{cell}(\omega t+\varphi)\}} = \frac{\tilde{E}(\omega)}{\tilde{I}(\omega)} = Z_0 e^{j\varphi} = Z' + jZ'' \quad \textbf{(Equation 2.4)}$$

Where:

- Z_{cell} is the complex impedance of the cell;
- E_{cell} is the sinusoidal potential of the cell;
- I_{cell} is the sinusoidal current of the cell;
- ω is the radial frequency in Hz ($2\pi f$);
- t is the time in s;
- φ is the phase angle between input and output signals;
- Z_0 is the impedance magnitude in Ω;
- Z' is the real part of the impedance in Ω;
- Z'' is the imaginary part of the impedance in Ω;
- j is the imaginary unit ($\sqrt{-1}$);

2.3. Electrochemical quartz crystal microbalance

The electrochemical quartz crystal microbalance (EQCM) is an electrogravimetric technique where the oscillating frequency of a quartz crystal is monitored during an electrochemical experiment [13,14]. The EQCM setup allows to track the deposition process of thin material layers, in real time, gathering information about the mass flux towards or against the surface of a specially designed quartz crystal electrode. The physical principle behind the microbalance functioning is the piezoelectric effect, where the electric polarization of a non-centrosymmetric crystalline material causes it to mechanically deform, or vice versa [14]. Due to this effect, a mechanical oscillation (standing wave) can be induced between two metallic electrodes placed in opposite sides of the crystal (**Figure 2.4a**). To efficiently induce an oscillating wave with a predominant displacement parallel to the surface (**Figure 2.4b**), quartz wafers obtained from an AT-cut are preferred [15]. This type of cut is specified as *ca.* 35º in relation to the optical axis of the crystal, originating crystals that, depending on their thickness, will have natural resonance frequencies between 2 and 20 MHz – a range that provides comparable sensitivity to that of some techniques used to monitor surface adsorption processes, for example, by the optical technique surface plasmon resonance. In some cases, QCM is even superior to those optical techniques since the piezoelectric mechanism can operate in opaque solutions [13].

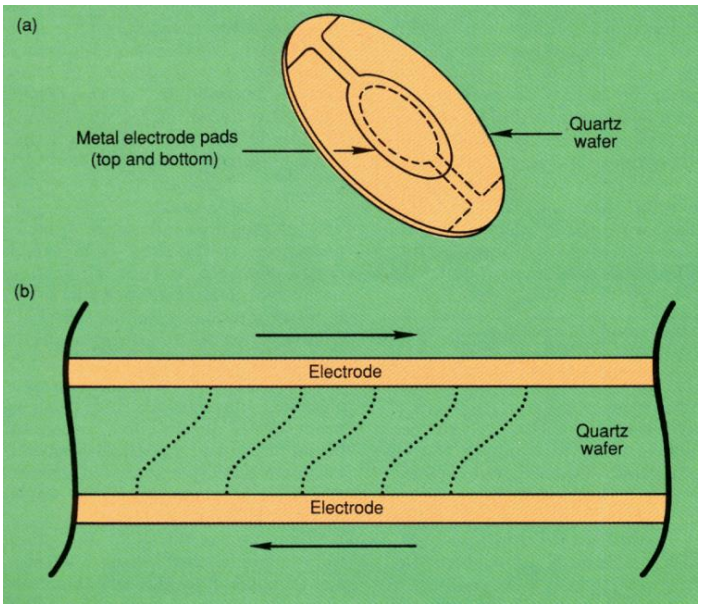

Figure 2.4: Quartz crystal sensor schematics **(a)**; shear deformation of an oscillating quartz wafer **(b)** – adapted from [15].

The oscillating frequency of the quartz crystal depends on several factors, that are usually constant throughout an experiment, namely the physical properties of the quartz material (thickness, density and shear modulus), physical properties of both adjacent media (gas or liquid density and viscosity), as well as pressure differences across the crystal and temperature. The mass of adsorbed material to the surface of the crystal is also a factor that affects the oscillating frequency and can thus be quantified by the Sauerbrey equation (**2.5**), considering all the other factors are constant. The conversion of frequency to mass variation is then a straightforward operation that depends on a sensitivity constant, usually denominated as C_f [13]. For instance, a quartz crystal with a fundamental frequency of 8 MHz would experience a damping of 0.145 Hz ng^{-1} cm^{-2}. Although the simple conversion of Sauerbrey is commonly used, this relationship is only valid when the bonded material is thin and rigid, since in this case the material will not experience any deformation during oscillation.

$$\Delta f = -\frac{2f_0^2}{A\sqrt{d_q \mu_q}}\Delta m = -C_f \Delta m \qquad \textbf{(Equation 2.5)}$$

Where:

- Δf is the variation in the oscillation frequency in Hz;
- Δm is the variation in the adsorbed mass in g;
- f_0 is fundamental resonant frequency in Hz;
- A is the piezoelectrically active area in cm^2;
- d_q is the density of quartz (2.648 g cm^{-3});
- μ_q is the shear modulus of an AT-cut quartz (2.947×10^{11} g cm^{-1} s^{-2});
- C_f is the integrated sensitivity constant in Hz g^{-1}.

2.4. Ellipsometry

At the beginning of the 20th century, knowledge of polarized light allowed for the first time the measurement of thin films on metallic surfaces by a technique called ellipsometry [16]. This technique, historically related to the electrochemical modification of surfaces, is based on the measurement of the polarization state of light reflected by a surface, thus allowing to deduce structural characteristics of a material and to estimate the thickness of thin coating layers. The way light interacts with a simple material can be described by its complex electrical permittivity ($\hat{\varepsilon}$) or by its complex refractive index ($\hat{n}$), which are mathematically related to each other by **Equation 2.6**. In the case of a transparent material ($k = 0$ and $\varepsilon'' = 0$) both complex quantities take only the real values of the dielectric constant (ε') and the real refractive index (n). While the dielectric constant is an attenuation factor of the electric field vector of light in the material relative to vacuum ($\varepsilon' = \varepsilon/\varepsilon_0$), the real refractive index (or optical density) describes the speed of light in vacuum relative to the speed in the material ($n = c/v$).

$$\hat{\varepsilon} = \hat{n}^2 \;\Leftrightarrow\; \varepsilon' - i\varepsilon'' = (n - ik)^2 \qquad \textbf{(Equation 2.6)}$$

Where:

- $\hat{\varepsilon}$ is the complex electric permittivity;
- ε' is the real electric permittivity or relative dielectric constant;
- ε'' is the imaginary permittivity;
- $\hat{n}$ is the complex refractive index;
- n is the real refractive index;
- k is the extinction coefficient;

In the case where the material is an absorber ($k \neq \varepsilon_2 \neq 0$) the two optical quantities necessarily take a real and an imaginary part, increasing the necessary effort for the mathematical treatment of the ellipsometric data. The imaginary part of the electrical permittivity is related to the energy dissipation after electromagnetic interaction with the material, while the imaginary part of the refractive index (k) is directly related to its absorptivity ($\alpha = 4\pi k/\lambda$). This interaction of light with the surface of the material will be even more complex if its structure presents a preferential electrical permittivity for one or more three-dimensional axes (anisotropy). This phenomenon can be observed by the variation of $\hat{\varepsilon}$ or $\hat{n}$ at different incidence angles and requires a more demanding mathematical treatment involving tensors. For this reason, the starting surface, also called substrate, should preferably be as close as possible to an ideally smooth, homogeneous and isotropic surface.

Defined as the orientation of the electric field over time (E), polarization is a characteristic of electromagnetic waves. When interacting with matter, the polarization state of light is disturbed [17]. Taking advantage of this interaction with the surface, an ellipsometric measurement involves the emission of a polarized beam of light, with a known wavelength, towards the sample at a fixed angle of incidence (φ_0) (**Figure 2.5**). Both components of the incident light, parallel (E_{ip}) and perpendicular (E_{is}) to the plane of incidence, are reflected, changing in intensity according to the optical properties of the surface. The reflected light, with typically elliptical polarization, is now defined by two new parallel (E_{rp}) and perpendicular (E_{rs}) components.

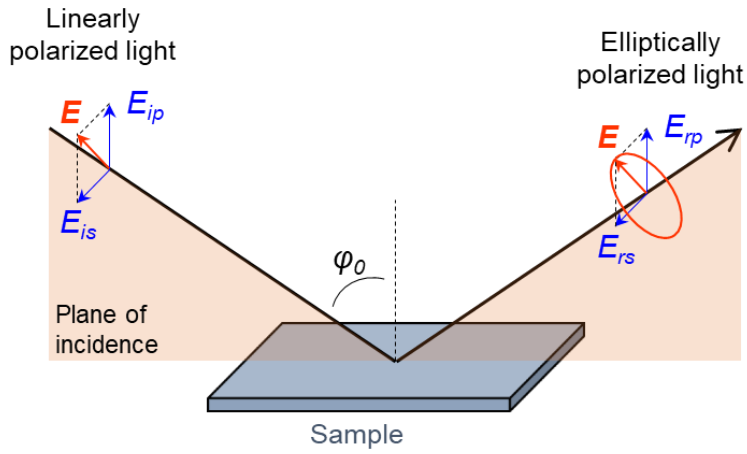

Figure 2.5: Specular reflection of polarized light in a flat surface – adapted from [16].

By the Fresnel **equations 2.7** and **2.8**, the components of incident and reflected light can then be correlated with the complex index of refraction of the material. Experimentally, the changes in the polarization state are measured by the phase difference Δ and azimuthal angle Ψ, also called ellipsometric angles, which derive from the ellipse geometry defined by the rotating electric field vector. Through the complex reflection coefficient (ρ) the experimental measurements are correlated with the optical properties of the surface by the fundamental equation of ellipsometry (**Equation 2.9**).

$$\widehat{r_p} = \frac{E_{rp}}{E_{ip}} = \frac{\hat{n}_1 cos\varphi_0 - \hat{n}_0 cos\varphi_1}{\hat{n}_1 cos\varphi_0 + \hat{n}_0 cos\varphi_1} \quad \textbf{(Equation 2.7)}$$

$$\widehat{r_s} = \frac{E_{rs}}{E_{is}} = \frac{\hat{n}_0 cos\varphi_0 - \hat{n}_1 cos\varphi_1}{\hat{n}_0 cos\varphi_0 + \hat{n}_1 cos\varphi_1} \quad \textbf{(Equation 2.8)}$$

$$\rho\,(\hat{n}_0, \hat{n}_1, \varphi_0, \lambda) = \frac{\widehat{r_p}}{\widehat{r_s}} = tan\Psi\, e^{i\Delta} \quad \textbf{(Equation 2.9)}$$

Where:

- $\widehat{r_p}$ and $\widehat{r_s}$ are the parallel (p) and perpendicular (s) complex Fresnel coefficients;
- E_{rp} and E_{rs} are the parallel (p) and perpendicular (s) components of the reflected electric field vector (r);
- E_{ip} and E_{is} are the parallel (p) and perpendicular (s) components of the incident electric field vector (r);
- $\hat{n}_0$ and $\hat{n}_1$ are the complex refractive indexes of ambient (0) and substrate (1);
- φ_0 and φ_1 are the incident (0) and refractive (1) angles; $\hat{n}_1 sen\varphi_1 = \hat{n}_0 sen\varphi_0$;
- λ is the light wavelength;
- Ψ is the azimuthal angle;
- Δ is the phase difference.

In the case of a smooth and homogeneous substrate, deriving its optical properties is a trivial calculation that uses **Equation 2.9**. The analytical solution is possible in this case because there are only two unknown variables (n_s, k_s) for two measured experimental values (Ψ, Δ). Considering more complicated interfaces, the complex reflection coefficient becomes dependent on a greater number of unknown variables than the measured ellipsometric angles Ψ and Δ, thus optical properties cannot be analytically derived. This is the case of a multi-phase model presented in **Figure 2.6**, comprising a semi-infinite ambient and substrate mediums, and a finite phase with thickness L_1. Considering that the optical properties of the ambient and substrate are known, the complex reflection coefficient will depend only on the three parameters of the finite phase (n_1, k_1, L_1) that cannot be analytically determined with a single ellipsometric measurement (that delivers only two experimental parameters). This problem can be solved either by reducing the number of unknown optical parameters through other characterization technique (for example, determining the film thickness by microscopy), or by increasing the number of measurements (multiangle or spectroscopic acquisitions) and perform a nonlinear fitting that will be discussed further in the text.

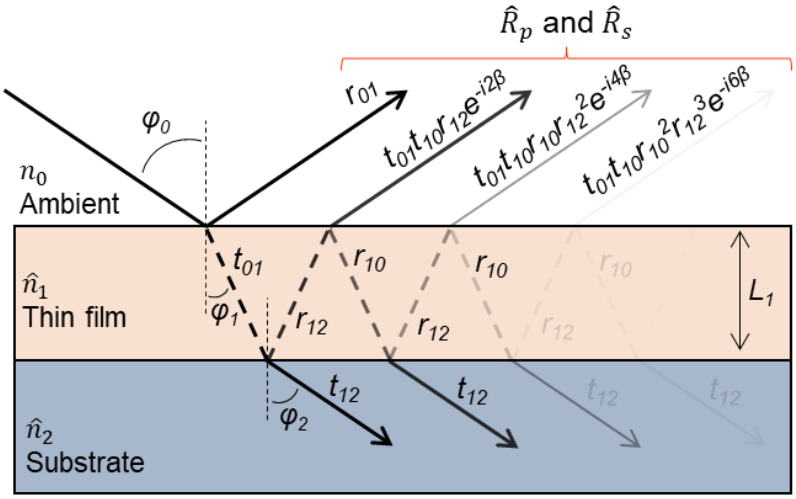

Figure 2.6: Reflection (r_{mn}) and transmission (t_{mn}) events of polarized light in a 3-phase isotropic model comprising a semi-infinite ambient medium (0), a finite thin film (1) and semi-infinite substrate (2) – adapted from [18].

As mentioned, the introduction of an isotropic layer on top of the substrate implies modifying the complex reflection coefficient (ρ) in order to take into account the various reflections and refractions that occur within the film (**Figure 2.6**). Two effective reflection coefficients ($\hat{R}$) can be mathematically deduced by the infinite sum of all light waves reflected by the thin film, one for the parallel component of light (**Equation 2.10**) and another for the perpendicular component (**Equation 2.11**). Ultimately, the overall reflection depends on the Fresnel coefficients regarding the reflection event on the upper (r_{01}) and lower (r_{12}) boundaries, and a phase factor β (**Equation 2.12**) that accounts for the film thickness (L_1). This model can be extended to a staking model of multiple finite phases by applying **Equations 2.10** and **2.11** in a recursive way [18], substituting the lower boundary Fresnel coefficients by the overall reflection coefficient $\hat{R}$ of the subsequent finite layer. Computationally, the recursive method is easier to implement and leads to faster calculations compared to other matrixial methods, such as the Abelès method and the Hayfield and White method [19].

$$\hat{R}_p = \frac{\hat{r}_{01p}+\hat{r}_{12p}e^{-i2\beta}}{1+\hat{r}_{01p}\hat{r}_{12p}e^{-i2\beta}} \quad \textbf{(Equation 2.10)}$$

$$\hat{R}_s = \frac{\hat{r}_{01s}+\hat{r}_{12s}e^{-i2\beta}}{1+\hat{r}_{01s}\hat{r}_{12s}e^{-i2\beta}} \quad \textbf{(Equation 2.11)}$$

$$\beta = \frac{2\pi L_1}{\lambda}\sqrt{\hat{n}_1^2 - n_0^2 sen^2\varphi_0} \quad \textbf{(Equation 2.12)}$$

Where:

- $\hat{R}_p$ and $\hat{R}_s$ are the complex parallel (p) and perpendicular (s) reflection coefficients.
- $\hat{r}_{mnl}$ are the complex Fresnel coefficients of interface *m,n* and orientation *l*;
- β is the phase factor;
- L_1 is the thickness of the thin film (1);
- λ, n_0, $\hat{n}_1$ and φ_0 are variables already described in **Equation 2.9**.

As mentioned before, if there is not an available analytical solution of the optical parameters of the materials, these may be attained by a nonlinear parameter estimation. To perform this mathematical procedure, one must select a figure of merit that quantifies the proximity between the experimental and theoretical data [16,19,20]. When the dispersion of the experimental data (error) is not available or is not possible to estimate, the mean squared error (MSE, **Equation 2.13**), also called the unbiased estimator, can be used as figure of merit. In this case, the residual sum of squares is only normalized by the degrees of freedom ($N - m - 1$), and the best parameters are expected to minimize MSE as much as possible, where MSE = 0 would correspond to a perfect fit. Although MSE is a good expression to look for parameters that will improve the fitting of the data, it does not quantify the quality of the fit. A more advantageous estimation of the parameters can be performed by the use of the reduced chi-square (**Equation 2.14**), that includes the experimental error. Since the residues are weighted by the experimental error, the quality of the fit can also be evaluated by the χ^2 itself: if this dimensionless quantity is close to the unit ($\chi^2 \approx 1$) then the model fits the data within the experimental error; whereas if it is too far from the unit ($\chi^2 >> 1$) then the model does not explain the data. The over-fitting of the data is also possible to identify by a χ^2 lower than the unit ($\chi^2 < 1$), which may indicate that the model is unproperly explaining the noise, or the experimental variance was overestimated. It is worth noting that even if a mathematically good fitting of the data is obtained, the relevance of the estimated parameters should always be carefully discussed and validated with information attained by other surface characterization techniques.

$$MSE = \frac{1}{N-m-1}\sum_{i=1}^{N}(\rho_i - \rho_{calc})^2 \qquad \textbf{(Equation 2.13)}$$

$$\chi^2_{red} = \frac{\chi^2}{N-m-1} = \frac{1}{N-m-1}\sum_{i=1}^{N}\frac{(\rho_i-\rho_{calc})^2}{\sigma_i^2} \qquad \textbf{(Equation 2.14)}$$

Where:

- N is the total number of experimental data points;
- m is the number of estimated parameters;
- ρ_i is value of the i-th experimental data point;
- ρ_{calc} is the calculated value;
- σ_i^2 is experimental variance of ρ_i.

2.5. Surface plasmon resonance

Surface plasmon resonance (SPR) is a refractometric technique that allows the measurement of small variations in the refractive index of the medium that is in close proximity with a metal surface [21,22]. Since it is a label-free, and noninvasive technique that allows for real-time monitoring of a surface, it has become an important optical biosensing technology in the areas of biochemistry, biology, and medical sciences [23]. This technique takes advantage of the total internal reflection phenomenon (TIR) that occurs when the light propagating in a higher refractive index media encounters a lower refractive index medium at an incident angle above a critical value. TIR condition is easily achieved using an optical prism of a higher refractive index than the external medium, where light propagating within the prism is internally reflected once it encounters one of its facets. Although there is no propagation of light into the external medium during a TIR event, there is the generation of a localized perturbation of the electromagnetic field in this medium called evanescent field wave. The penetrating depth of this perturbation is around one light wavelength and decays exponentially [24]. A common configuration implemented in SPR measurements that exploits the evanescent wave is the Kretschmann configuration (**Figure 2.7a**). A thin layer of a conductive material – usually gold, and more rarely silver, aluminum, or copper – is placed in the prism facet, causing the evanescent field wave to perturb the electron density of the metal which in turn leads to some energy transfer in the form of a surface plasmon – an oscillation in the electron density that propagates in the metal surface. Thus, part of the p-polarized light is absorbed, and the optical phenomenon is better described as attenuated total reflection (ATR). The excitation of a surface plasmon, with the consequent absorption of light, occurs when the wave vector of the incident light couples with the wave vector of the surface plasmon [25], which is maximized at a specific resonance angle. The SPR angle is then characteristic for each optical system since it depends on the light frequency, dielectric properties of the prism, external medium, and metal, as well as, the thickness of the metal layer. **Figure 2.7b** shows a typical reflectivity curve presenting a dip at the resonance angle of the system. Since the resonance angle is sensitive to minute changes of the refractive index of the external medium, the adsorption of large molecules (*e.g.*, proteins, polynucleotides) at the surface of the metal will cause a shift in the reflectivity curve of the bare metal. In fact, variations of the refractive index in the micro-scale cause angle shifts typically in the milli-degree scale [25]. A nearly linear relationship between the amount of surface-bound macromolecules and the resonance shift angle ($\Delta\theta_{SPR}$) makes the SPR technique a very useful tool to quantify and monitor adsorption and desorption events. To acquire real-

time data of the interfacial events with high time resolution, the reflectivity curve should be ideally captured in a smallest time possible, which is achievable in more advanced SPR equipment [21]. In this case, a sensorgram can be constructed by plotting the resonance angle as a function of time. However, other cost-effective SPR equipments measure the reflectivity over time at a fixed angle, producing a similar sensorgram that is relatable to the first. To conveniently compare sensorgrams obtained from different optical responses, a resonance unit (RU) was defined as the optical response produced by a variation of 1×10^{-6} RIU (refractive index units) [21]. Thus, calibration of the optical signal is of upmost importance to acquire meaningful data to explain and model the kinetics of interfacial events.

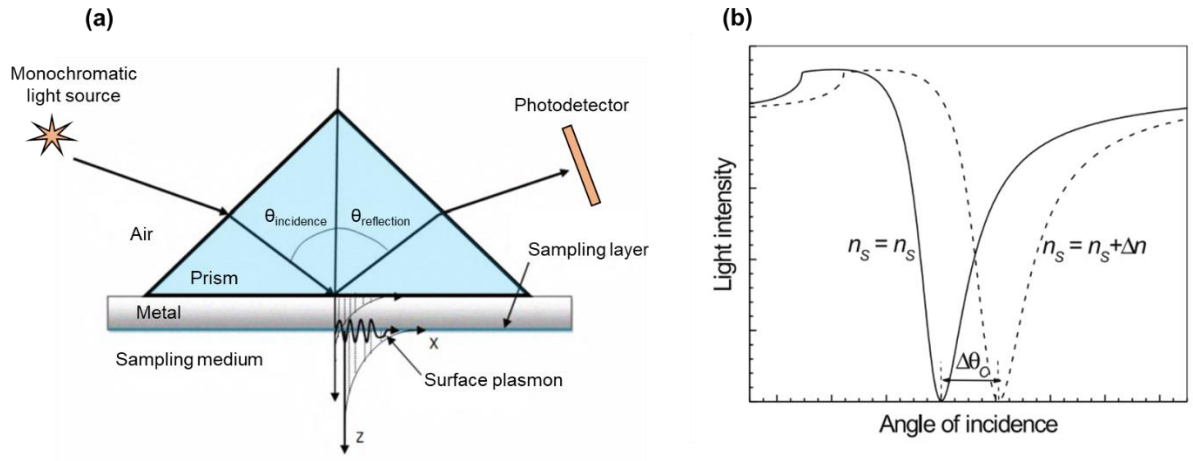

Figure 2.7: Surface plasmon generation in a Kretschmann configuration **(a)**; shift of the SPR reflectivity curve upon the increase of the refractive index of the sampling medium **(b)** – adapted from [22,25].

2.6. X-ray photoelectron spectroscopy

The X-ray photoelectron spectroscopy (XPS) is an analytic surface technique commonly used to probe the elemental composition and chemical state of a vacuum stable sample by means of the photoelectric effect [26,27]. As suggested by the name, X-ray radiation in the range of 100 eV to 10 keV is used to excite the deep core levels of the sample atoms, and the energy of the emitted electrons is analyzed. The photoelectric process is constrained, nonetheless, by the penetration depth of the incident X-ray photons and by the electron mean free path in solid materials. Although the penetration power of photons is in the range of 1 to 10 μm, electrons can only escape from depths in the nanometers scale (1–10 nm) [27,28]. As a consequence, electrons that escape in a vertical path will accentuate the emission spectrum of the bulk, whereas shallow electron take-off angles will produce spectra with a higher surface

component. This effect can be used, for instance, to obtain a composition depth profile of the sample [29].

In simple terms, the XPS setup (**Figure 2.8a**) is an ultravacuum system comprising the monochromatic source of photons (generated by an aluminum or magnesium cathodic tube), the sample (usually solid due to the vacuum conditions), and the hemispherical analyzer that separates electrons by their kinetic energies. To analyze the photoelectron emission spectra (**Figure 2.8b**), one should consider that the kinetic energy of the ejected electrons is related to the binding energies of specific atomic orbitals. Thus, sharp peaks of discrete energy values appear in the emission spectra that are characteristic of each chemical element. Qualitative and quantitative information of the chemical composition of the sample is then possible to extract from an XPS spectrum, considering the peaks position and intensity, respectively. High resolution spectrum allows even to visualize the fine structure of the core levels of the sample that are, not only influenced by the electrostatic attraction to the nucleus (intra-atomic effects), but also by the coulombic effects of the neighboring atoms (interatomic effects). Shifts to the core energy levels caused by the chemical environment are designated as chemical shifts (usually of 1 to 10 eV) [26], and convey important information about the chemical bonds and oxidation states. A process of curve fitting is then routinely applied to XPS spectra to separate core-level peaks, allowing to resolve and infer about the chemical structure of the sample [29].

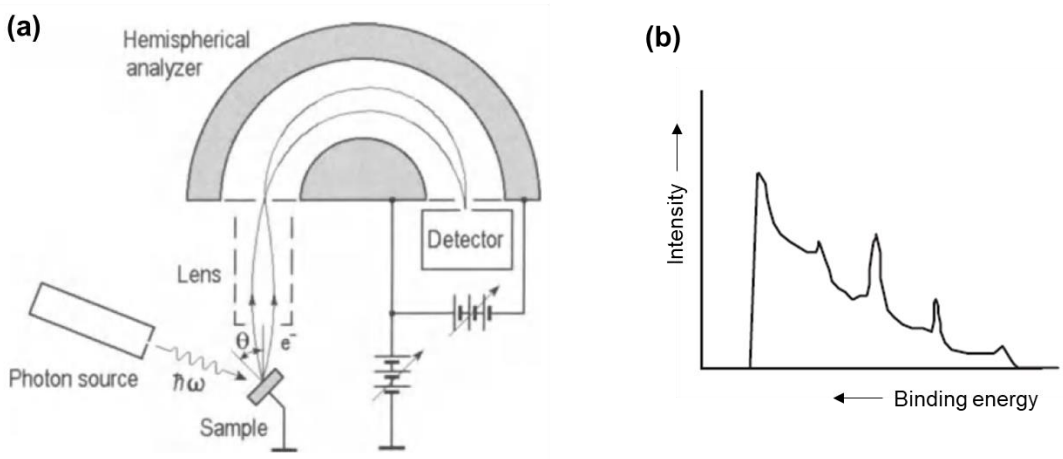

Figure 2.8: Photoelectron spectroscopy experimental setup **(a)**; Typical XPS spectrum **(b)** – adapted from [26,27].

2.7. Atomic force microscopy

Microscopies with atomic resolution appeared as a response to the technological interest for the nanoscale [30]. Scanning Probe Microscopies (SPM) are a group of techniques that can provide images with a resolution of 10^{-10} m from the interaction of the sample surface and a sharp tip that moves across it in a zigzag movement. The first kind of a scanning probe microscope was the scanning tunneling microscope (STM), created in the 1980 decade, it is able to deliver topographic information by the measurement of the tunneling currents between a metallic tip and a conductive surface. Later, a different type of scanning microcopy was developed to analyze the topography of samples regardless of their conductivity: the atomic force microscopy (AFM) [30, 31]. Instead of tunneling currents, the AFM microscope measures the interacting force between the cantilever (usually made of silicon or silicon nitride) and the surface, opening the possibility to study the surface of polymers, biological materials, and other non-conducting materials.

The topographic image is generated by a feedback mechanism, keeping the interaction between the cantilevers tip and the surface constant, while the two horizontal directions, x and y, are varied (**Figure 2.9a**). To keep the interaction constant, the vertical position of the sample (z) is adjusted according to the information received about the deflection or oscillation of the cantilever, which, in turn, is obtained from a photodiode that detects the beam of light reflected at the top of the cantilever [30, 32].

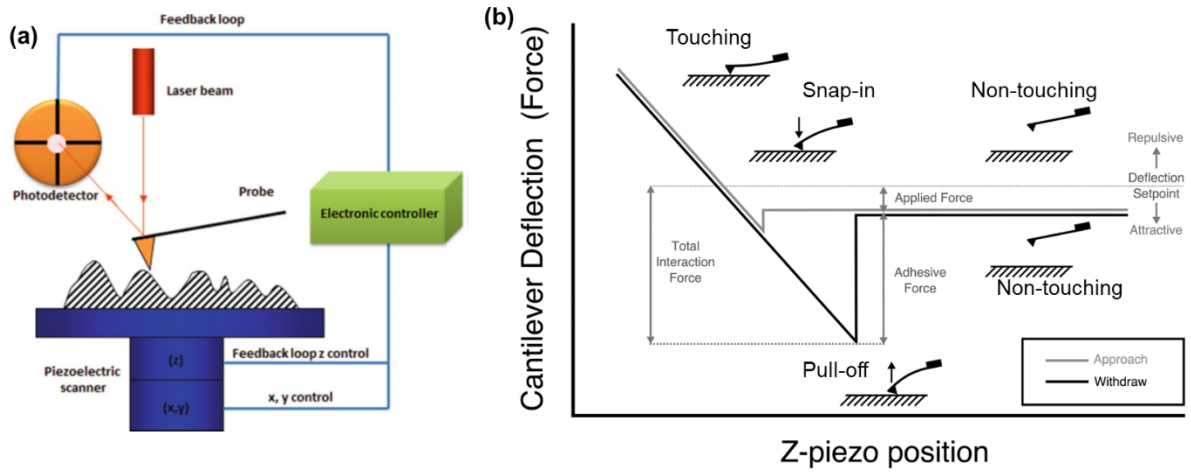

Figure 2.9: Simplified scheme of the feedback loop circuitry in AFM **(a)**; Typical force-distance curve **(b)** – adapted from [33] and [34], respectively.

Depending on the vertical distance between tip and surface, the resultant force exerted on the cantilever can be attractive (deflection towards the surface) or repulsive (deflection away

from the surface) – see **Figure 2.9b**. Taking advantage of the strong repulsive force, operation in the contact mode allows fast scanning speeds with atomic resolution on smooth, non-deformable surfaces. In this mode, the topographic information can be obtained by force modulation: maintaining a constant deflection of the cantilever, meaning a constant force between the tip and the surface. Additionally, the torsional deformation of the cantilever is another parameter that can be measured within the contact regime, offering information about friction coefficients of different regions of the sampled surface – lateral force microscopy.

Besides the contact mode, there are dynamic modes that operate in the region of attractive force (farther from the surface – **Figure 2.9b**) and prevent definitive deformation of the sample and contamination of the tip. This is the case of the tapping mode [30–33] – also known as intermittent mode – where the cantilever oscillates near its resonant frequency above the surface, and its tip only reaches the surface briefly, making this mode suitable for analyzing soft surfaces, such as polymers, biological material, among others. In tapping mode, the topography can be inferred by the changes in the amplitude of the cantilever. For instance, a stronger interaction with the surface lowers the cantilevers frequency, and thus its amplitude [31]. In addition to the height image, the phase difference between the excitation signal and the one measured by the photodiode is typically used to create a simultaneous image than can map differences in the mechanical properties of the surface. The phase image is then useful to distinguish materials with different stiffnesses or to evaluate chemical homogeneity in a qualitative manner. Quantitative information is challenging to obtain since the phase variation are dependent on several mechanical properties simultaneously, namely, the viscoelasticity and adhesion.

More recently, the PeakForce Tapping mode was developed where the cantilever is set to oscillate at a much lower frequency than its resonance frequency (0.25 to 2 kHz), which allows to approximate the ramping process as quasi-static [35]. As so, the maximum interaction force (peak force) between the tip and the sample can be measured and controlled with great precision, and force-distance curves can be acquired quickly for each image pixel. The fast recording of force-distance curves brings the capability of multi-parameter acquisition in real time in simultaneous with the topography, namely, surface deformation, Young's modulus, energy dissipation and adhesion force [36]. These nanomechanical parameters are obtained from the force-distance curves as shown in **Figure 2.10**. The deformation is simply attained from the difference between the tip positions at the peak force position (maximum force) and at the snap-in position on the approach curve. The dissipation energy originates from the hysteresis observed when plotting the approach and retract curves in the same graph, as properly

highlighted by the yellow area. The adhesion force refers to the minimum force in the retract curve. The Young's modulus can be calculated from the repulsive region of the retract curve (marked in green), using an appropriate mechanical model that considers adhesion, such as the Derjaguin-Muller-Toporov (DMT) model, that describes stiff contact events characterized by low adhesion forces and small tip radius [32]. Alternatively, the Johnson-Kendall-Roberts (JKR) model is a better option to describe contacts with low stiffness, high adhesion forces, and large tip radius.

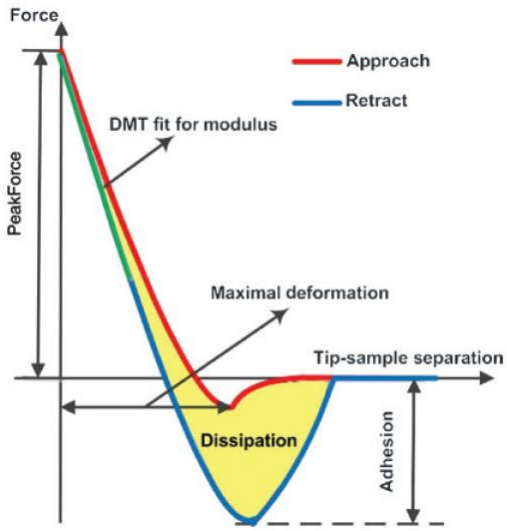

Figure 2.10: Force-distance curve in a PeakForce Tapping experiment; Approach and retract curves are displayed in red and blue color, respectively – adapted from [35].

Another possible parameter to be estimated by atomic force microscopy is the surface roughness, evaluating the height differences of prominences and depressions on the surface. Several mathematical treatments can be used in the roughness calculation, however the root mean square roughness (R_q, R_{RMS} or *RMS*) is the one that is usually used due to its simplicity and because it corresponds to a standard deviation to the average of heights [30]. The calculation of the R_q is commonly integrated in the AFM software, and it is based on the **equation 2.15** [37].

$$R_q = \sqrt{\frac{\sum_{i=1}^{N}(z_i - \bar{z})^2}{N}} \qquad \textbf{(Equation 2.15)}$$

Where:

- R_q is the root mean square roughness in a given area;
- N is the number of points;
- z_i is the height in point i;
- $\bar{z}$ is the height average in a given area.

2.8. References

[1] J. Wang, Analytical Electrochemistry, Second Edition, John Wiley & Sons, Inc., New York, USA, 2000. doi:10.1002/0471228230.

[2] C.G. Zoski, Handbook of electrochemistry, First Edition, Amsterdam, The Netherlands, 2007. doi:10.1016/B978-0-444-51958-0.X5000-9.

[3] J.C. Myland, K.B. Oldham, Cottrell's equation revisited: An intuitive, but unreliable, novel approach to the tracking of electrochemical diffusion, Electrochemistry Communications. 6 (2004) 344–350. doi:10.1016/j.elecom.2004.01.013.

[4] D. R. Lide, CRC Handbook of Chemistry and Physics, 89th Edition, Florida, USA, 2009. doi:10.1136/oem.53.7.504.

[5] L.R. Bard, A. J.; Faulkner, Electrochemical Methods: Fundamentals and Applications, Second Edition, New York, USA, 2001.

[6] J.R. Macdonald, Impedance spectroscopy, Annals of Biomedical Engineering. 20 (1992) 289–305. doi:10.1007/BF02368532.

[7] C.M.A. Brett, A.M.O. Brett, Electrochemistry - Principles, Methods, and Applications, Oxford University Press, Oxford, UK, 1993.

[8] S. Wang, J. Zhang, O. Gharbi, V. Vivier, M. Gao, M.E. Orazem, Electrochemical impedance spectroscopy, Nature Reviews Methods Primers. 1 (2021) 41. doi:10.1038/s43586-021-00039-w.

[9] H. Cesiulis, N. Tsyntsaru, A. Ramanavicius, G. Ragoisha, Nanostructures and Thin Films for Multifunctional Applications, Springer International Publishing, Cham, Switzerland, 2016. doi:10.1007/978-3-319-30198-3.

[10] V.S. Muralidharan, Warburg impedance - Basics revisited, Anti-Corrosion Methods and Materials. 44 (1997) 26–29. doi:10.1108/00035599710157387.

[11] A. Lasia, The Origin of the Constant Phase Element, Journal of Physical Chemistry Letters. 13 (2022) 580–589. doi:10.1021/acs.jpclett.1c03782.

[12] M.R. Shoar Abouzari, F. Berkemeier, G. Schmitz, D. Wilmer, On the physical interpretation of constant phase elements, Solid State Ionics. 180 (2009) 922–927. doi:10.1016/j.ssi.2009.04.002.

[13] K.A. Marx, Quartz Crystal Microbalance: A Useful Tool for Studying Thin Polymer Films and Complex Biomolecular Systems at the Solution−Surface Interface, Biomacromolecules. 4 (2003) 1099–1120. doi:10.1021/bm020116i.

[14] J. Tichý, J. Erhart, E. Kittinger, J. Přívratská, Fundamentals of Piezoelectric Sensorics, Springer Berlin Heidelberg, Berlin, Germany, 2010. doi:10.1007/978-3-540-68427-5.

[15] M.R. Deakin, D.A. Buttry, Electrochemical applications of the quartz crystal microbalance, Analytical Chemistry. 61 (1989) 1147A-1154A. doi:10.1021/ac00195a001.

[16] M. Losurdo, K. Hingerl, Ellipsometry at the Nanoscale, Springer Berlin Heidelberg, Berlin, Germany, 2013. doi:10.1007/978-3-642-33956-1.

[17] R.M.A. Azzam, N.M. Bashara, Ellipsometry and Polarized Light, North-Holland Publishing Company, Amsterdam, The Netherlands, 1977.

[18] H. Fujiwara, Spectroscopic Ellipsometry - Principles and Applications, John Wiley & Sons, Tokyo, Japan, 2007.

[19] G.E. Jellison, Data analysis for spectroscopic ellipsometry, Thin Solid Films. 234 (1993) 416–422. doi:10.1016/0040-6090(93)90298-4.

[20] H.G. Tompkins, E.A. Irene, Handbook of Ellipsometry, William Andrew, New York, USA, 2005. doi:10.1016/B978-0-12-405889-7.01001-7.

[21] R.B.M. Schasfoort, A.J. Tudos, Handbook of Surface Plasmon Resonance, Royal Society of Chemistry, Cambridge, 2017. doi:10.1039/9781788010283.

[22] J. Homola, Surface Plasmon Resonance Based Sensors, Springer-Verlag Berlin Heidelberg, Berlin, Germany, 2006. doi:10.1007/b100321.

[23] Y. Tang, X. Zeng, J. Liang, Surface Plasmon Resonance: An Introduction to a Surface Spectroscopy Technique, Journal of Chemical Education. 87 (2010) 742–746. doi:10.1021/ed100186y.

[24] P. Pattnaik, Surface Plasmon Resonance: Applications in Understanding Receptor–Ligand Interaction, Applied Biochemistry and Biotechnology. 126 (2005) 079–092. doi:10.1385/ABAB:126:2:079.

[25] M.S. Islam, A.Z. Kouzani, X.J. Dai, W.P. Michalski, Parameter sensitivity analysis of surface plasmon resonance biosensor through numerical simulation, in: IEEE/ICME International Conference on Complex Medical Engineering, IEEE, 2010: pp. 171–176. doi:10.1109/ICCME.2010.5558850.

[26] P. van der Hiede, X-ray Photoelectron Spectroscopy: An Introduction to Principles and Practices, John Wiley & Sons, New Jersey, USA, 2012.

[27] K. Oura, M. Katayama, A. V. Zotov, V.G. Lifshits, A.A. Saranin, Surface Science: An Introduction, Springer-Verlag Berlin Heidelberg, Berlin, Germany, 2003. doi:10.1007/978-3-662-05179-5.

[28] A.J. Milling, Surface Characterization Methods: Principles, Techniques and Applications, Marcel Deker, New York, USA, 1999.

[29] J.F. Moulder, W.F. Stickle, P.E. Sobol, K.D. Bomben, Handbook of X-ray Photoelectron Spectroscopy, Perkin-Elmer Corporation, Minnesota, USA, 1992. doi:10.1002/0470014229.ch22.

[30] B. Voigtländer, Scanning Probe Microscopy, Springer Berlin Heidelberg, Berlin, Germany, 2015. doi:10.1007/978-3-662-45240-0.

[31] S.N. Magonov, M.-H. Whangbo, Surface Analysis with STM and AFM: Experimental and Theoretical Aspects of Image Analysis, VCH Verlagsgesellschaft, Weinheim, Germany, 1996. doi:10.1055/s-0031-1276420.

[32] R. García, Amplitude Modulation Atomic Force Microscopy, WILEY-VCH Verlag & Co., Weinheim, Germany, 2010.

[33] S. Pisano, E. Gilson, Analysis of DNA–Protein Complexes by Atomic Force Microscopy Imaging: The Case of TRF2–Telomeric DNA Wrapping, in: N.C. Santos, F.A. Carvalho (Eds.), Atomic Force Microscopy - Methods and Protocols, Humana Press, 2019: pp. 75–97. doi:10.1007/978-1-4939-8894-5_5.10.1017/9781107707399.005.

[34] A.F. Wallace, Scanning Probe Microscopy, in: J.P. Kenney, H. Veeramani, D.S. Alessi (Eds.), Analytical Geomicrobiology, Cambridge University Press, 2019: pp. 121–147. doi:10.1017/9781107707399.005.

[35] K. Xu, W. Sun, Y. Shao, F. Wei, X. Zhang, W. Wang, P. Li, Recent development of PeakForce Tapping mode atomic force microscopy and its applications on nanoscience, Nanotechnology Reviews. 7 (2018) 605–621. doi:10.1515/ntrev-2018-0086.

[36] M. Pfreundschuh, D. Martinez-Martin, E. Mulvihill, S. Wegmann, D.J. Muller, Multiparametric high-resolution imaging of native proteins by force-distance curve-based AFM, Nature Protocols. 9 (2014) 1113–1130. doi:10.1038/nprot.2014.070.

[37] D.L. Sedin, K.L. Rowlen, Influence of tip size on AFM roughness measurements, Applied Surface Science. 182 (2001) 40–48. doi:10.1016/S0169-4332(01)00432-9.

Chapter III

Experimental conditions and procedures

3. Experimental conditions and procedures

3.1. Chemicals

Dopamine hydrochloride (DA, Sigma-Aldrich), *DL*-norepinephrine hydrochloride (NE, Sigma-Aldrich), 3,4-dihydroxy-*L*-phenylalanine (DOPA, Sigma-Aldrich), catechol (CA, Alfa Aesar), caffeic acid (CAF, Sigma-Aldrich), rosmarinic acid (Sigma-Aldrich), gallic acid (Sigma-Aldrich), (±)-catechin hydrate (Sigma-Aldrich), 2,6-dimethylphenol (DMP, Sigma-Aldrich), 2,2′-azino-bis(3-ethylbenzothiazoline-6-sulfonic acid) diammonium salt (ABTS, Sigma Chemical), potassium hexacyanoferrate(III) (Merck), hexaammineruthenium(III) chloride (Sigma-Aldrich), aminoferrocene ($FcNH_2$, Sigma-Aldrich), potassium chloride (Merck), potassium nitrate (Merck), ethanolamine (ETA, Fisher Scientific), immunoglobulin G from human serum (IgG, Sigma-Aldrich), polyclonal Anti-human immunoglobulin G (whole molecule) produced in goat (Anti-IgG, Sigma-Aldrich) and bovine serum albumin (BSA, Sigma-Aldrich) were all used without further purification. The following buffers were used in the modification steps and characterizations of electrodes:

i) Tris-HCl buffer pH 8.5 containing 50 mM tris(hydroxymethyl)aminomethane (≥99.8%, Sigma-Aldrich) was adjusted with hydrochloric acid (Fisher Scientific);

ii) citrate-phosphate buffers (CPB) were prepared using citric acid ($C_6H_8O_7{\cdot}H_2O$, Sigma-Aldrich) and di-sodium hydrogen phosphate anhydrous (Na_2HPO_4, Merck) – CPB pH 4.6 (27 mM $C_6H_8O_7{\cdot}H_2O$ and 47 mM Na_2HPO_4) and CPB pH 6.0 (17 mM $C_6H_8O_7{\cdot}H_2O$ and 66 mM Na_2HPO_4); and CPB pH 7.0 (17 mM $C_6H_8O_7{\cdot}H_2O$ and 66 mM Na_2HPO_4).

iii) Phosphate buffer solutions (PB) with several pH values were prepared by mixing two 100 mM stock solutions of phosphoric acid (H_3PO_4, Merck), Na_2HPO_4, and monosodium phosphate (NaH_2PO_4, Merck) until the desired pH value is reached: pH 2.0 (H_3PO_4 and Na_2HPO_4), pH 4.0 (NaH_2PO_4 and H_3PO_4), pH 6.0 and 8.0 (NaH_2PO_4 and Na_2HPO_4).

iv) Phosphate buffer saline (pH 7.4, 0.01 M phosphate buffer containing 0.138 M sodium chloride and 0.0027 M potassium chloride), obtained from Sigma-Aldrich was used without (PBS) or with (PBST) 0.05 % (v/v) of polysorbate-20 (Tween® 20).

Fungal laccase preparation NS-51003 (LacNZ) was kindly provided by Novozymes A/S (Denmark), whereas the bacterial laccase cocktail MetZyme® LIGNO™ (LacMG) was kindly provided by MetGen (Finland) [1]. Chestnut shells and olive oil dregs were kindly provided by a factory located in Campania region (Italy), and the aqueous extracts were prepared according to previously procedures reported elsewhere [2,3]. Ultrapure water, obtained from a purification

MILLI-Q A10 system (18.2×10^6 Ω cm), was used to prepare buffers, rinsing steps and electrodes polishing.

3.2. Instrumentation

3.2.1. Electrodes, cells, and electrochemical equipment

Throughout this work the electrochemical surface modification procedures were applied to two conductive materials: gold and carbon. These are common working electrode materials used for electrochemical purposes, due to their conductive and electrocatalytic properties [4,5]. For the general purpose, thin layer evaporated gold from Arrandee™ is used, consisting on 200 nm of gold deposited on borosilicate glass (**Figure 3.1a**). For electrochemical quartz crystal microbalance assays, the working electrode consisted on a 8 MHz AT-cut quartz crystal with an integrated sensitivity constant of 0.739 Hz ng^{-1} coated with a 100 nm gold layer, acquired from CHInstruments (**Figure 3.1b**). In the surface plasmon resonance assays, glass slides purchased from NanoSPR LLC are coated with a 45 nm gold layer (**Figure 3.1c**). All the electrodes have a pre-layer of chromium (2–5 nm) to enhance gold adhesion to the crystal or glass substrates. Gold electrodes from Arrandee™ and CHInstruments are reusable electrodes that were washed repeatedly with ethanol and water, dried in a nitrogen stream, and cleaned in a Diener Electronics ZEPTO plasma chamber for 4 min at a pressure of 0.3 mbar. After one cleaning cycle the quality of the surface was assessed by visual inspection and by ellipsometry. If necessary, the cleaning cycle was repeated. Gold slides from NanoSPR LLC are single-use surfaces that were washed and dried as mentioned before and cleaned in a UV/ozone ProCleaner™ Plus chamber (Bioforce Nanosciences) for 40 min before each assay.

The three types of carbon electrodes used are presented in the lower row of **Figure 3.1**: glassy carbon disk (GC, **Figure 3.1d**), polycrystalline graphite plates cut from an Alpha Aesar rod (graph, **Figure 3.1e**), and highly oriented pyrolytic graphite (HOPG, **Figure 3.1f**). The surface of glassy carbon was firstly polished with alumina suspension of 5 μm grain size (Buehler Alpha Micropolish), using a synthetic fiber cloth (Buehler Microcloth). After 3 min of ultrasonic cleaning in water, the polishing step was repeated using decreasing alumina grain sizes 1 and 0.3 μm. To eliminate any remaining organic residue, the electrode was placed for 40 min in the UV/ozone chamber. Regarding the polycrystalline plate (**Figure 3.1e**), the cleaning procedure started by polishing its edges and faces using a waterproof sandpaper p1200 (SiC), followed by ultrasonic cleaning in water until there was no visible dispersed carbon

powder. Both electrodes were dried under a nitrogen stream. HOPG cleaning procedure consisted of peeling the surface by the action an adhesive tape.

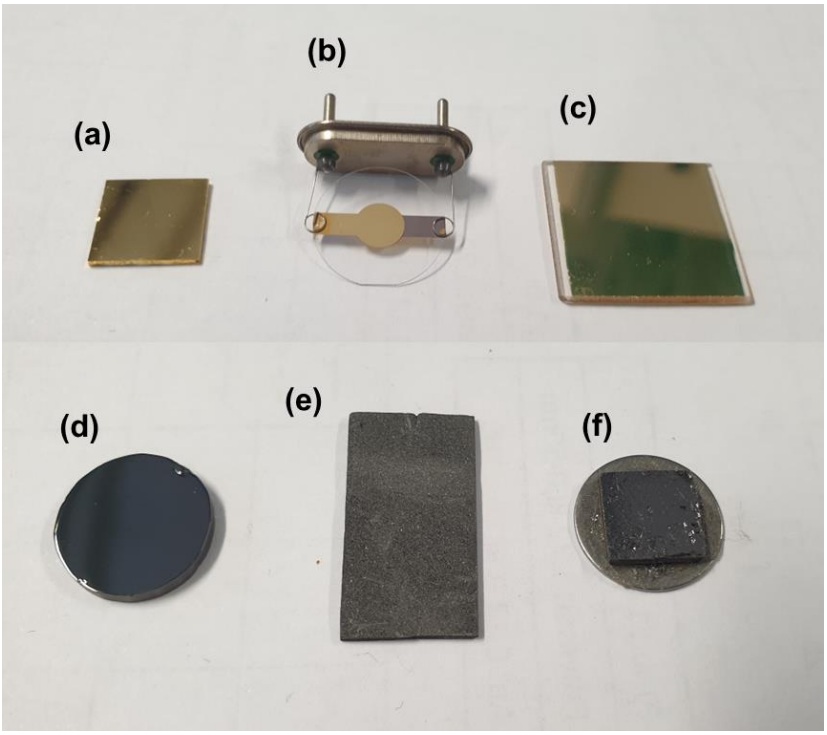

Figure 3.1: Upper row shows the evaporated gold electrodes from Arrandee **(a)**, CHInstruments (b), and NanoSPR LLC **(c)**; Lower row shows the glassy carbon electrode **(d)**, polycrystalline graphite **(e)**, and HOPG **(f)**.

In electrochemical assays, the usual configuration of 3 electrodes was used: a gold or carbon working electrode, a platinum counter electrode and a saturated calomel electrode (SCE) as reference. Several electrochemical cells were used throughout this work, as presented in **Figures 3.2** and **3.3**. Whenever possible the electrochemical cell was placed inside of a Faraday cage. All the conventional electrochemical assays that do not required a large surface area, were performed in the one-compartment acrylic cell (**Figure 3.2**) with an area-defining O-ring of 0.47 cm^2, and equipped with one of the three reusable stand-alone working electrodes (**Figure 3.1a, d, f**) at the bottom of the cell. Cyclic voltammetry and chronoamperometry were performed using a PARSTAT 2263 potentiostat from AMETEK (Princeton Applied Research), while electrochemical impedance spectroscopy was performed using a Vertex.One.EIS potentiostat/galvanostat from Ivium Technologies B. V.. Experimental parameters such as, potential values, scan rate, or assay duration are defined later in the section 3.4 (Electrode modification approaches) or along the results discussion. Impedance spectra were recorded at 0.2 V (half-wave potential of $K_3Fe(CN)_6$ on bare gold electrode) within a frequency range from

10 kHz to 100 mHz and a perturbation amplitude of 10 mV. Equivalent circuit fitting was performed with IviumSoft software (v 4.985).

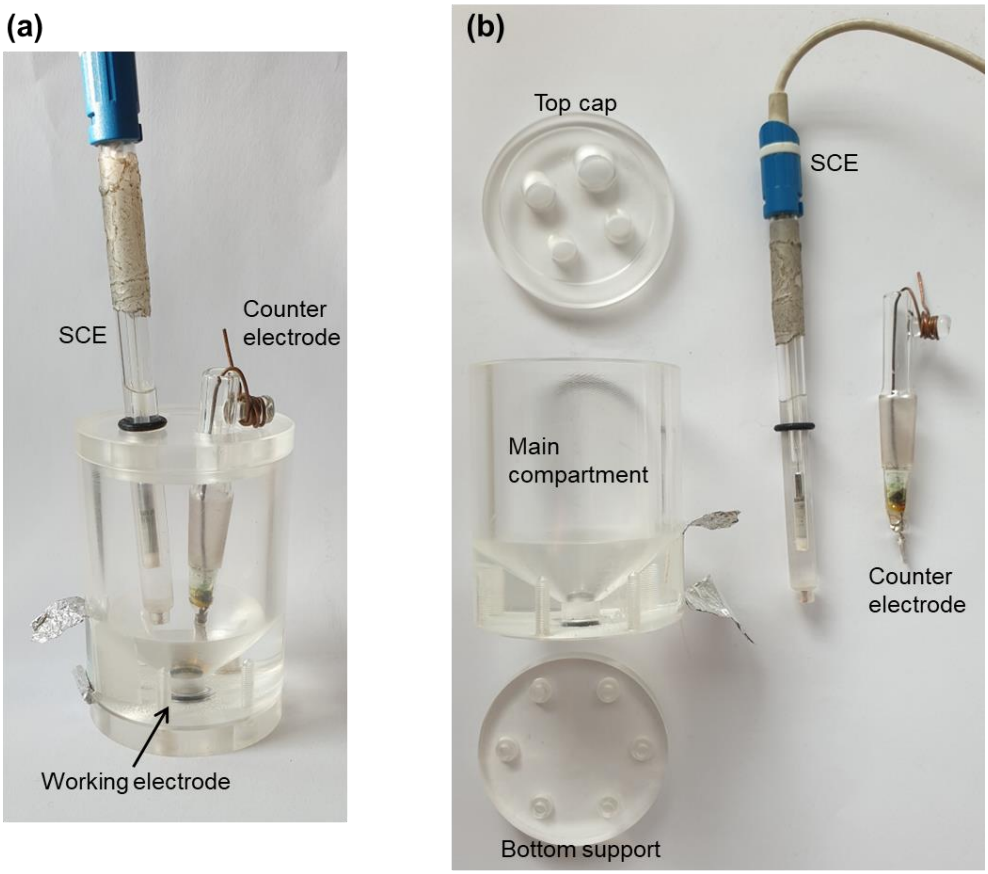

Figure 3.2: Photographs of the assembled **(a)** and disassembled **(b)** one-compartment acrylic cell.

In the case of the larger working electrodes (**Figure 3.1c** and **3.1e**), the geometric area was defined by a Teflon tape, providing its electrical isolation from the holder. Typically, the area of the graphite electrode was 2.5 cm^2, whereas the area of the SPR slide was 3.3 cm^2. Due to their sizes, these two electrodes worked in a one-compartment electrochemical cell comprising of a 20 mL glass beaker equipped with a Styrofoam cap to hold working, reference and counter electrodes in a vertical position and parallel to each other.

For non-conventional electrochemical assays, namely, *in situ* gravimetric or ellipsometric assays, the specialized cells of **Figure 3.3a** and **3.3b,c** were used. The electrochemical quartz crystal microbalance assays were performed fitting the gold-coated quartz electrode aforementioned (**Figure 3.1b**) on the bottom of the appropriate one-compartment EQCM Teflon cell provided by CHInstruments, Inc. (**Figure 3.3a**). This system was connected to a CHI420 Electrochemical Analyzer (CHInstruments, Inc.) equipped with an oscillator accessory. In the case of *in situ* ellipsometric assays, the Arrandee gold electrode of **Figure 3.1a** was fitted into a home-made two-compartment Teflon cell containing two optical windows

at 20° from the bottom plane (**Figure 3.2b,c**). A Pt mesh was used in this case as counter electrode. The electrochemical parameters of the *in situ* ellipsometric assays were controlled by a Vertex.One.EIS potentiostat/galvanostat (Ivium Technologies B. V., The Netherlands).

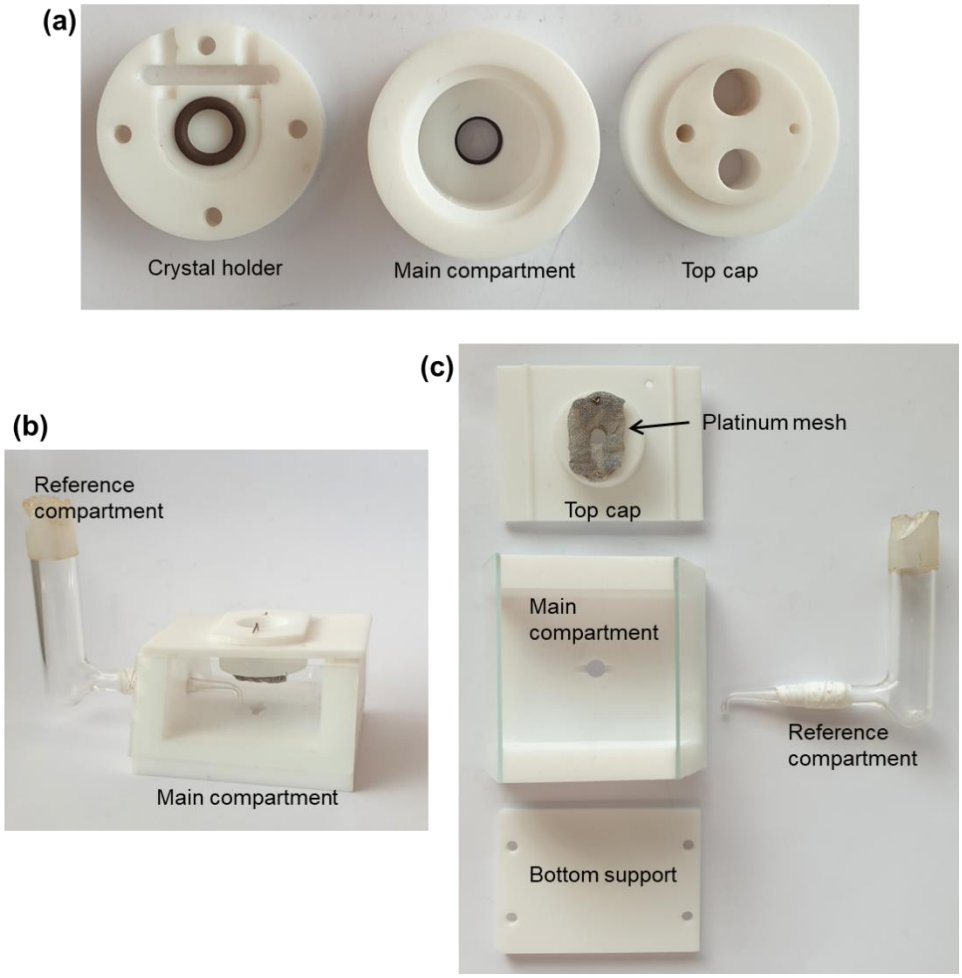

Figure 3.3: Photographs of the cells utilized in *in situ* electrochemical assays: disassembled EQCM cell **(a)**; and the assembled **(b)** and dissembled **(b)** two-compartment cell for the *in situ* ellipsometric assays.

3.2.2. Ellipsometry

Ellipsometric measurements were carried out, *ex situ*, at single or multiple angles of incidence (values are specified along the text), and *in situ* at a single incidence angle of 70˚, using the monochromatic ellipsometer SE400 (SENTECH Instruments GmbH), fitted with a He-Ne laser light source (632.8 nm) in a PCSA configuration. In the *ex situ* setup, multiple points of the bare and modified surface were acquired, whereas in the *in situ* setup a single point of the surface was analyzed through time. A common routine to determine the dielectric properties of the analyzed samples started by the determination of refractive index and extinction coefficient of the bare substrate (gold or glassy carbon), at the selected angles of

incidence, considering a semi-infinite two-phase model for the substrate/ambient interface. The refractive index values of the ambient phases were assumed to be transparent, in particular, for the *ex situ* measurements, the ambient air was assumed to have $n = 1$, while for *in situ* measurements, the Abbe refractometer NAR-1T Liquid (ATAGO) was used to acquire the refractive index value of the buffered solution of dopamine ($n = 1.335 \pm 0.001$). After trivial calculation of the substrates dielectric parameters, surface modifications derived from the deposition of polymers or proteins was subsequently evaluated using a model comprising a homogenous, isotropic, and finite phase, or phases, to described the deposited material. Unless specified along the text, the thin layer parameters (n, k, L) were considered to be unknown and allowed to vary during the mathematical fitting of the data. The fittings were performed in the MATLAB R2016b software translating the **Equations 2.7** to **2.14** (described in chapter II) into MATLAB script. The fitting procedure differs conceptually between the *ex situ* and *in situ* data. Regarding the first case, the iterative minimization of the residues was performed considering a merit function that encompassed the standard deviation as measure of the experimental error (**Equation 2.14**, chapter II). In the case of the *in situ* data, and due to the single-point nature of the setup, the merit function is simplified to the mean square error estimator (**Equation 2.13**, chapter II). Furthermore, to complete the fitting of the *in situ* data (Δ *vs.* Ψ curve) to a multiphase model, the residues minimization procedure is repeatedly applied to an increasingly complex model, as it is constructed and fine tuned regarding growth velocities and phase changes, until all the possible time segments are explained.

3.2.3. Surface plasmon resonance

Surface plasmon resonance measurements were carried out at a fixed angle of incidence in a Kretschmann configuration by the monochromatic (630 – 670 nm) SPR equipment Biosuplar 400T, (Analytical μ-Systems), coupled to a peristaltic pump from ISMATEC running at 25 μL min^{-1}. The optical prism (F1-65) and the contact liquid (Cargille-Sacher Laboratories Inc) have a refractive index of 1.61, compatible with the gold-coated glass slide of **Figure 3.1c**. Before the antigen–antibody assay, water and PBS were pumped into the cell to normalize the equipment reflectivity response (RU) according to the equation: $RU_{norm} = RU/(RU_{PBS} - RU_{water})$. Considering the reported refractive index values of water (1.3328) and PBS (1.3342) [6,7], the normalized optical response (RU_{norm}) is a dimensionless quantity and its unitary value is equivalent to a variation of 0.0014 RIU. In order to better visualize and compare sensorgrams,

the optical responses are corrected considering the response of the film before IgG injection (RU_0) as the starting value, following the equation: $\Delta RU = RU - RU_0$.

3.2.4. Reflectance IR spectroscopy

FTIR spectra were obtained with a Nicolet Nexus 6700 FTIR spectrometer using the Specular Apertured Grazing Angle module (Smart SAGA™). During spectra acquisition, 128 scans were collected for each sample, using 4 cm^{-1} resolution.

The Raman experiments were carried out in the University of Warsaw using a DXR SmartRaman spectrometer (Thermo Scientific). The instrument was operated using a 633 nm excitation line. For typical experiments, the spectral resolution was equal to 1 cm^{-1}. The 50/0.50 objective was used. In the configuration used, the signal was collected from the 1 μm^3 spot.

3.2.5. X-ray photoelectron spectroscopy

XPS spectra were collected in an Ultra High Vacuum (UHV) system with a base pressure of 2×10^{-10} mbar (TEMA, University of Aveiro). The system is fitted with a hemispherical electron energy analyser (SPECS Phoibos 150), a delay-line detector and a monochromatic X-ray source AlK_α (1486.71 eV). High resolution spectra were recorded at normal emission take-off angle and with a pass-energy of 20 eV, providing an instrumental peak broadening of 0.5 eV. The effect of the electric charge was corrected using C 1s peak (285.0 eV) as reference [8]. The spectra were deconvoluted with XPSPEAK software, using a Gaussian–Lorentzian peak shape and Shirley (or Linear) type background subtraction.

3.2.6. Atomic force microscopy

AFM measurements were performed in air at 23 ± 1 °C, using a Multimode 8 HR microscope coupled to Nanoscope V (Digital Instruments, Bruker). The images were acquired in Peak Force Tapping (at a frequency of 2 kHz) using ScanAsyst mode, with Silicon Nitride ScanAsyst-Air probes (spring constant of *ca.* 0.4 N m^{-1}, Bruker), at a scan rate of ca. 1.0 Hz. For the acquisition of adhesion images, the quantitative nanomechanical mapping (QNM)s software was used and the probes were modified with amine groups using a previously reported method [9] with some modifications. Briefly, the probes were activated in Diener Electronics ZEPTO plasma cleaner, setting the air pressure at 0.3 mbar for 1.5 min. Afterwards, the tips were incubated overnight in 0.3% ethanolamine in dried DMSO, following an extensive washing with this solvent.

3.2.7 Water contact angle goniometry

Water contact angle measurements of the modified electrodes were performed using the goniometer KRÜSS DSA30, through the analysis of the shape water sessile drops (1 µL), using the software ImageJ and the automatic adjustment of plugin DropSnake [10]. At least five drops have been analyzed for each sample.

3.3. Laccases activity and protein content

Enzymatic activity of the laccase cocktails were assessed by UV-Vis spectroscopy (UV 2600 spectrophotometer, Shimadzu) following the oxidation of ABTS at 420 nm ($\varepsilon = 3.6 \times 10^4$ M^{-1} cm^{-1}) [11]. The assay was performed at 22 ± 2°C, by mixing 250 µL of 2 mM ABTS with 2 µL of diluted LacNZ (1:400) or 5 µL of diluted LacMG (1:50), in 1 mL total volume of CPB pH 4.6. The increase in absorbance was recorded over 2 minutes, yielding a value of 478 and 40 U mL^{-1} for LacNZ and LacMG, respectively (one unit of enzyme activity is defined as the amount of enzyme required to oxidize 1 µmol ABTS per minute). The protein content of LacNZ and LacMG was estimated to be 9 ± 1 mg mL^{-1} and 14.0 ± 0.5 mg mL^{-1}, respectively, by the Bradford assay using bovine serum albumin for the calibration curve.

3.4. Electrode modification approaches

3.4.1. Electropolymerization of catechol derivatives

Carbon and gold electrodes were coated with thin polymeric films through the electropolymerization of bio-inspired molecules such as catecholamines (dopamine, norepinephrine, DOPA), catechol and caffeic acid. The electropolymerization of these monomers was performed by potentiostatic or potentiodynamic methods using a 5 mM monomer in CPB pH 7.0 solution, deaerated with pure N_2 for 20 minutes. Unless stated otherwise, the potentiostatic depositions were performed by chronoamperometry at 0.3 V for 120 s, whereas the potentiodynamic depositions were performed by cyclic voltammetry from -0.6 to +0.8 V at 200 mV s^{-1} using different numbers of potential cycles. The resulting thin polymeric films of polycatechol, polydopamine, polynorepinephrine, polyDOPA, and poly(caffeic acid) were labeled as ePCA, ePDA, ePNE, ePDOPA, and ePCAF, respectively. After polymerization, the modified electrodes, were washed with ultrapure water and dried under a nitrogen stream, before subsequent modification steps or characterization assays.

3.4.2. Synthesis of polymeric films comprising aminoferrocene or ethanolamine

The electropolymerization of catechol derivatives was also performed potentiodynamically in the presence amine-containing molecules: aminoferrocene (2.5 mM) or ethanolamine (10, 50 and 100 mM). The concentration of monomer, supporting electrolyte and potential window are mentioned above. Whenever indicated in the text, pristine ePDA films were also incubated in 5 mM or 100 mM ethanolamine PBS solution for 3 hours. The modified gold electrodes were washed with water and dried with nitrogen flux.

3.4.3. Laccases immobilization and catalytic activity assessment

The immobilization of laccases LacNZ and Lac MG was carried out either by a one-step or a two-step approach. The one-step approach concerns a potentiostatic co-deposition of laccase during the electrosynthesis of the polycatechol or polycatecholamine film at 0.3 V for 120, 200, 300 or 600 s. The two-step approach concerns the incubation of a previously modified electrode (with polycatechol or polycatecholamine) in a laccase solution for 3 hours. Details of the electropolymerization conditions are stated above.

The catalytic activity assessment of laccase modified electrodes was carried out by spectroscopic and electrochemical methods. Regarding the spectroscopic method, the modified electrodes were placed inside the UV-Vis cuvette in 500 µM ABTS solution (CPB pH 4.6), and the formation of oxidized ABTS was followed at 420 nm. For the electrochemical method, the catalytic activity was measured by the chronoamperometric reduction of the enzymatic products at different concentrations of initial substrate, stepping the potential from open-circuit potential to 0.4 V in the case of ABTS [12], or to 0.0 V (pH 5), -0.1 V (pH 7), and -0.2 V (pH 9) in the case of phenolic compounds [13]. The electrolyte solution was aerated during the measurements to ensure a constant oxygen concentration. Plotting catalytic current density obtained the chronoamperometric assays against the substrate concentration, a Michaelis-Menten type curve is obtained, which was fitted using the non-linear regression tools of the OriginPro 9.0 software (OriginLab). Taking into account the direct proportionality between the catalytic current density and the oxidation rate ($j \propto v$), the following adapted Michaelis-Menten equation [14] was used:

$$|j - j_b| = \frac{j_{max}\,[S]}{K_M^{app} + [S]} \qquad \textbf{(Equation 3.1)}$$

Where:

- j is the measured current density in A cm^{-2};

- j_b is the background current density (before substrate addition) in A cm^{-2};
- j_{max} is the maximum catalytic current density in A cm^{-2};
- $[S]$ is the substrate concentration in mol cm^{-3};
- K_M^{app} is the apparent Michaelis-Menten constant in mol cm^{-3}.

3.4.4. Antigen-antibody optical assays

The optical performance of modified gold interfaces was evaluated through ellipsometric measurements (static conditions) and through surface plasmon resonance assays (dynamic conditions). In static conditions, the optical parameters of the surfaces were measured by ellipsometry upon each modification step: polymer modified surfaces were incubated with 0.1 mg/mL of IgG in PBS for 1.5 h, at room temperature, thoroughly rinsed with PBST and water, and dried under nitrogen flow, followed by immersion in 0.1 mg/mL of Anti-IgG in PBS for 1.5 h. An intermediate blocking step was performed for 30 min with 5 mM of ETA or 0.1 mg/mL of BSA, both in PBS, for some modified electrodes, as explained along the text. Afterward, a 0.1 mg/mL IgG solution was pumped into the system and left to incubate till a stable optical signal was acquired. After PBST washing, a 0.1 mg/mL Anti-IgG solution was pumped and left to incubate again until the optical signal was stable. In some cases, a blocking step was also performed after IgG incubation, using 5 mM of ETA or 0.1 mg/mL of BSA.

3.5. References

[1] V. Hämäläinen, T. Grönroos, A. Suonpää, M.W. Heikkilä, B. Romein, P. Ihalainen, S. Malandra, K.R. Birikh, Enzymatic Processes to Unlock the Lignin Value, Frontiers in Bioengineering and Biotechnology. 6 (2018) 1–10. doi:10.3389/fbioe.2018.00020.

[2] G. Squillaci, F. Apone, L.M. Sena, A. Carola, A. Tito, M. Bimonte, A. De Lucia, G. Colucci, F. La Cara, A. Morana, Chestnut (Castanea sativa Mill.) industrial wastes as a valued bioresource for the production of active ingredients, Process Biochemistry. 64 (2018) 228–236. doi:10.1016/j.procbio.2017.09.017.

[3] G. Squillaci, A. Marchetti, O. Petillo, M. Bosetti, F. La Cara, G. Peluso, A. Morana, Olive oil dregs as a novel source of natural antioxidants: extraction optimization towards a sustainable process, Processes. 9 (2021) 1064. doi:10.3390/pr9061064.

[4] L.D. Burke, P.F. Nugent, The electrochemistry of gold: I the redox behaviour of the metal in aqueous media, Gold Bulletin. 30 (1997) 43–53. doi:10.1007/BF03214756.

[5] Richard L. McCreery, Advanced Carbon Electrode Materials for Molecular Electrochemistry, Chemical Reviews. 108 (2008) 2646–2687. doi:10.1021/CR068076M.

[6] T. Akimoto, S. Sasaki, K. Ikebukuro, I. Karube, Refractive-index and thickness sensitivity in surface plasmon resonance spectroscopy, Applied Optics. 38 (1999) 4058. doi:10.1364/ao.38.004058.

[7] P. Pilla, P.F. Manzillo, V. Malachovska, A. Buosciolo, S. Campopiano, A. Cutolo, L. Ambrosio, M. Giordano, A. Cusano, Long period grating working in transition mode as promising technological platform for label-free biosensing, Optics Express. 17 (2009) 20039. doi:10.1364/OE.17.020039.

[8] O. Okhay, S. Zlotnik, W. Xie, K. Orlinski, M.J. Hortiguela Gallo, G. Otero-Irurueta, A.J.S. Fernandes, D.A. Pawlak, A. Weidenkaff, A. Tkach, Thermoelectric performance of Nb-doped SrTiO3 enhanced by reduced graphene oxide and Sr deficiency cooperation, Carbon. 143 (2019) 215–222. doi:10.1016/j.carbon.2018.11.023.

[9] L. Wildling, B. Unterauer, R. Zhu, A. Rupprecht, T. Haselgrübler, C. Rankl, A. Ebner, D. Vater, P. Pollheimer, E.E. Pohl, P. Hinterdorfer, H.J. Gruber, Linking of sensor molecules with amino groups to amino-functionalized AFM tips, Bioconjugate Chemistry. 22 (2011) 1239–1248. doi:10.1021/bc200099t.

[10] A.F. Stalder, G. Kulik, D. Sage, L. Barbieri, P. Hoffmann, A snake-based approach to accurate determination of both contact points and contact angles, Colloids and Surfaces A: Physicochemical and Engineering Aspects. 286 (2006) 92–103. doi:10.1016/j.colsurfa.2006.03.008.

[11] C. Johannes, A. Majcherczyk, Laccase activity tests and laccase inhibitors, Journal of Biotechnology. 78 (2000) 193–199. doi:10.1016/S0168-1656(00)00208-X.

[12] X. Wu, Y. Hu, J. Jin, N. Zhou, P. Wu, H. Zhang, C. Cai, Electrochemical Approach for Detection of Extracellular Oxygen Released from Erythrocytes Based on Graphene Film Integrated with Laccase and 2,2-Azino-bis(3-ethylbenzothiazoline-6-sulfonic acid), Analytical Chemistry. 82 (2010) 3588–3596. doi:10.1021/ac100621r.

[13] A. Jarosz-Wilkołazka, T. Ruzgas, L. Gorton, Amperometric detection of mono- and diphenols at Cerrena unicolor laccase-modified graphite electrode: Correlation between sensitivity and substrate structure, Talanta. 66 (2005) 1219–1224. doi:10.1016/j.talanta.2005.01.026.

[14] B. Haghighi, L. Gorton, T. Ruzgas, L. J. Jönsson, Characterization of graphite electrodes modified with laccase from Trametes versicolor and their use for bioelectrochemical

monitoring of phenolic compounds in flow injection analysis, Analytica Chimica Acta. 487 (2003), 3–14. doi:10.1016/S0003-2670(03)00077-1.

Chapter IV

Electrosynthesis of polydopamine films for electrode biofunctionalization

Most of the content found in this chapter is published in:

- L.C. Almeida, R.D. Correia, A. Marta, G. Squillaci, A. Morana, F. La Cara, J.P. Correia, A.S. Viana, Electrosynthesis of polydopamine films – tailored matrices for laccase-based biosensors, Applied Surface Science. 480 (2019) 979–989, doi:10.1016/j.apsusc.2019.03.015.

4. Electrosynthesis of polydopamine films for electrode biofunctionalization

In this chapter the electrochemical synthesis of biocompatible polydopamine films on carbon electrodes is explored, overcoming problems concerning low reproducibility, stability and electroactivity of chemically synthesized films. A number of techniques, including cyclic voltammetry, ellipsometry, UV-Vis, FTIR and X-ray Photoelectron spectroscopies, goniometry and atomic force microscopy, have been used to fully characterize the modified electrodes. These studies enable to compare the electrochemical, optical, dielectric and permeability properties of films prepared on glassy carbon by chemical and electrochemical synthesis, and to propose a refinement of mechanistic description of electrochemical polymerization, as well as the resulting co-polymeric structure of electrosynthesized polydopamine. It is generally accepted that the Raper-Mason reaction scheme [1] proposed for chemically prepared polydopamine, also describes the electrochemical polymerization, where chains of poly(5,6-dihydroxyindole) are assumed to be the main structural motif (Chapter I, **Figure 1.4**). Distinct electrosynthesis conditions were tested (potentiodynamic growth at different potential sweep rates and number of cycles), aiming the construction of biosensing ePDA matrices with optimized redox responses and ability to robustly immobilize biomolecules, probably through the reaction of their amine groups to the polymer catechol moities. To this end, laccase immobilization is performed on films with distinct chemical properties. The catalytic activity of laccase linked to chemically or electrochemically prepared graphite/PDA electrodes is also evaluated by amperometric and spectroscopic detection of ABTS, a model substrate.

4.1. Electrosynthesis and surface characterization of polydopamine films on glassy carbon electrode

Electrochemical synthesis of polydopamine was carried out potentiodynamically in a wide potential range (between −0.6 and 0.8 V) in order to have a clear picture of the redox processes occurring during dopamine polymerization. The cyclic voltammograms recorded during polymer growth for a selected number of cycles are shown in **Figure 4.1**, using a faster and slower potential sweep rate (20 and 200 mV s^{-1}). Two distinct quinone/hydroquinone (Q/QH_2) electrochemical conversions are observed at both sweep rates, whose intensity decreases during polymerization due to the formation of a poorly conducting polymeric phase. This behavior is more pronounced at 20 mV s^{-1}, where more material is deposited after each polymerization cycle. Firstly, as illustrated in **Figure 4.2**, dopamine (DA) in the open form is

oxidized to dopaminequinone (DAQ) by a two-electron two-proton conversion [2], displaying anodic peaks at *ca.* 0.6 and 0.4 V at 200 and 20 mV s^{-1}, respectively. On the subsequent cathodic scan, the corresponding reduction of DAQ is observed at *ca.* −0.1 V, only when a fast potential scan rate is used. The irreversible DA oxidation at 20 mV s^{-1} clearly proves the occurrence of fast chemical steps that consume the electrogenerated DAQ molecules, commonly attributed to the intramolecular cyclization, with the formation of leucodopaminochrome (LDAC), known to occur at neutral or basic conditions [3]. When sweeping the potential up to 0.8 V, where DAQ is formed, the chemically generated LDAC is concomitantly oxidized to dopaminechrome (DAC), which allows the observation of its reduction peak at the first cathodic scan, either at 200 mV s^{-1} (−0.44 V) or at 20 mV s^{-1} (−0.41 V). On the second anodic scan, the LDAC oxidation process is observed for the first time at both 200 mV s^{-1} (−0.16 V) and 20 mV s^{-1} (−0.10 V) potential scans. The significant negative potential shift of this redox process regarding that of DAQ/DA is explained by the strong electron-donating character of the nitrogen atom linked to the catechol ring [4,5] that happens as a consequence of the intramolecular cyclization, allowing a clear distinction of these two types of Q/QH_2 processes.

Since a potentiodynamic method was used to polymerize DA, kinetic information about the two identified Q/QH_2 processes can also be deduced. Contrary to the redox behavior of DAQ/DA, the indoline forms DAC/LDAC oxidize and reduce reversibly, even at slow sweep rates (**Figure 4.1b**). This reflects the relative stability of these latter species in solution, which do not undergo fast transformations during the electropolymerization process. Instead, the continuous cycling at 200 mV s^{-1} results in a current increase of the DAC/LDAC redox peaks until the 5th cycle is reached (**Figure 4.1c**), which indicates the accumulation of DAC/LDAC stable monomers. Indeed, the appearance of an intense orange color was observed near the electrode surface during the electropolymerization processes. To investigate this fact, we have analyzed the electrolyte solution by UV-Vis spectroscopy after 3, 6 and 9 potential cycles. As shown in **Figure 4.3a**, the typical absorption band of DAC [6,7] can be clearly depicted at a maximum wavelength of 472 nm, proving that an excess of this molecule is present near the working electrode after each electropolymerization assay. In fact, the amount of generated DAC increases from the 3rd to the 9th potential cycle, undoubtedly confirming its accumulation near the electrode surface and, therefore, the existence of a bottleneck step in the electropolymerization mechanism. Most recent publications on PDA potentiodynamic synthesis do not highlight these observations [8–10], most probably because at slow sweep rates (*e.g.* 20 mV s^{-1} or lower) the blocking effect of the thick and poorly conductive film precludes the observation of DAC/LDAC redox conversion.

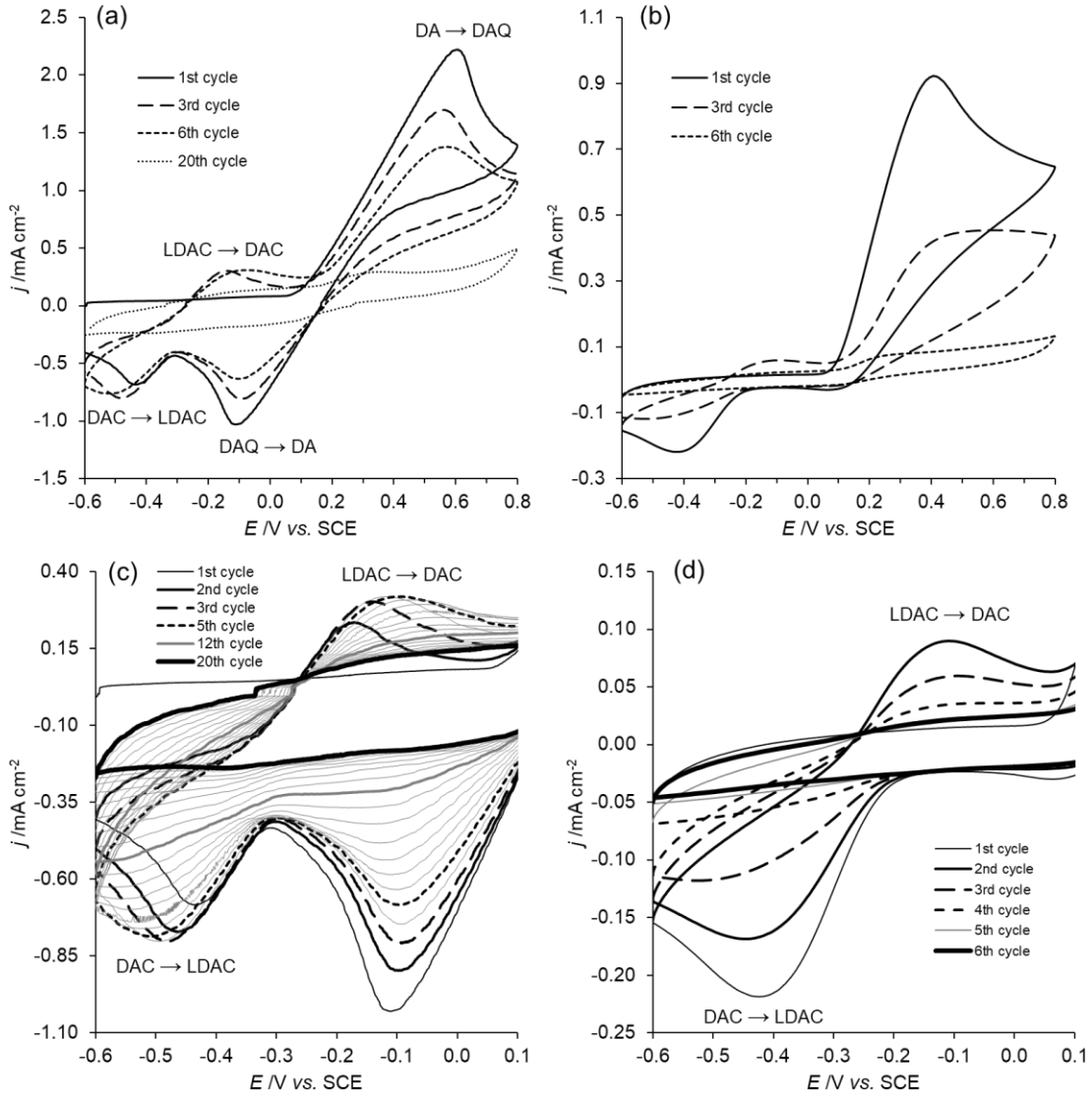

Figure 4.1: Potentiodynamic growth of polydopamine at 200 mV s^{-1} (a) and 20 mV s^{-1} (b) in a deoxygenated CPB pH=7.0 solution containing 5 mM of dopamine. Detailed potential window of potentiodynamic growth at 200 mV s^{-1} (c) and 20 mV s^{-1} (d).

After the 5th potential cycle at 200 mV s^{-1} (**Figure 4.1a** and **4.1b**), the current of DAC/LDAC redox peaks decrease slowly due to the charge transfer blocking of a growing polymer, and not because DAC is being incorporated into the polymer structure (**Figure 4.2B**). At 20 mV s^{-1}, the same behavior is observed right from the 2nd potential cycle, since more polymeric material is deposited upon each potential cycle (**Figure 4.1b** and **4.1c**). To further investigate the accumulation of DAC/LDAC molecules, we have recorded the UV-Vis spectra of the collected electrolyte solutions over an extended period (**Figure 4.3b**). DAC displays a slow concentration decay at neutral buffer over the course of a 30 min period. Although thermodynamically favorable, isomerization of DAC to 5,6-dihydroxyindole (DHI) requires an

activation step with the possible formation of a dopamine-methide intermediate, which is known to be slow at room temperature and enzymatically catalyzed in living systems [3,11,12]. This isomerization step is commonly reported in either chemical [3,13] or electrochemical PDA polymerization mechanisms [8–10], however, we have found that it is less important within the time scale of short electropolymerization processes. As depicted in **Figure 4.3c**, by limiting the potential cycling between −0.6 and 0.0 V, upon electrogeneration of LDAC (using a larger potential window), the redox conversion of DAC/LDAC is clearly depicted for 20 potential cycles, indicating that a polymeric phase (**Figure 4.2B**) should not be formed quantitatively from DAC/LDAC monomers. We attributed the slight decrease of peak currents to the diffusion of LDAC and DAC from the vicinity of the electrode towards the bulk solution. In addition, due to the slow conversion of DAC to DHI, it was also observed a more pronounced decrease in the reduction peak regarding its oxidation counterpart. Since DAC is not significantly incorporated into the polymeric structure during electrosynthesis of ePDA, it is foreseen that electrochemical growth will produce structurally different matrices than chemically synthesized ones, especially those prepared with long times.

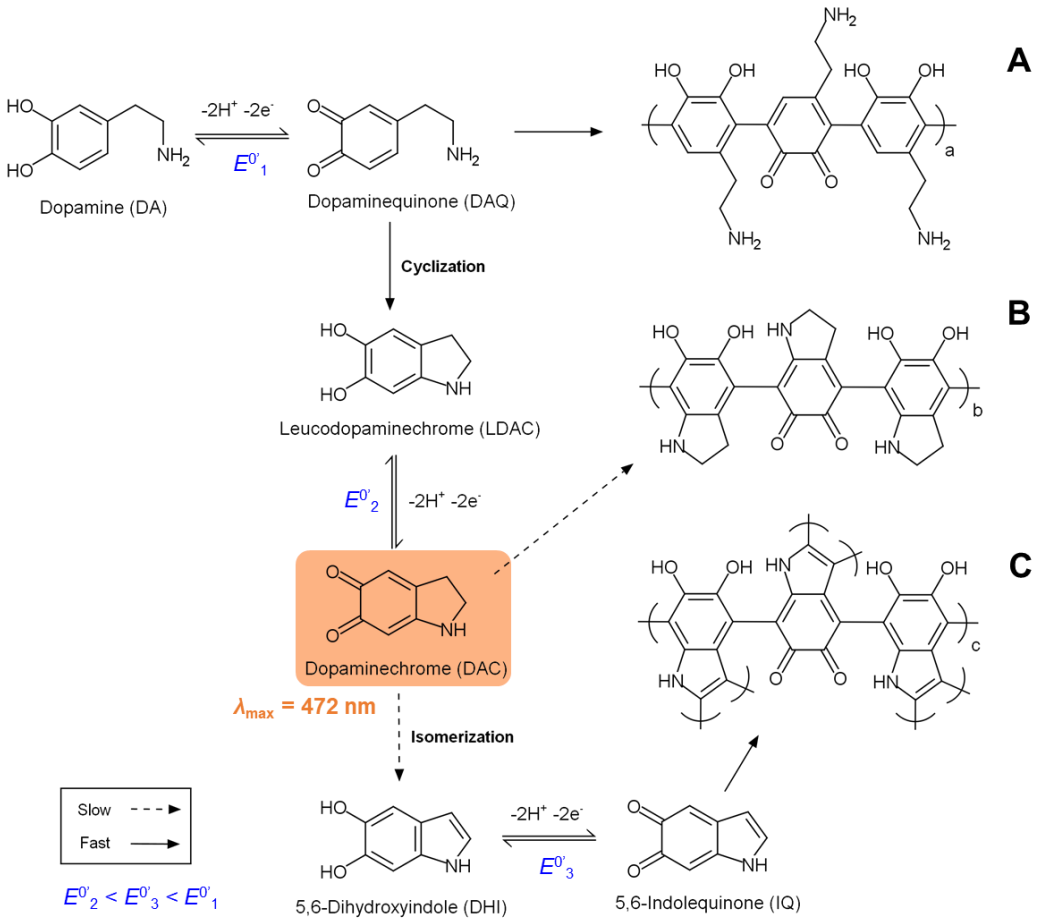

Figure 4.2: Proposed mechanism for the electropolymerization of dopamine. The final polymer will contain different proportions of type A (dopamine in the open form), B (indoline type) and C chains (indole type), where a > c > b.

The absence of clear redox peaks corresponding to DHI electrochemical activity on the cyclic voltammograms (**Figure 4.1**) is an additional characteristic of ePDA potentiodynamic synthesis. This redox process should occur at intermediate potential values between DAQ/DA and DAC/LDAC conversions [5,14], due to the poor electrodonating effect of the pyrrole ring. Since conversion from DAC to DHI was proven to be slow, the produced isomerization products must exist in a quite limited amount. In fact, IQ/DHI molecules did not accumulate in a sufficient extent to be detected during the electropolymerization process, as confirmed by UV-Vis spectroscopy (**Figure 4.3a**). Summarizing our evidences and the consulted studies, we suggest the direct polymerization of open-chain dopamine molecules as the main electrosynthesis pathway (**Figure 4.2A**).

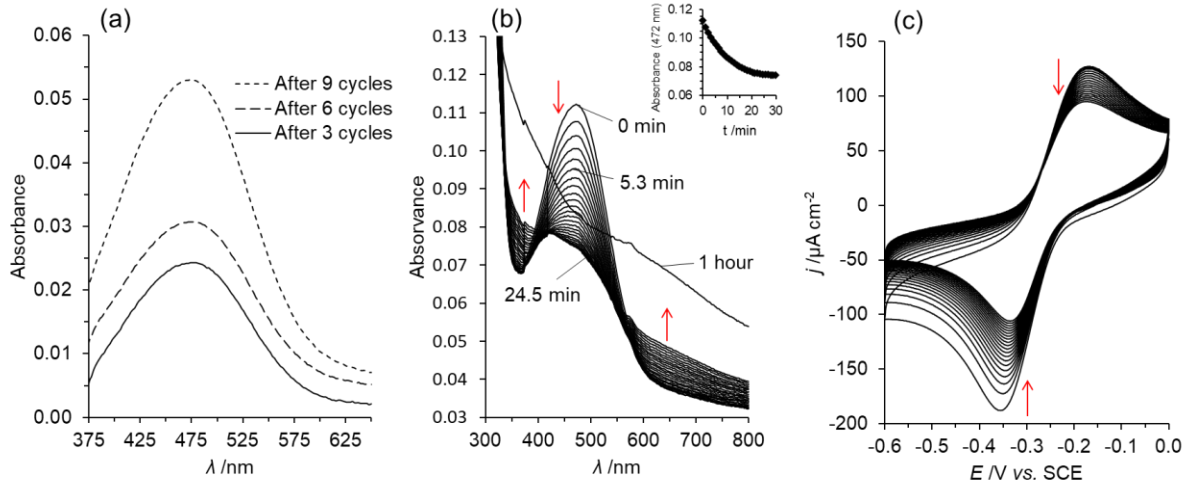

Figure 4.3: UV-Vis spectra of the collected electrolyte solution (750 µL) near the working electrode after potential cycling at 200 mV s^{-1}, between −0.6 and 0.8 V (a). Time-dependent UV-Vis spectra of the collected electrolyte solution after 20 potential cycles at 200 mV s^{-1} between −0.6 and 0.8 V. Inset shows the absorbance value at 472 nm for 30 min (b). Cyclic voltammograms in a 5 mM dopamine CPB pH 7.0 solution showing the redox conversion DAC/LDAC (20 cycles at 200 mV s^{-1}) in a narrowed potential window (−0.6 to 0.0 V), after 2 cycles between −0.6 and 0.8 V (c).

Figure 4.4 shows the electrochemical response of the synthesized ePDA films on glassy carbon electrodes, investigated at several potential sweep rates in a monomer-free CPB pH 4.6 solution (same electrolyte selected for the enzymatic catalytic assays). The bulged shape of the voltammograms is typical for polymers where the charge delocalization along the chains takes place over segments with many different lengths. Therefore, the electrochemical response of the films is dominated by the formation of charge carriers by oxidation and its extinction by reduction of the polymer chains backbone, over a large potential window (*ca.* -0.20 to 0.25 V), due to the multitude of polymeric segment lengths. In addition to the common charge/discharge behaviour of the delocalized regions of the polymer, the films also have functional groups that

undergo electrochemical transformations. The films are indeed enriched with Q/QH_2 groups, exhibiting a major redox process at $E^I_{1/2}$ = 0.28 V, with a potential peak separation of *ca.* 0.09 V. The linear relationship between oxidation and reduction peak currents and the potential sweep rate (inset of **Figure 4.4**) confirms the charge-controlled redox processes of ePDA films, as well as the lower peak potential separation when compared to the diffusion-controlled redox response of 1 mM dopamine at bare GC electrode (ΔE_p = 0.25 V) [15]. The most intense and well define process ($E^I_{1/2}$) matches the redox potential value of a Q/QH_2 group without strong electron-donating substitutions. For this reason, it is ascribed to polymeric chains of dopamine moieties, contributing with primary amine groups to the ePDA structure. It is expected that dopamine molecules are linked by the 3 and 6 positions of the phenolic ring (**Figure 4.2A**), while retaining their catechol electroactivity. The other redox conversion process of ePDA, detected at a lower potential ($E^{II}_{1/2}$ = 0.12 V) and overlapping polymer backbone doping/undoping as discussed above, is also consistent with the presence of Q/QH_2 groups substituted with slightly electron-donating groups. Thus, the redox conversion of a small amount of IQ/DHI originated from the slow isomerization of DAC (**Figure 4.2C**) should also be considered. In fact, the potential value of $E^{II}_{1/2}$ is in perfect agreement with the redox potential of poly(5,6-dihydroxyindole) [16]. PDA electrosynthesis was already performed using noble metals as working electrodes [8–10], however, the generated films do not show well-defined redox peaks precluding a clear identification of different Q/QH_2 moieties. In addition, in **Figure 4.4** only weak and broad bands can be observed below $E^{II}_{1/2}$, agreeing with the difficulty of incorporating indoline-type species into the polymeric structure (**Figure 4.2B**), even for the prolonged electropolymerizations. In agreement with the previous discussion, polymeric chains of DAC/LDAC seem to represent the smallest fraction of polydopamine structure.

The surface coverage of electroactive Q/QH_2 groups was estimated for the main ePDA redox process (I_a), through the slopes shown on **Figure 4.4** insets, assuming a two-electrons electrochemical conversion [2,17]. **Table 4.1** summarizes relevant data retrieved from the electrochemical and non-electrochemical characterization of the modified electrodes, namely Q/QH_2 coverage, refractive index, thickness and roughness. Regarding electrosynthesized films, a decrease of the number of electroactive sites, as revealed by the Q/QH_2 coverage values, is observed with the increment of polymerization cycles. This decrease in electroactivity also correlates with an increase in film thickness as estimated by *ex situ* ellipsometric measurements, using a three-layer model as reported elsewhere [15]. This behavior can be explained by a lower

accessibility to the electroactive moieties on thicker polymeric phases, or/and by an increase in the disorder of the polymeric structure, yielding a less conductive film. Indeed, a decrease of refractive indexes is also verified with film thickening, which is consistent with the formation of less dense and branched polymer as electropolymerization develops. For example, the ePDA film grown at 20 mV s^{-1} with 6 potential cycles, with an estimated thickness of 33 nm, displays the lowest refractive index amongst all electrosynthesized films (n = 1.5), indicating a high degree of branching for the longest electropolymerization process. Since IQ/DHI moieties are known to dimerize through several positions of the indole ring [18], their incorporation into the polymer structure, may result in higher branching, justifying the lower densities of thicker ePDA films. Likewise, fast polymerizations favor the formation of linear dopamine chains resulting in a more organized and denser structure.

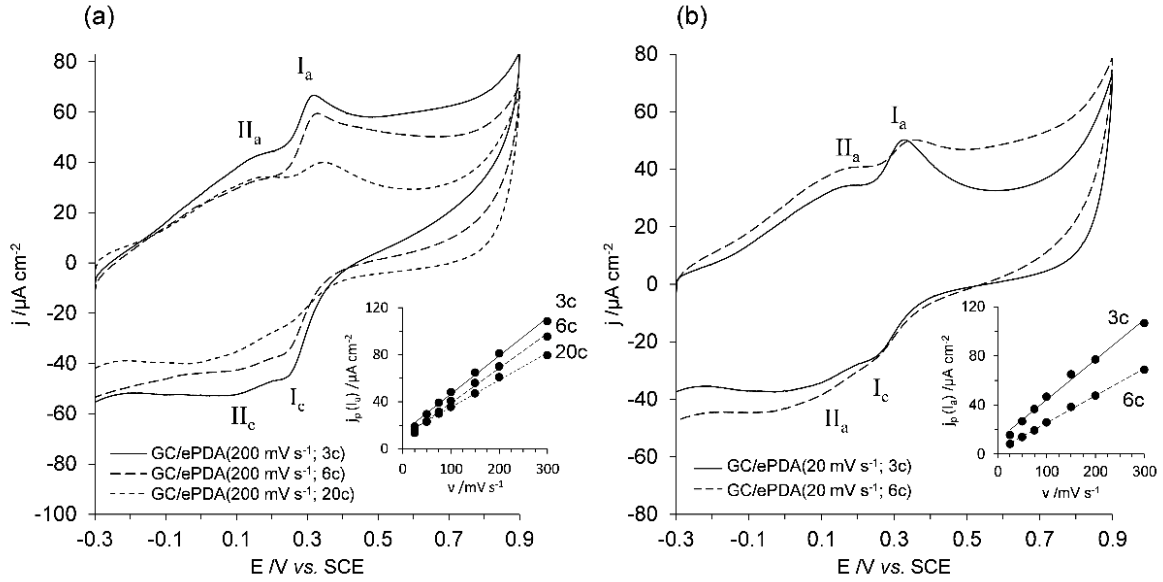

Figure 4.4: Cyclic voltammograms at 50 mV s^{-1} of GC/ePDA electrodes in deoxygenated CPB pH=4.6 buffer, electrosynthesized at 200 mV s^{-1} **(a)** and 20 mV s^{-1} **(b)**. Figure insets show the linear relationship between the oxidation peak (I_a) current density and potential sweep rate.

It is worth to highlight that thin films grown potentiodynamically in just 84 s (200 mV s^{-1}; 6c) display a similar thickness than those prepared chemically for 1 h (3 nm [15]) and more importantly exhibit a much higher Q/QH_2 coverages (4.7×10^{-11} *versus* 2.2×10^{-11} mol cm^{-2} for PDA (1h) [15]). This behavior confirms the influence of polymerization method on the final properties of the films. If polydopamine films are to be employed as biosensor matrices [15,19,20], a high number of available quinone groups should be advantageous for the covalent immobilization of biomolecules.

Table 4.1: Surface coverage (Γ^1), water contact angle (θ_{WCA}), refractive index (n_{ePDA}), optical thickness (L_{ePDA}), and root mean square roughness (R_q, 2×2 μm^2) of GC modified with polydopamine films. Multiangle ellipsometry is carried out *ex situ* at 60° and 70°, assuming a fixed extinction coefficient (k = 0.4 [15]).

Films	$\Gamma^1 \times 10^{11}$ /mol cm^{-2}	θ_{WCA} /°	n_{ePDA}	L_{ePDA} /nm	R_q/nm
ePDA (200 mV s^{-1}; 3c)	4.8	24 ± 1	1.9	2.1	–
ePDA (200 mV s^{-1}; 6c)	4.7	29 ± 3	1.9	2.9	4.4
ePDA (200 mV s^{-1}; 20c)	2.5	35 ± 1	1.7	18.7	4.6
ePDA (20 mV s^{-1}; 3c)	3.8	23 ± 2	1.8	16.6	5.1
ePDA (20 mV s^{-1}; 6c)	2.6	25 ± 2	1.5	33.0	7.5

The morphological characterization of the electrosynthesized films over GC electrodes was carried out by *ex situ* AFM (**Figure 4.5**). Uniform and highly adherent granular polymers, covering the electrode surface were obtained for all the conditions tested. It was observed that very thin films (*ca.* 3 nm) electrochemically or chemically synthesized with strikingly different electrochemical properties, display a similar roughness (R_q= 4.4 *versus* 4.0 nm, respectively), highly dependent on the R_q of the underlying electrode surface (R_q = 4.9 nm). To ensure that ePDA fully covers GC electrodes, the thinnest film (200 mV s^{-1}; 3c) was also grown on atomically flat HOPG surface and the topographical images are provided in **Figure 4.5g**–**h**. Although only 3 potential cycles were performed at a fast scan rate, the HOPG surface is totally covered with granular and polymeric material (**Figure 4.5h**), and thus a complete coverage is also assumed in the case of GC. The highest R_q values (**Table 4.1**) were obtained for the films synthesized with the lowest potential scan rate, corroborating the thickening of the films with the increasing number of potential cycles and the presence of a less dense polymers. In contrast, films prepared with a faster sweep rate (200 mV s^{-1}; 6 and 20 cycles) exhibit comparable roughness independently on their thickness, as expected for more compact films.

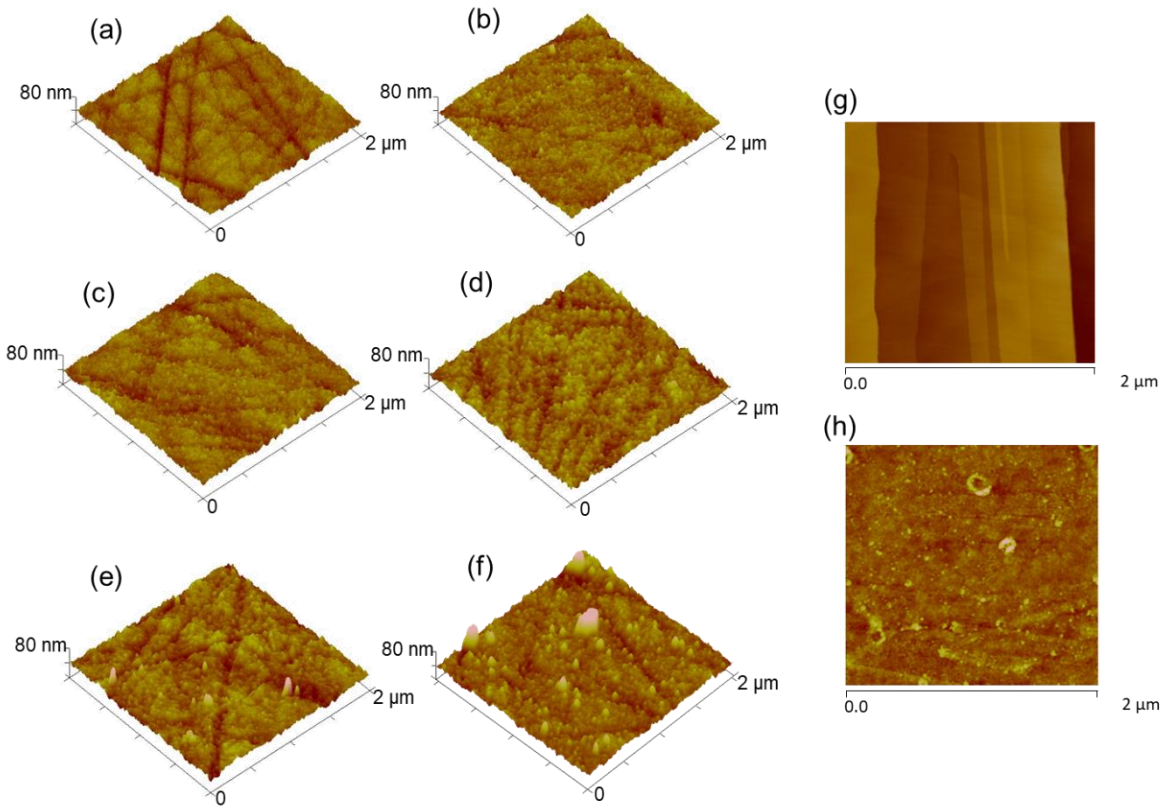

Figure 4.5: AFM 3D images of bare **(a)** and modified GC electrodes with PDA(1h) **(b)**, ePDA(200 mV s^{-1}; 6c) **(c),** ePDA(200 mV s^{-1}; 20c) **(d),** ePDA(20 mV s^{-1}; 3c) **(e)**, and ePDA(20 mV s^{-1}; 6c) **(f)**. AFM topographic images (Z = 20 nm) of bare HOPG **(g)** and HOPG/ePDA(200 mV s-1, 3c) **(h)**.

The wettability of the films was obtained by water contact angle measurements (**Table 4.1**). It was found that the electrochemically synthesized films exhibit higher hydrophilicity than chemically prepared polymers, independently on their thickness. One possible explanation would be the presence of a vestigial amount of carboxyl groups generated during electropolymerization, with the corresponding loss of amine moieties. This mechanism has been reported for dopamine polymerization in the presence of strong oxidants, such as $NaIO_4$, with the consequent formation of more hydrophilic films that those generated in basic aerated solutions [21]. To further investigate the structural differences among PDA and ePDA films, XPS and reflectance IR spectroscopy were used. Polymeric coatings were grown on Au substrates for XPS analysis to avoid the contribution of large background signals from C and O regions, characteristic of GC electrodes. It was found that PDA and ePDA had atomic ratios of: 0.216 and 0.219 for O/C and 0.104 and 0.088 for N/C, respectively. Although, both polymers exhibit a very similar composition, the slightly differences in the ratios agrees with the hypothesis raised above, where a residual substitution of amine functions by carboxyl groups occurs. In addition, the O/C ratio is much lower than that reported for superhydrophilic

degraded PDA (*ca.* 0.3), that underwent extensive oxidative *o*-quinone cleavage [21], supporting the presence of polymers mainly composed of intact catechol groups.

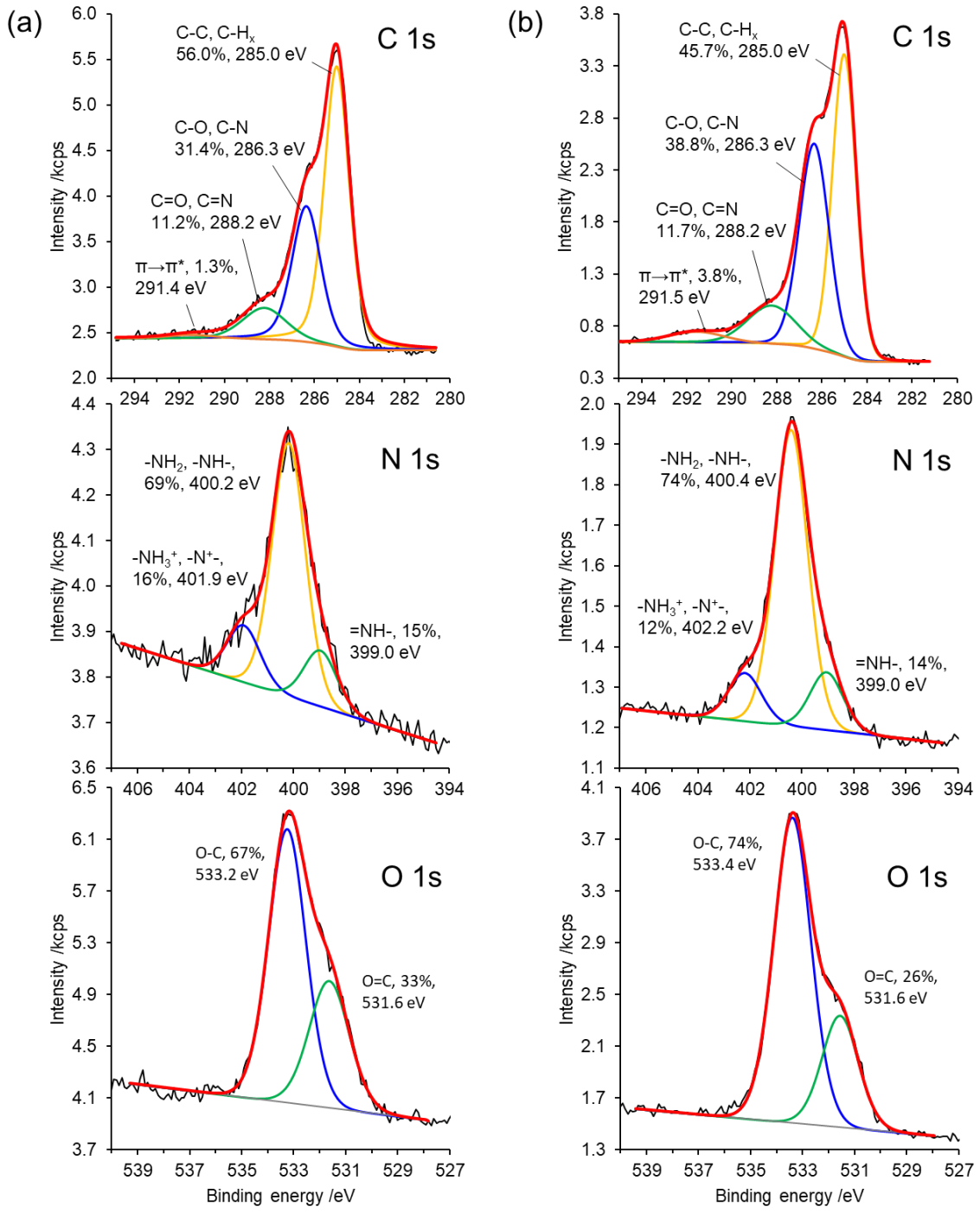

Figure 4.6: XPS spectra of C 1s, N 1s and O 1s regions of Au/ePDA(200 mV s^{-1}; 20c) (a) and Au/PDA(24h) (b) modified electrodes. Peak binding energy assignments and functional group contents are also presented.

The spectral regions of C 1s, N 1s and O 1s presented in **Figure 4.6** show structural differences between chemically and electrochemically synthesized films. The C 1s signal was

deconvoluted into 4 peaks attributed to the hydrocarbon skeleton (C-C, C-H_x), heteroatoms (C-O, C-N), aromatic components (C=O, C=N) and to the graphitic π→π* transition [13], all expected to exist in a polydopamine structure composed by dopamine and its derivatives (**Figure 4.2**). However, chemically synthesized PDA displayed a higher signal contribution from the C-O/C-N bond (*ca.* 39 %) when compared to the potentiodynamically grown film (*ca.* 31 %), indicating a higher content of cyclic amine groups in chemically prepared films. This difference is in agreement with the small incorporation extent of DAC/LDAC chains in the polymer matrix expected for the electrochemical polymerizations. At the spectral region of N 1s, three main peaks were deconvoluted, displaying common binding energies of amines. The lowest energy peak (*ca.* 399 eV), assigned to a deprotonated pyrrolic nitrogen [22], strongly indicates the presence of indole moieties in both types of polymers, originated from IQ/DHI monomers. The other two nitrogen peaks are characteristic of an aliphatic contribution (-NH_2, -NH-) and its respective ammonium state contribution (-NH_3^+, -N^+-) [23,24]. It is clear that ePDA film has less aliphatic amines and a slightly higher fraction of ammonium state, which is in perfect agreement with a higher amount of linear dopamine chains when compared with PDA film. From the analysis of O 1s spectral region, it was found that the electrochemical preparation method yields a polydopamine film with a higher amount of stable quinones (C=O), while the chemical synthesis favored the presence of hydroquinone groups (C-OH). This is of particular interest for the straightforward covalent attachment of biomolecules on electrogenerated polymers. Again, there might be also some contribution of carboxyl functionalities on ePDA films, but as mentioned above this must be vestigial, since the overall ratio O/C for both films are close to the expected for polydopamine films.

FTIR characterization was also carried out using highly reflective Au surfaces. The data presented in **Figure 4.7** reveals noticeable differences in the molecular structures of the synthesized polydopamine films. The most prominent differences are found below 1800 cm^{-1} where eight distinct IR absorption bands were assigned. Two intense peaks were observed in PDA spectrum centered at 1593 and 1513 cm^{-1}, corresponding to the asymmetric and symmetric C=C stretching modes of the benzene ring, respectively [25,26]. In fact, these are doubly degenerated modes characteristic of a dihydroxyphenol ring, appearing also in FTIR spectra of catechol [27], dopamine [26,28], indoline [29] and indole [30], which suggest that chemically prepared polydopamine contains the aromaticity of the catechol ring identical to its monomers. Remarkably, the spectrum of ePDA shows a suppressed absorption at 1513 cm^{-1}, displaying only the doubly degenerated asymmetric mode at 1635 and 1593 cm^{-1}. We assign this disappearance to an effective C-C coupling between dihydroxyphenolic rings of dopamine

(**Figure 4.2A**), resulting in the formation of a linear and conjugated polymeric backbone similar to poly(*p*-phenylene) [31] and polycatechol-based films (without amine moieties) [27,32,33]. In addition, the indolic component of the chemically grown PDA structures can be identified by the presence of peaks at 1450 and 1361 cm^{-1}, corresponding to C=N and CNCC vibrational modes, characteristic of indole and polyindole [13,30]. As mentioned above, the extensive isomerization of DAC to DHI in the chemical polymerization is therefore consistent with the sharpening of such IR bands at PDA spectrum, whereas ePDA structure have a less important indolic component. In addition, an ill-defined C=O vibrational mode [21,34] at 1725 cm^{-1} can be denoted for ePDA film, that could be assigned to the residual presence of carboxyl groups. Below 1350 cm^{-1} two IR absorptions at can be depicted in ePDA spectrum, at 1304 and 1277 cm^{-1}, which may be due to CH_2 wagging mode from open-chained dopamine and to the phenolic C-OH stretching mode, respectively [28]. PDA spectrum only shows the last peak, clearly demonstrating that the use of a chemical or electrochemical synthetic method results in films with distinct functional groups composition, as suggested by the aforementioned characterizations.

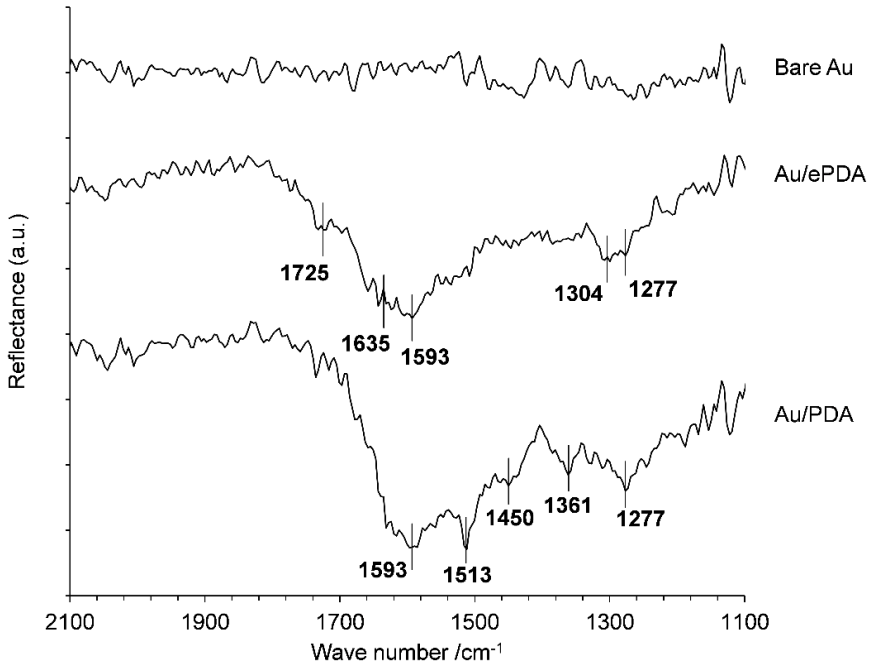

Figure 4.7: FTIR reflectance spectra of bare gold, Au/ePDA(20 mV s^{-1}; 9c) and Au/PDA(24h) electrodes.

Aiming to employ these films as electrochemical transducers, the charge transfer properties of the modified electrodes were accessed using $Fe(CN)_6^{4-}/Fe(CN)_6^{3-}$ redox probe, as presented in **Figure 4.8**. As soon as the GC electrode is covered with a thin layer of PDA(1h), a slight hinder effect is observed (**Figure 4.8a**), as expected for a poorly-conducting layer.

Remarkably, thin ePDA films of comparable thickness (< 3 nm, **Figure 4.8b**) display the opposite effect characterized by a slight increment of the anionic probe peak currents. This behavior points to a small increase of the electroactive area through the formation of a non-isolating film. This finding shows that thin ePDA films are better electrochemical transducers for $Fe(CN)_6^{4-}/Fe(CN)_6^{3-}$ redox probe when compared with PDA films of the same thickness. It was also found that thicker PDA(14h) film (*ca.* 11 nm) [15], synthesized by oxygen-driven dopamine oxidation, significantly hinders the redox process of the $Fe(CN)_6^{4-}/Fe(CN)_6^{3-}$ (**Figure 4.8a**). In contrast, thicker ePDA(20 mV s^{-1}; 3c) film (*ca.* 17 nm), only partially blocked the redox signal of the anionic probe in use (**Figure 4.8c**), thus highlighting a clear benefit of using electrosynthetic method. Electrosynthesized films at 200 mV s^{-1}, 20 cycles (18 nm) and 20 mV s^{-1}, 6 cycles (33 nm) totally hinder the electrochemical process (**Figure 4.8c**). The observed broad peaks correspond to the polymer redox processes, and therefore, these modified electrodes were not used as matrices for further biosensing studies with electrochemical transduction.

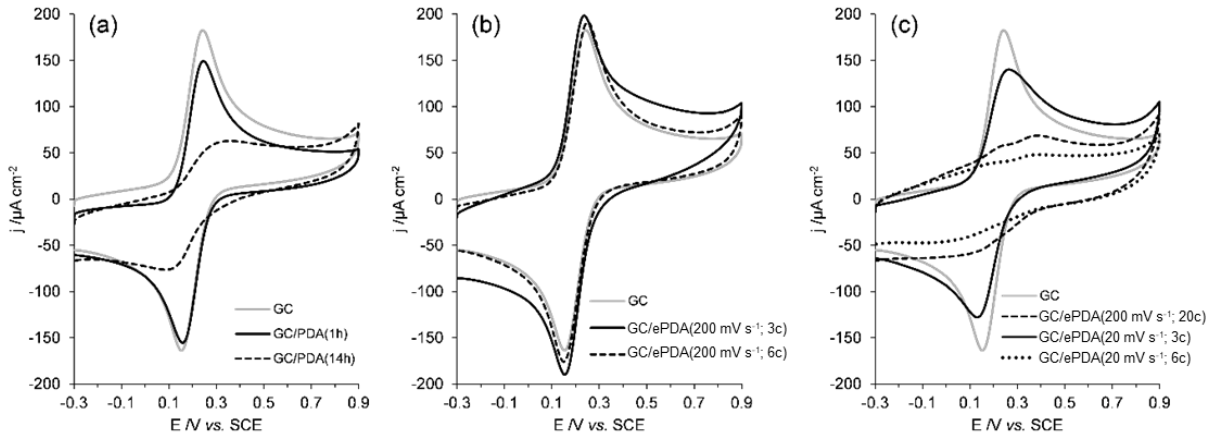

Figure 4.8: Cyclic voltammograms of GC electrode before and after polydopamine deposition by chemical and electrochemical methods, recorded at 50 mV s^{-1} in a 1 mM $K_3Fe(CN)_6$ and 0.25 M KNO_3 solution; chemically deposited PDA films are shown in panel **(a)**, electrochemically deposited thin ePDA films (< 3 nm) on panel **(b)** and thick ePDA films (17 – 33 nm) on panel **(c)**.

4.2. Catalytic activity of immobilized laccase on electrochemically and chemically prepared polydopamine films

The applicability of polydopamine as supporting interface for biomolecules was evaluated through the catalytic performance of graphite/ePDA/Lac electrodes towards ABTS detection. Laccase was immobilized on ePDA(200 mV s^{-1}; 6c), ePDA(20 mV s^{-1}; 3c) films, and also on chemically synthesized PDA(1h) and PDA(14h) for comparison, on cheap and disposable graphite electrodes. The immobilization procedure consists on the incubation of polydopamine modified electrodes in a laccase preparation, with a measured catalytic activity of 345.5 U mL^{-1} for ABTS oxidation (420 nm), for 3 h at room temperature. An extensive rinsing step after enzyme incubation was carried out to ensure that the measured activity only relates to enzyme firmly immobilized in the polymer. In the presence of laccase, ABTS is oxidized and the reduced enzyme is regenerated by the concomitantly reduction of oxygen to water, as represented schematically in **Figure 4.9a** [35]. This catalytic behavior can be observed by cyclic voltammetry in successive additions of ABTS to the electrolyte solution using, for instance, the ePDA(200 mV s^{-1}; 6c) film as immobilization matrix of laccase (**Figure 5.9b**). Sigmoidal shaped voltammograms develop with increasing reduction currents upon each addition of ABTS substrate in a micromolar range, while its corresponding anodic process is not quantitively observed. The immobilized laccase is then catalyzing the oxidation of ABTS, depleting the electrode vicinity very rapidly, which avoids its electrochemical oxidation. At the same time, the $ABTS^{\bullet+}$ radical accumulates near the electrode surface enabling its detection by electrochemical reduction. This result confirms the robust immobilization of active enzymes on biocompatible polymer, that resists to potential cycling within the redox conversion of the polymer.

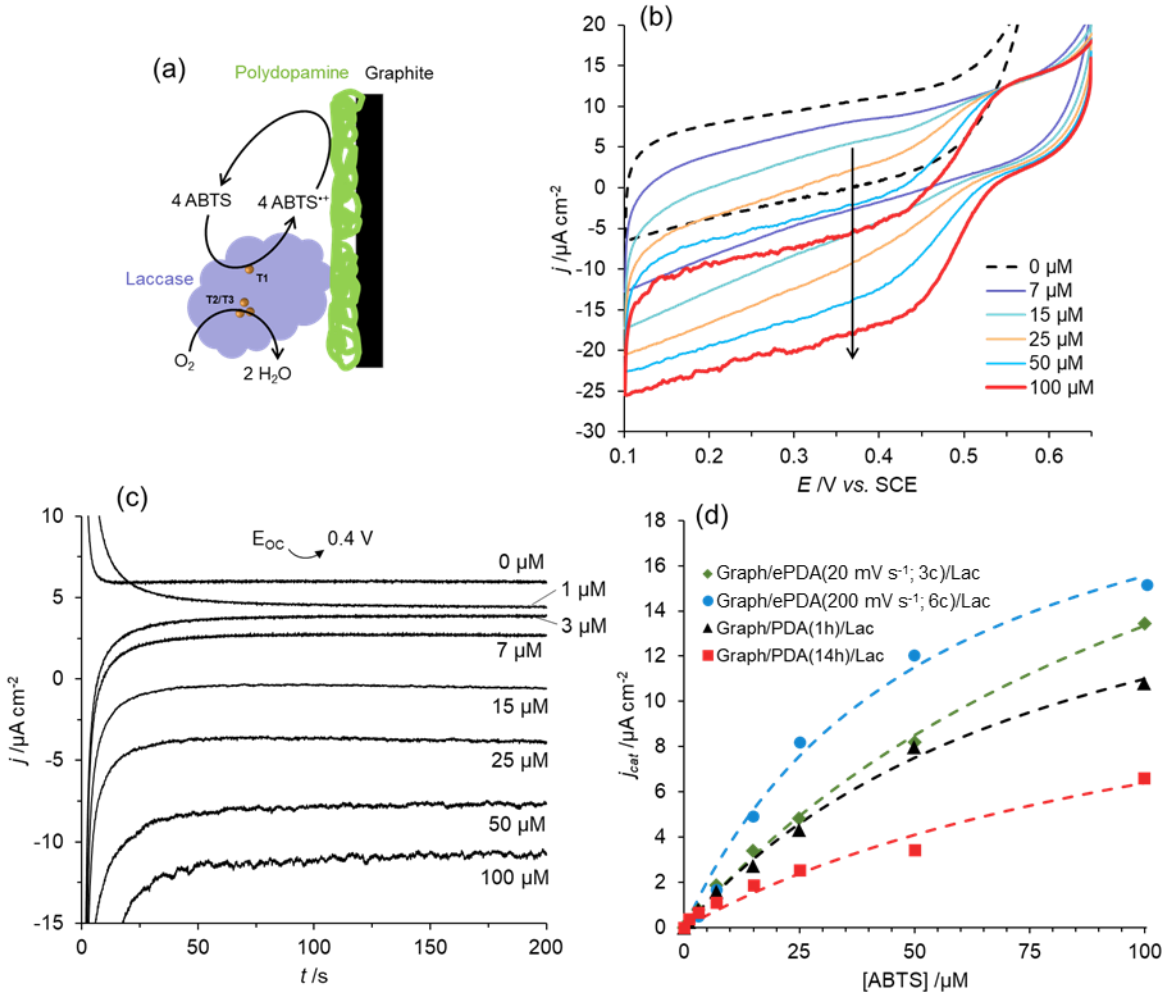

Figure 4.9: Schematic illustration of ABTS enzymatic oxidation by the immobilized laccase in the presence of oxygen and electrochemical detection of oxidized form ($ABTS^{\bullet+}$) by the electrode surface **(a)**; Cyclic voltammetric **(b)** and chronoamperometric **(c)** responses of graphite/ePDA(200 mV s^{-1}; 6c)/Lac to different additions of ABTS; Catalytic current densities ($j_{cat} = |j - j_b|$) *versus* ABTS concentration, obtained by chronoamperometric assays (0.4 V) of graphite modified with ePDA(200 mV s^{-1}; 6c)/Lac, ePDA(20 mV s^{-1}; 3c)/Lac, PDA(1h)/Lac and PDA(14h)/Lac **(d)**. Experiments were performed in oxygenated CPB pH 4.6.

Chronoamperometric assays were performed for the distinct modified electrodes, at an optimized pH for the enzymatic oxidation of ABTS [35], applying a potential of 0.4 V (reduction potential value for ABTS on bare GC electrode [15]) for 200 s to allow its detection on the electrode surface (**Figure 4.9b**). All the modified electrodes showed a decrease in the cathodic current upon ABTS additions, as depicted in **Figure 5.9d**. It was verified that the catalytic responses follow a Michaelis-Menten behavior (*cf.* **Equation 3.1**, chapter III), allowing to estimate the analytical parameters summarized in **Table 4.2**. There is a clear difference between the catalytic activity of laccase immobilized on thin ePDA(200 mV s^{-1}; 6c) and PDA(1h) films. Higher catalytic currents, sensitivity and apparent Michaelis Menten

constant (K_M^{app}) were achieved for electrosynthesized film (200 mV s^{-1}; 6c), which can be correlated with a facile electron transfer through the interface, greater electroactivity and structural order of ePDA compared to PDA. Also, in the case of thicker films, ePDA(20 mV s^{-1}; 3c) polymer enabled a much better catalytic response than the PDA (14h) film, accordingly to their electrochemical properties. Comparing the four modified electrodes, the best performance was obtained for the thin electrochemically synthesized film. Its sensitivity value of 342 mA M^{-1} cm^{-2} obtained from the linear range (1 – 25 μM) is superior to that reported for modified gold electrodes [35] and close to modified carbon paste electrodes [36] where the enzyme load is typically very high. Indeed, an estimation the amount of active enzyme by spectrophotometric assays was performed and the result presented in **Table 4.2**. The modified graphite electrodes were placed inside the UV-Vis cuvette in 500 μM ABTS solution (CPB pH 4.6), and the formation of oxidized ABTS was followed at 420 nm. Average values of 6.5 ± 0.9 U cm^{-2} were obtained for laccase immobilized on ePDA(200 mV s^{-1}; 6c), ePDA(20 mV s^{-1}; 3c) and PDA(14h), whereas for PDA(1h) electrode, the enzymatic activity was lower 1.6 ± 1.4 U cm^{-2}. The data agrees with the observed catalytic performances and is also related to the amount of Q/QH_2 estimated by electrochemistry, which is lower for the thin PDA (1h).

Table 4.2: Amperometric response parameters towards ABTS oxidation of graphite modified electrodes with laccase and polydopamine films synthesized by chemical (PDA) or electrochemical methods (ePDA): apparent Michaelis-Menten constant (K_M^{app}), saturation current density (j_{max}), sensitivity of the linear range (1 – 25 μM) and respective R^2.

Modified graphite electrode	K_M^{app} /μM	j_{max} /μA cm^{-2}	Sensitivity /mA M^{-1} cm^{-2}	R^2	Laccase activity / U cm^{-2}
PDA(1h)/Lac	87	21	158	0.9959	1.6 ± 1.4
PDA(14h)/Lac	128	14	105	0.9942	
ePDA(20 mV s^{-1}; 3c)/Lac	79	21	228	0.9925	6.5 ± 0.9
ePDA(200 mV s^{-1}; 6c)/Lac	54	24	342	0.9935	

By electrochemical methods it is thus possible to grow electroactive and biocompatible polydopamine films on carbon surfaces. Quinone groups should provide the anchoring points for enzyme attachment, whereas the structural regularity and charge transfer properties enable the electrochemical detection of enzymatically oxidized ABTS. Both factors are crucial to better tune the catalytic response of the modified electrode.

4.3. Conclusions

In summary, it is demonstrated that electropolymerization of dopamine is an advantageous route to tune the chemical structure and thickness of polydopamine films, which dictate their electrochemical and optical properties. Such fine control enables the improvement of biosensing performances regarding the widespread chemical polymerization in alkaline medium. The detected excess of orange indoline type intermediaries (DAC/LDAC) during electropolymerization process allowed to identify a crucial bottleneck step. We propose that electropolymerization favors the formation of linear chains of dopamine in the open form, with a quite limited incorporation of branched 5,6-dihydroxyindole chains, in agreement with the XPS and FTIR structural analysis of the prepared films. In fact, the thinnest ePDA films behave as a more organized polymeric structure, displaying well-defined quinone/hydroquinone redox peaks and enabling a facile $Fe(CN)_6^{4-}/Fe(CN)_6^{3-}$ redox conversion, when compared to PDA films with a similar thickness (*ca.* 3 nm). Independently of film thickness, electrochemical synthesis yields more hydrophilic polymers (θ_{WCA}: 23 – 35°) than chemically synthesized ones (θ_{WCA}: 46 – 49°), highlighting their structural differences.

The subsequent catalytic activity assessments of immobilized Lac on graphite/ePDA and graphite/PDA electrodes clearly show the importance of the films physicochemical properties on the success of immobilization step. Graphite/ePDA(200 mV s^{-1}; 6c)/Lac electrode displayed the best catalytic performance towards ABTS detection (linear sensitivity: 342 mA M^{-1} cm^{-2}) which can be attributed to a better polymeric organization, as seen by its greater electroactivity and electron transfer properties, when compared to a PDA film with identical thickness. These results highlight the great potential of electrosynthesized polydopamine films as electrochemical transducing interfaces for biosensing devices.

4.4. References

[1] M.E. Lynge, R. van der Westen, A. Postma, B. Städler, Polydopamine—a nature-inspired polymer coating for biomedical science, Nanoscale. 3 (2011) 4916–4928. doi:10.1039/c1nr10969c.

[2] I. Ismail, T. Okajima, S. Kawauchi, T. Ohsaka, Studies on the early oxidation process of dopamine by electrochemical measurements and quantum chemical calculations, Electrochimica Acta. 211 (2016) 777–786. doi:10.1016/j.electacta.2016.05.056.

[3] M. Sugumaran, Reactivities of quinone methides versus o-Quinones in catecholamine metabolism and eumelanin biosynthesis, International Journal of Molecular Sciences. 17 (2016) 1–23. doi:10.3390/ijms17091576.

[4] T.A. Enache, A.M. Oliveira-Brett, Phenol and para-substituted phenols electrochemical oxidation pathways, Journal of Electroanalytical Chemistry. 655 (2011) 9–16. doi:10.1016/j.jelechem.2011.02.022.

[5] F. Zhang, G. Dryhurst, Oxidation chemistry of dopamine: Possible insights into the age-dependent loss of dopaminergic nigrostriatal neurons, Bioorganic Chemistry. 21 (1993) 392–410. doi:10.1006/bioo.1993.1033.

[6] N. González-Diéguez, A. Colina, J. López-Palacios, A. Heras, Spectroelectrochemistry at screen-printed electrodes: Determination of dopamine, Analytical Chemistry. 84 (2012) 9146–9153. doi:10.1021/ac3018444.

[7] J. Di, S. Bi, Effect of aluminum (III) on the conversion of dopachrome in the melanin synthesis pathway, Spectrochimica Acta - Part A: Molecular and Biomolecular Spectroscopy. 59 (2003) 1689–1696. doi:10.1016/S1386-1425(02)00403-1.

[8] J.L. Wang, B.C. Li, Z.J. Li, K.F. Ren, L.J. Jin, S.M. Zhang, H. Chang, Y.X. Sun, J. Ji, Electropolymerization of dopamine for surface modification of complex-shaped cardiovascular stents, Biomaterials. 35 (2014) 7679–7689. doi:10.1016/j.biomaterials.2014.05.047.

[9] Y. Li, M. Liu, C. Xiang, Q. Xie, S. Yao, Electrochemical quartz crystal microbalance study on growth and property of the polymer deposit at gold electrodes during oxidation of dopamine in aqueous solutions, Thin Solid Films. 497 (2006) 270–278. doi:10.1016/j.tsf.2005.10.048.

[10] F. Bernsmann, J.C. Voegel, V. Ball, Different synthesis methods allow to tune the permeability and permselectivity of dopamine-melanin films to electrochemical probes, Electrochimica Acta. 56 (2011) 3914–3919. doi:10.1016/j.electacta.2011.02.028.

[11] R. Kishida, Y. Ushijima, A.G. Saputro, H. Kasai, Effect of pH on elementary steps of dopachrome conversion from first-principles calculation, Pigment Cell & Melanoma Research. 27 (2014) 734–743. doi:10.1111/pcmr.12256.

[12] M. García-Moreno, J. Rodríguez-López, F. Martínez-Ortiz, J. Tudela, R. Varón, F. García-Cánovas, Effect of pH on the oxidation pathway of dopamine catalyzed by tyrosinase, Archives of Biochemistry and Biophysics. 288 (1991) 427–434. doi:10.1016/0003-9861(91)90216-6.

[13] R.A. Zangmeister, T.A. Morris, M.J. Tarlov, Characterization of polydopamine thin films deposited at short times by autoxidation of dopamine, Langmuir. 29 (2013) 8619–8628. doi:10.1021/la400587j.

[14] H. Muguruma, Y. Inoue, H. Inoue, T. Ohsawa, Electrochemical Study of Dopamine at Electrode Fabricated by Cellulose-Assisted Aqueous Dispersion of Long-Length Carbon Nanotube, Journal of Physical Chemistry C. 120 (2016) 12284–12292. doi:10.1021/acs.jpcc.6b03715.

[15] L.C. Almeida, J.P. Correia, A.S. Viana, Electrochemical and optical characterization of thin polydopamine films on carbon surfaces for enzymatic sensors, Electrochimica Acta. 263 (2018) 480–489. doi:10.1016/j.electacta.2018.01.077.

[16] S. Gidanian, P.J. Farmer, Redox Behavior of Melanins: Direct Electrochemistry of DHI-melanin and its Cu and Zn Adducts, J. Inorg. Biochem. 89 (2002) 54–60.

[17] C. Lin, L. Chen, E.E.L. Tanner, R.G. Compton, Electroanalytical study of dopamine oxidation on carbon electrodes: from the macro- to the micro-scale, Physical Chemistry Chemical Physics. 20 (2018) 148–157. doi:10.1039/C7CP07450F.

[18] J. Liebscher, R. Mrówczyński, H.A. Scheidt, C. Filip, N.D. Haìdade, R. Turcu, A. Bende, S. Beck, Structure of polydopamine: A never-ending story?, Langmuir. 29 (2013) 10539–10548. doi:10.1021/la4020288.

[19] H. Lee, J. Rho, P.B. Messersmith, Facile conjugation of biomolecules onto surfaces via mussel adhesive protein inspired coatings, Advanced Materials. 21 (2009) 431–434. doi:10.1002/adma.200801222.

[20] L.P. Zhu, J.H. Jiang, B.K. Zhu, Y.Y. Xu, Immobilization of bovine serum albumin onto porous polyethylene membranes using strongly attached polydopamine as a spacer, Colloids and Surfaces B: Biointerfaces. 86 (2011) 111–118. doi:10.1016/j.colsurfb.2011.03.027.

[21] F. Ponzio, J. Barthès, J. Bour, M. Michel, P. Bertani, J. Hemmerlé, M. D'Ischia, V. Ball, Oxidant Control of Polydopamine Surface Chemistry in Acids: A Mechanism-Based Entry to Superhydrophilic-Superoleophobic Coatings, Chemistry of Materials. 28 (2016) 4697–4705. doi:10.1021/acs.chemmater.6b01587.

[22] R. Cruz-Silva, E. Amaro, A. Escamilla, M.E. Nicho, S. Sepulveda-Guzman, L. Arizmendi, J. Romero-Garcia, F.F. Castillon-Barraza, M.H. Farias, Biocatalytic synthesis of polypyrrole powder, colloids, and films using horseradish peroxidase, Journal of Colloid and Interface Science. 328 (2008) 263–269. doi:10.1016/j.jcis.2008.09.021.

[23] N. Graf, E. Yegen, T. Gross, A. Lippitz, W. Weigel, S. Krakert, A. Terfort, W.E.S. Unger, XPS and NEXAFS studies of aliphatic and aromatic amine species on functionalized surfaces, Surface Science. 603 (2009) 2849–2860. doi:10.1016/j.susc.2009.07.029.

[24] J.-P. Sylvestre, S. Poulin, A. V. Kabashin, E. Sacher, M. Meunier, J.H.T. Luong, Surface Chemistry of Gold Nanoparticles Produced by Laser Ablation in Aqueous Media, J. Phys. Chem. B. 108 (2004) 16864–16869. doi:10.1021/jp047134.

[25] M. Preuss, F. Bechstedt, Vibrational spectra of ammonia, benzene, and benzene adsorbed on Si (001) by first principles calculations with periodic boundary conditions, Physical Review B - Condensed Matter and Materials Physics. 73 (2006). doi:10.1103/PhysRevB.73.155413.

[26] S. Gunasekaran, R.T. Kumar, Vibrational spectra and normal coordinate analysis of adrenaline and dopamine, Indian Journal of Pure & Applied Physics. 45 (2007) 884–892.

[27] P.K. Jha, G.P. Halada, The catalytic role of uranyl in formation of polycatechol complexes, Chemistry Central Journal. 5 (2011) 12. doi:10.1186/1752-153X-5-12.

[28] O. Jha, T.K. Yadav, R.A. Yadav, Structural and vibrational study of a neurotransmitter molecule: Dopamine [4-(2-aminoethyl) benzene-1,2-diol], Spectrochimica Acta - Part A: Molecular and Biomolecular Spectroscopy. 189 (2018) 473–484. doi:10.1016/j.saa.2017.07.067.

[29] D.G. O'Sullivan, 657. Vibrational frequency correlations in heterocyclic molecules. Part VI. Spectral features of a range of compounds possessing a benzene ring fused to a five-membered ring, Journal of the Chemical Society (Resumed). (1960) 3278. doi:10.1039/jr9600003278.

[30] H. Talbi, E.B. Maarouf, B. Humbert, M. Alnot, J.J. Ehrhardt, J. Ghanbaja, D. Billaud, Spectroscopic studies of electrochemically doped polyindole, Journal of Physics and Chemistry of Solids. 57 (1996) 1145–1151. doi:10.1016/0022-3697(95)00413-0.

[31] J.C. Soares, M. Foschini, C. Eiras, E.A. Sanches, D. Gonçalves, Electrosynthesis and optical characterization of poly(p-phenylene), polypyrrole and poly(p-phenylene)-polypyrrole films, Materials Research. 17 (2014) 332–337. doi:10.1590/S1516-14392014005000008.

[32] H. Coskun, A. Aljabour, L. Uiberlacker, M. Strobel, S. Hild, C. Cobet, D. Farka, P. Stadler, N.S. Sariciftci, Chemical vapor deposition - based synthesis of conductive polydopamine thin-films, Thin Solid Films. 645 (2018) 320–325. doi:10.1016/j.tsf.2017.10.063.

[33] W. Zheng, H. Fan, L. Wang, Z. Jin, Oxidative Self-Polymerization of Dopamine in an Acidic Environment, Langmuir. 31 (2015) 11671–11677. doi:10.1021/acs.langmuir.5b02757.

[34] T. An, N. Lee, H.-J. Cho, S. Kim, D.-S. Shin, S.-M. Lee, Ultra-selective detection of Fe2+ion by redox mechanism based on fluorescent polymerized dopamine derivatives, RSC Advances. 7 (2017) 30582–30587. doi:10.1039/c7ra04107a.

[35] I. Almeida, F. Henriques, M.D. Carvalho, A.S. Viana, Carbon disulfide mediated self-assembly of Laccase and iron oxide nanoparticles on gold surfaces for biosensing applications, Journal of Colloid and Interface Science. 485 (2017) 242–250. doi:10.1016/j.jcis.2016.09.042.

[36] A. Jarosz-Wilkołazka, T. Ruzgas, L. Gorton, Amperometric detection of mono- and diphenols at Cerrena unicolor laccase-modified graphite electrode: Correlation between sensitivity and substrate structure, Talanta. 66 (2005) 1219–1224. doi:10.1016/j.talanta.2005.01.026.

Chapter V

Electrosynthesis of polycatechol and polycatecholamine films on gold electrodes

Most of the content found in this chapter is published in:

- L.C. Almeida, R.D. Correia, B. Palys, J.P. Correia, A.S. Viana, Comprehensive study of the electrochemical growth and physicochemical properties of polycatecholamines and polycatechol, Electrochimica Acta. 386 (2021) 138515, doi:10.1016/j.electacta.2021.138515.

- L.C. Almeida, R.D. Correia, J.P. Correia, A.S. Viana, Combined Electrochemical, Ellipsometric and Microgravimetric Study of Ion Permeable Polydopamine Films, J. Electrochem. Soc. 169 (2022) 046503, doi: 10.1149/1945-7111/ac60f0.

5. Electrosynthesis of polycatechol and polycatecholamine films on gold electrodes

Catechol is well-known for its presence in natural adhesives [1], leading to the development of bio-inspired coatings as a surface anchoring group with versatile chemistry. Polydopamine is the most studied catechol-based material, however, the role of other chemical functionalities combined with catechol, on the synthesis and materials properties is far less explored. Only recently, the synergetic effect of having catechol next to amine groups was clearly demonstrated [2] in high salt concentration solutions. This chapter presents a detailed investigation of the potentiodynamic polymerization of catecholic monomers containing different chemical functions, namely, amine, hydroxyl and carboxyl groups. Catecholamines such as, dopamine, norepinephrine and *L*-DOPA were selected, as well as catechol and caffeic acid, to evaluate electropolymerization kinetics and final physicochemical properties of the deposited films. The electrochemical data is supported by gravimetry, spectroscopy (FTIR, Raman, UV-Vis, XPS), atomic force microscopy (AFM), ellipsometry and wettability assays. Discussion about the structure-property relationships of polycatecholamines is provided, focusing on the biosensors developments challenges: biomolecules immobilization and signal transduction by electrochemical or optical means.

Envisaging the improvement of the development biosensing interfaces, a detailed ellipsometric and gravimetric studied focused on the conductivity and permeability properties of polydopamine is also presented. The electropolymerization of dopamine on gold surfaces, using a potentiodynamic mode with a high anodic limit (1.1 V *vs.* SCE) allows the synthesis of polymeric films with higher thickness, roughness, porosity, electroactivity and ion permeability compared to those synthesized using lower anodic limits (up to 0.8 V). Further studies are necessary to assess the applicability of thicker catechol-based polymers to the biosensing field.

5.1. Electropolymerization of catechol derivatives under potentiodynamic mode

The electrochemical polymerization of catechol, caffeic acid and catecholamines, namely dopamine, norepinephrine and DOPA, was investigated in potentiodynamic mode. **Figure 5.1a–e** shows the cyclic voltammograms corresponding to 50 potential cycles of a gold electrode in deaerated 5 mM solutions of the five monomers, at 200 mV s^{-1}. In the first anodic scan, all the monomers display an oxidation peak (I_a) at *ca.* 0.3 V (**Figure 5.1a–e**) with similar

intensities, corresponding to the two-proton two-electron conversion [3] of the *o*-diphenolic group to a *o*-quinone group (**Figure 5.2**). The electrochemically generated quinone species can be detected in the subsequent cathodic scan (I_c), displaying distinct reduction intensities. In the case of quinone species originated from dopamine, catechol and caffeic acid (**Figure 5.1a,d,e**), the reduction peaks I_c occur at *ca.* 0.0 V, while norepinephrine and DOPA quinones reduction peaks develop at *ca.* 0.1 V (**Figure 5.1b,c**). The oxidized form of catechol and caffeic acid display the most intense reductions (**Figure 5.1d,e**), whereas the quinones derived from dopamine, norepinephrine, and DOPA show an irreversible behaviour (**Figure 5.1a–c**), that is accentuated for DOPA and norepinephrine. In fact, I_c/I_a peak current ratios for the first potential cycle are 0.93 for catechol, 0.76 for caffeic acid, 0.62 for dopamine, 0.41 for norepinephrine and 0.23 for DOPA. The irreversibility associated with catecholamines, compared to the monomers without amine groups in their structures (catechol and caffeic acid), can be explained by the intramolecular cyclization that is known to occur for catecholamines through Michael addition [4]. The nucleophilic amine readily attacks the quinone group, originating 5,6-dihydroxyindoline derivatives (**Figure 5.2**). The extent of intramolecular cyclization is then greater for DOPA, smaller for norepinephrine and even smaller for dopamine. An explanation of the different stabilities of the electrogenerated quinones lay on the small differences in the nucleophilicities of their amine groups and in the electrophilicities of their benzene rings, which depends on the inductive effects caused by the nearby substituents. In the case of DOPA, the presence of a carboxylate group at pH 7 (pK_a = 2.29) [5] has an electron donating effect, leading to a more nucleophilic amine than dopamine, explaining a fast intramolecular cyclization. Regarding norepinephrine, the hydroxyl group in the vicinity of the catechol group, with an electron withdrawing effect, enhances the electrophilicity of the ring towards the amine nucleophilic attack, also justifying a faster intramolecular cyclization than dopamine. The working pH is also an important parameter since the degree of amine group deprotonation determines the nucleophilic attack [6], however, the reported pK_a values for these three catecholamines [5,7,8] do not allow to establish a correlation between pK_a and the differences in the irreversibility found for processes I.

In **Figure 5.1a–c**, concerning catecholamines polymerization, the identified redox process II can be assigned to the products of intramolecular cyclization: oxidation of 5,6-dihydroxyindolines (II_a) and reduction of their corresponding redox pairs, 5,6-indolinequinones (II_c). The $E_{1/2}$ values associated with these cyclized products (*ca.* -0.3 V in **Figure 5.1a,c**, and -0.2 V in **Figure 5.1b**) are significantly lower than the potential value associated to process I, due to the electrodonating effect of the nitrogen atom to the catechol ring in the cyclized forms

[3,9]. The redox process II of dopamine and DOPA occurs at $E_{1/2}$ values of *ca.* -0.3 V (**Figure 5.1a,c**), whereas in the case of norepinephrine this parameter is slightly higher, *ca.* -0.2 V (**Figure 5.1b**). This difference may be explained by the electron withdrawing effect of the hydroxyl group, hampering the removal of electrons from the catechol ring in the case of norepinephrine's products.

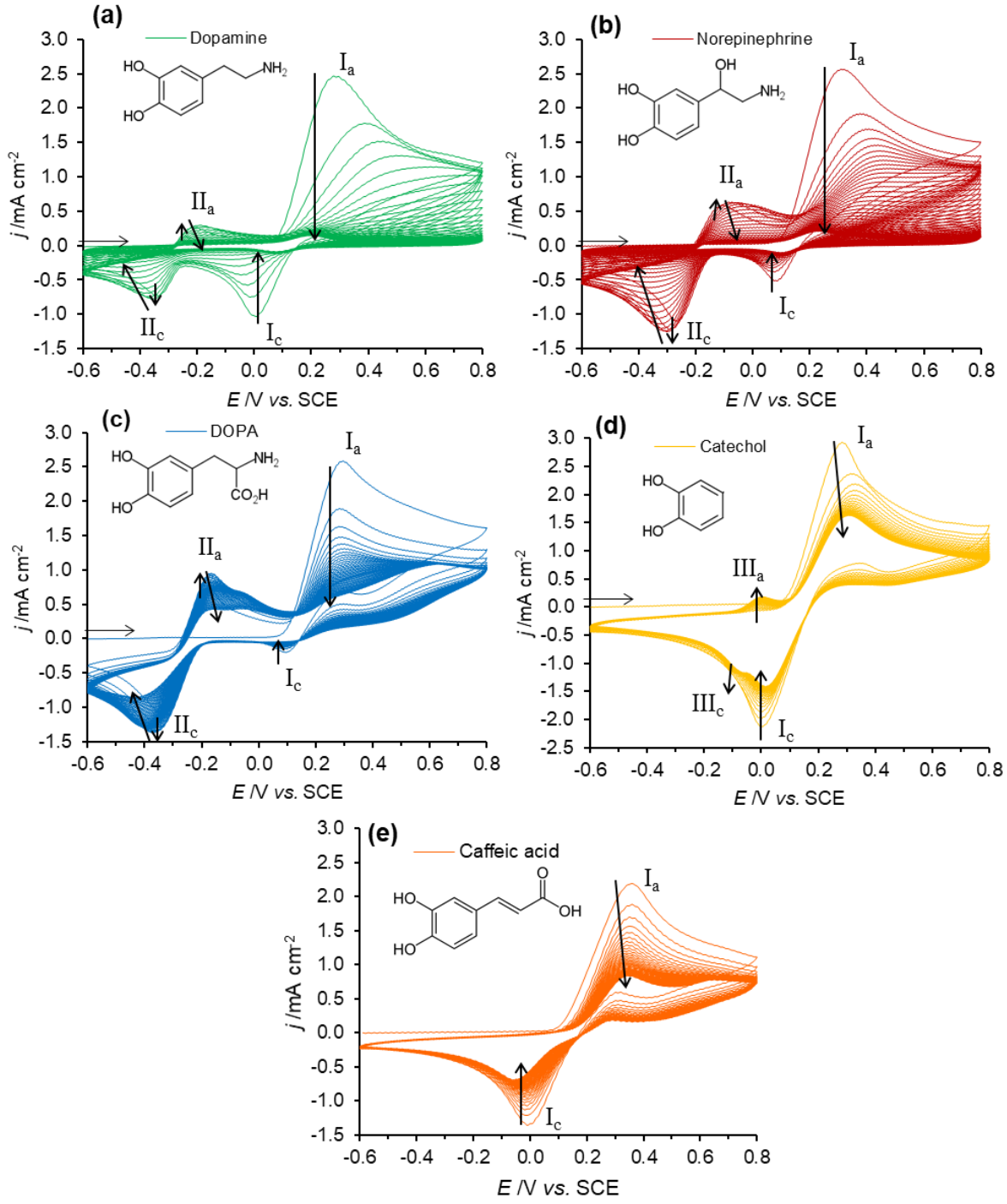

Figure 5.1: Potentiodynamic growth of ePDA **(a)**, ePNE **(b)**, ePDOPA **(c)**, ePCA **(d)** and ePCAF **(e)** at 200 mV s^{-1} for 50 potential cycles in a deoxygenated CPB pH=7.0 solution containing 5 mM of monomer.

In addition to processes I and II, there is the appearance of a less intense redox process, centred at -0.04 V, exclusive to catechol cyclic voltammograms (**Figure 5.1d**, process III). This redox process is not present in the beginning of catechol electropolymerization, but it becomes noticeable as potential cycling continues and its intensity increases. These peaks were previously assigned to a redox process of a new polymeric phase [10,11], although the exact polymeric structure is not clearly assigned in the literature. In fact, the intensity of redox process III and its peak separation (ΔE_p) are considerably lower than those observed for indoline type species in solution (redox processes II, **Figure 5.1a–c**), supporting an electron transfer of surface confined molecules. Compared to the other monomers, catechol does not have any substituents in the positions 3 to 6, thus it is considered to be more prone to dimerization and hydroxylation [12], following an additional polymerization pathway that may not be relevant for its substituted analogues. For instance, caffeic acid cyclic voltammograms do not encompass process III (**Figure 5.1e**), clearly suggesting a different electropolymerization process apart from catechol. It has been reported that catechol electropolymerization occurs by C-C and C-O-C coupling of monomers [11,13,14], whereas caffeic acid moieties are mostly linked by C-C bonds [15] (**Figure 5.2**). For this reason, process III is most likely related to the redox conversion of polymeric chains of catechol molecules linked by C-O-C bonds.

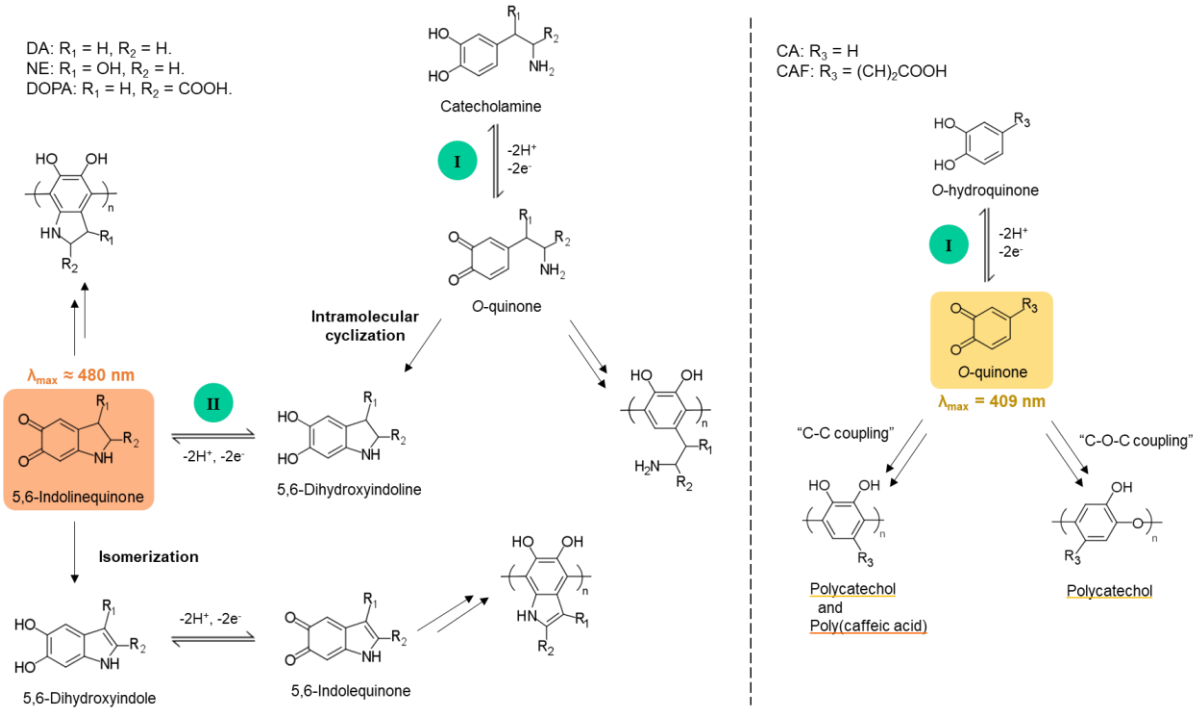

Figure 5.2: Proposed redox processes and chemical steps involved in electrochemical polymerization of catecholamines, catechol and caffeic acid.

To further investigate the accumulation of intermediate species in solution, UV-Vis spectra of the electrolyte solution were acquired during the electropolymerization of catecholamines and catechol in a quartz cuvette (**Figure. 5.3a**). A characteristic absorbance band of 5,6-indolinequinone chromophores [3,16,17] appears in the three spectra of catecholamines, proving the formation of such intermediates during the electropolymerization process. Dopachrome exhibit a maximum of absorbance at 478 nm, noradrenochrome at 486 nm and dopaminechrome at 476 nm, close to previously reported values obtained for catecholamine chemical oxidation by metals ions [16,18]. The origin of such bands has been assigned to a $n \rightarrow \pi^*$ transition occurring at carbonyl group linked to an indoline moiety [17], as the result of monomers intramolecular cyclization (**Figure 5.2**). It is possible to observe that these species accumulate in solution according to their cyclization extent discussed previously: the most intense absorbance peak is attributed to dopachrome due to the fastest cyclization, followed by noradrenochrome and dopaminochrome with respectively slower cyclization rates. By fixing the wavelength of maximum absorbance (**Figure 5.3b**) or the potential of the oxidation peak II (**Figure 5.3c**) of these intermediates, it is possible to depict different accumulation profiles for dopachrome compared to the other two species. The molecules originated from the intramolecular cyclization of dopamine and norepinephrine accumulate in solution until the 25th cycle of electropolymerization (**Figure 5.3b**), after which the oxidation of monomers (process I_a) is partially hindered by the formation of a polymeric phase (**Figure 5.3d**). Besides, after some time chemical conversion to indolic species [3], from indoline moieties, becomes the predominant process (**Figure 5.2**). In contrast, dopachrome continues to accumulate during all the electropolymerization process (**Figure 5.3b**), due to the uninterrupted electrogeneration of dopaquinone throughout the 50 potential cycles. The differences in the hinderance of monomers oxidation over the distinct polymers, suggests a poor coverage of the surface in the case of polyDOPA and thicker films in the case of ePDA and ePNE. The charge transfer constrain is also observed in the current profiles of oxidation peaks II_a (**Figure 5.3c**). As proved by UV-Vis (**Figure 5.3b**) and mentioned above, dopaminechrome and noradrenochrome accumulate in solution until 25th potential cycle, however the formation of a polymeric phase causes the oxidation peaks II_a to decrease rapidly, becoming barely detectable at the electrode surface after 12 and 20 potential cycles (**Figure 5.3c**), respectively.

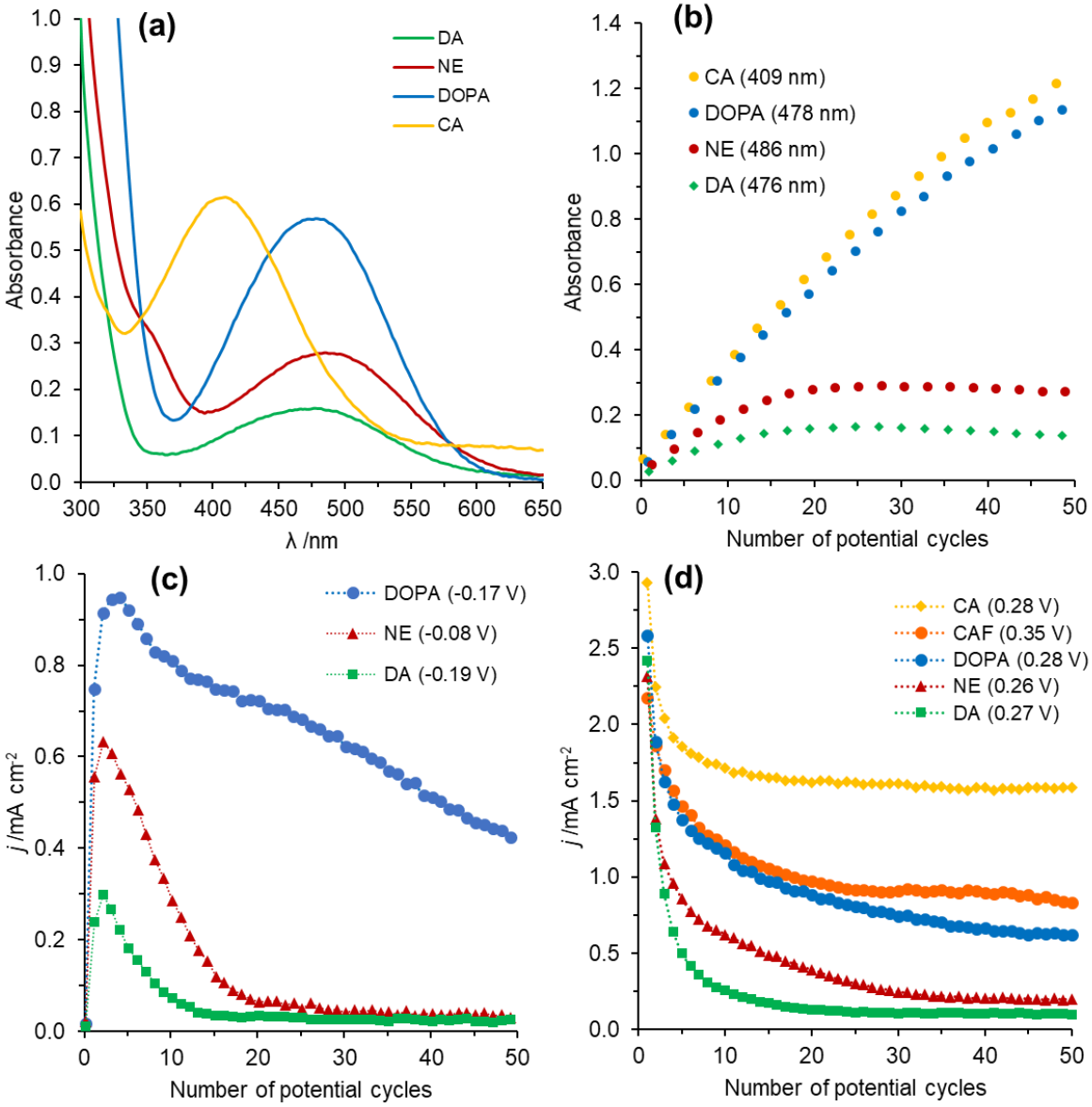

Figure 5.3: UV-Vis spectra of the electrolyte solution taken at the 20th potential cycle of electropolymerization of 5 mM DA, NE, DOPA and CA (a). Absorbance values at λ_{max} for each monomer during potential cycling (b). Current values at the oxidation peak II_a (c) and at oxidation peak I_a (d) taken from cyclic voltammograms presented in **Figure 5.1**.

The UV-Vis spectra acquired during the electropolymerization of catechol shows the appearance of an absorbance band centred at 409 nm (**Figure 5.3a**), previously assigned to *o*-benzoquinone [19,20], that increases during the 50 potential cycles (**Figure 5.3b**). Distinctly from the catecholamines electropolymerization, the oxidation current at catechol oxidation peak (**Figure 5.3d**), does not decrease significantly after the 10th potential cycle, indicating that the polymeric phase growing at the electrode surface is not hindering the monomer oxidation as in the case of catecholamines. To complement the spectroelectrochemical studies of intermediate species, EQCM was used to further analyse the polymers deposition on the gold surfaces.

The mass variations of the working electrode recorded during the potentiodynamic cycling of the five monomers is presented in **Figure 5.4**. The representation of mass changes *versus* applied potential is shown in **Figure A1** (Annex). Clearly the four monomers display very different mass profiles, revealing distinct film thickening progression. Regarding the initial 5 potential cycles, the average growth rate of polydopamine, polynorepinephrine, polyDOPA, poly(caffeic acid) and polycatechol is 7.3, 6.5, 0.3, 2.1 and 4.5 ng cm^{-2} s^{-1}, respectively. In the case of catecholamines, the initial growth rate is deeply related with the intramolecular cyclization extent of each oxidized monomer, which is acting as a competitive step against polymerization (**Figure 5.2**). As so, when quinones species originated in redox process I_a are chemically converted to indoline type species, there is less available monomer to undergo oligomerization and further deposition of polymer at the electrode surface. As a consequence, polyDOPA mass growth is much slower than the other polycatecholamines studied, due to the rapid depletion of dopaquinone from the vicinity of the working electrode. In addition, the presence of a carboxylic acid in DOPA structure may also negatively affect oligomer formation/polymer deposition, as hypothesized before [21]. The slower growth rate of polyDOPA demonstrated by EQCM is also in agreement with the poorly pronounced charge transfer blocking effect of redox process I (**Figure 5.3d**) and II (**Figure 5.3c**) observed during DOPA electropolymerization. The intramolecular cyclization extent is less evident in the case of norepinephrine, leading to a faster polymerization growth compared to DOPA, and for the case of dopamine polymer growth is even faster due to the larger amount of available dopaminequinone monomers. In the case of polyDOPA, only after 8 potential cycles (**Figure 5.4**), there is a slow but approximately constant polymer growth up to 50 cycles (*ca.* 2.2 ng cm^{-2} s^{-1}), which is consistent with almost no hinderance effect by the film towards DOPA oxidation (process I_a), as observed in **Figure 5.1c** and **5.3d**.

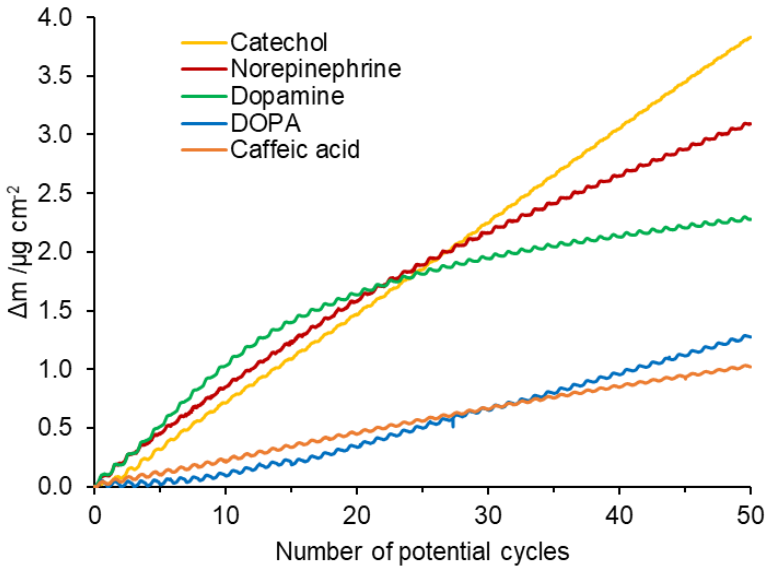

Figure 5.4: Mass variation during the potentiodynamic polymerization of dopamine (DA), norepinephrine (NE), DOPA, catechol (CA) and caffeic acid (CAF) for 50 potential cycles at 200 mV s^{-1} in a deoxygenated CPB pH=7.0 solution containing 5 mM of monomer.

Polydopamine displays the fastest initial growth, however around the 11th potential cycle the mass increments drastically drop, almost stagnating, reaching a constant and slow growth rate (1.1 ng cm^{-2} s^{-1}) from the 30th potential cycle onwards. This behaviour can be explained by the increasingly difficulty in oxidizing dopamine at the working electrode that is being covered by a low conductive film, in agreement to reported data [22,23]. As polymerization progresses, the amount of indole type species available in solution is expected to increase, which will raise the probability of chain branching though their incorporation. Differently, polynorepinephrine growth profile follows approximately two linear growth regimes, the first up to 20 potential cycles (5.6 ng cm^{-2} s^{-1}) and a second one with a lower rate (3.5 ng cm^{-2} s^{-1}), which implies that this polymer should be more conductive and/or more porous compared to polydopamine. This allows to extend potential cycling, forming thicker polynorepinephrine films and overcoming the difficulties found for the electrochemical growth of polydopamine.

Differently to polydopamine and polynorepinephrine polymerizations, the mass growth profiles of polycatechol and poly(caffeic acid) are approximately linear during the 50 polymerization cycles, varying at a rate of 5.5 and 1.6 ng cm^{-2} s^{-1}, respectively. This linear behavior corroborates the continuous oxidation of monomer without obvious signs of electrode surface passivation, as discussed before for polyDOPA formation. As seen in **Figure 5.3d**, catechol, DOPA and caffeic acid oxidations are only partially hindered during the 50 potential cycles. Even so, polycatechol stands out by its higher deposition rate, which strongly suggests

the formation of a conductive and/or porous polymeric matrix that do not hinder monomer oxidation regardless of the polymeric phase thickness. In contrast, poly(caffeic acid) growth is characterized by a much slower deposition rate than polycatechol's and similar to polyDOPA's. As mentioned before, the presence of a carboxylic group seems to inhibit polymer formation and deposition. In fact, the chemical polymerization of caffeic acid was already reported to be much slower compared to other catechol-containing molecules, requiring accelerating agents to produce useful polymeric coatings [15,24].

5.2. Thin film characterization

The polymeric films electrosynthesized on gold substrates were characterized by several surface techniques to study their physicochemical properties. *Ex situ* ellipsometry was used to estimate the optical properties (refractive index (*n*), extinction coefficient (*k*)) and thickness (*L*) of the investigated polymeric matrices in dry conditions (**Table 5.1**). After 50 potential cycles, polydopamine and polynorepinephrine exhibit a similar thickness of *ca.* 20 nm, followed by polycatechol (*ca.* 13 nm), polyDOPA (*ca.* 6 nm) and poly(caffeic acid) (*ca.* 3 nm). As expected, based on electropolymerization data discussed above, the thickness of polyDOPA and poly(caffeic acid) are lower than the other polymers. In contrast, polycatechol exhibited the highest mass gain during electrogravimetric experiments, however its thickness is inferior to polydopamine and polynorepinephrine, measured *ex situ*. The estimated extinction coefficients for the thin polymeric layers reveals that polycatecholamines and poly(caffeic acid) are more absorbing than polycatechol at this wavelength (632.8 nm). However, *k* values obtained for polydopamine on gold are much lower than those estimated on carbon electrodes (*ca.* 0.4) [3,25], disclosing distinct polymer electronic structures over the two electrode materials. Polydopamine and polynorepinephrine display the highest refractive indexes pointing to the presence of optically denser polymeric matrices, in contrast with polyDOPA and polycatechol that exhibit the lowest refractive indexes, thus indicating differences in polymer compactness in dry conditions. Poly(caffeic acid) differs from the other polymers by exhibiting an intermediate refractive index value.

In order to evaluate the porosity of the polymers, the mass differences in wet and dry conditions have been measured allowing to estimate the fraction of incorporated electrolyte solution, $\chi_{ie} = (\Delta m_{(wet)} - \Delta m_{(dry)})/\Delta m_{(wet)}$, during the electropolymerization process (**Table 5.1**). It is observed that both ePDA and ePNE do not incorporate a high amount of electrolyte solution (*ca.* 10 %), in contrast with polycatechol, polyDOPA and poly(caffeic acid), in which a large

fraction of mass change is due to electrolyte solution entrapment in the polymer (>50 %). This behaviour may reflect a more branched and porous structure for the three polymers, alike other conductive polymers [26,27], when compared to considerably more compact structures of ePDA and ePNE. The fact that catechol polymerization may occur through both C-C and C-O-C coupling [11,13,14] (**Figure 5.2**), may explain the more porous morphology due to a larger polymer branching. The presence of the carboxyl group in polyDOPA and poly(caffeic acid) may be the cause for the high porosity of these two matrices. As discussed before, the carboxyl function seems to slow down polymer growth, which may be interpreted as a difficulty in polymer assembly. As a result, polyDOPA and poly(caffeic acid) present a more porous structure, able to incorporated a large amount of electrolyte. The polymer density values in dry conditions were also calculated by dividing $\Delta m_{(dry)}$ by the optical thickness (L), as presented in **Table 5.1**. Despite the differences of thickness, refractive index and solvent intake, ePNE and ePCA display similar densities (*ca.* 1.3 g cm^{-3}), as well as ePDA and ePDOPA (*ca.* 1.0 g cm^{-3}). It is worth mentioning that polycatechol and polynorepinephrine should continue to grow further and faster than polydopamine, if a higher number of potential cycles is performed, due to their almost linear growth profiles. This behaviour is important for the preparation of thick films, which are required for many applications, for instance, in the optimization of the amount of catalytic material (*e.g.* enzymes) that may be co-deposited with the polymer.

The average contact angle of the air-water-film interface (**Table 5.1**) corroborate that ePDA and ePCA films are, as expected, less hydrophilic than ePNE and ePDOPA, which present additional hydroxyl and carboxyl groups, respectively. The data points to the presence of intact functional groups, from monomeric units, in the backbone structure of polymers. Indeed, electrosynthesized polycatechol shows a similar wettability than thin chemically synthesized films [28], whereas ePNE and ePDOPA are considerably more hydrophilic than those formed by chemical routes, namely 30º [28] and 38º [29] for PNE and 68º [30] for PDOPA, demonstrating the relevance of electrosynthetic methods to better control the polymer growth process. Hydrophilic polymers may be of great advantage to be employed in biosensing applications, in particular for blocking non-specific interactions [31].

Table 5.1: Refractive index (*n*), extinction coefficient (*k*), thickness (*L*), water contact angle (θ_{WCA}), mass variations (Δm), electrolyte fraction (χ_{ie}) and density (*d*) of modified gold with polymeric films grown under the conditions of **Figure 5.1**. Ellipsometry performed *ex situ* at an incident angle of 70°.

Film	***n***	***k***	***L* /nm**	θ_{WCA} /°	$\Delta m_{(wet)}$ /µg cm^{-2}	$\Delta m_{(dry)}$ /µg cm^{-2}	χ_{ie} %	***d*** /g cm^{-3}
ePDA	1.75 ± 0.01	0.05 ± 0.01	18.5 ± 0.9	49 ± 3	2.19 ± 0.09	1.98 ± 0.02	10 ± 5	1.07 ± 0.06
ePNE	1.78 ± 0.03	0.048 ± 0.006	21.8 ± 0.9	18 ± 2	3.08 ± 0.02	2.82 ± 0.03	8 ± 2	1.29 ± 0.07
ePDOPA	1.65 ± 0.02	0.07 ± 0.01	6.2 ± 0.2	18 ± 3	1.3 ± 0.1	0.61 ± 0.06	53 ± 8	1.0 ± 0.1
ePCAF	1.71 ± 0.01	0.03 ± 0.01	3.2 ± 0.1	–	1.06 ± 0.03	0.41 ± 0.05	61 ± 5	1.3 ± 0.2
ePCA	1.66 ± 0.03	0.006 ± 0.006	12.5 ± 0.8	37 ± 3	4.0 ± 0.2	1.58 ± 0.08	61 ± 4	1.3 ± 0.1

Figure 5.5a shows the cyclic voltammograms of the polymers films in monomer free electrolyte solution. All the polymers are electroactive at neutral pH, displaying a predominant redox process centred at *ca.* 0.15 V, which is attributed to the quinone/hydroquinone redox conversion of the catechol moieties without electrodonating groups in the benzene ring, *i.e.* units of pristine catechol and catecholamines in the open form, polymerized by C-C coupling [3,10] (see **Figure 5.2**). This redox potential value matches the corresponding quinone/hydroquinone electrochemical process of monomers in solution (**Figure 5.1**). Less intense and more negative processes (occurring below or at 0 V) can be depicted for all the polycatecholamines (**Figure 5.5a**), particularly noticeable for ePDA, which can be attributed to the quinone/hydroquinone conversion of indoline type moieties, and other substituted species. These match the redox potential of *para*-quinones [9]. No clear redox process assigned to 5,6-dihydroxyindole (DHI) moieties could be detected in the electrochemical responses shown in **Figure 5.5a**, which are expected to occur between 0 V and the main redox peak [3,16]. Therefore, our results indicate that electrogenerated polymer matrixes, grown upon 50 potential cycles, are mainly formed by uncyclized catecholamines. Indeed, our conclusions agree with recent studies concerning chemical polymerization, which clearly demonstrate from mass spectrometry studies that DHI plays a minor role in the final structure of polydopamine [32,33]. Nevertheless, the voltammetric response of very thin polymers, grown with only 6 potential cycles (**Figure 5.5b**), reveals distinct redox responses, where indoline type species become more evident, supporting their integration in polycatecholamines matrices. In addition, indole moieties can be also depicted in ePNE and ePDOPA cyclic voltammograms, through a small oxidation peak at around 0.08 V. The species are incorporated in the initial potential scans, becoming less noticeable along potential cycling.

The polymers electroactivity does not directly relate with the estimated thickness or deposited mass, yet the less intense oxidation process is obtained for ePDOPA, as expected for

a very thin (6 nm) and light film (0.6 μg cm^{-2}). ePCAF, although thin and electroactive, displays a much larger peak separation, suggesting a more difficult charge transfer across the polymer material compared to the other matrices. In fact, a similar electrochemical behaviour was already observed in carbon electrodes modified with this polymer, yet a clear explanation couldn't be raised [10]. ePNE with a similar thickness of ePDA but higher polymer mass, has shown the most intense redox response amongst polycatecholamines, corroborating the presence of more electroactive material, hence more electrochemically available quinone/hydroquinone groups. This suggests that ePNE film displays a higher organization on its polymeric structure when compared to ePDA film, with similar porosity (**Table 5.1**). In addition, the high amount of quinone groups present in ePNE matrix, highlights its very promising aptitude to anchor biomolecules through Michael addition reaction. Polycatechol shows a distinct electrochemical behaviour, since it presents a very well-defined redox process at *ca.* 0 V, which increases progressively with potential cycling. As mentioned, this process has been observed before [10,11], however its exact nature is still unclear. The range of potential where it occurs may suggest a redox conversion involving *p*-quinone/*p*-hydroquinones moieties [9]. There is one more reduction peak at *ca.* -0.3 V, in the cyclic voltammogram of polycatechol, that may be assigned to new species formed from the nucleophilic attack of water molecules to the catechol ring [14], shifting the potential value of hydroquinone/quinone conversion to more negative values.

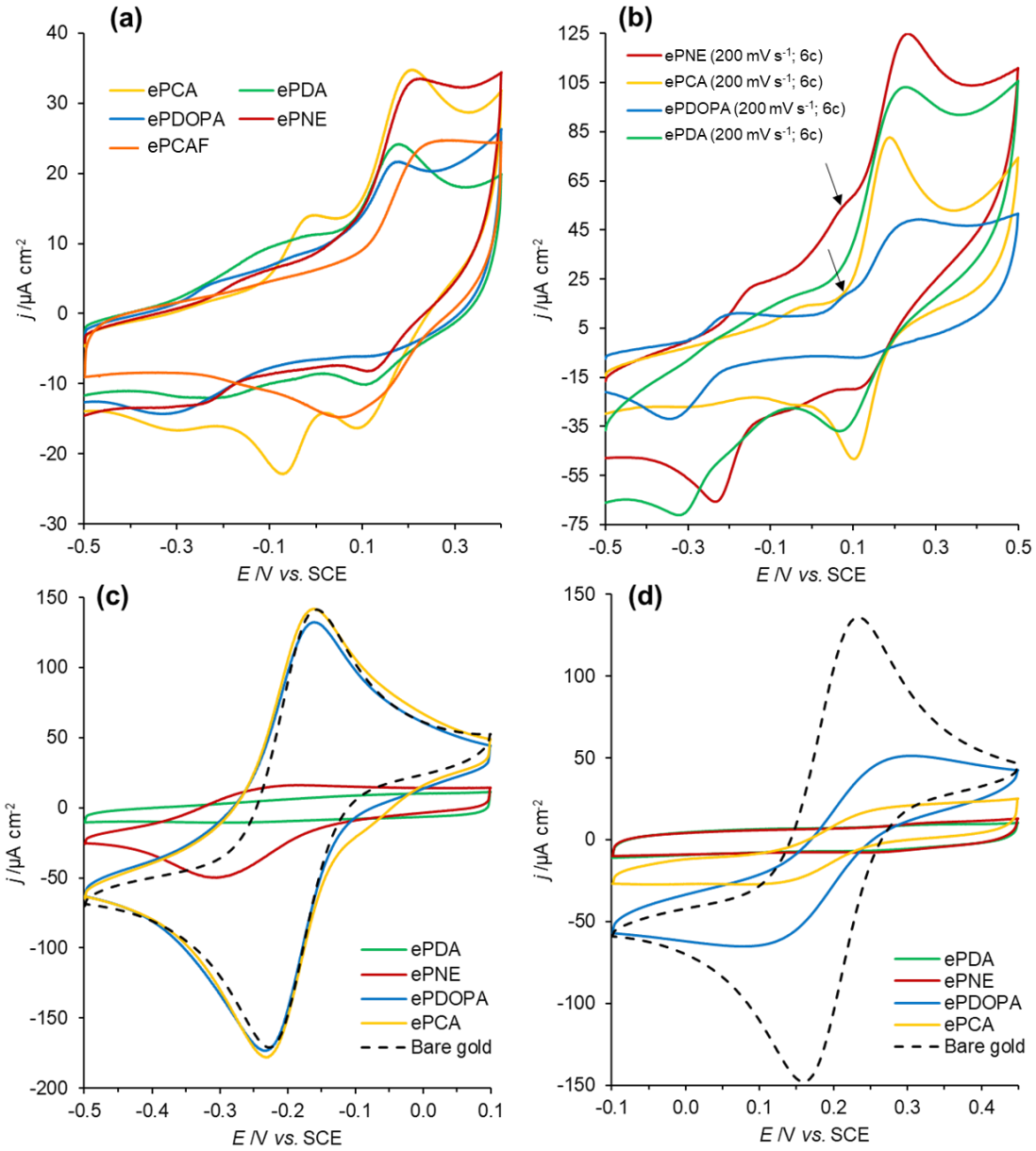

Figure 5.5: Cyclic voltammograms, recorded at 50 mV s^{-1} in deoxygenated CPB pH=7.0 buffer, of gold electrodes modified with ePDA, ePNE, ePDOPA, ePCA and ePCAF synthesized with 50 **(a)** and 6 potential cycles **(b)**. Cyclic voltammograms of the modified electrodes of panel (a) in 0.25 M KCl solution of 1 mM $Ru(NH_3)_6Cl_3$ **(c)** and 0.25 M KCl solution of 1 mM $K_3Fe(CN)_6$ **(d)** recorded at 50 mV s^{-1}. Arrows in panel (b) point to the identified oxidation process of 5,6-dihydroxyinole moieties (*ca.* 0.08 V) present in ePNE and ePDOPA.

Figure 5.5c shows the cyclic voltammetric responses of the several films in a solution containing 1 mM $[Ru(NH_3)_6]Cl_3$ and 0.25 M KCl. It can be observed that ePDA is the only polymer that totally hinders the electron transfer of $[Ru(NH_3)_6]^{3+/2+}$, whereas ePNE, with a similar thickness and porosity still enables a partial electrochemical conversion of this redox mediator. ePCA and ePDOPA do not have any blocking effect on the electron transfer of this positively charged redox probe, likely due to their higher porosity and lower thickness. The

electrochemical responses of $[Fe(CN)_6]^{3-/4-}$ over the investigated polymers was also carried out and is shown in **Figure 5.5d**. Contrarily to the observed for the positive redox probe, both ePNE and ePDA totally hamper the anionic probe electron transfer, in agreement with previous work for polydopamine [23,34], pointing out the negative charge of this polymer at neutral pH, that above a given thickness do not allow the transduction of negatively charged analytes. ePCA and ePDOPA partially hinder $[Fe(CN)_6]^{3-/4-}$ redox process in agreement with their lower thickness and higher porosity. To further elucidate the blocking properties of the films as a function of pH, a study of the polymers protonated/deprotonated groups has been carried out by recording cyclic voltammograms in phosphate buffer solutions (pH 2, 6, 4 and 8) containing 1.0 mM of $K_3Fe(CN)_6$ [35–37], upon 5, 20 and 50 polymerization cycles. The representations of the oxidation peak current density *versus* pH for the investigated polymers are compiled in **Figure 5.6**. As expected, the thickening of the films results in a considerable blocking effect towards the anionic probe conversion, especially for ePDA and ePNE, which are the thickest and less porous polymers. Nevertheless, upon 5 potential cycles, one can observe that at pH 2 and 4 all the modified electrodes enable the electrochemical conversion of $[Fe(CN)_6]^{3-/4-}$ ions. However, ePDA and ePNE films, at pH 6, block the anionic probe charge transfer, which can be related with a change in polymer overall charge, that above pH 4 should be negative making it harder for the negatively charged ion to approach the interface. Roughly, the data indicates pK_a values of *ca.* 5 for ePDA and lower than 4 for ePNE, resulting from the balance between the formation of a negatively charged semiquinone (pK_a = 4.7 for dopamine semiquinone [38]), and the protonated amine. We anticipate that the OH group, adjacent to the catechol ring in norepinephrine, may contribute to an easier protonation of semiquinones, lowering its pK_a. The pK_a should be even lower for ePDOPA, as suggested by data in **Figure 5.6c**, due to the presence of a carboxylic acid (pK_a 2.29 [5]) that must be deprotonated in the polymer at pH 4, contributing to the overall negative charge. Opposite to catecholamines, ePCA electrochemical transduction of an anionic redox probe is not greatly affected by pH (**Figure 5.6d**), which can be possibly explained by its large porosity and the absence of a positively charged amine group. It is worth to emphasize that even the thickest ePCA film do not hinder the electrochemical transduction of a positively charged ion (**Figure 5.5c**).

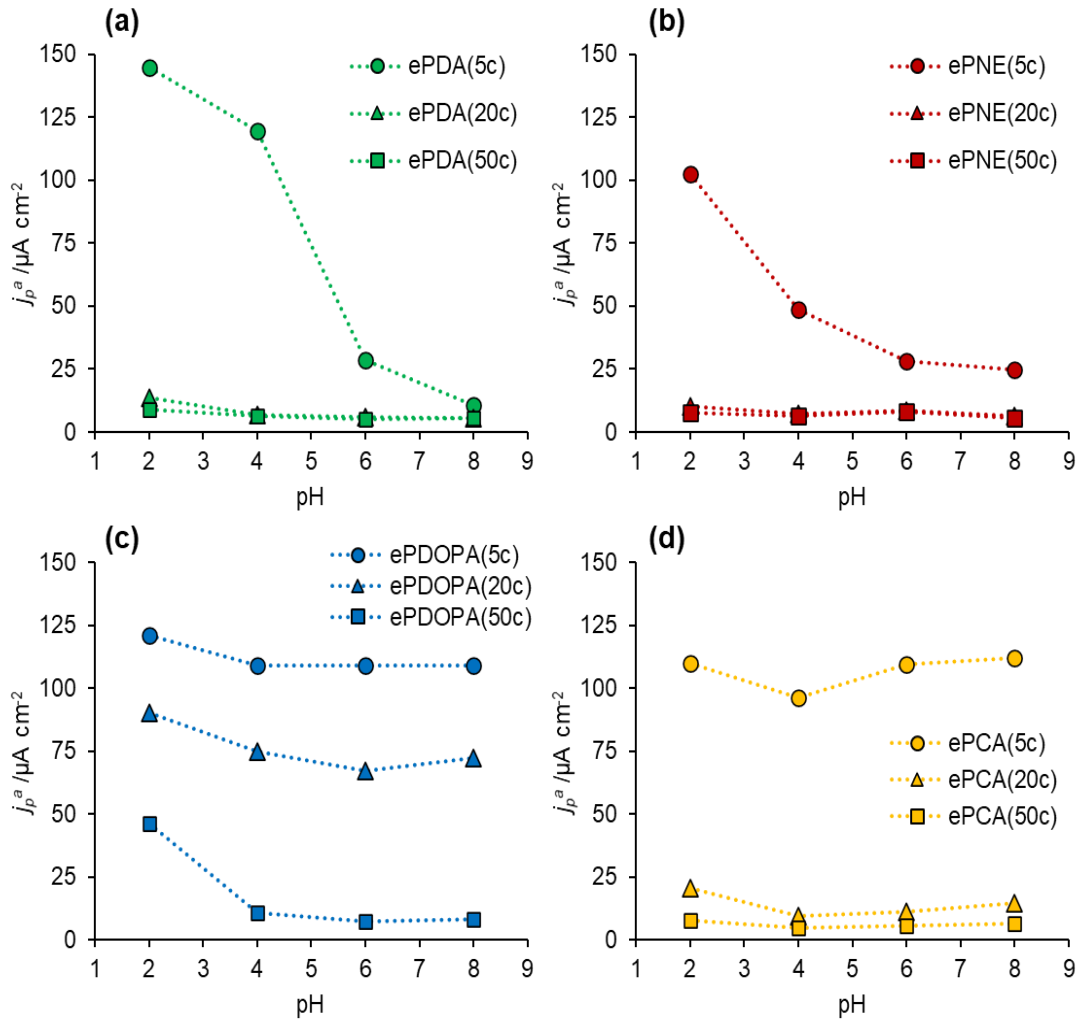

Figure 5.6: Representation of oxidation peak current *vs.* pH obtained from cyclic voltammograms, recorded at 50 mV s^{-1}, of gold modified electrodes with polydopamine (ePDA) **(a)**, polynorepinephrine (ePNE) **(b)**, polyDOPA (ePDOPA) **(c)**, and polycatechol (ePCA) **(d)**, with 5, 20 and 50 electropolymerization cycles, in 1 mM $K_3Fe(CN)_6$ and 0.1 M sodium phosphate buffer solutions.

Electrochemical impedance spectroscopy (EIS) was also conducted at different growth stages of the polymer (5, 20 and 50 cycles) to further support cyclic voltammetric and gravimetric data, as illustrated by the Nyquist plots shown in **Figure 5.7a–c**. Upon 5 polymerization cycles, the EIS spectra of all polymers present clear semicircles corresponding to charge transfer resistance (R_{ct}) within the high-frequency range, and typical semi-infinite diffusion regions for middle-range frequencies [23]. Yet, considerably smaller semicircles were recorded for ePCA and ePDOPA, much closer to the behaviour of bare gold. Spectra exhibiting these two regions were best fitted to the modified Randles circuit (**Figure 5.7d**, circuit 1). This circuit comprises the electrolyte resistance (R_s) in series with a parallel circuit composed by R_{ct}, in series with a Warburg impedance element (W), associated to diffusion, and a constant phase

element (CPE) accounting for a non-ideal double-layer capacitance. For ePDA and ePNE, after 20 or 50 cycles, the experimental data showed a very resistive behaviour towards $[Fe(CN)_6]^{3-/4-}$ ions redox conversion, thus the simplified equivalent circuit 2 has been used instead. **Table 5.2** compiles the R_{ct} values fitted for all the modified surfaces.

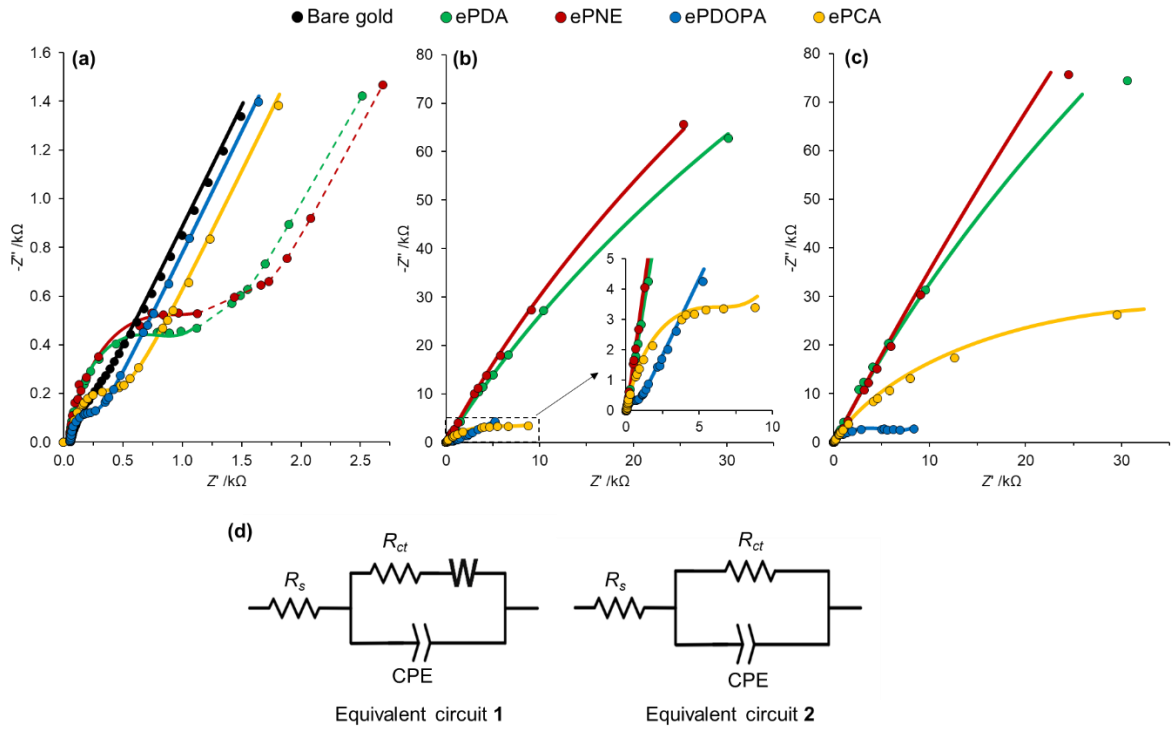

Figure 5.7: Nyquist plots of gold electrode before and after modification with ePDA, ePNE, ePDOPA and ePCA, recorded in deoxygenated solutions of 1mM $K_3Fe(CN)_6$ and 0.25 M KNO_3, as a function of the number of polymerization cycles: 5 (a), 20 (b) and 50 (c). Solid lines represent the fitting of the experimental data to the equivalent circuits shown in (d). EIS data obtained for ePDOPA (5, 20 and 50 cycles), ePCA (5 and 20 cycles), ePDA (5 cycles) and ePNE (5 cycles) were fitted with equivalent circuit 1; ePDA and ePNE with 20 or 50 cycles and ePCA (50 cycles) were fitted to equivalent circuit 2. Bare gold was fitted with circuit 1, but replacing CPE by an ideal capacitor. Dashed lines are only guides to the eyes.

The estimated R_{ct} values for the redox conversion of an anionic probe increase with the number of polymerization cycles, in agreement with the voltammetric data presented in **Figure 5.6**, confirming charge transfer limitation due to polymer thickening. R_{ct} values are consistent with overall mass increase and expected level of porosity (**Table 5.1**). The larger R_{ct} values are obtained for ePNE followed by ePDA, which are the thickest and less porous films. ePDOPA is the film that offers less resistance to the redox conversion of $[Fe(CN)_6]^{3-/4-}$ ionic species, probably due to its lower thickness and high porosity, as above discussed. The very low R_{ct} value estimated for ePDOPA after 5 polymerization cycles (196 Ω) is close to that obtained for bare gold (81 Ω), strongly supporting the irrelevant mass increase obtained after 5 cycles

(**Figure 5.4**). This is consistent with the presence of a very low polymer surface coverage, as confirmed by AFM imaging (discussed below). ePCA, which has a two-times larger thickness that ePDOPA (after 50 cycles) also displays low R_{ct} values compared to ePDA and ePNE, which fully agrees with the high incorporation of electrolyte solution (*ca.* 60%) within the polymer matrix, as deduced by EQCM experiments. The level of porosity of ePCA has revealed to be beneficial to compensate the polymer negative charge still enabling a partial electrochemical transduction of $[Fe(CN)_6]^{3-/4-}$ ionic species.

Table 5.2: Estimated charge transfer resistance (R_{ct}) values for the EIS data shown in **Figure 5.7**.

R_{ct} / Ω	ePDA	ePNE	ePDOPA	ePCA
5 cycles	8.76×10^2	1.09×10^3	1.96×10^2	3.85×10^2
20 cycles	5.32×10^5	6.63×10^5	6.86×10^2	7.85×10^3
50 cycles	8.01×10^5	2.85×10^6	6.21×10^3	7.55×10^4

To better elucidate the polymeric structures, the films were characterized by FTIR, XPS, and in some cases Raman spectroscopy. **Figure 5.8** shows the FTIR spectra of polymers grown with 50 potential cycles. There is a clear difference in the overall spectral intensity of the ePNE film comparing to the other polymers, though the spectra are collected from exactly the same sample area. Indeed, after drying, ePNE displays the highest deposited mass and thickness, being also a very dense polymer (**Table 5.1**), which justifies its relatively intense spectrum. The O-H, C=C, C-O stretching bands can be depicted in all spectra as expected for polymers containing catechol groups in their molecular structure [39,40]. In fact, ePCA spectrum shows nearly all bands present in the spectra of remaining polymers, confirming that the existence of characteristic polycatechol chain. The presence of amine groups in polycatecholamines is confirmed by the broad mixed O-H, N-H stretching band. Indeed, in polycatechol spectrum, the band in this region is blue-shifted, resulting from the lack of amine groups. Due to the broad and intense O-H, N-H stretching band, it is not possible to distinguish aliphatic C-H stretching around 2900 cm^{-1}, as foreseen for polymeric chains of catecholamine monomers [41]. The two characteristic vibrational modes of the benzene ring (C=C asymmetric and symmetric stretches) [3,41] are observed in all polymers with different relative intensities, which indicates different chemical environments near the phenolic rings. The C=C symmetric stretch of polycatechol is particularly sharp compared to polycatecholamines, probably due to the absence of overlapping N-H bending modes, occurring at 1600 cm^{-1} [40,42]. In contrast, polynorepinephrine and polydopamine spectra display broad benzene ring bands that should encompass amine bending modes. In addition, ePCA displays a very strong υ_{C-O} band, compared to polycatecholamines,

which supports the hypothesized polymerization via C-O-C coupling, in addition to the C-C coupling route. Low intensity bands corresponding to the presence of indole type moieties ($\upsilon_{C=N}$ and υ_{CNCC} [43–45]) are also depicted in polycatecholamine spectra, especially visible for the more intense ePNE spectra. The characteristic stretching band of carbonyl group is observed in the spectra of polyDOPA, confirming the presence of the carboxylic group in the polymer.

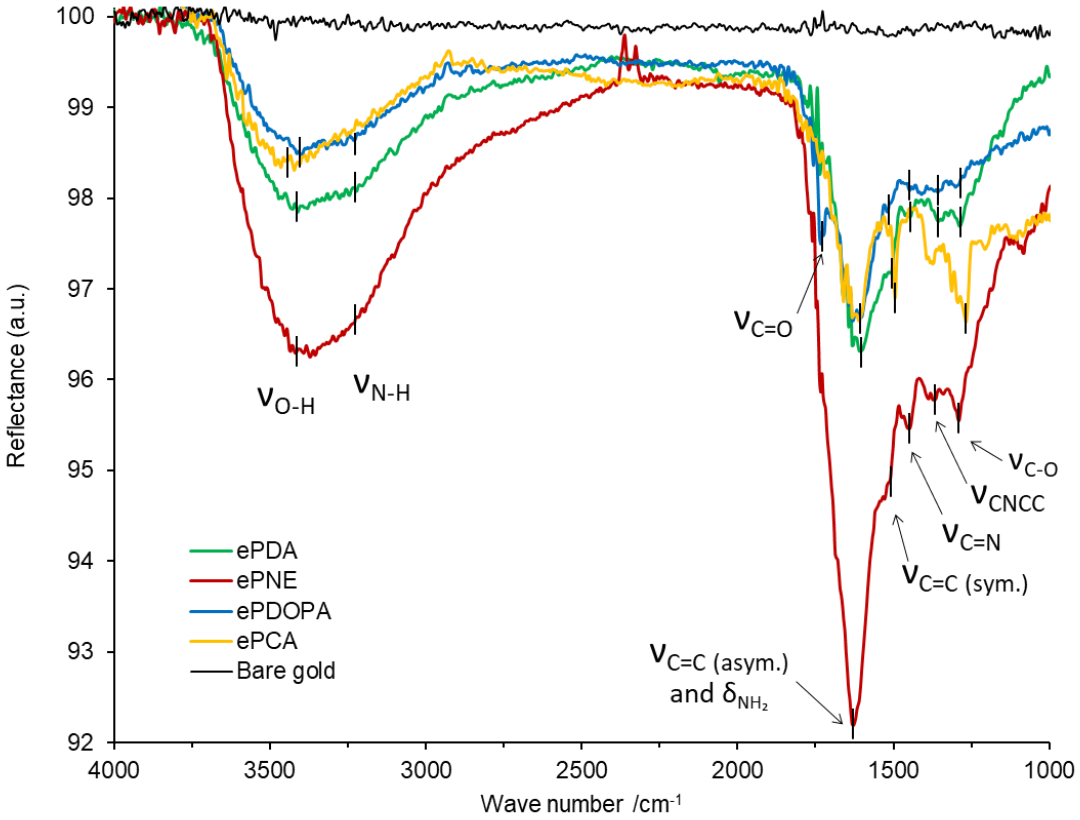

Figure 5.8: FTIR spectra of gold modified with ePDA, ePNE, ePDOPA and ePCA electrosynthesized at 200 mV s^{-1} for 50 potential cycles.

To complement the FTIR characterization, Raman spectroscopy was also used to characterize the three polycatecholamines: ePDA, ePNE and ePDOPA (**Figure 5.9**). Generally, the shape of the spectra is dominated by the strong absorption bands of the C=C ring stretches, similarly to the FTIR spectra and resembling eumelanin Raman spectra published elsewhere [46]. Polynorepinephrine and polydopamine exhibit fluorescence, as seen by the broad emission between 1600 and 500 cm^{-1} affecting the peak assignment, especially in thicker films. In the particular case of polyDOPA, the sharp spectra is very similar to polyindole [47], strongly indicating the incorporation of indole type species. Since the O-H and N-H stretching are weak in Raman, it was possible to clearly observe the aliphatic C-H stretching in thinner polymers

(at *ca.* 2900 cm^{-1}). This finding corroborates the electrochemical data where the expected polymeric chains comprise non-cyclized catecholamines and indoline type moieties, both containing aliphatic carbons. For thicker films the C-H stretching band is less evident, as a consequence of indole type species incorporation for longer polymerization.

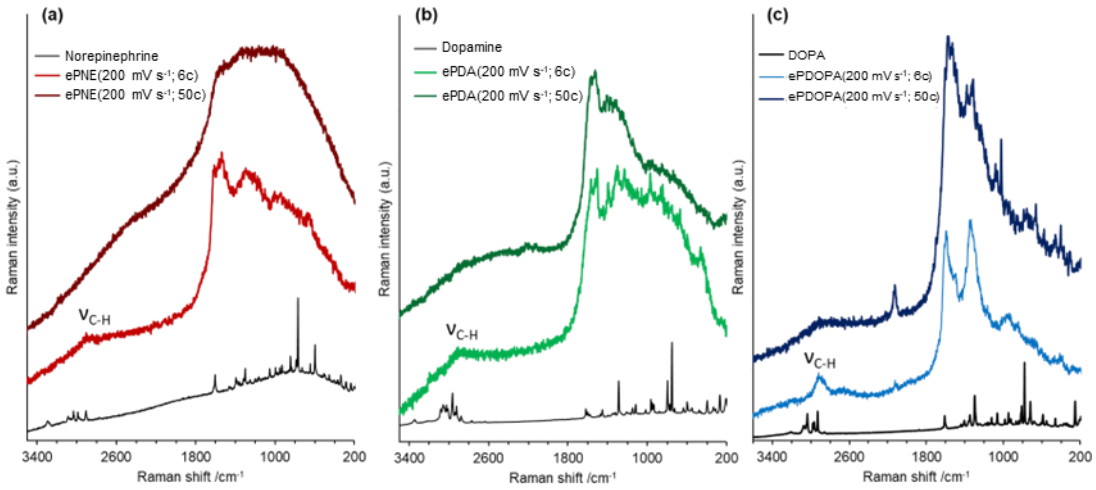

Figure 5.9: Raman spectra of gold modified electrode with polynorepinephrine (a), polydopamine (b) and polyDOPA (c) electrosynthesized at 200 mV s^{-1} for 6 and 50 potential cycles, using an excitation wavelength of 633 nm. The Raman spectra of the monomers' powder is also presented.

The chemical composition of the polymers grown with 50 potential cycles was further explored by XPS. The O/C atomic ratios estimated for the polymers agree with the calculated values for the corresponding monomers (**Table 5.3**), with the exception of ePDOPA that presents a slightly lower O/C ratio. This might be explained by a small loss of carboxylic acid groups, as suggested for chemically grown eumelanin [48]. In addition, the N/C ratio obtained for all the polycatecholamines matches those calculated for their monomers, indicating that most of the polymeric chains are mainly formed by non-degraded monomeric units, as also pointed out by the contact angle measurements (**Table 5.1**).

Table 5.3: Atomic ratio values calculated for monomers (DA, NE, DOPA and CA) and those experimentally obtained for polymers (ePDA, ePNE, ePDOPA and ePCA) based on XPS analysis.

Atomic ratio	DA	ePDA	NE	ePNE	DOPA	ePDOPA	CA	ePCA
O/C	0.25	0.27	0.38	0.33	0.44	0.36	0.33	0.34
N/C	0.13	0.11	0.13	0.10	0.11	0.11	–	–

Figure 5.10 shows the C 1s region of the four polymers. The O 1s and N 1s regions were also acquired and can be retrieved in **Figure A2** and **A3** (Annex), respectively. The C1s spectra

were fitted into four components ascribed to i) C-C, C-H_x, ii) C-O, C-N, iii) C=O and iv) π-π*. The C-O component of polynorepinephrine spectra is particularly higher than that of the other polymers, confirming the presence of the hydroxyl group, whereas the C=O peak in polynorepinephrine, polydopamine and polycathechol spectra is similar and should correspond to quinone groups. In the case of polyDOPA, the (C=O) component exhibits a higher intensity than the other polymers, which is attributed to a mixture of quinones and carboxylic acid, confirming the presence of this latter group in the final polymeric structure. This is corroborated by the larger C=O fraction obtained in O1s spectrum of polyDOPA (**Figure A2**, Annex) in comparison with the other polymers. It is worth noting that C1s spectrum of polycatechol shows well-defined and separated C-O and C-C, C-CH_x peaks due to the absence of C-N bonds that enlarge the C-O peak in the case of polycatecholamines.

The N 1s spectra of polycatecholamines (**Figure. A3**, Annex) were fitted for three components: protonated amine species (*ca.* 402 eV), aliphatic amines NH_2, -NH- (*ca.* 400 eV) and deprotonated pyrolytic nitrogen C=N (*ca.* 399 eV). For the all the polymers the major contribution arises from aliphatic amines, as reported before for electrochemically [3] and chemically synthesized polydopamine films [43,49]. Polydopamine seems to be the most heterogeneous polymer with a higher fraction of both aromatic C=N and -NH_3^+ species.

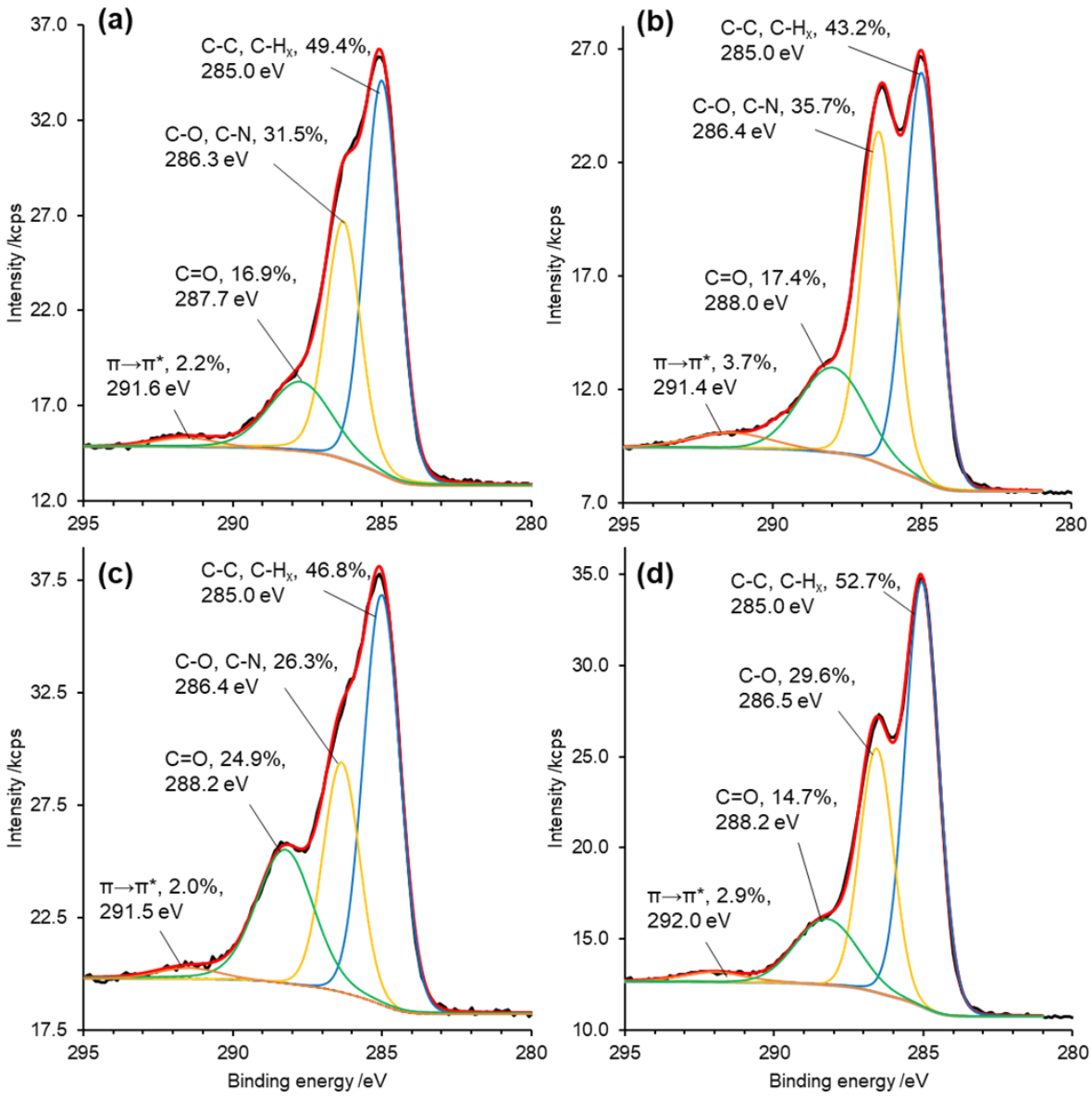

Figure 5.10: XPS spectra of C 1s region of gold modified electrode with ePDA **(a)**, ePNE **(b)**, ePDOPA **(c)** and ePCA **(d)**, electropolymerized at 200 mV s^{-1} for 50 potential cycles.

5.3. Polymer morphology and adhesion properties

The polymers morphology was characterized by AFM imaging, as shown in **Figure 5.11**. Overall the electrosynthesized polymers with 50 cycles exhibit a very smooth granular topography, where ePDA and ePDOPA are the most regular films, with an R_q of 3.6 ± 0.2 nm, followed by ePNE (R_q = 5.2 ± 0.1 nm), and finally by ePCA with an estimated R_q value of 5.7 ± 0.2 nm. ePCA topography is alike thin conducting polymers (*e.g.* polypyrrole [50]), showing the initial stages of a typical 3D cauliflower shape. Polycatecholamines also exhibit aggregates of polymeric granules, with a more regular size and distribution, yielding more

uniform morphologies, probably due to slower growth rates, as observed for ePDOPA and for ePNE and ePDA, towards the end of polymerization, when compared to ePCA.

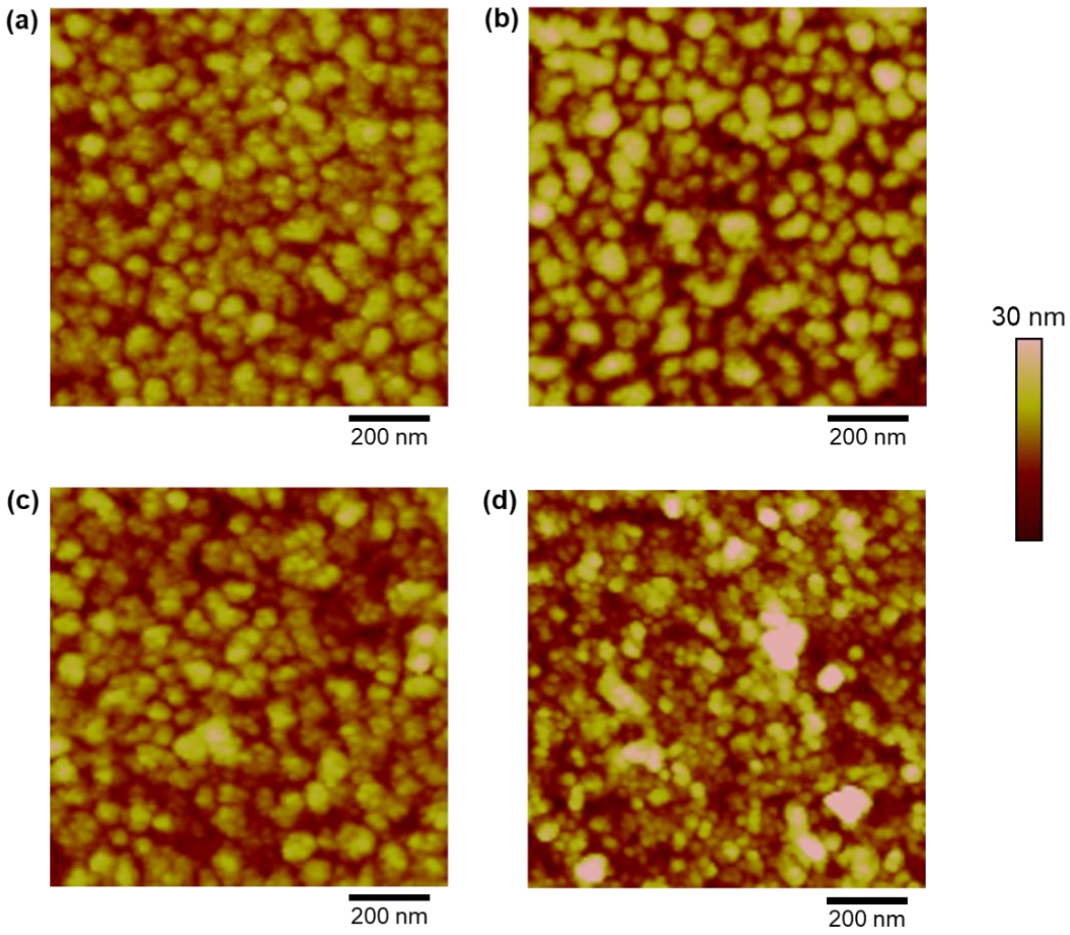

Figure 5.11: AFM morphological images of gold modified electrode with ePDA **(a)**, ePNE **(b)**, ePDOPA **(c)** and ePCA **(d)**, electropolymerized at 200 mV s^{-1} for 50 potential cycles.

To better elucidate the EIS and gravimetric data, AFM analysis at an early stage of polymer formation (5 cycles) was also carried out, as illustrated in **Figure 5.12**. As expected, the fastest growing films, ePDA, ePNE and ePCA covered gold surfaces with polymer grains, whereas gold modified with ePDOPA revealed only few agglomerated grains spread over the surface. One can depict an extremely thin layer (**Figure 5.12c**), probably corresponding to DOPA monomers or short oligomers. In addition, smaller grain sizes could be depicted in ePCA modified gold, which should account for the much lower charge transfer resistance (**Table 5.2**) observed by this film towards a negatively charged probe.

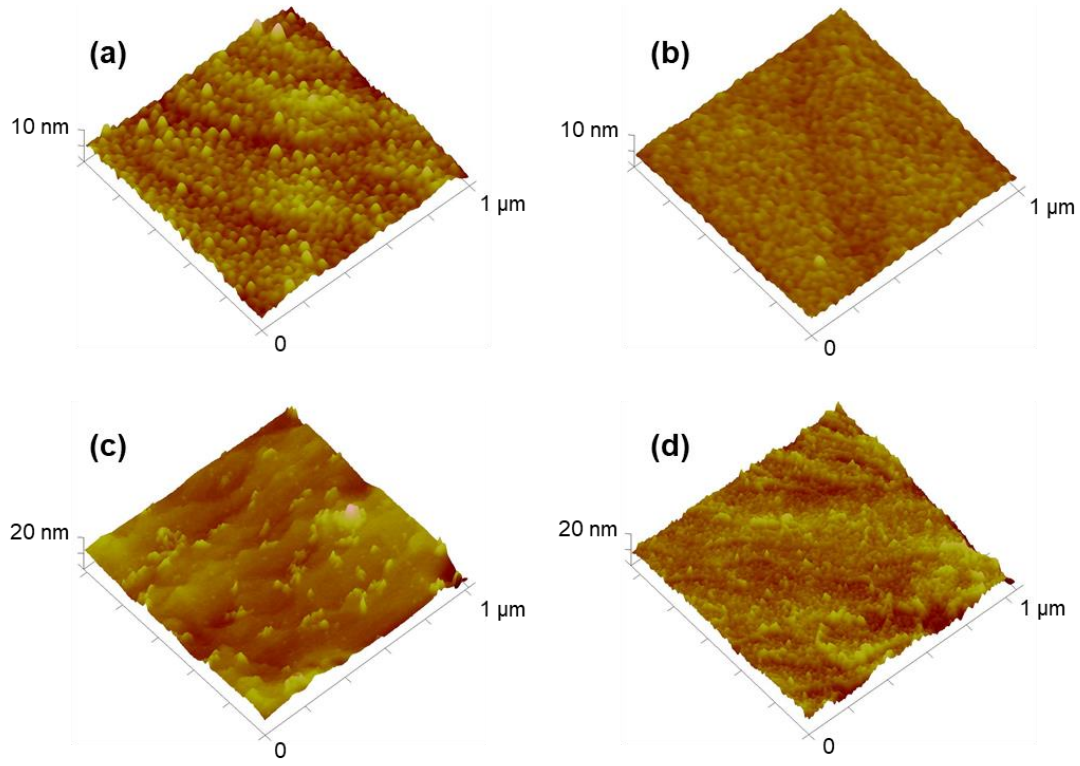

Figure 5.12: AFM 3D images of gold modified electrode with polydopamine **(a)**, polynorepinephrine **(b)**, polyDOPA **(c)**, and polycatechol **(d)**, electropolymerized at 200 mV s^{-1} for 5 potential cycles.

The efficient interaction of these polymers, containing catechol/quinone moieties with amine groups is a requirement when these films are to be used as biofunctionalization matrices, mimicking the adhesion properties of mussel foot proteins. To measure these types of forces, the surface of an AFM tip was modified with amine groups and allowed to interact with polycatechol and polycatecholamines. As it can be seen by the representative force curves in **Figure 5.13a**, the adhesion forces between an amine-functionalized tip to the four polymers tested are similar. Peak Force tapping and Quantitative nanomechanical mapping software were combined to collect simultaneously with topography, adhesion forces distribution over a surface area of 2×2 μm^2. **Figure 5.13b** shows the calculated histogram based on the recorded adhesion map for each polymer. The three polycatecholamines display a similar range of adhesion forces centred around 4 nN, which agrees with a value found for electrosynthesized polydopamine [22]. However, polynorepinephrine displays slightly higher adhesion characterized by a second distribution peak shifted to higher values. Polycatechol exhibits a gaussian distribution of adhesion forces, reflecting a more chemically homogeneous film with an average value of 4.8 nN, that is slightly higher when compared to polycatecholamines. For reference, by mapping a mica surface, which is known to be very hydrophilic, with the same tip, an adhesion force of *ca.* 1.3 nN was obtained. Overall, the *ex situ* nanomechanical

measurements emphasize the pivot role of catechol group in the adhesion properties of these polymers.

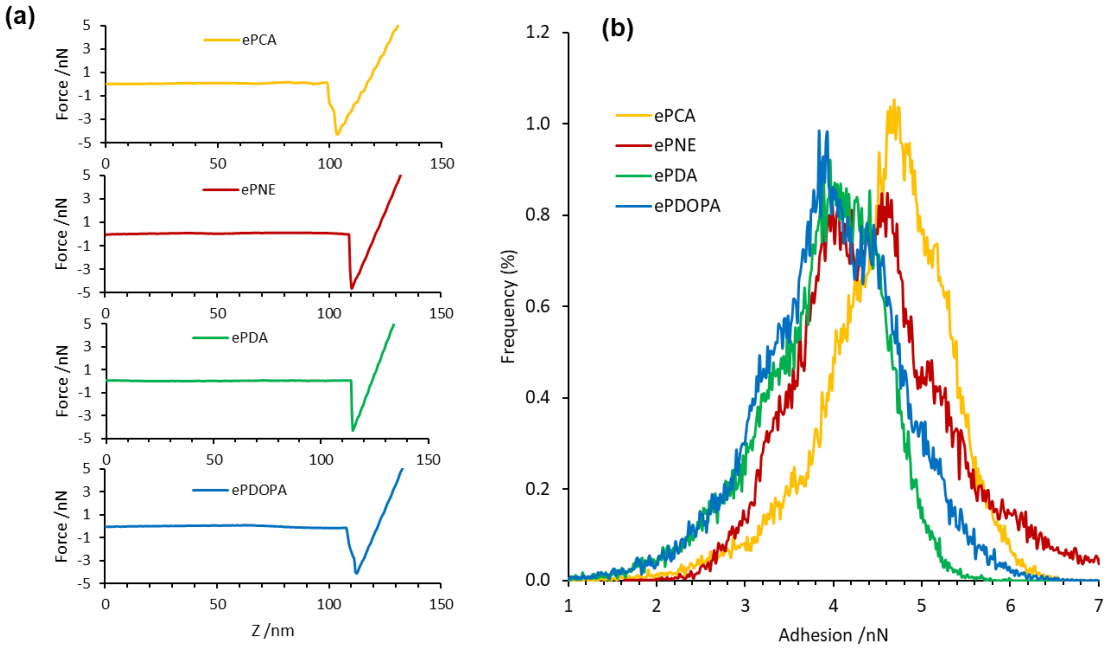

Figure 5.13: Representative force curves of polycatechol (ePCA), polynorepinephrine (ePNE), polydopamine (ePDA) and polyDOPA (ePDOPA) **(a)**; Adhesion forces histogram of each polymeric surface acquired using an amine-modified AFM tip and scanning a 2×2 μm^2 area **(b)**.

To further evaluate possible interactions of polycatechol and polycatecholamine coatings with amine groups present in target molecules, the immobilization of an amine derivative of ferrocene was attempted during the electropolymerization of catechol, dopamine, norepinephrine and DOPA. As depicted in the cyclic voltammograms of **Figure 5.14a**, the aminoferrocene complex displays a well-behaved charge transfer process on bare gold, displaying a diffusion-controlled redox process characterized by a redox potential of -0.10 V. It is previously described elsewhere [51] that aminoferrocene exhibits a one-electron one-proton redox conversion, and due to the weak alkalinity of its aromatic amine (pK_a = 5.9), it is expected that both reduced and oxidized species would be deprotonated at the neutral working pH (7), as represented in the chemical structures of **Figure 5.14b**. The electroactivity of such complex is a desirable feature since, upon its immobilization onto the several polymeric matrices, qualitative and quantitative analysis can be envisaged regarding the immobilized amount.

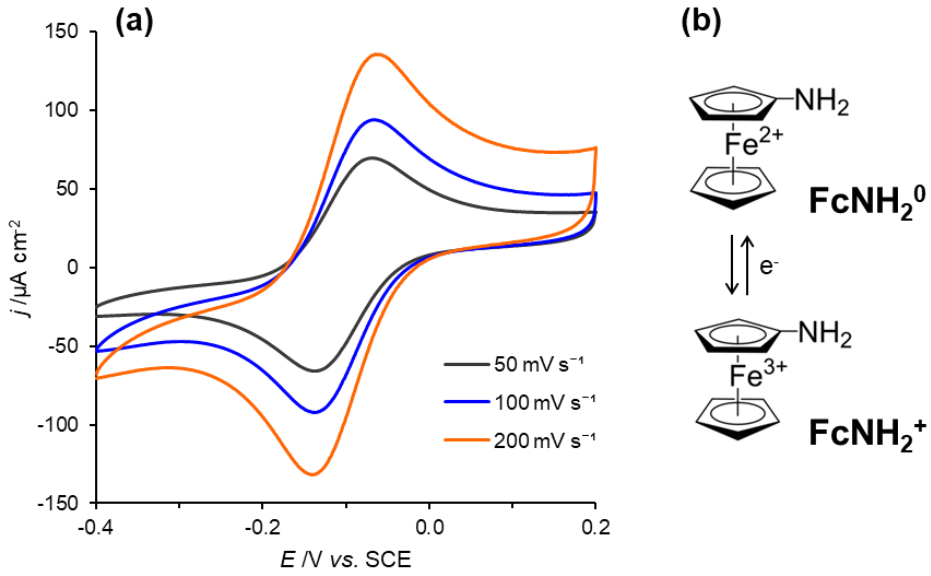

Figure 5.14: Cyclic voltammograms recorded at 50, 100 and 200 mV s^{-1}, of bare gold electrode in a deoxygenated CPB pH 7.0 solution containing 0.5 mM of aminoferrocene **(a)**; Redox conversion of aminoferrocene at neutral pH **(b)** – adapted from [51].

In a first trial, 0.5 mM of aminoferrocene was added to the electropolymerization solution of norepinephrine, although no redox peaks attributable to aminoferrocene were found in the voltametric characterization of the polymer formed after 6 potential cycles at 200 mV s^{-1} (data not shown). An increase in concentration to 2.5 mM of aminoferrocene allowed a clear visualization of its redox peak during the electropolymerization process, and also in the subsequent redox response of the modified polymers, and thus, 2.5 mM was the selected concentration to carried out the comparative studied of polycatecholamine ability to immobilized the redox active compound. **Figure 5.15** shows the potentiodynamic growth of the different polycatecholamine films in the presence of 2.5 mM of aminoferrocene at a previously used scan rate (200 mV s^{-1}). In these cyclic voltammograms there is the obvious appearance of a redox conversion, centred at *ca.* -0.1 V, that is not present in the electropolymerizations of each monomer in the absence of aminoferrocene (*cf.* **Figure 5.1**), and thus it can be attributed to the presence of aminoferrocene in the solution. Since the effect of aminoferrocene presence in the thickness of the resulting coatings was not known at this point, the same number of potential cycles was chosen to the faster growing polymers (ePDA, ePNE and ePCA), while a higher number of 50 potential cycles was selected for the slowest growing polymer (ePDOPA).

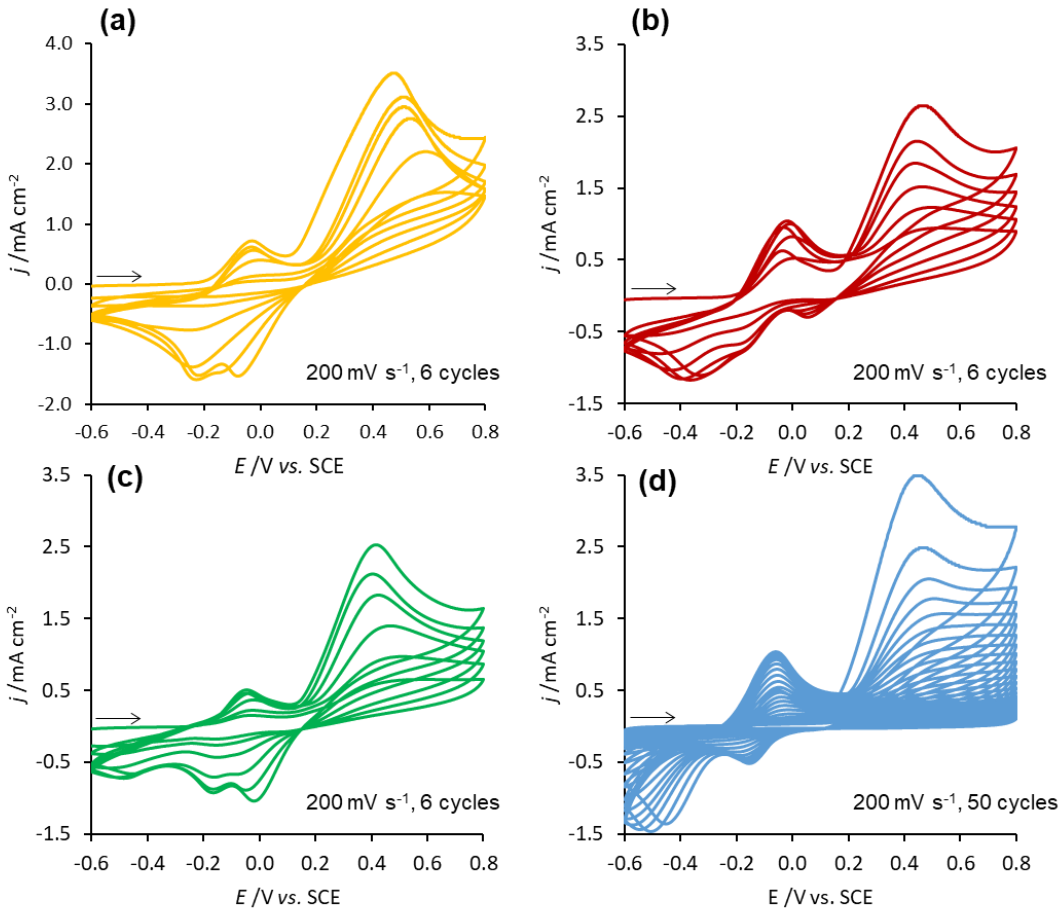

Figure 5.15: Potentiodynamic growth of polycatechol (a), polynorepinephrine (b), polydopamine (c) and polyDOPA (d) in the presence of 2.5 mM of aminoferrocene, performed at 200 mV s^{-1} for 6 or 50 potential cycles (as indicated in the graphs) in a deoxygenated CPB pH 7.0 solutions containing 5 mM of monomer.

It is important to mention that the oxidation of the monomer generates quinone species in solution that are ready to react with nucleophilic species. In this case, the deprotonated aminoferrocene may act as a nucleophile and attack the quinone groups, being incorporated in the polymer through covalent bonding. Although this particular reaction is not found in the literature, the reaction of aniline and 4-methylcatechol is reported [52]. Covalent binding is therefore a possibility to consider, although it was not possible to detect any new redox process attributable to such theoretical covalent adduct which implies it does not form quantitatively in solution.

The cyclic voltammetric response of the new modified films in a narrow potential window is shown in **Figure 5.16**. A redox process centred at *ca.* -0.1 V can be clearly depicted for the case of ePDA, ePNE and ePCA matrices, confirming a successful immobilization of aminoferrocene. Although the exact type of immobilization of this redox active compound can not be clearly deduce from the gathered data, the stable redox signal in the studied potential

window of **Figure 5.16** indicates a stable immobilization. Since no electrochemical direct evidence for the formation of covalent adducts between aminoferrocene and monomers or oligomers is found, the most probable immobilization type is the electrostatic entrapment and the least probable scenario is the superficial adsorption.

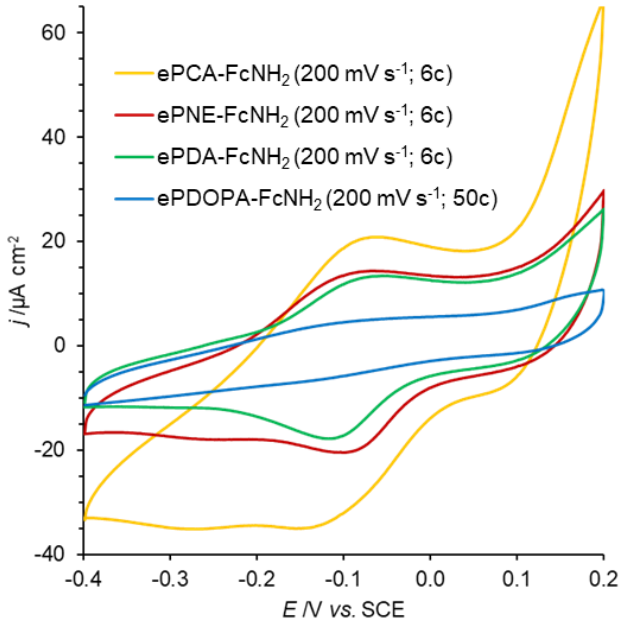

Figure 5.16: Cyclic voltammograms, recorded at 50 mV s^{-1} in deoxygenated CPB pH = 7.0 buffer, of gold modified electrodes with polycatechol (ePCA), polynorepinephrine (ePNE), polydopamine (ePDA) and polyDOPA (ePDOPA) electrosynthesized in the presence of 2.5 mM aminoferrocene ($FcNH_2$).

The average charge integrated from the area under each oxidation and reduction peak outputs the following estimates for the amount of immobilized aminoferrocene in polydopamine, polynorepinephrine and polycatechol, respectively: 1.9×10^{-10}, 2.5×10^{-10} and 6.2×10^{-10} mol cm^{-2}. Given the similar amount of estimate $FcNH_2$ in the ePDA and ePNE matrices, and considering the possible overlap between ePCA *p*-Q/HQ redox conversion – previously discussed (*cf.* **Figure 5.5**) – with $FcNH_2$ redox conversion, it can be reasoned that the real amount of immobilized $FcNH_2$ is similar for the three types of polymeric matrices. However, in the case of ePDOPA no redox signal attributable to aminoferrocene was detected, indicating that either the immobilization did not occur in similar extent as in the case of the other polymeric matrices, or the immobilization occurred and led to an electrochemically inactive film. Further optimization of the potential cycles may be carried out in order to fully evaluate the ability of ePDOPA regarding the immobilization of amine-containing compounds.

Nonetheless, the other three polymeric matrices are promising to the functionalization of electrode surfaces with small amines, biomolecules and nanometric entities.

5.4. Potentiostatic synthesis of polydopamine films

The electrochemical polymerization of catechol derivatives by potentiostatic methods is also a possible route to modify conductive surfaces with polymeric films, quickly and reproducibly. Since the polymerization of catechol derivatives is driven by its oxidation and formation of quinone species, the application of a fixed anodic potential is, in principle, an efficient way to grow a polymeric layer. As seen by the cyclic voltammograms of **Figure 5.1**, the minimum potential value to initiate the electropolymerization of the studied catechol derivatives at neutral conditions is *ca.* 0.1 V. From this value forward, potential is sufficiently high to promote the oxidation of the catechol function at the gold surface. Thus, several anodic potential values were chosen to study the potentiostatic synthesis of polydopamine, namely 0.2, 0.6 and 0.8 V, as seen in **Figure 5.17**. All the current profiles indicate the formation of low conducting polymeric layers since the current is gradually decaying towards zero (**Figure 5.17a**). The same behavior was already discussed previously in the potentiodynamic growth of polydopamine, where the thickening of the polymeric layer hinders the charge transfers processes across it. An opposite behavior is observed in the potentiostatic growth of electronically conducting polymers [26,53], where the increase in electroactive area leads to the increase of current during growth. The potentiostatic growths of polydopamine were followed by the gravimetric measurements shown in **Figure 5.17b**. Independently of the applied potential, the mass deposition profiles are characterized by an initial regime of fast and nearly linear growth with time, that further progresses into a constant regime of maximum mass – a mass variation behavior expected for the formation of a low-conducting layer. Importantly, the maximum of the deposited mass at the electrode can be tuned by the applied potential, revealing that higher potential values may be used to achieved higher polydopamine thicknesses.

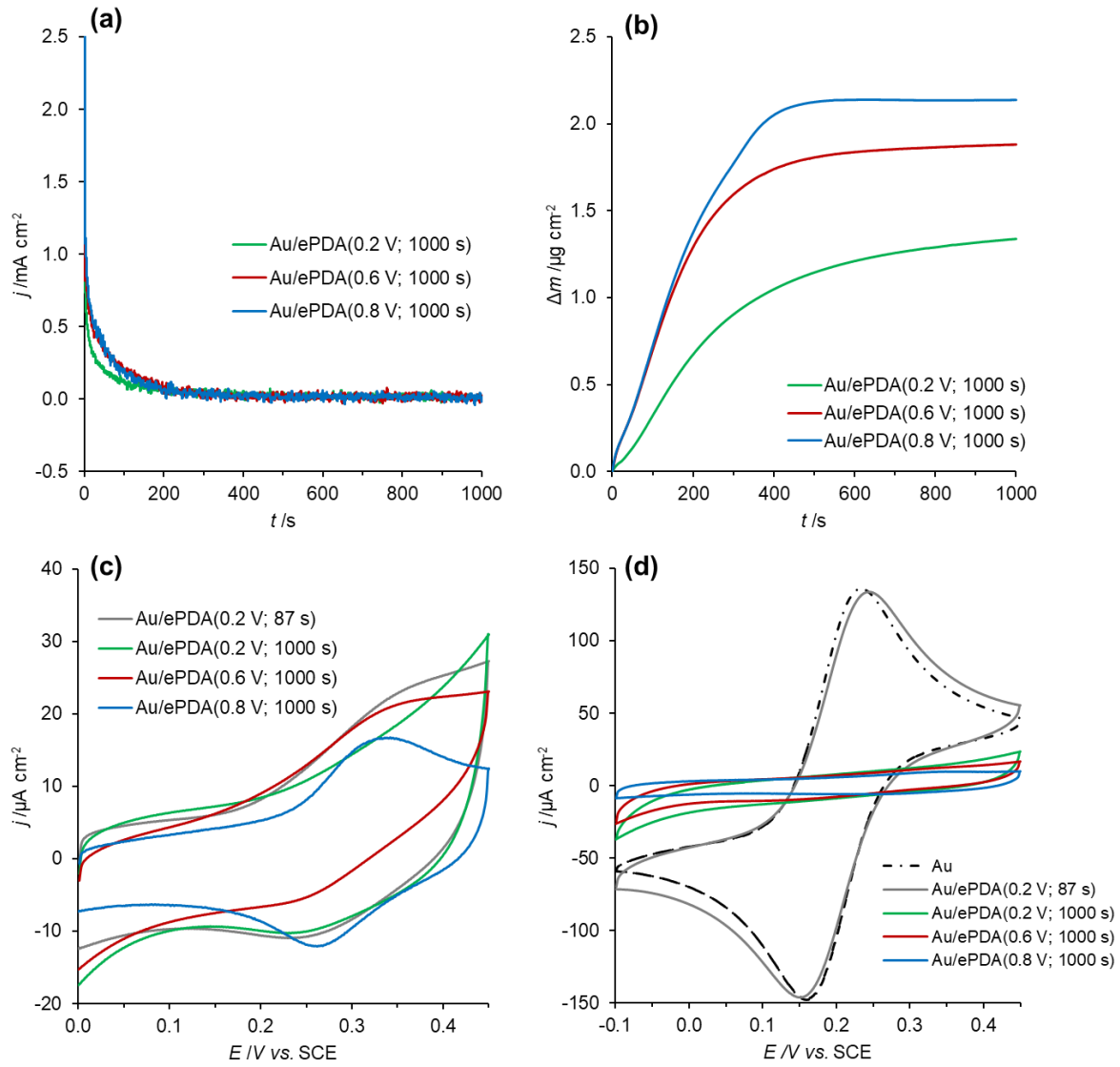

Figure 5.17: Chronoamperograms **(a)** and mass variation **(b)** profiles of the potentiostatic growth of polydopamine, at gold electrodes, applying 0.2, 0.6 and 0.8 V for 1000 s in a CPB pH=7.0 solution containing 5 mM of dopamine. Cyclic voltammograms of the modified electrodes in CPB pH=4.6 buffer **(c)** and in 0.25 M KNO_3 solution of 1 mM $K_3Fe(CN)_6$ **(d)** recorded at 50 mV s^{-1}. All solutions were deoxygenated with nitrogen.

The gold modified electrodes with potentiostatically synthesized polydopamine films were characterized in slightly acidic solution as depicted in the cyclic voltammograms of **Figure 5.17c**. The polydopamine film grown at 0.2 V for 1000 s do not show a significant redox activity since only a low intensity reduction wave is depicted around 0.23 V. However, if the growth is stopped at 87 s, the polymeric material deposited at the gold electrode displays the characteristic quinone/hydroquinone redox process (centered at *ca.* 0.3 V) of polydopamine. This decrease of redox activity with polymer thickening can be explained by the increase of the charge transfer resistance of a progressively thicker non-conducting polymeric phase, as discussed previously in Chapter IV. The cyclic voltammetric characterization of polydopamine

film grown after 87 and 1000 s in a ferricyanide solution (**Figure 5.17d**) also reveals that polymer thickening leads to the complete blocking of the charge transfer between the anionic probe and the electrode. This behavior is expected for compact and non-conducting films. When using higher potential values (0.6 and 0.8 V) to prepare the polydopamine films, the voltammetric responses in the ferricyanide solution of the electrode modified with those films displayed a more planar shape compared to the polydopamine film prepared using 0.2 V (**Figure 5.17d**). This is indicative of the formation of thicker films with increasing blocking properties as the applied potential increases, with similarly compactness and conductivity. However, the Q/HQ redox response of ePDA(0.6 V, 1000 s) film is more significant compared to ePDA(0.2 V, 1000 s) (**Figure 5.17c**). Furthermore, ePDA(0.8 V, 1000 s) film displays even better-defined Q/HQ redox peaks with a smaller peak separation. These results show that the electrochemical accessibility to the redox active groups of polydopamine improves when higher growth potential is used, although the thickening of the polymer is expected. The improvement of electrochemical accessibility may occur by the increase of protons mobility within the polymeric phase since these are necessary to electrochemically convert quinones to hydroquinones, and vice-versa. Therefore, the results point to the formation of thicker polydopamine films with a proton-conductive behavior, which may be interesting for diverse electrochemical applications [54].

In order to roughly evaluate the thickness of the polydopamine films after 1000 s of growth, the gold modified electrodes were characterized by *ex situ* ellipsometry using a single incident angle (**Table 5.4**). The pairs of Ψ,Δ measured for each polydopamine film are not successfully fitted assuming the same complex refractive index (varying only the thickness of the polymeric layer). In fact, Ψ values should decrease with polymer thickening for this hypothesis to be true, however, this parameter increased with the increase of growth potential. Although the exact complex refractive index cannot be determined for each polymer using data of a single incident angle, it is clear that the use of different applied potentials results in the formation of polymeric layers with distinct optical properties (distinct n,k values). This point corroborates the variation of redox activity exhibited by the three polymers that is indicative of clear differences in the polymeric structures.

Table 5.4: Average ellipsometric parameters (Ψ, Δ) measured at 70° of gold modified electrodes with polydopamine films grown potentiostatically at 0.2, 0.6 and 0.8 V for 1000 s, and respective fitted values of extinction coefficient (k) and thickness (L), considering fixed refractive indexes (n) of 1.45, 1.60 and 1.75.

E_{growth} /V	Ψ /°	Δ /°	n	k	L /nm
0.2	43.57 ± 0.03	98.7± 0.4	1.45	0.055	11.4
			1.60	0.074	9.4
			1.75	0.090	8.1
0.6	43.68 ± 0.03	92.7 ± 0.8	1.45	0.036	19.0
			1.60	0.047	15.6
			1.75	0.056	13.4
0.8	43.87 ± 0.03	86.0 ± 0.3	1.45	0.025	29.7
			1.60	0.031	23.7
			1.75	0.034	20.2

In addition, the observed decrease in Δ values is a strong indication of polymer thickness increase as the applied potential increases. To enable an evaluation of the effect of growth potential on the variations of *n*, *k*, and *L*, the experimental data is fitted using a large variation of *n* (from 1.45 to 1.75) as compiled in **Table 5.4** and better depicted in **Figure 5.18**. The wide variation in the obtained *k* values suggests distinct optical properties of the different polydopamine films, however, due to the assumptions used to obtain such values no further interpretations should be done. Analyzing the obtained thickness values, it is possible to confirm the thickening of polydopamine as the applied potential increases. Although the obtained thickness values are in the same order of magnitude as those obtained by the potentiodynamic method (*cf.* **Table 5.1**), the high hinderance to charge transfer observed for the ferricyanide probe (*cf.* **Figure 5.10d**) invalidates the use of such films in the construction of biosensing interfaces with electrochemical transduction. Nonetheless, the potentiostatic method hereby presented allows a fast and controllable deposition of polydopamine at the electrode surface, which can be adjusted to synthesize thinner films where charge transfer is still occurring.

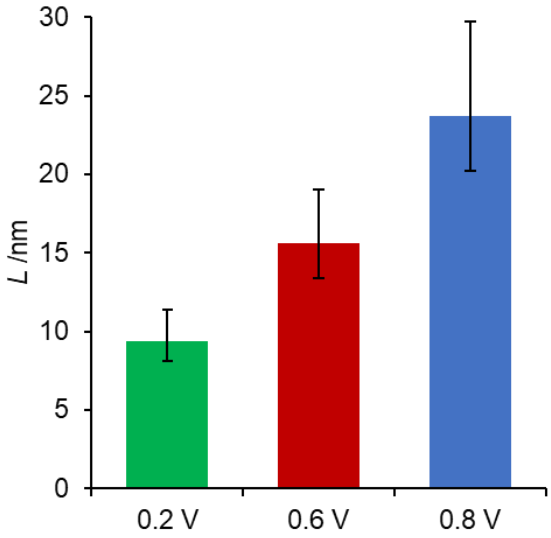

Figure 5.18: Fitted thicknesses of **Table 5.4** regarding polydopamine films grown potentiostatically at 0.2, 0.6 and 0.8 V for 1000 s. Bar heights display the thickness at n = 1.60, while the error bars display the variation of thickness at n = [1.45; 1.75].

5.5. Ion permeable polydopamine films

Previous works have shown that electrochemically synthesized polydopamine is a poorly conductive material that precludes its continuous thickening, reaching a plateau after a certain number of potential cycles, as observed by electrochemical quartz crystal microbalance (**Figure 5.4**). Although, typically, electropolymerization yields more permeable films than chemically synthetized ones, with the same thickness, it was shown that after *ca.* 30 nm both types of polydopamine films block the electron transfer of anionic species, still allowing for the transduction of neutral and cationic species. Nevertheless, after *ca.* 45 nm polydopamine coatings totally inhibit charge transfer of multivalent metal complexes [23,55]. Thus, improving the permeability and conducting properties of the highly adherent polydopamine films is still an important challenge that hampers the further development of biomimetic electrochemical applications, namely biosensing. With the purpose of increasing thickness, electroactivity and permeability of polydopamine, the electropolymerization of dopamine was performed potentiodynamically by increasing the upper potential limit to 1.1 V, instead of the commonly used 0.5 V [22,56] or 0.8 V [3,57,58]. The gold electrode was chosen to facilitate the accomplishment of a combined gravimetric and ellipsometric in-depth study of dopamine electropolymerization in this new condition. **Figure 5.19** shows the cyclic voltammograms recorded between -0.8 V and two different anodic limits, 0.8 V (**Figure 5.19a)** and 1.1 V (**Figure 5.19b**), for 100 potential cycles at 200 mV s^{-1}. The overall shape of the two voltammograms is identical and encompasses two main redox processes, assigned to the

dopamine/dopaminequinone (I) and dopaminechrome/leucodopaminechrome conversion (II) [55,57]. When the potential is cycled until 0.8 V, the intensity of both redox processes decreases progressively, indicating the formation of a polydopamine film that, due to its low conductivity compared to bare gold, hinders monomer and its derivatives electrochemical conversions. However, when the potential is cycled until 1.1 V, the intensity of process I only decreases initially (1 – 25th cycle), increasing afterwards, as shown in the current profiles of **Figure 5.19c**. This contrasting behavior is better illustrated in **Figure 5.19d** and **5.19e**, where both oxidation and reduction currents of process I clearly increase from the 25th to the 100th cycle (**Figure 5.19e**). As far it is concerned, this is the first report showing the increment of polydopamine redox conversion during potential cycling, reflecting its greater ability for monomer conversion, compared to polydopamine films prepared up to 0.8 V. It is worth noting that cycling the gold electrode at neutral pH between 0.8 and 1.1 V will slightly oxidize the metal with a consequent formation of gold oxide (Au_2O_3) [58], which is then reduced back to Au^0 on the reverse sweep, at *ca.* 0.5 V (**Figure 5.19e**). Thus, the distinct electrochemical polymerization process observed for ePDA(1.1 V) may also be related with the roughness increase of the underlying gold [59], which is responsible for an increase of surface area.

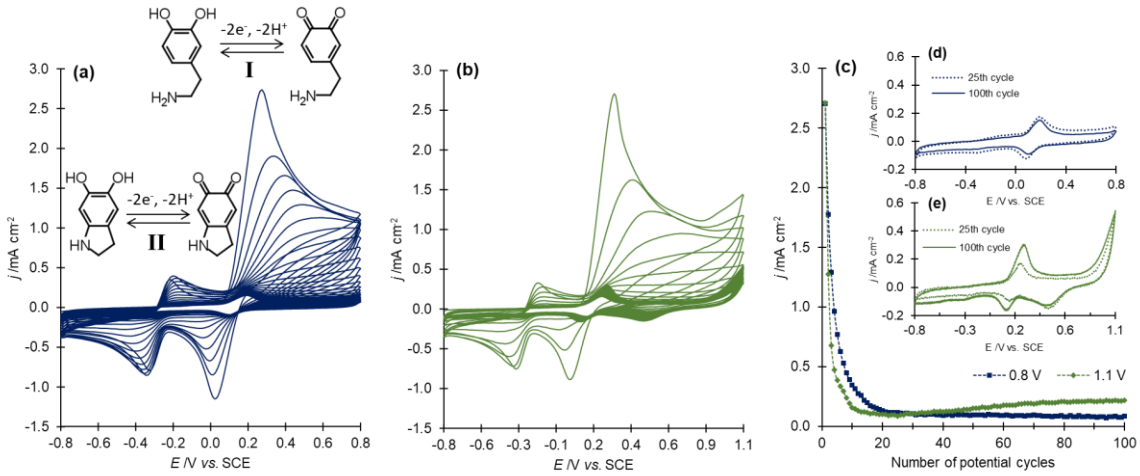

Figure 5.19: Potentiodynamic polymerization of 5 mM dopamine in CPB pH 7 at 200 mV s^{-1}, for 100 cycles between -0.8 V and 0.8 V **(a)** and 1.1 V **(b)**; Anodic current values *versus* number of potential cycles **(c)**, obtained at 0.28 V from the cyclic voltammograms shown in (a) and (b). The insets **(d)** and **(e)** compare the 25th and the 100th cyclic voltammogram of (a) and (b), respectively.

The electropolymerization kinetics of ePDA(0.8 V) and ePDA(1.1V) was followed by EQCM (**Figure 5.20**). The change in frequency obtained for ePDA(0.8 V) indicates a fast initial deposition rate, followed by a plateau which reveals the formation of a poorly conducting polymeric phase that does not allow the oxidation of dopamine quantitatively. In fact, after the 25th potential cycle the polymer growth drastically slows down, keeping a constant and very

slow deposition rate (**Figure 5.20a**), as reported recently for ePDA(0.8 V) grown with only 50 polymerization cycles [55]. In the case of ePDA(1.1 V), the change in frequency up to approximately 25 cycles is similar, although slightly larger than that observed for ePDA(0.8 figure 5.20V), which is consistent with a higher amount of deposited polymer, due to the application of a more positive anodic potential limit, promoting oxidation of more monomers. Nevertheless, as clearly depicted, there is a drastic change in frequency from the 25^{th} to 100^{th} cycle, denoting the formation of a much thicker and probably porous film (**Figure 5.20b**). By converting the change in frequency to mass variation using the Sauerbrey equation (*cf.* **Equation 2.5**), values of 3.0 μg cm^{-2} is obtained at the end of ePDA(0.8 V) potentiodynamic polymerization, whereas 5.2 times more mass is obtained for ePDA(1.1 V) case (15.7 μg cm^{-2}). Interestingly, the estimated optical thicknesses upon drying are 27 nm and 66 nm for ePDA(0.8 V) and ePDA(1.1 V) films, respectively, representing a lower proportion. The lack of proportionality between the calculated mass and thickness suggests that ePDA(1.1 V) should be much more porous in comparison to ePDA(0.8 V), incorporating a larger amount of electrolyte solution during its electrochemical growth. According to these results, the linear frequency-to-mass relation of the Sauerbrey equation is compromised for ePDA(1.1 V) film. Furthermore, although the origin for the drastic change in frequency is not fully understood, we postulate the hypothesis that upon consecutive cycling the film loses adherence to the gold electrode locally, which may allow electrolyte incorporation and further polymer growth. It is worth noting that there are no drastic changes occurring in the cyclic voltammograms of ePDA(1.1 V) film around the 25^{th} cycle nor upon (**Figure 5.19e**), proving that the film is attached to the electrode surface throughout potential cycling.

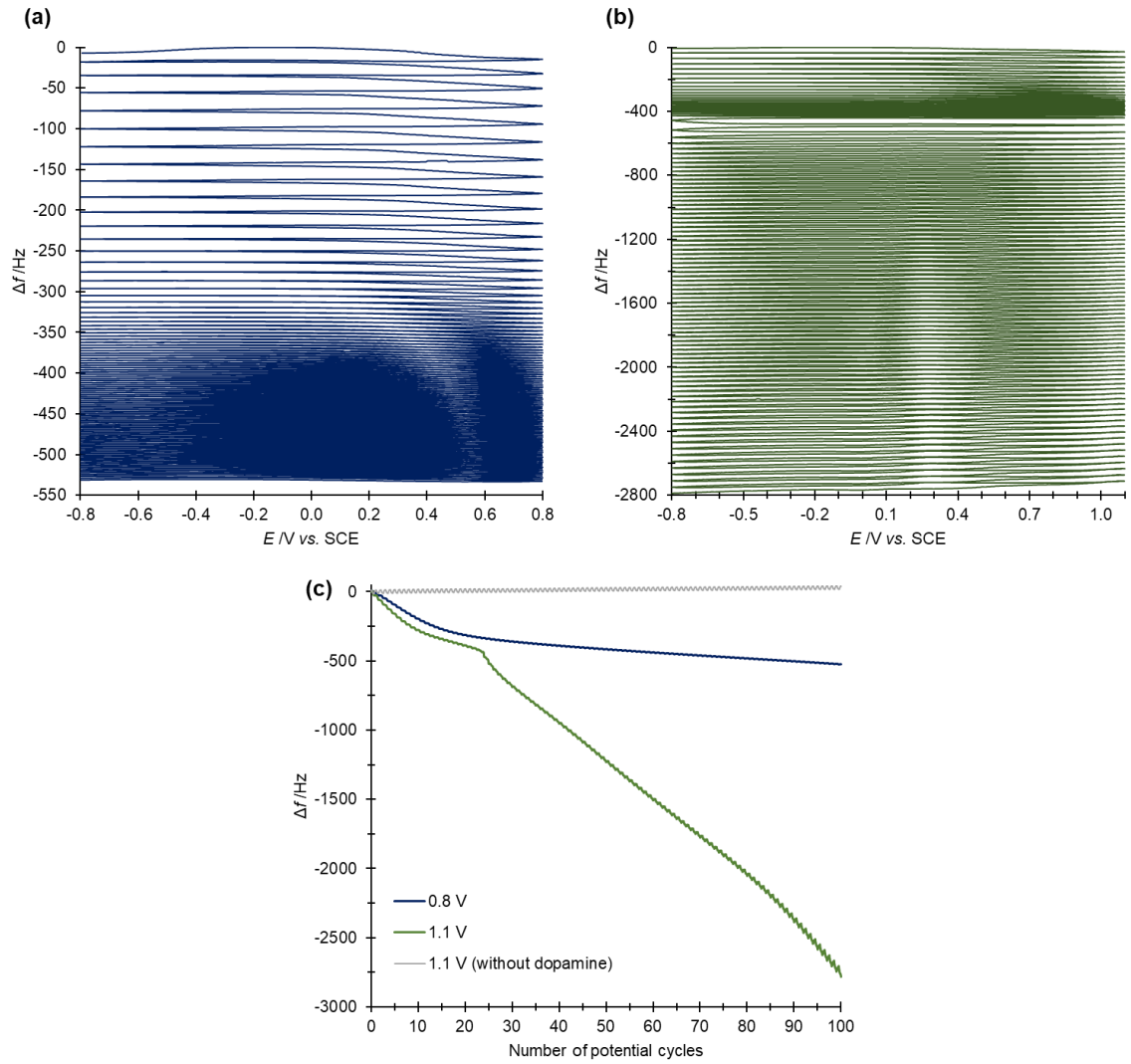

Figure 5.20: EQCM mass variation during the potentiodynamic polymerization of 5 mM dopamine in CPB pH 7 at 200 mV s^{-1}, for 100 cycles using an upper limit of 0.8 V **(a)** or 1.1 V **(b)**; EQCM mass variations**(c)** of panels (a) and (b) as a function of number of potential cycles; Gold cycling, without dopamine, in CPB pH 7 at 200 mV s^{-1} for 100 cycles using an upper limit of 1.1 V is also presented in panel (c).

To further understand the phenomenon observed by EQCM, around the 25th potential cycle, the potentiodynamic growth was also monitored by *in situ* ellipsometry. **Figure 5.21a** and **5.21b** show the raw data regarding the change in the ellipsometric parameters Ψ (azimuth angle) and Δ (phase difference) acquired during the growth of ePDA(0.8 V) and ePDA(1.1 V), respectively. It is worth to note that in the absence of dopamine in solution consecutive potential cycling (up to 100 cycles) does not produce important variation of the ellipsometric parameters of gold electrode (**Figure 5.21b**). In contrast, there is a drastic difference in the evolution of the ellipsometric parameters over the two electropolymerization processes, exhibiting very distinct profiles amongst them. Since Ψ and Δ at the cathodic and anodic limits are very similar, as observed in **Figure 5.21a** and **5.21b**, the physical models were fitted to the ellipsometric data

(**Figure 5.21c** and **5.21d**) acquired at the cathodic limit (-0.8 V). The complexity of the data requires multi-phase models to reasonably predict the experimental variations. Thus, several isotropic, homogeneous and finite layers were necessary to model the overall polydopamine growth: for ePDA(0.8 V) growth one layer was used (**Figure 5.21e**), whereas for ePDA(1.1 V) growth three layers were necessary (**Figure 5.21f**). The initial polymer layer formation occurs up to the 20th cycle of ePDA(0.8 V) growth (segment A) and up to the 18th cycle of ePDA(1.1 V) growth (segment C), where similar ellipsometric curves were fitted, differing manly in the rate of growth per cycle: 1.9 nm/cycle and 2.9 nm/cycle, respectively. Hence, at these initial segments, the use of a higher anodic limit (1.1 V) results in the increase of thickening rate of a layer with similar optical properties (1.48-0.020i, 52.2 nm), compared to that obtained for ePDA(0.8 V) (1.49-0.024i, 38.0 nm). It is worth noting that both ePDA(0.8 V) and ePDA(1.1 V) growth profiles (segments A and C, respectively) exhibit an intricate behavior that was simplified by fitting one global effective layer, in order to extract *n* and *k* values with physical meaning, and to allow the computation of the following layers. In **Figure 5.21c**, the dotted lines demonstrate that segment A can also be described (better, but not fully) by two homogenous layers with different *n* values, suggesting that ePDA films are optically denser up to *ca.* 13 nm, and less dense afterwards. This result corroborates the decrease of *n* values with polymer thickening, previously observed for thin polydopamine films electrodeposited on glassy carbon electrodes, estimated by *ex situ* ellipsometry (**Table 4.1**).

After the initial polymer layers formation, very distinct ellipsometric curves develop depending on the electropolymerization conditions. Concerning ePDA(0.8 V), upon the formation of the first effective layer (**Figure 5.21e**), between the 21st and 92nd potential cycle, the ellipsometric data are consistent with a change in the rate of polymer thickening, from 1.9 to 0.2 nm/cycle. This much slower growing stage (segment B) is characterized by the conversion of the pre-exiting layer to a denser material, with a final complex refractive index of 1.52-0.026i. This result corroborates the EQCM data for this polymer, ePDA(0.8 V), in which frequency values attain a plateau near the same polymerization stage. After the 92nd cycle, the data was not fitted to a reasonable model with physical meaning.

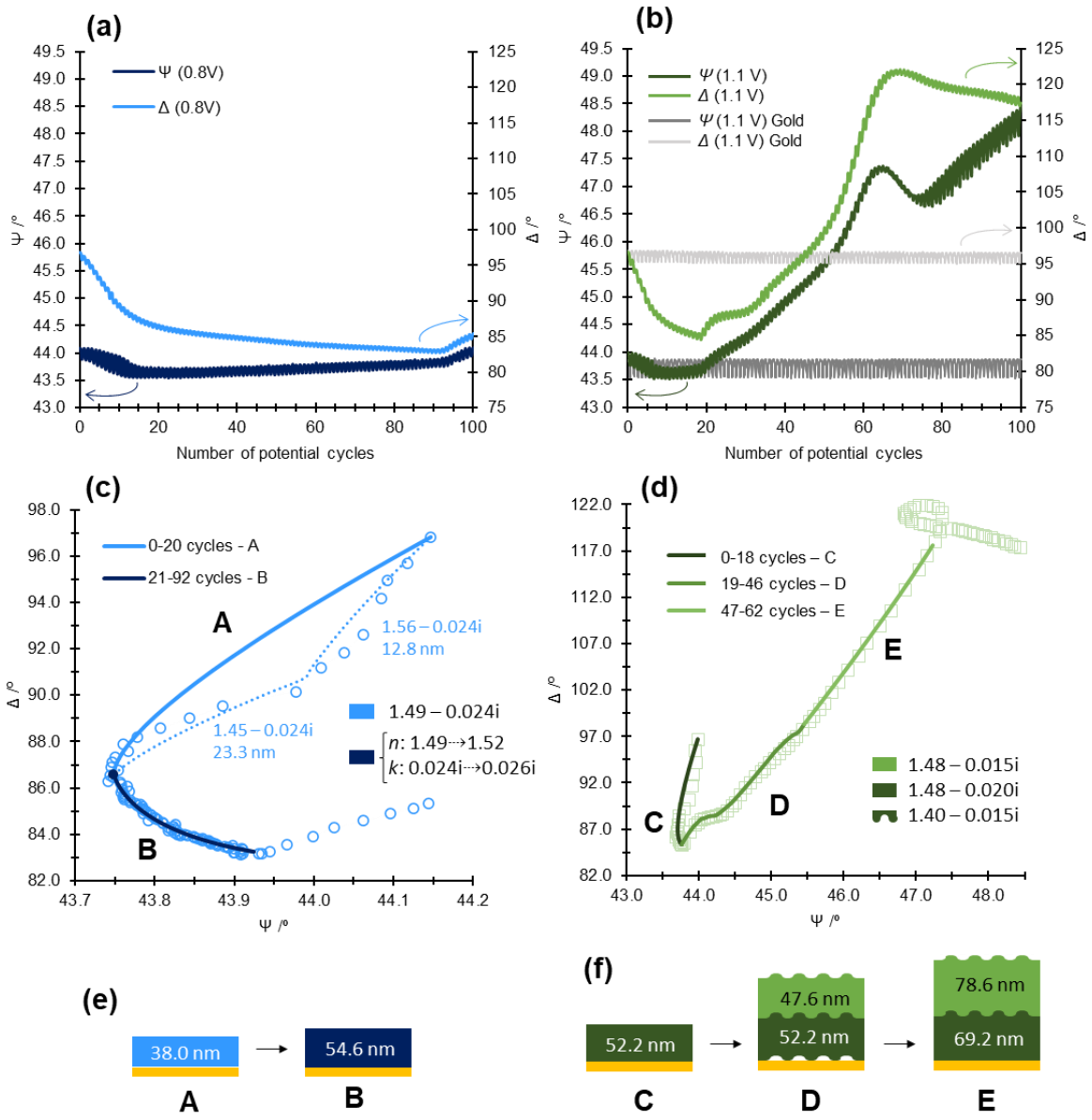

Figure 5.21: Evolution of the experimental ellipsometric parameters, *Ψ* and *Δ*, *versus* number of polymerization cycles during the electropolymerization of 5 mM dopamine, at pH 7.0, up to 0.8 V **(a)**; and up to 1.1 V **(b)**; Representation of the *Δ versus Ψ* collected at the cathodic limit during the potentiodynamic polymerization up to 0.8 V **(c)** and up to 1.1 V **(d)**, and corresponding theoretical trajectory (line) generated by assuming the models represented in panel **(e)** and **(f)**, respectively. Details of the fitting process are given in the text.

In the case of ePDA(1.1 V), between 19 and 46 potential cycles (segment D), the *Ψ-Δ* curve follows an unexpected shape which is not explained by the simple thickening of the already fitted layer, neither through the simulation of the growth a new isotropic layer in contact with solution. For this reason, the data was best fitted considering the formation of a very porous polymer layer adjacent to the electrode surface, containing a high percentage of electrolyte, as revealed by its *n* and *k* values (1.40-0.015i), that lie between those obtained for polymer (1.48-0.020i) and electrolyte (1.335-0i). Nevertheless, in order to have a proper fitting, this very

porous layer should only exist during segment D, growing 17 nm in the first 4 potential cycles, and decreasing afterwards until it disappears at the 46th potential cycle. The regression of the porous layer is interpreted as polymer growth in the interstitial vacancies previously occupied by the electrolyte solution, occurring in the direction of the electrode. Concomitantly with the presence of this interlayer, ePDA continues to grow on the top of the first polymer layer (up to 47.6 nm) with very similar dielectric properties (1.48-0.015i) – **Figure 5.21f**, segment D. After 46 and up to 62 potential cycles (segment E), polymer thickening occurs at 1.7 nm/cycle until the 54th cycle, and thereafter the rate of deposition increases to 2.5 nm/cycle, keeping the same complex refractive index. An abnormal ellipsometric behavior occurs after this segment, precluding the correct fitting of the experimental data to a physically meaningful model. However, the data points to the presence of a less dense layer that could not be fitted as a homogeneous and isotropic layer. In spite of this, the *in situ* ellipsometric data undoubtedly reveals that the application of 1.1 V as anodic limit, yields a considerably thicker and more porous polymer (lower *n* and *k* values) than when limiting the upper limit potential as 0.8 V.

The morphology of the thicker ePDA(1.1 V) films synthesized with 20 and 100 potential cycles was characterized by AFM. Representative images are shown in **Figure 5.22**. Upon 20 potential cycles (**Figure 5.22a**), a smooth and uniform granular morphology, typical of this type of polymer [55], is observed; whereas a radically different morphology was consistently recorded for films prepared with 100 cycles. From **Figure 5.22b**, one can depict two distinct morphologies: (A) an underlying polymer layer, less uniform than that formed upon 20 cycles, exhibiting small globular clusters of about 50 nm diameter; and (B) fiber-like polymeric structures (50 – 100 nm diameter), most of them forming a kind of opened rings on top of slightly elevated polymer circular platforms protruding from the bottom of the polymeric layer. In addition, the fiber structures are apparently coming out from the polymer, as illustrated in more detail in **Figure 5.19c**. From phase contrast imaging (data not shown), the fibers consist of polydopamine that grew in a preferential manner, and this observation is confirmed by XPS studies, as discussed below. The average thicknesses of the films after 20 and 100 cycles, measured by AFM, are *ca.* 18 and 60 nm, respectively, corroborating the values estimated by ex situ ellipsometry (*ca.* 17 and 66 nm). It is worth to point out that after 25 cycles (data not shown), there are already fibers deposited on the top of the polymeric layer. The drastic change in morphology must be related to the disruptive phenomena observed during the electrosynthesis of ePDA(1.1 V), followed by EQCM and ellipsometry.

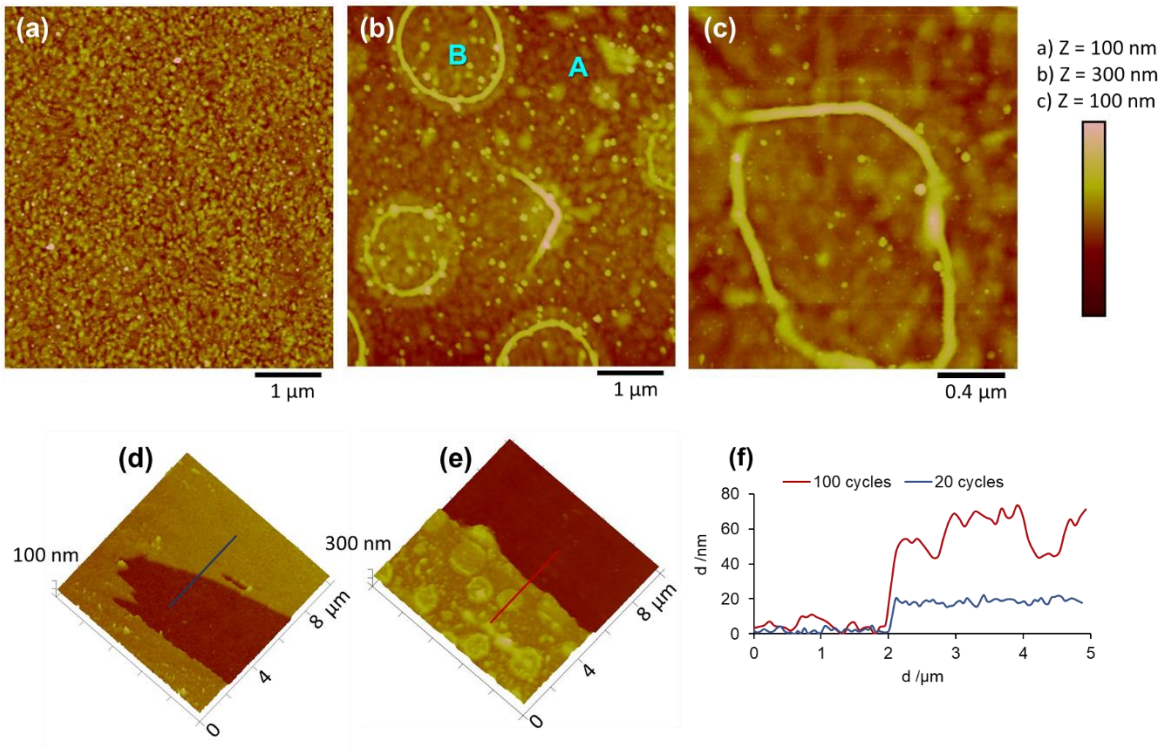

Figure 5.22: AFM morphological images of gold modified with ePDA(1.1 V) after 20 **(a)** and 100 **(b)** potential cycles; Amplified image of fiber-like structures of ePDA(1.1 V) grown after 100 potential cycles **(c);** 3D topographical images of the same modified surfaces intentionally scratched – 20 **(d)** and 100 **(e)** growth cycles– and respective high profiles **(f)**.

As clearly seen from the three-dimensional image of ePDA(1.1 V), formed with 100 cycles (**Figure 5.22e**), there are circular platforms protruding from the polymer matrix, which should be due to the local and temporary loss of polymer adhesion around the 20th cycle, which should be progressively filled with new polymeric segments during polymer thickening, as suggested during ellipsometric data discussion, and illustrated in **Figure 5.21f**.

FTIR and XPS analyses were carried out to disclose the differences in the chemical compositions of polymers formed upon 20 and 100 potential cycles (**Figure 5.23**). FTIR spectra reveal typical bands expected for polydopamine on both films (**Figure 5.23a**). Briefly, the broad band between 3700 – 3000 cm^{-1} corresponds to ν(O-H) and ν(N-H) stretching modes; the low intensity peak at *ca.* 2900 cm^{-1} can be assigned to the alkane ν(C-H), whereas the strong band at 1600 cm^{-1} is due to the ν_{as}(CC)aromatic mode. Consistently with reported studies of electrosynthesized polydopamine films [3,55], there is a suppression of the ν_{s}(CC)aromatic mode at around 1510 cm^{-1}, present in dopamine monomer spectrum, indicating a different aromaticity of the catechol moieties within the polymer, probably due to the establishment of C-C bonds amongst monomeric units. As foreseen, the bands are much better defined for the thicker film, grown with 100 cycles, although the spectra reveal the same chemical composition

for both polymers. According to the XPS characterization, the O/C, N/C and N/O atomic ratios of polydopamine synthesized with 20 and 100 cycles are 0.28, 0.10, 0.38 and 0.29, 0.10, 0.35, respectively, also disclosing a very similar composition. In addition, the values are close to those calculated for the dopamine monomer (ratios of 0.25, 0.12, 0.50, respectively), which indicates that no other chemical functions are present, resulting, for instance, from polymer degradation. It is noteworthy, that both films exhibit less than 1% of gold in their composition, indicating that there was no contamination of polydopamine by the underlying substrate, which oxidized and reduced during this process. In fact, a thorough analysis of C 1s, O 1s (**Figure A5**) and N 1s regions (**Figure 5.23b,c**) confirm the presence of chemically identical polymers after 20 and 100 cycles. Moreover, the carbon and oxygen spectra are in great agreement with those obtained for ePDA(0.8 V) with 50 cycles, suggesting a great structural similarity in the overall polycatecholic backbone of the polymers regardless of the used anodic limit. However, analyzing the N 1s region of polydopamine films grown using high (1.1 V) and low (0.8 V) anodic limits, it is possible to find a significant difference amongst the pyrolitic contributions to their spectra (**Figure 5.23b–d**). The two spectra of ePDA(1.1 V) films exhibit a very low aromatic contribution compared to that of ePDA(0.8 V), strongly suggesting the absence of indolinic moieties in the first cases. Furthermore, the greater aliphatic amine contribution in ePDA(1.1 V) spectra, is also indicative of a more homogeneous polymer compared to the one synthesized with a lower anodic limit.

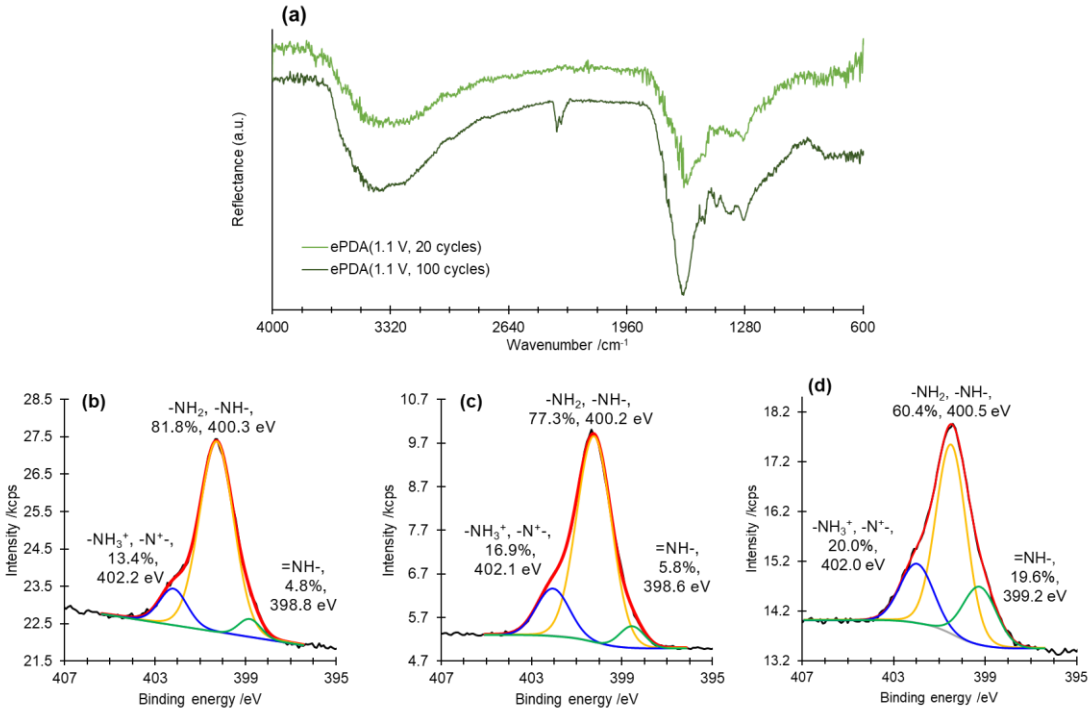

Figure 5.23: FTIR **(a)** and XPS spectra of N 1s region **(b, c)** of ePDA(1.1 V) synthesized with 20 cycles **(b)** and 100 **(c)** cycles; XPS spectra of N 1s region of ePDA(0.8 V) synthesized with 50 cycles **(d)**.

So far, it is demonstrated that dopamine can electropolymerize using an anodic limit of 1.1 V, yielding coatings with higher thickness and very distinct morphology than the typical smooth films of this type of material [3,78], although chemically identical. A very important goal is to prove that this new coating exhibit good electroactivity and permeability to redox species, in contrast with previously reported polydopamine films. **Figure 5.24a** shows the electrochemical behavior of ePDA(1.1 V) formed with 20 and 100 potential cycles, where there is only one main redox process, centered at 0.3 V (ΔE_p = 0.004 V and 0.007 V, respectively) attributed to the uncyclized form of polydopamine, as discussed before. The electrochemical data does not reveal the presence of other indolinic or indolic polymeric forms, commonly detected for thinner polydopamine films prepared with lower anodic limits. This agrees with the previous XPS analysis of the nitrogen spectral regions. The other striking difference is the much higher faradaic current observed for the thicker film, in contrast with previous reports where electroactivity decreased with polymer thickness. This agrees with the increase in current at dopamine oxidation potential, detected upon the 25th cycle during the electropolymerization process carried out up to 1.1 V (**Figure 5.16c** and **5.15e**). These results indicate the presence of a rougher and probably porous film that allow a better electron transfer across it. In fact, by recording the cyclic voltammograms of ePDA(1.1 V) in the presence of hexaaminеruthenium chloride (**Figure 5.24b**), this species could be detected by both films, although much better by the thicker and more electroactive film. This phenomenon, also involving adsorption of the ruthenium complex in the film, is in great contrast with the observed for other thinner polydopamine films presented before, grown up to 0.8 V (*ca.* 20 nm), which totally hampered the electrochemical conversion of this redox species. This result highlights the suitability of extending the anodic potential limit to create polymers with enhanced permeability properties.

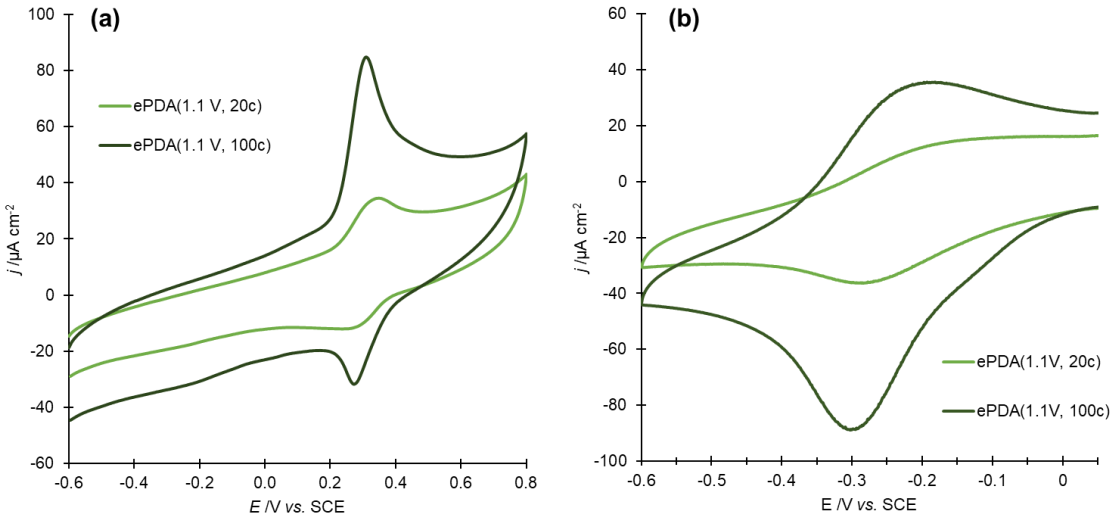

Figure 5.24: Cyclic voltammograms of ePDA(1.1 V) films in deaerated **(a)** CPB solution pH 4.6 and **(b)** 1 mM $[Ru(NH_3)_6]Cl_3$ 0.25 M KCl solution, recorded at 20 mV s^{-1}.

5.6. Conclusions

The detailed investigation presented in this chapter allowed to disclose the effects of several chemical functions (amine, hydroxyl and carboxyl) in the electropolymerization process of catechol derivatives, and consequently in the physicochemical properties of the resulting thin polymeric films. Parameters such as the morphology and adhesion forces, evaluated by AFM, were not significantly affected by the pendant chemical groups, since all the polymers display a smooth, uniform, and granular morphology with similar adhesion forces towards an amine-functionalized tip.

The proximity between the amine and catechol groups leads to the formation of cyclized species, increasing the complexity of the electropolymerization process and chemical composition of the resulting polycatecholamines. By combining the EQCM and *ex situ* ellipsometric data, it is possible to infer that the amine group, in dopamine and norepinephrine monomers, accelerates polymer thickening, although the resulting films are more compact and less electroactive comparing to polycatechol. In contrast, catechol, caffeic acid and DOPA generate very porous films, since more than half of the mass change over polymerization is caused by electrolyte entrapment. Furthermore, the carboxyl group is clearly identified as an inhibitor of polyDOPA and poly(caffeic acid) growth, as seen by their low mass deposition rates and low thicknesses. Thus, the amine and carboxyl groups of the starting monomers are crucial in determining the polymers growth rate and porosity, while the hydroxyl group do not play a significant role.

The polymers hydroquinone/quinone redox conversions indicate that the major polymeric units should consist on pristine uncyclized monomers, incorporating a lower amount of indoline and indolic type species. Amongst polycatecholamines, ePNE is the most electroative polymer and possess the lowest fraction of cyclized species. Regarding ePCA, the main polymeric species should derive from C-C coupling of oxidized catechol units, but polymerization via C-O-C coupling should also take place. Detailed XPS analysis shows the conservation of monomers specific structural groups, hydroxyl and carboxylic acid of ePNE and ePOPA, respectively, and confirms that ePDA contains the highest fraction of aromatic amines amongst polycatecholamines. ePDOPA and ePNE are very hydrophilic, corroborating the presence of OH and COOH groups, and present lower water contact angle values compared to chemically synthetized PNE and PDOPA coatings, demonstrating that electrochemical synthetic routes are advantageous to control the polymerization process.

As a final conclusion, all the polymers display a thickness-dependent electroactivity and charge transfer properties that reflect their low conductivity and overall negative net charge. Thus, electrochemical methods are crucial to finely tune polymer thickness and accomplish the optimal requirements for a given application, namely those requiring electrochemical transduction. According to the selected monomer and electrosynthesis conditions, different charge transfer properties can be achieved, at distinct pH solutions, making possible the detection of negatively or positively charged species.

Further possible enhancements of the biosensing performances are envisaged by the electrochemical synthesis of polycatecholamines using higher anodic limits. As demonstrated for dopamine case, the use of a high anodic limit leads to a distinct polymeric growth profile and allows the formation of polymeric films with higher roughness, porosity, electroactivity and ion permeability compared to those synthesized using lower anodic limits. These are critical parameters to increase enzyme load without compromising electrochemical signals. FTIR and XPS data indicate that the thicker polydopamine films display typical chemical compositions of polydopamine, and good electroactivity of the quinone/hydroquinone pendant groups. Regrettably, endeavors to immobilize fungal laccase did not yield electrodes with noteworthy electrocatalytic properties, prompting the discontinuation of the use of such polymers.

5.7. References

[1] H. Lee, S.M. Dellatore, W.M. Miller, P.B. Messersmith, Mussel-inspired surface chemistry for multifunctional coatings, Science. 318 (2007) 426–430. doi:10.1126/science.1147241.

[2] G.P. Maier, M. V. Rapp, J.H. Waite, J.N. Israelachvili, A. Butler, Adaptive synergy between catechol and lysine promotes wet adhesion by surface salt displacement, Science. 349 (2015) 628–632. doi:10.1126/science.aab0556.

[3] L.C. Almeida, R.D. Correia, A. Marta, G. Squillaci, A. Morana, F. La Cara, J.P. Correia, A.S. Viana, Electrosynthesis of polydopamine films - tailored matrices for laccase-based biosensors, Applied Surface Science. 480 (2019) 979–989. doi:10.1016/j.apsusc.2019.03.015.

[4] E. Faure, C. Falentin-Daudré, C. Jérôme, J. Lyskawa, D. Fournier, P. Woisel, C. Detrembleur, Catechols as versatile platforms in polymer chemistry, Progress in Polymer Science. 38 (2013) 236–270. doi:10.1016/j.progpolymsci.2012.06.004.

[5] A. Afkham, D. Nematollahi, L. Khalafi, M. Rafiee, Kinetic study of the oxidation of some catecholamines by digital simulation of cyclic voltammograms, International Journal of Chemical Kinetics. 37 (2005) 17–24. doi:10.1002/kin.20046.

[6] I. Ismail, T. Okajima, S. Kawauchi, T. Ohsaka, Studies on the early oxidation process of dopamine by electrochemical measurements and quantum chemical calculations, Electrochimica Acta. 211 (2016) 777–786. doi:10.1016/j.electacta.2016.05.056.

[7] D. Nematollahi, H. Shayani-Jam, M. Alimoradi, S. Niroomand, Electrochemical oxidation of acetaminophen in aqueous solutions: Kinetic evaluation of hydrolysis, hydroxylation and dimerization processes, Electrochimica Acta. 54 (2009) 7407–7415. doi:10.1016/j.electacta.2009.07.077.

[8] F. Mack, H. Bönisch, Dissociation constants and lipophilicity of catecholamines and related compounds, Naunyn-Schmiedeberg's Archives of Pharmacology. 310 (1979) 1–9. doi:10.1007/BF00499868.

[9] T.A. Enache, A.M. Oliveira-Brett, Phenol and para-substituted phenols electrochemical oxidation pathways, Journal of Electroanalytical Chemistry. 655 (2011) 9–16. doi:10.1016/j.jelechem.2011.02.022.

[10] J. Davis, D.H. Vaughan, M.F. Cardosi, Modification of catechol polymer redox properties during electropolymerization in the presence of aliphatic amines, Electrochimica Acta. 43 (1998) 291–300. doi:10.1016/S0013-4686(97)00086-8.

[11] R. Pourghobadi, D. Nematollahi, M.R. Baezzat, S. Alizadeh, H. Goljani, Electropolymerization of catechol on wireless graphite electrode. Unusual cathodic polycatechol formation, Journal of Electroanalytical Chemistry. 866 (2020) 114180. doi:10.1016/j.jelechem.2020.114180.

[12] T. Palomäki, S. Chumillas, S. Sainio, V. Protopopova, M. Kauppila, J. Koskinen, V. Climent, J.M. Feliu, T. Laurila, Electrochemical reactions of catechol, methylcatechol and dopamine at tetrahedral amorphous carbon (ta-C) thin film electrodes, Diamond and Related Materials. 59 (2015) 30–39. doi:10.1016/j.diamond.2015.09.003.

[13] S. Dubey, D. Singh, R.A. Misra, Enzymatic synthesis and various properties of poly(catechol), Enzyme and Microbial Technology. 23 (1998) 432–437. doi:10.1016/S0141-0229(98)00063-5.

[14] M.A. Rahman, H.A. Al-Abadleh, Surface Water Structure and Hygroscopic Properties of Light Absorbing Secondary Organic Polymers of Atmospheric Relevance, ACS Omega. 3 (2018) 15519–15529. doi:10.1021/acsomega.8b02066.

[15] Y. He, Q. Chen, Y. Zhang, Y. Zhao, L. Chen, H_2O_2 -Triggered Rapid Deposition of Poly(caffeic acid) Coatings: A Mechanism-Based Entry to Versatile and High-Efficient Molecular Separation, ACS Applied Materials & Interfaces. 12 (2020) 52104–52115. doi:10.1021/acsami.0c13382.

[16] J. Di, S. Bi, Effect of aluminum (III) on the conversion of dopachrome in the melanin synthesis pathway, Spectrochimica Acta - Part A: Molecular and Biomolecular Spectroscopy. 59 (2003) 1689–1696. doi:10.1016/S1386-1425(02)00403-1.

[17] N. González-Diéguez, A. Colina, J. López-Palacios, A. Heras, Spectroelectrochemistry at screen-printed electrodes: Determination of dopamine, Analytical Chemistry. 84 (2012) 9146–9153. doi:10.1021/ac3018444.

[18] W.J. Barreto, S. Ponzoni, P. Sassi, A Raman and UV-Vis study of catecholamines oxidized with Mn(III), Spectrochimica Acta - Part A: Molecular and Biomolecular Spectroscopy. 55 (1998) 65–72. doi:10.1016/S1386-1425(98)00164-4.

[19] H. Hu, J.C. Dyke, B.A. Bowman, C.-C. Ko, W. You, Investigation of Dopamine Analogues: Synthesis, Mechanistic Understanding, and Structure–Property Relationship, Langmuir. 32 (2016) 9873–9882. doi:10.1021/acs.langmuir.6b02141.

[20] G. Albarran, W. Boggess, V. Rassolov, R.H. Schuler, Absorption Spectrum, Mass Spectrometric Properties, and Electronic Structure of 1,2-Benzoquinone, The Journal of Physical Chemistry A. 114 (2010) 7470–7478. doi:10.1021/jp101723s.

[21] S. Li, H. Wang, M. Young, F. Xu, G. Cheng, H. Cong, Properties of Electropolymerized Dopamine and Its Analogues, Langmuir. 35 (2019) 1119–1125. doi:10.1021/acs.langmuir.8b01444.

[22] B. Stöckle, D.Y.W. Ng, C. Meier, T. Paust, F. Bischoff, T. Diemant, R.J. Behm, K.-E. Gottschalk, U. Ziener, T. Weil, Precise control of polydopamine film formation by electropolymerization, Macromolecular Symposia. 346 (2014) 73–81. doi:10.1002/masy.201400130.

[23] F. Bernsmann, J.C. Voegel, V. Ball, Different synthesis methods allow to tune the permeability and permselectivity of dopamine-melanin films to electrochemical probes, Electrochimica Acta. 56 (2011) 3914–3919. doi:10.1016/j.electacta.2011.02.028.

[24] M. Iacomino, J.I. Paez, R. Avolio, A. Carpentieri, L. Panzella, G. Falco, E. Pizzo, M.E. Errico, A. Napolitano, A. del Campo, M. D'Ischia, Multifunctional Thin Films and Coatings from Caffeic Acid and a Cross-Linking Diamine, Langmuir. 33 (2017) 2096–2102. doi:10.1021/acs.langmuir.6b04079.

[25] L.C. Almeida, J.P. Correia, A.S. Viana, Electrochemical and optical characterization of thin polydopamine films on carbon surfaces for enzymatic sensors, Electrochimica Acta. 263 (2018) 480–489. doi:10.1016/j.electacta.2018.01.077.

[26] A.I. Melato, A.S. Viana, L.M. Abrantes, Different steps in the electrosynthesis of poly(3,4-ethylenedioxythiophene) on platinum, Electrochimica Acta. 54 (2008) 590–597. doi:10.1016/j.electacta.2008.07.030.

[27] L.M. Abrantes, J.P. Correia, A.I. Melato, An ellipsometric study of poly(3,4-ethylenedioxythiophene) electrosynthesis - From the initial stages to thick layers formation, Journal of Electroanalytical Chemistry. 646 (2010) 75–84. doi:10.1016/j.jelechem.2010.02.025.

[28] C. Lim, J. Huang, S. Kim, H. Lee, H. Zeng, D.S. Hwang, Nanomechanics of Poly(catecholamine) Coatings in Aqueous Solutions, Angewandte Chemie International Edition. 55 (2016) 3342–3346. doi:10.1002/anie.201510319.

[29] V. Baldoneschi, P. Palladino, M. Banchini, M. Minunni, S. Scarano, Norepinephrine as new functional monomer for molecular imprinting: An applicative study for the optical sensing of cardiac biomarkers, Biosensors and Bioelectronics. 157 (2020) 112161. doi:10.1016/j.bios.2020.112161.

[30] J. Kang, S. Tada, T. Kitajima, T. Il Son, T. Aigaki, Y. Ito, Immobilization of Bone Morphogenetic Protein on DOPA- or Dopamine-Treated Titanium Surfaces to Enhance

Osseointegration, BioMed Research International. 2013 (2013) 1–6. doi:10.1155/2013/265980.

[31] V. Baldoneschi, P. Palladino, S. Scarano, M. Minunni, Polynorepinephrine: state-of-the-art and perspective applications in biosensing and molecular recognition, Analytical and Bioanalytical Chemistry. 412 (2020) 5945–5954. doi:10.1007/s00216-020-02578-9.

[32] Q. Lyu, N. Hsueh, C.L.L. Chai, Unravelling the polydopamine mystery: Is the end in sight?, Polymer Chemistry. 10 (2019) 5771–5777. doi:10.1039/c9py01372e.

[33] M.L. Alfieri, R. Micillo, L. Panzella, O. Crescenzi, S.L. Oscurato, P. Maddalena, A. Napolitano, V. Ball, M. D'Ischia, Structural Basis of Polydopamine Film Formation: Probing 5,6-Dihydroxyindole-Based Eumelanin Type Units and the Porphyrin Issue, ACS Applied Materials & Interfaces. 10 (2018) 7670–7680. doi:10.1021/acsami.7b09662.

[34] V. Ball, Physicochemical perspective on "polydopamine" and "poly(catecholamine)" films for their applications in biomaterial coatings (Review), Biointerphases. 9 (2014) 030801. doi:10.1116/1.4875115.

[35] J.J. Gooding, P.S. Hale, L.M. Maddox, J.G. Shapter, Surface pKa of Self-Assembled Monolayers, Journal of Chemical Education. 82 (2005) 779. doi:10.1021/ed082p779.

[36] F.C.M. de Oliveira, S.H.P. Serrano, Electrochemically Active L-Cysteine Gold Modified Electrodes, Electrochimica Acta. 125 (2014) 566–572. doi:10.1016/j.electacta.2014.01.079.

[37] R.M. Buoro, R.P. Bacil, C.G. Sanz, O.S. Campos, S.H.P. Serrano, Biomimetic behavior and nanomolar detection of hydrogen peroxide on an electrochemically pre-treated hematin modified glassy carbon electrode, Sensors and Actuators B: Chemical. 250 (2017) 169–178. doi:10.1016/j.snb.2017.03.176.

[38] M. Salomäki, L. Marttila, H. Kivelä, T. Ouvinen, J. Lukkari, Effects of pH and oxidants on the first steps of polydopamine formation: a thermodynamic approach, The Journal of Physical Chemistry B. 122 (2018) 6314–6327. doi:10.1021/acs.jpcb.8b02304.

[39] Y. Kong, S.L. Mu, B.W. Mao, Synthesis of polycatechol with electrochemical activity and its properties, Chinese Journal of Polymer Science (English Edition). 20 (2002) 517–524.

[40] J. Wu, C. Cai, Z. Zhou, H. Qian, F. Zha, J. Guo, B. Feng, T. He, N. Zhao, J. Xu, Low-cost mussel inspired poly(catechol/polyamine) coating with superior anti-corrosion capability on copper, Journal of Colloid and Interface Science. 463 (2016) 214–221. doi:http://dx.doi.org/10.1016/j.jcis.2015.10.056.

[41] S. Gunasekaran, R.T. Kumar, Vibrational spectra and normal coordinate analysis of adrenaline and dopamine, Indian Journal of Pure & Applied Physics. 45 (2007) 884–892.

[42] Z. Bacsik, N. Ahlsten, A. Ziadi, G. Zhao, A.E. Garcia-Bennett, B. Martín-Matute, N. Hedin, Mechanisms and Kinetics for Sorption of CO_2 on Bicontinuous Mesoporous Silica Modified with n-Propylamine, Langmuir. 27 (2011) 11118–11128. doi:10.1021/la202033p.

[43] R.A. Zangmeister, T.A. Morris, M.J. Tarlov, Characterization of Polydopamine Thin Films Deposited at Short Times by Autoxidation of Dopamine, Langmuir. 29 (2013) 8619–8628. doi:10.1021/la400587j.

[44] K.E. and S.S. of P.F. on P.E. Jackowska, J. Bukowska, Electrochemical and Spectroscopic Studies of Polyindole Films on Pt Electrodes, Polish Journal of Chemistry. 66 (1992) 1477–1486.

[45] Inamuddin, N. Shakeel, M. Imran Ahamed, S. Kanchi, H. Abbas Kashmery, Green synthesis of ZnO nanoparticles decorated on polyindole functionalized-MCNTs and used as anode material for enzymatic biofuel cell applications, Scientific Reports. 10 (2020). doi:10.1038/s41598-020-61831-4.

[46] Z. Huang, H. Lui, X.K. Chen, A. Alajlan, D.I. McLean, H. Zeng, Raman spectroscopy of in vivo cutaneous melanin, Journal of Biomedical Optics. 9 (2004) 1198. doi:10.1117/1.1805553.

[47] H. Talbi, J. Ghanbaja, D. Billaud, B. Humbert, Vibrational properties and structural studies of doped and dedoped polyindole by FTi.r., Raman and EEL spectroscopies, Polymer. 38 (1997) 2099–2106. doi:10.1016/S0032-3861(96)00759-8.

[48] M. Sugumaran, Reactivities of quinone methides versus o-Quinones in catecholamine metabolism and eumelanin biosynthesis, International Journal of Molecular Sciences. 17 (2016) 1–23. doi:10.3390/ijms17091576.

[49] S. Rella, E. Mazzotta, A. Caroli, M. De Luca, C. Bucci, C. Malitesta, Investigation of polydopamine coatings by X-ray Photoelectron Spectroscopy as an effective tool for improving biomolecule conjugation, Applied Surface Science. 447 (2018) 31–39. doi:10.1016/j.apsusc.2018.03.057.

[50] A. Mourato, A.S. Viana, F.-P. Montforts, L.M. Abrantes, Polypyrrole on self-assembled monolayers of a pyrrolyl lipoic acid derivative—electrosynthesis and polymer film characterization, Journal of Solid State Electrochemistry. 14 (2010) 1985–1995. doi:10.1007/s10008-010-1036-6.

[51] J. Věžník, M. Konhefr, L. Trnková, P. Skládal, K. Lacina, Elusive pKa' of aminoferrocene determined with voltammetric methods in buffered and unbuffered systems and practical aspects of such experiments, Electrochimica Acta. 318 (2019) 534–541. doi:10.1016/j.electacta.2019.05.113

[52] G. Li, H. Zhang, F. Sader, N. Vadhavkar, D. Njus, Oxidation of 4-methylcatechol: Implications for the oxidation of catecholamines, \Biochemistry. 46 (2007) 6978–6983. doi:10.1021/bi061699+.

[53] D. Sazou, M. Kourouzidou, E. Pavlidou, Potentiodynamic and potentiostatic deposition of polyaniline on stainless steel: Electrochemical and structural studies for a potential application to corrosion control, Electrochimica Acta. 52 (2007) 4385–4397. doi:10.1016/j.electacta.2006.12.020.

[54] K. Kreuer, Proton Conductivity: Materials and Applications, Chemistry of Materials. 8 (1996) 610–641. doi:10.1021/cm950192a.

[55] B. Gao, L. Su, Y. Tong, M. Guan, X. Zhang, Ion Permeability of Polydopamine Films Revealed Using a Prussian Blue-Based Electrochemical Method, The Journal of Physical Chemistry B. 118 (2014) 12781–12787. doi:10.1021/jp507617t.

[56] J.L. Wang, B.C. Li, Z.J. Li, K.F. Ren, L.J. Jin, S.M. Zhang, H. Chang, Y.X. Sun, J. Ji, Electropolymerization of dopamine for surface modification of complex-shaped cardiovascular stents, Biomaterials. 35 (2014) 7679–7689. doi:10.1016/j.biomaterials.2014.05.047.

[57] L.C. Almeida, R.D. Correia, B. Palys, J.P. Correia, A.S. Viana, Comprehensive study of the electrochemical growth and physicochemical properties of polycatecholamines and polycatechol, Electrochimica Acta. 386 (2021) 138515. doi:10.1016/j.electacta.2021.138515.

[58] L.C. Almeida, T. Frade, R.D. Correia, Y. Niu, G. Jin, J.P. Correia, A.S. Viana, Electrosynthesis of polydopamine-ethanolamine films for the development of immunosensing interfaces, Scientific Reports. 11 (2021) 1–12. doi:10.1038/s41598-021-81816-1.

[59] S.H. Hong, S. Hong, M.-H. Ryou, J.W. Choi, S.M. Kang, H. Lee, Sprayable ultrafast polydopamine surface modifications, Advanced Materials Interfaces. 3 (2016) 1500857. doi:10.1002/admi.201500857.

[60] M. Pourbaix, Atlas of Electrochemical Equilibria in Aqueous Solutions, 2nd Edition, National Association of Corrosion Engrneers, Houston, Texas, 1974.

[61] P. Gao, D. Gosztola, L.W.H. Leung, M.J. Weaver, Surface-enhanced Raman scattering at gold electrodes: dependence on electrochemical pretreatment conditions and comparisons with silver, Journal of Electroanalytical Chemistry. 233 (1987) 211–222. doi:10.1016/0022-0728(87)85017-9.

Chapter VI

Development of laccase-based biosensing interfaces for polyphenols detection

Most of the content of this chapter can be found in the following published paper and submitted manuscript:

- L.C. Almeida, R.D. Correia, G. Squillaci, A. Morana, F. La Cara, J.P. Correia, A.S. Viana, Electrochemical deposition of bio-inspired laccase-polydopamine films for phenolic sensors, Electrochimica Acta. 319 (2019) 462-471, doi:10.1016/j.electacta.2019.06.180.

- L.C. Almeida, J.F. Zeferino, C. Branco, A. Morana, G. Squillaci, R. Santos, P. Ihalainen, L. Sobhana, J.P. Correia, A.S. Viana, Polynorepinephrine and polydopamine-bacterial laccase coatings for phenolic amperometric biosensors, *submitted manuscript*.

6. Development of laccase-based biosensing interfaces for polyphenols detection

The search for new materials and optimal strategies to attach enzymes to electrodes have been an intensive area of research over the last decades. One of the major problems that rises when developing enzymatic biosensors is the maintenance of biological activity of the enzyme and, equally important, the robustness of the protein bond to the surface [1].

Due to the capacity of oxidizing a broad range of phenolic molecules, laccases are suitable to construct amperometric biosensors that can detect and quantify relevant polyphenols in agroforestry and food industries (*e.g.* caffeic acid, rosmarinic acid, gallic acid and catechin) and xenobiotics in thermoplastics industry (*e.g.* dimethylphenol). As mentioned in chapter I (section 1.4), polydopamine-based methods have already been shown to successfully immobilize technologically pertinent enzymes (glucose oxidase and laccase), albeit the practicality of the presented amperometric biosensors is deeply dependent on the incorporation of nanomaterials. Commonly, drop-casting strategies in combination with the chemically driven polymerization of dopamine are reported due to their simplicity to implement in the laboratory, although the control over the properties of the deposited biosensing film is compromised. In contrast, surface modifications driven by the electrochemical deposition of catechol-containing molecules can be envisaged to finely control the properties of the immobilization matrix (*cf.* chapters IV and V), maximizing immobilization robustness and the biosensing reproducibility of the interface. It is worth noting that the group of S. Yao and collaborators have reported the entrapment of glucose oxidase [2] and anti-human immunoglobulin G [3] during the potentiodynamic synthesis of polydopamine, demonstrating superior immobilization performance against a well-known organic conducting polymer, polypyrrole. Although there is not a current consensus about the type of chemical bond between proteins and catechol-containing polymers, potentiostatic or potentiodynamic deposition strategies can be envisaged as efficient ways to provide high concentration of quinone groups at the surface, thus increasing the probability of covalent and robust immobilization of laccases within the polymeric matrices by known Michael-type addition or Schiff base reactions [4].

In this chapter, the immobilization of two industrial laccases from fungal and bacterial origin (provided by Novozymes and MetGen, LacNZ and LacMG, respectively) is explored during or upon electrodeposition of polycatecholamines on carbon electrodes, later denominated in the text as one-step and two-step modification strategies, respectively. To confirm and optimize the catalytic activity of laccases before and after surface immobilization,

spectroscopic and chronoamperometric assays are performed in the presence of the standard substrate ABTS. Subsequently, the best procedure is implemented on cheap disposable graphite electrodes, approaching the technological demands of a sensitive, rapid and easy to use point-of-use biosensing device, useful for industrial residues and nutritional quality assessments or pollution control of wastewaters.

6.1. Fungal laccase-polycatecholamine hybrid films prepared by one-step potentiostatic method

6.1.1. Electrochemical synthesis and characterization of polydopamine-laccase films

A typical cyclic voltammetric response of a potentiodynamic growth of ePDA film, recorded in 5 mM dopamine (DA) in CPB pH 7.0, on a glassy carbon electrode, is illustrated in **Figure 6.1a**. Two main redox processes, centered at 0.23 and -0.29 V, are clearly depicted during growth, and correspond to two-electron two-proton quinone/hydroquinone electrochemical conversions, as described elsewhere [5–7]. The higher potential redox conversion corresponds to the open forms dopaminoquinone (DAQ)/ DA, whereas the lower potential redox conversion is assigned to the cyclized forms leucodopaminechrome (LDAC)/ dopaminechrome (DAC) due to the electrodonating effect of the nitrogen atom to the catechol ring (*cf.* **Figure 4.2**, chapter 4). The current decrease of DAQ/DA redox process, along the potential cycles is due to the formation of a poorly conductive polymeric phase, which precludes the detection of the monomeric species in solution. In contrast, the redox peaks corresponding to LDAC/DAC increase along the first potential cycles indicating the formation of these electroactive species, not present initially. However, for a large number of cycles, this process is also precluded.

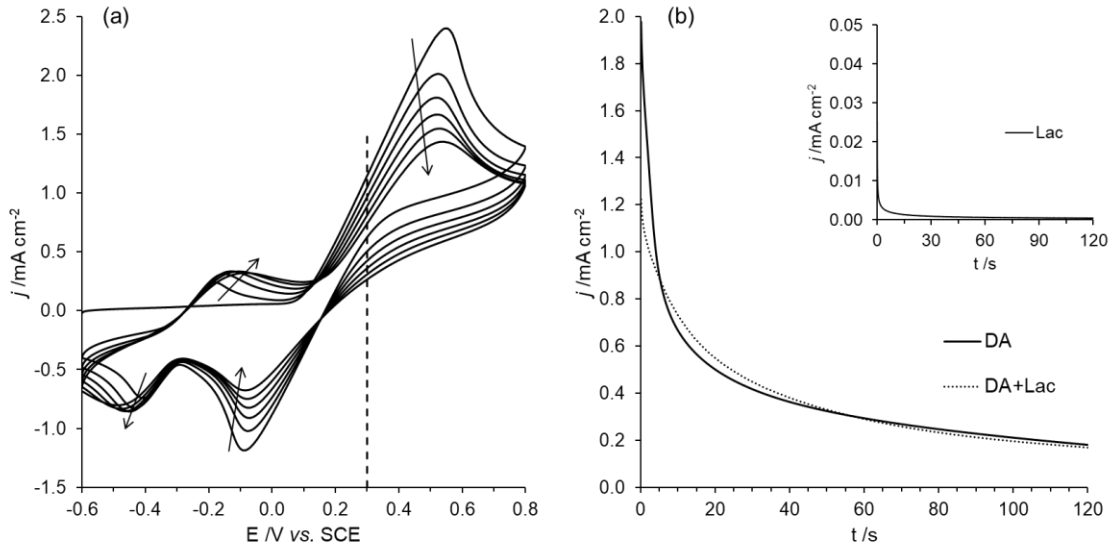

Figure 6.1: Potentiodynamic growth (6 cycles at 200 mV s^{-1}) of ePDA films from 5 mM DA solution **(a)**; potentiostatic synthesis (120 s at 0.3 V) of ePDA films, using 5 mM DA solution in the absence (solid line) and presence of 18 μg mL^{-1} of LacNZ (dotted line) **(b);** Inset of **(b)** shows the chronoamperometric assay in 18 μg mL^{-1} LacNZ solution. All assays were carried out on GC electrodes, in CPB pH 7.0 deaerated solutions.

According to the voltammograms of **Figure 6.1a**, we have selected 0.3 V as the potential to grow ePDA polymeric matrix potentiostatically, as shown in **Figure 6.1b**. The low energy (low overpotential) for monomer oxidation leads to the production of radical cations in moderate amounts, which contributes for the regioregularity of the oligomer/polymeric segments, avoiding the polymer branching and its overoxidation. ePDA was synthesized in the presence and absence of LacNZ, in deaerated solutions to prevent dopamine enzymatic oxidation [8] and chemical oxidation [9], both driven by the presence of oxygen. The current profiles on both chronoamperograms are very similar and reveal the formation of polymers with low conductivities when compared with conventional electronically conducting polymers, such as polyaniline [10] and poly(3,4-ethylenedioxythiophene) [11]. In fact, there is no evidence of the nucleation and 2D or 3D growth of a new conducting phase at the electrode surface, as it happens when the electrodeposited material is a good electronic conductor like a metal or a conventional conducting polymer. In this case, only a current decay is observed that does not follow the Cottrell behavior ($I \propto t^{-1/2}$), indicating that the process is not diffusion controlled and the reaction rate is determined by the decreasing ability for charge transfer of the electrode surface. By co-depositing ePDA and LacNZ at 0.3 V, it is expected that generated quinone groups are readily available to react with nucleophilic groups of laccase, such as amines, creating a stable and functional enzyme/polymeric matrix [9]. When GC electrode is polarized in a solution containing only laccase, as shown in the inset of **Figure 6.1b**, almost no oxidation

current develops, as expected in the absence of a monomer in solution. The cyclic voltammetric responses of ePDA films, potentiostatically formed in the presence and absence of laccase, recorded in a monomer free CPB pH 4.6 electrolyte solution, after 5 potential cycles of stabilization in the same solution [5] are shown in **Figure 6.2a**. The electrochemical responses of deposited ePDA and hybrid ePDA-LacNZ polymers are very similar, exhibiting a well-defined redox process at 0.28 V, and a broader wave at lower potentials, centered at 0.13 V. We attribute the more positive process to the quinone/hydroquinone redox conversion of non-cyclized dopamine chains within the polymer, once it perfectly matches the value of dopamine in solution [5]. As expected, relevant redox processes (**Figure 6.2a**) are not detected in the cyclic voltammogram obtained for GC after the polarization in a dilute laccase solution (in the absence of dopamine). The linear relationship between the peak current and potential sweep rate for this process on both ePDA and hybrid ePDA-LacNZ polymers, as illustrated in the inset of **Figure 6.2a**, reveals an electrochemical conversion controlled by charge transfer, as expected for surface-confined electroactive species when the diffusion is not the rate limiting factor. The broader wave, at lower potential, comprises at least two processes which we assign mainly to the polymer backbone redox conversion (of segments with a wide distribution of sizes) and possibly also to the cyclized dopamine residues, such as 5,6-dihydroxyindole (DHI), that is formed through isomerization of DAC [7,12]. In fact, upon cyclization, the electrodonating effect of the nitrogen in the catechol ring will facilitate the quinone/hydroquinone redox conversion, shifting the potential towards lower values [13]. The similarity between ePDA and ePDA-LacNZ cyclic voltammetric responses reveals that enzyme immobilization does not affect the redox response of the polymeric matrix, as would be anticipated if there was a significant nucleophilic attack by functional groups of the enzyme, such as amines, to the available quinones within the polymer, resulting in covalent linkages. As discussed above, a negative potential shift of the Q/HQ redox conversion would be expected in this case [7,13]. Thus, the absence of such behavior suggests that most probably the majority of laccase molecules are physically entrapped in ePDA films. Still, the ePDA-LacNZ interaction is sufficiently strong to resist to potential cycling, supporting a robust immobilization of the enzyme. This is an encouraging result since it indicates that the native form of the enzyme is preserved in the polymeric matrix and should display a similar catalytic activity than that of free laccase. Nevertheless, based on the well-described nucleophilic attack of amines to quinones, through Michael-type addition or Schiff base reactions [4], a partial covalent binding, not inferred by cyclic voltammetry, should also occur.

ePDA and ePDA-LacNZ films partially hinder the redox process of $K_3Fe(CN)_6$ (**Figure 6.2b**), revealed by the decrease in the oxidation and reduction peak currents and also by a slight increase in peak potential separation, in comparison to those peaks observed for bare GC electrode. The partial blocking of the anionic probe indicates the presence of somewhat resistive polymers towards the $K_3Fe(CN)_6$ charge transfer process. In ePDA-LacNZ film, an additional blocking effect compared to ePDA layer is observed due to the presence of proteic material. Furthermore, enzyme may confer an extra negative charge to the interface at the experimental conditions (pH *ca.* 6), since laccase isoelectric point is reported to lie between 4 and 7 [14]. Notwithstanding, the hybrid ePDA-LacNZ interface is capable to detect the redox process of this anionic probe, which demonstrates its potential as electrochemical transducer in biosensors.

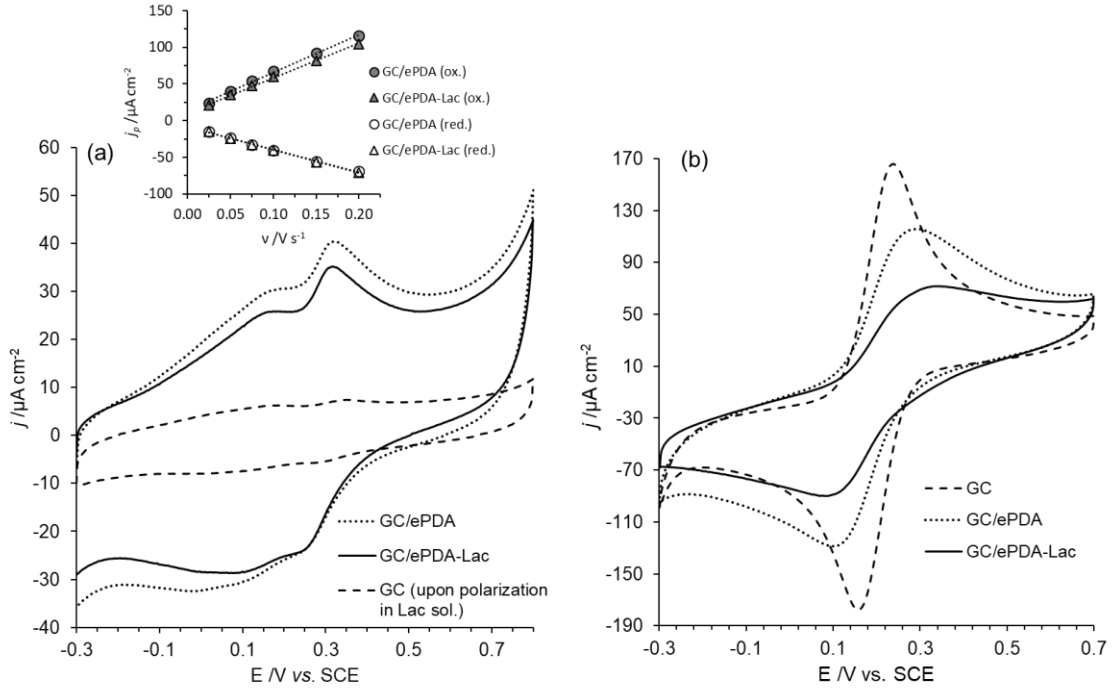

Figure 6.2: Cyclic voltammograms (50 mV s^{-1}) of GC electrode upon polarization at 0.3 V, 120 s, in 5 mM DA, 5 mM DA and LacNZ (18 µg mL^{-1}), and only LacNZ (18 µg mL^{-1}), recorded in deoxygenated solutions of CPB pH 4.6 **(a)**; bare GC and GC after polarization at 0.3 V, 120 s, in 5 mM DA in the presence or absence of LacNZ (18 µg mL^{-1}), recorded in 1 mM $K_3Fe(CN)_6$, 0.25 M KNO_3 solution **(b)**.

The optical thickness and dielectric properties (refractive index and extinction coefficient) of polymeric films on GC electrodes were evaluated by multiangle ellipsometry, and the computed data are summarized in **Table 6.1**. ePDA-LacNZ film was found to have an average optical thickness higher than ePDA (for the same growth charge), proving the

incorporation of LacNZ molecules within the polymeric matrix. There are small differences in the optical density (revealed by real part of the refractive index, *n*) and extinction coefficient, *k*, between polymers, indicating the formation of a slightly less dense and more optically absorbing film when laccase is present. In addition, ePDA-LacNZ is less hydrophilic than pristine ePDA (**Table 6.1**), corroborating the immobilization of the enzyme. Indeed, a value of water contact angle of 53° has been reported for laccase modified surfaces [15].

Table 6.1: Complex refractive index ($\hat{n}$), thickness (L), water contact angle (θ_{WCA}) and root mean square roughness (R_q) of GC modified electrode with ePDA and ePDA-LacNZ films. The multiangle ellipsometry is carried out at the incident angles: 40°, 45°, 50°, 55°, 60°, 65° and 70°.

Film	$\hat{n} = n - ki$	L **/nm**	θ_{WCA} **/°**	R_q **/nm**
ePDA	1.84 (± 0.09) – 0.363 (± 0.006)*i*	5.2 ± 0.7	35 ± 2	3.4
ePDA-LacNZ	1.74 (± 0.04) – 0.41 (± 0.06)*i*	8 ± 1	48 ± 5	5.0

Topographic images obtained by AFM, shown in **Figure 6.3**, disclose very smooth and regular globular morphology for both films. Polymeric grains are similar in size to single laccase molecules [16] as well as their expected viscoelastic properties, which precludes a clear distinction of the embedded biomolecules. However, slightly larger globular features can be depicted on ePDA-LacNZ film, in agreement with the height profiles (**Figure 6.3**) and root-mean-square (R_q) values presented in **Table 6.1**. It is worth noting from the results presented so far, that enzyme molecules should be evenly distributed within the polymeric matrix, in a way that its morphology and redox properties are not drastically altered.

The catalytic performance of the GC/ePDA-LacNZ electrode was firstly attempted towards ABTS oxidation reaction. ABTS was chosen since it is an electroactive compound, with a well-behaved redox conversion and also displaying a high affinity for laccase [17]. In the presence of molecular oxygen, the immobilized laccase is expected to oxidize ABTS with the concomitant formation of water molecules (**Figure 6.4a**). The oxidized ABTS can then be detected on the electrode surface by applying a proper reducing potential. As expected for a catalytic process followed by cyclic voltammetry (**Figure 6.4b**), successive additions of ABTS to the electrolyte solution result in an absolute increase of its reduction peak current (at 0.4 V), which is only followed by a similar increase of the oxidation peak currents upon enzyme saturation. A stepwise decrease in current, after each ABTS addition, is better depicted by chronoamperometry (**Figure 6.4c**) carried out at 0.4 V [5,7]. The current background from the ePDA-LacNZ film, in the absence of ABTS, is also provided (**Figure 6.4c**), illustrating the

stability of this matrix under these experimental conditions. In fact, the current responses as function of ABTS concentration follow a typical Michaelis-Menten behavior (**Figure 6.4c**), definitively proving the presence of active immobilized enzyme in ePDA-LacNZ modified by the one-step electrodeposition of DA and LacNZ (18 μg mL^{-1}). A more concentrated solution in laccase (180 μg mL^{-1}) was also tested during electropolymerization, although it did not improve the catalytic activity of the ePDA-LacNZ film (**Figure 6.4c**). In fact, the K_M^{app} and j_{max} parameters from the non-linear fitting of ePDA-LacNZ (18 μg mL^{-1}) film response are 8.8 μM and 2.7 μA cm^{-2}, whereas for ePDA-LacNZ (180 μg mL^{-1}) film these values are 10.0 μM and 2.5 μA cm^{-2}, respectively (*cf.* **Equation 3.1**, chapter III). The data indicates that a laccase concentration of 18 μg mL^{-1} is enough and adequate to prepare highly catalytic surfaces. It is worth to note that there was no detected enzyme activity, measured by spectrophotometric assay, in the washing discards of the modified electrodes, proving a very robust one-step surface bio-functionalization. In addition, the estimated K_M^{app} values for the catalytic performance of GC/ePDA-LacNZ towards ABTS oxidation are considerably lower than most of the published data using different systems (enzyme, immobilization method, electrode material) [18], including previous works carried out by the authors using distinct PDA films [5,7], reinforcing the efficacy of the described methodology.

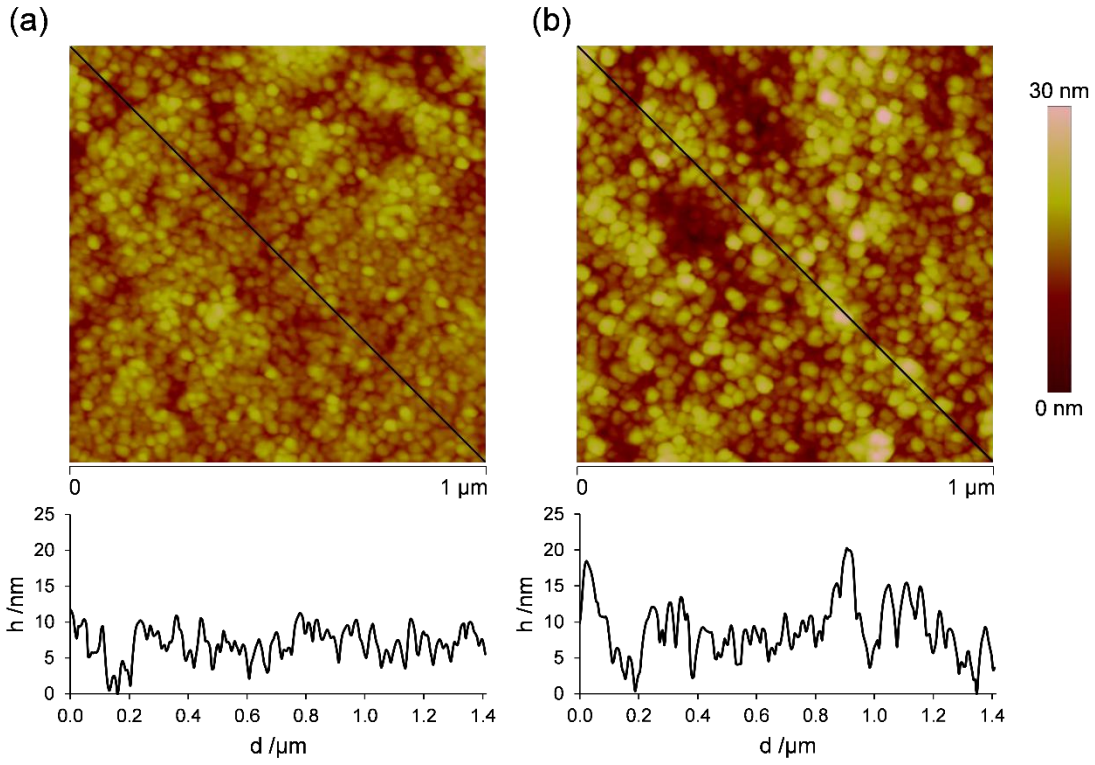

Figure 6.3: AFM topographic images and corresponding height profiles of GC modified with ePDA **(a)** and ePDA-LacNZ **(b)** films.

To demonstrate the importance of dopamine as an efficient immobilization agent during electrodeposition, a blank assay was performed in which GC was polarized at 0.3 V for 120 s in the presence of LacNZ (18 μg mL^{-1}), without DA. After this electrochemical step, the electrode did not display any enzymatic activity towards ABTS oxidation (**Figure 6.4d**). Instead, the anodic current only slightly increased as ABTS concentration was augmented. This is a typical behavior expected for a non-enzymatic electrochemical detection, where the current is proportional to the concentration of analyte. Furthermore, the pristine ePDA film response to the addition of ABTS was also studied (**Figure 6.4d**). In spite of a slight increase of the low reduction current for substrate concentrations below 50 μM of ABTS, maybe induced by the polymer redox process, ePDA does not have a coherent response to ABTS addition, since at higher concentrations the current starts to increase. Both control assays discussed above for the model substrate, ABTS, validate the new one-step bio-functionalization method, allowing a robust immobilization of an active enzyme.

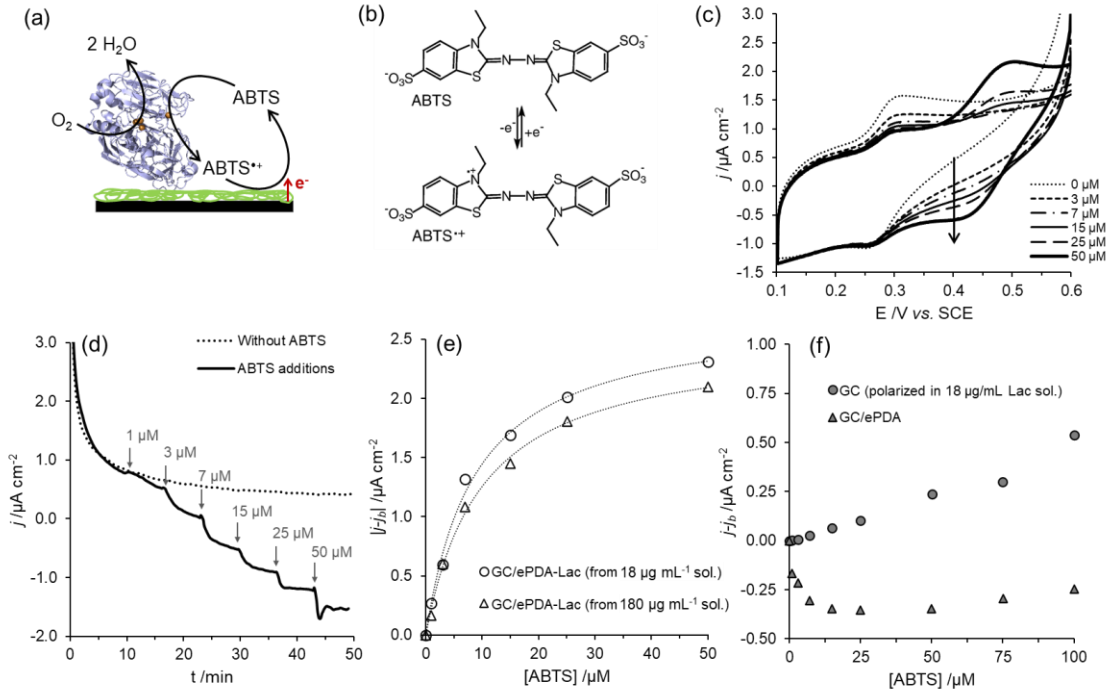

Figure 6.4: Simplified scheme of ABTS enzymatic oxidation by immobilized laccase, in the presence of oxygen, and electrochemical regeneration of the oxidized substrate ($ABTS^{\bullet+}$) **(a)**; Chemical structures of ABTS and $ABTS^{\bullet+}$ **(b)**; Cyclic voltammetric **(c)** and chronoamperometric **(d)** responses of ePDA-LacNZ film (grown from 18 μg mL^{-1} LacNZ and 5 mM DA solution) in the absence and upon stepwise additions of ABTS. The chronoamperometric response of the same ePDA-LacNZ film without ABTS is represented by the dashed line; Current *versus* ABTS concentration (j_b is the background current recorded in the absence of ABTS), showing a non-linear fitting of the Michaelis-Menten type curves for ePDA-LacNZ films electrosynthesized from 5 mM DA and 18 μg mL^{-1} or 180 μg mL^{-1} LacNZ solutions **(e)**; Current *versus* ABTS concentration for GC after ePDA deposition (5 mM DA, without LacNZ; triangles), and GC upon polarization (0.3 V, 120s, CPB pH 7.0) in 18 μg mL^{-1} LacNZ solution (without DA; circles) **(f)**; All ABTS detection assays were performed in aerated CPB pH 4.6, at 0.4 V.

6.1.2. Catalytic properties of the modified electrodes towards phenolic acids

Caffeic, rosmarinic and gallic acid were the low molecular weight phenolic compounds selected to evaluate and calibrate the amperometric responses of graphite disposable electrodes modified with ePDA-LacNZ films. These substrates are electroactive due to the presence of phenolic functional groups in their molecular structures (as presented in **Figure 6.5**), that are able to undergo redox reactions at electrode surfaces [19–21]. The electrochemical behavior of such compounds was firstly evaluated by cyclic voltammetry on bare GC. Caffeic acid (**Figure 6.5a**) and its derivative rosmarinic acid (**Figure 6.5b**) display a quite reversible behavior at the working acidic pH (4.6), which is attributed to the two-electron two-proton redox conversion of their catechol moieties [19,22]. In the case of rosmarinic acid, broader oxidation and reduction peaks are observed, which correspond to the almost concomitant redox conversions of the two catechol groups, at acidic pH [19]. In contrast to caffeic and rosmarinic acid, gallic acid cyclic voltammograms (**Figure 6.5c**) display an almost irreversible electrochemical response. This behavior is known for derivatives of pyrogallol, where the instable quinone species generated upon oxidation undergo further chemical reactions [23,24], precluding their electrochemical reduction in the subsequent cycle. After 3 potential cycles, there is a significant decrease in the oxidation peak current of gallic acid, which is less pronounced for the two hydroxycinnamic acids. This decrease is caused by the deposition of electrogenerated oxidation products on GC surface, which is known to occur for the three compounds [23,25,26], especially at higher pH values. Therefore, the chronoamperometric enzymatic assays targeting the detection of these compounds were carried out at 0.0 V, that is a sufficiently low potential to avoid electrode poisoning [27]. In this way, as soon as the enzymatic oxidation of the substrate occurs, the produced *o*-quinones will be immediately reduced at the electrode surface, and the enzyme regenerated by the molecular oxygen (*cf.* **Figure 6.4a**).

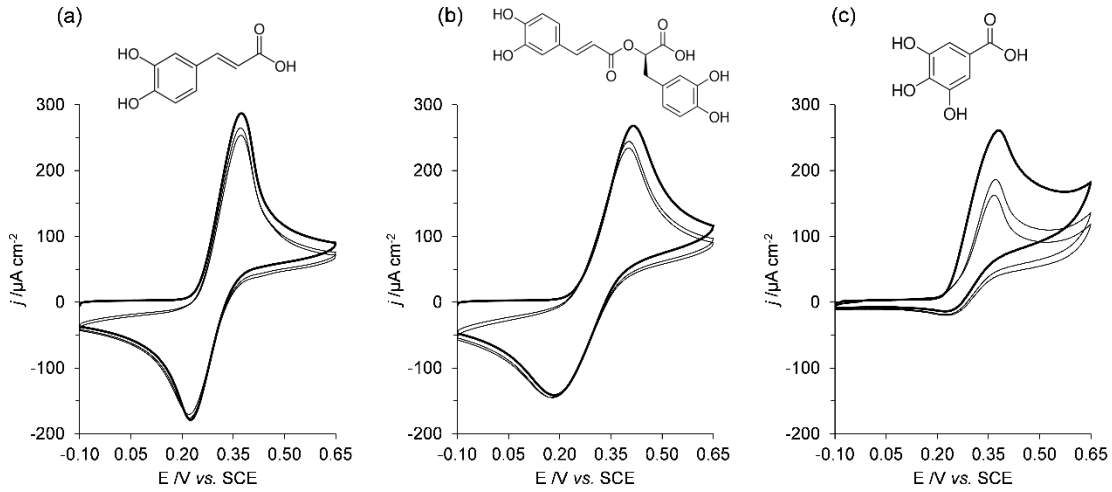

Figure 6.5: Cyclic voltammograms of bare GC electrode in 0.5 mM caffeic acid **(a)**, rosmarinic acid **(b)** and gallic acid **(c)** solutions, recorded at 50 mV s^{-1} in deoxygenated CPB pH 4.6. The corresponding molecular structures are shown above each voltammogram.

Figure 6.6 shows the chronoamperometric responses (insets) and the corresponding Michaelis-Menten type curves (*cf.* **Equation 3.1**, chapter III) obtained for the detection of caffeic, rosmarinic and gallic acid using graphite/ePDA-LacNZ modified electrodes. **Table 6.2** compiles analytical parameters extracted from **Figure 6.6**. As it is clearly seen, the disposable graphite/ePDA-LacNZ electrodes display very reproducible catalytic responses to the three phenolic compounds tested, proving a great control over electrode biofunctionalization by the one-step potentiostatic method proposed in this work. It is worth to note, as shown in **Figure A4** (Annex), that cyclic voltammetric curves of the modified electrode, ePDA-LacNZ, in electrolyte solution before and after a calibration curve of gallic acid (within the linear range of the sensor, 1 – 150 µM), do not exhibit any redox peaks that correspond to gallic acid redox process, indicative of no fouling phenomenon during the catalytic assay. Furthermore, the redox response of the polymer has not significantly changed after calibration plot. In addition, the low fitting errors regarding the Michaelis-Menten kinetics (**Table 6.2**) also show that the immobilized laccase preserves its catalytic properties, maintaining a stable response throughout the amperometric measurements. Although good sensitivity values were obtained for the three compounds tested, they are in general inferior to those reported for electrodes modified with drop-casting of complex nanoarchitectures [28–33], which are prepared with a much higher amount of catalyst, than that used in this study (electrodeposition from 1.0 U mL^{-1} LacNZ solution). On the other hand, as shown in **Table 6.3**, the limit of detection (LOD) values are in line with those published for the same phenolic derivatives, whereas the linear ranges of detection obtained for our biosensing interface are wider for all the phenolic compounds tested.

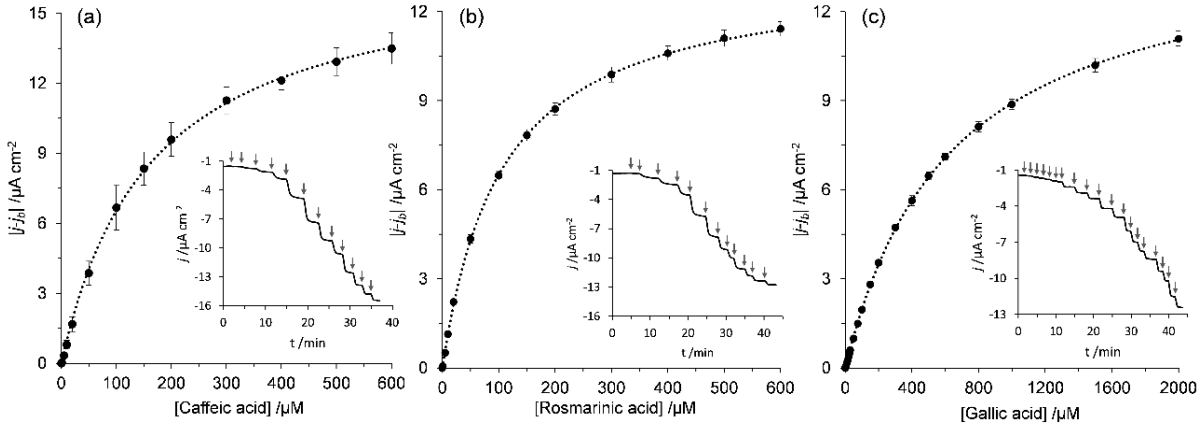

Figure 6.6: Current responses of the graphite/ePDA-LacNZ modified electrode to different concentrations of caffeic acid **(a)**, rosmarinic acid **(b)** and gallic acid **(c)** measured by chronoamperometry at an applied potential of 0.0 V, in oxygenated CPB pH 4.6 buffer. Presented data were obtained from 3 independent assays for each phenolic compound. Insets show representative chronoamperograms where the additions of phenolic compounds are indicated by the vertical arrows.

Table 6.2: Analytical parameters (apparent Michaelis-Menten constant, K_M^{app}; saturation current, j_{max}; limit of detection, LOD*; linear range; sensitivity; and coefficient of determination, R^2) extracted from the chronoamperometric assays presented in **Figure 6.6**, for caffeic, rosmarinic and gallic acid.

Phenolic compound	K_M^{app} /mM	j_{max} /μA cm^{-2}	LOD /μM	Linear range /μM	Sensitivity /μA cm^{-2} mM^{-1}	R^2
Caffeic acid	0.16 ± 0.01	17.2 ± 0.4	0.14	1 – 50	81 ± 2	0.9965
Rosmarinic acid	0.106 ± 0.003	13.4 ± 0.1	0.09	1 – 20	114 ± 1	0.9995
Gallic acid	0.63 ± 0.01	14.6 ± 0.1	0.29	1 – 150	19.3 ± 0.2	0.9986

*LOD values were calculated using the expression $3\sigma/m$, where σ is the standard deviation of the blank current and m is the sensitivity of the sensor.

Table 6.3: Analytical parameters of other laccase-based amperometric biosensors found in the literature.

Biosensor	Measuring conditions	Phenolic compound	K_M^{app} /mM	LOD /μM	Linear range /μM	Refs.
Au/Lacc-CS-MWCNT[a]	-0.2 V *vs.* Ag/AgCl, pH 4.5	Caffeic acid Rosmarinic acid Gallic acid	0.0518 0.0252 –	0.151 0.233 –	0.735 – 10.5 0.91 – 12.1 0.79 – 2.1	[28]
laccase-PAP-MWCNT[b]	-0.1 V *vs.* Ag/AgCl, pH 5.5	Caffeic acid Gallic acid	0.005 0.115	0.06 1.41	0.17 – 3.33 4.64 – 117.0	[29]

AuSPE/laccase/Nafion[c]	-0.2 V *vs.* Ag/AgCl, pH 4.5	Caffeic acid Rosmarinic acid Gallic acid	0.0066 0.0043 0.0412	2.5 2.4 1.55	3 – 15 3 – 15 2 – 7	[30]
TvL-MWCNTs-SPE[d]	-0.1 V *vs.* Ag/AgCl, pH 5.0	Gallic acid	0.81± 0.09	0.6	0.6 – 99.9	[31]
Graphite/Lac[e]	-0.050 V *vs.* Ag/AgCl, pH 5.0	Caffeic acid	0.0274	0.56 ± 0.03	1 – 10	[32]
CSPE/TLV-PVA-AWP[f]	-0.30 V *vs.* Ag/AgCl, pH 4.7	Caffeic acid	–	0.524	0.5 – 130	[33]

[a]Au/Lacc-CS-MWCNT: electrodeposition on gold foil from a suspension containing laccase (25 U mL^{-1}), chitosan and multiwall carbon nanotubes; [b]laccase-PAP-MWCNT: Drop-cast deposition of polyazetidine prepolymer (PAP®) and laccase (2500 U mL^{-1}) solution over a multi-walled carbon nanotubes screen printed electrode; [c]AuSPE/Lac/Nafion: drop-cast laccase on a screen-printed gold electrode followed by a nafion deposition; [d]TvL-MWCNTs-SPE: drop-cast deposition of polyazetidine prepolymer (PAP®) and laccase (26.7 U mL^{-1}) solution over a multi-walled carbon nanotubes screen printed electrode; [e]Graphite/Lac: laccase (3.05 U mL^{-1}) adsorbed on spectrographic graphite; [f]CSPE/TLV-PVA-AWP: Screen-printed disposable graphite electrode modified with entrapped laccase (180,000 U mL^{-1}) on a polyvinyl alcohol photopolymer.

The sensitivity achieved towards gallic acid detection is important to enable the accurate estimation of its content in real samples, rich on this phenolic derivative, such as in the chestnut shell extract [34]. To this purpose, stepwise additions of chestnut shell extract to the electrolyte solution were performed (**Figure 6.7** inset), and the current measured at the same experimental conditions of the phenolic calibration curves. For extract concentrations in the range of 20 – 80 mg L^{-1}, the graphite/ePDA-LacNZ responds linearly (6.3 ± 0.1 nA cm^{-2} mg^{-1} L), whereas for higher concentrations the amperometric signal is no longer proportional to extract additions (**Figure 6.7**), tending to a plateau. The determination of this linear region is of utmost importance since it indicates that target electroactive compounds can be quantitatively detected, in the complex mixture. The amount of gallic acid equivalents (GAE) in chestnut shell extract was estimated through the ratio between the sensitivity of the sample and sensitivity of the standard (**Figure 6.6c**), yielding a value of 56 ± 2 mg GAE g^{-1} DE (expressed per grams of dried extract). This value is close to that determined for gallic acid content by HPLC (63.51 ± 1.32 mg g^{-1} DE) [34]. Therefore, the novel ePDA-LacNZ interface has demonstrated a great potential towards the detection of low molecular weight phenolic compounds in real samples.

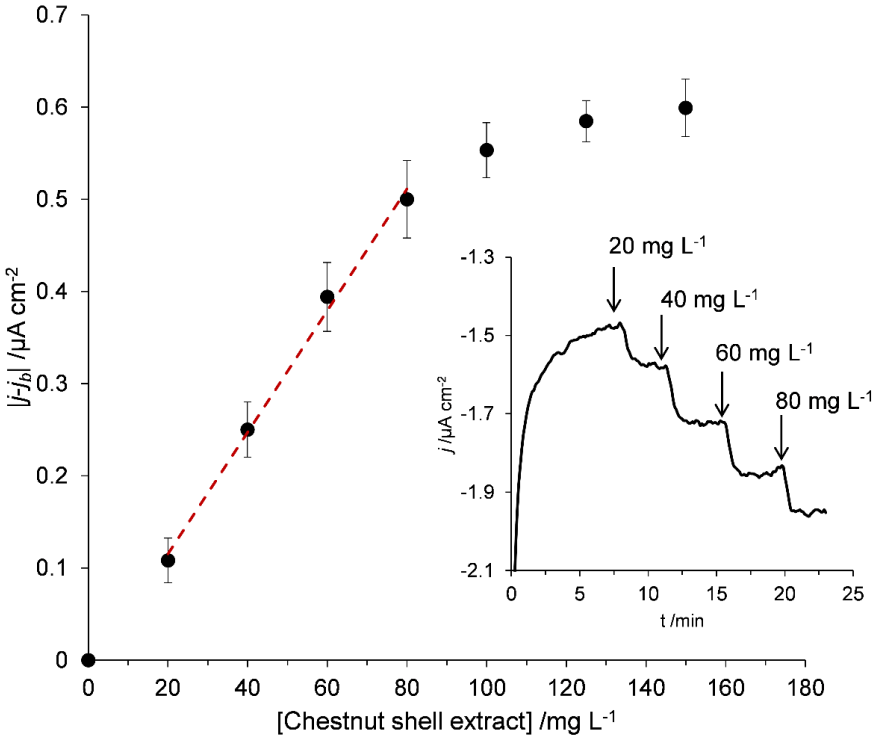

Figure 6.7: Current response of the graphite/ePDA-LacNZ modified electrode to different concentrations of chestnut shell extract (20 – 150 mg L^{-1}) measured at an applied potential of 0.0 V in oxygenated CPB pH 4.6 buffer. Error bars represent the standard deviation of 3 independent assays. Inset shows a representative chronoamperometric assay where additions of extract are indicated by the arrows.

6.1.3. Polycatecholamines comparative performance in laccase-based biosensing interfaces

Previously, it was demonstrated that cheap graphite electrodes could be successfully modified with thin polydopamine-laccase films by a simple and fast potentiostatic method that allowed the development of reproducible biosensors for the detection of phenolic compounds. To further complement this work, dopamine was substituted by norepinephrine and catechol in the one-step potentiostatic deposition of polymer-laccase films. As represented in the scheme of **Figure 6.8a**, the same potentiostatic deposition method was used, applying 0.3 V for 120 s to pristine graphite electrodes immersed in solutions containing 5 mM of monomer and 0.65 U mL^{-1} of LacNZ. After the electrode modification, their catalytic activity was assessed by chronoamperometry using gallic acid as a phenolic compound model. **Figure 6.8b** shows the catalytic curves of the modified electrodes with the three polymer-laccase thin films. Polynorepinephrine performed very similarly to polydopamine, displaying a sensitivity for gallic acid detection of 15.0 and 14.6 µA cm^{-2} mM^{-1}, respectively, both in the linear range of 0.005 – 0.200 mM. In what regards the analytical performance, both polycatecholamines were

shown to be suitable for the attachment of active LacNZ. Although slightly higher currents were observed for the case of polynorepinephrine at gallic acid concentrations higher than 0.5 mM, this is not analytically relevant since the saturation region is characterized by a very low sensitivity. The slightly better biosensing performance polynorepinephrine against polydopamine can be due to its possible lower thickness that allowed a more facile electron transfer while working with a similar amount of immobilized laccase. Given the data of the potentiodynamic growth of polycatechol (*cf.* **Figure 5.1**), polycatechol-laccase hybrid film is expected to be thinner than polycatecholamines-laccase films synthesized with the same polymerization time. That would enable a better electron transfer across polycatechol-laccase compared to the other polymers; however, the catalytic currents after the co-deposition of laccase were considerably lower than those observed for polydopamine and polynorepinephrine. In fact, the measured sensitivity in the polycatechol case was 9.8 μA cm^{-2} mM^{-1}, with the same linear range. It is possible that the amount of immobilized laccase is lower compared to the other cases, as suggested by the lower saturation current.

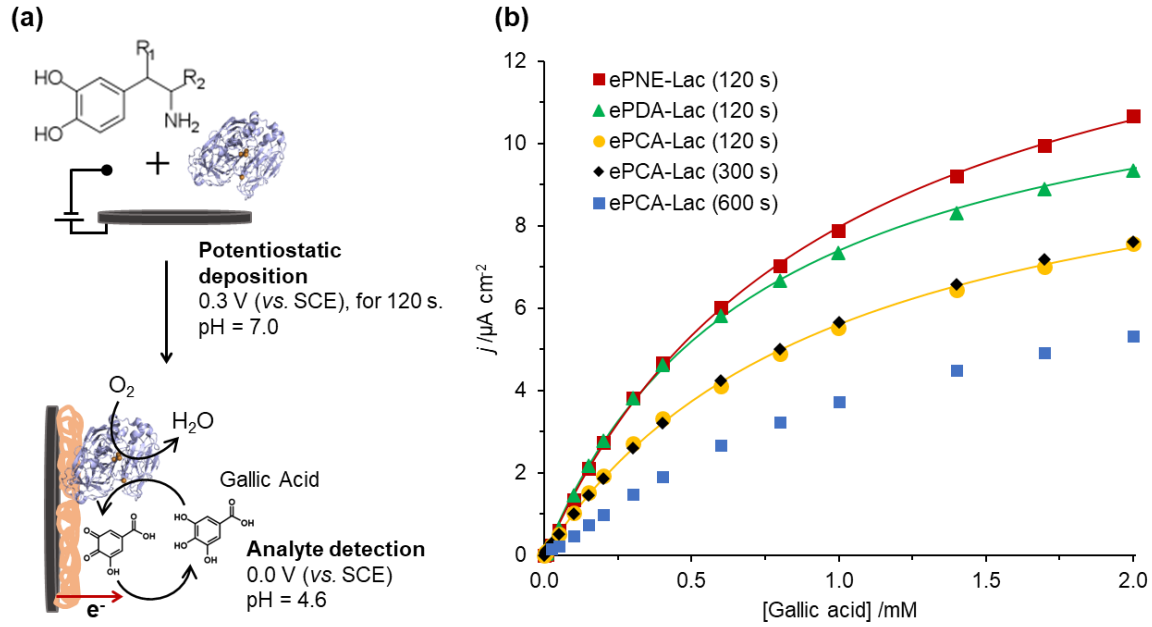

Figure 6.8: Scheme of the one-step potentiostatic deposition of polymer-laccase thin films in graphite electrodes and further amperometric detection of gallic acid **(a)**; Current responses of the graphite/polymer-LacNZ modified electrodes to different concentrations of gallic acid measured by chronoamperometry at an applied potential of 0.0 V, in oxygenated CPB pH 4.6 buffer **(b)**.

In an effort to improve the catalytic signal of polycatechol-laccase film, the polymerization was also conducted for 300 and 600 s (**Figure 6.8b**). However, the use of longer polymerization times did not improve the catalytic profile already obtained with 120 s. Then, the results indicate that electrodepositions longer than 300 s do not increase the amount of useful laccase. Since graphite electrodes were used in these assays, it is challenging to have a precise measure of the polymers thickness, and relate this parameter with the catalytic currents. However, to estimate the thickening behavior of potentiostatic synthesized polycatechol, *ex situ* multiangle ellipsometric measurements were conducted to glassy carbon electrodes modified with this polymer after 120, 300 and 600 s of electrodeposition. The experimental and calculated ellipsometric angles Ψ and Δ are provided in the **Table A1** of Annex, as well as the estimated parameters that concern the thin polycatechol films (*n*, *k* and *L*). Thicknesses of 1.4 ± 0.3, 2.8 ± 0.5 and 4.1 ± 0.8 nm are estimated for the films prepared after 120, 300 and 600 s of electrodeposition, respectively, revealing a slower growth compared with polydopamine. For comparison, a polydopamine film grown potentiostatically using the same potential for 120 s, renders a 5.2 nm layer (*cf.* **Table 6.1**) that is thicker than the polycatechol film grown after 600 s. Since the polycatechol-laccase films are expected to be thinner than polycatecholamines-laccase films, it is reasonable to conclude that lower catalytic currents are not caused by charge transfer hindering of the analyte. Instead, the lower performance of polycatechol may be related with the absence of an amine group in its structure, preventing an even more effective co-deposition of polymer and LacNZ at the electrode surface. It is worth noting that in this experiment LacNZ is immobilized during the electrodeposition of polycatechol, which is a different strategy than adsorbing the enzyme on top of a pre-synthesized film. Further laccase adsorption assays in the several polycatecholamine films, monitored by SPR or gravimetric techniques, may disclose the role of catechol and amine groups in the immobilization capabilities of catechol-related polymers.

6.2. Modification of polycatecholamine films with bacterial laccase

Bacterial laccases are promising biocatalysts for industrial processes, such as textile wastewater treatments [35] and lignin valorization [36,37], since they are active in a wider range of pH, stable at higher temperatures, and less susceptible to inhibitory agents compared to the eukaryotic laccases extracted from fungi and plants [38]. These same characteristics are also important to consider in the development of enzymatic fuel cells and biosensors, however, bacterial laccases are typically low redox potential enzymes which discourages their study and

application in electrochemical devices [39]. It is worth noting that, besides the redox potential of a laccase, substrate affinity also affects the oxidation rate. For example, it has been shown that a low redox potential laccase from *Bacillus subtilis* oxidizes aromatic amines faster than high redox potential fungal laccases [40]. In addition, the immobilization of the same laccase at glassy carbon electrodes modified with thiolated graphene and gold nanoparticles, allowed improvements in the stability and reusability of the resulting biosensor when compared to the use of the widely studied fungal laccase from *Trametes versicolor* [41]. Since the bacterial laccases are less studied than fungal laccases, the advantages and disadvantages of bacterial laccases in the electrochemical field are still not clear, thus it is a scientific topic that should be pursued.

6.2.1. Catalytic profile of the bacterial laccase

Although laccases are known for oxidizing a wide range of substrates, bacterial laccases are generally more selective enzymes compared to eukaryotic laccases [42]. To assess the catalytic profile of the bacterial laccase cocktail provided by MetGen (LacMG), the UV-Vis spectra of several phenolic solutions was recorded at pH 4.6 and 7.0 in the presence of the enzyme (**Figure 6.9**). The chemical structures of the selected phenols are presented in **Figure 6.9a**, comprising a toxic monophenol, 2,6-DMP, the simplest ortho-diphenol, catechol, an hydroxycinnamic acid, caffeic acid, an hydroxybenzoic acid, gallic acid, and a flavonoid, catechin.

Regarding 2,6-DMP, catechol and catechin, there is almost no catalytic activity at pH 4.6, as seen by the absence of products formation after *ca.* 3 min (**Figure 6.9b**). This agrees with the published catalytic profiles of bacterial laccases towards proton donating substrates (*e.g.* phenols), where the optimum pH value ranges from 6 to 9 [43,44]. At neutral pH (**Figure 6.9c**), the spectra of the three aforementioned substrates present new absorption bands, namely, those related to the oxidation products of 2,6-DMP at 440 nm, of catechol at 400 nm, of catechin at 440/473 nm [45,46]. In contrast, the two phenolic compounds bearing a carboxyl group (caffeic acid and gallic acid) showed significant oxidation rates at acidic and neutral media (**Figure 6.9d**). Caffeic acid spectra display absorption bands at 420 nm at both pH, while gallic acid spectra display absorption bands at 390/570 nm at pH 4.6, and 370(*sh.*)/457/580 nm at pH 7.0. The appearance of absorption bands in caffeic acid and gallic acid spectra at both pH values (**Figure 6.9b** and **6.9c**) denotes the formation of their oxidation products, clearly confirming significant catalytic activity of LacMG. The observed catalytic activity at acidic media has not yet been described in the literature, and its worth exploring, since a LacMG-based biosensor

may be able to identify different classes of phenols in complex mixtures by changing the operational pH.

Another catalytic feature of LacMG that deserves mentioning, concerns the higher formation rate of catechin oxidation products compared to the other phenolic compounds (**Figure 6.9d**). Although the presented results are expressed as relative formation rates (empiric absorbance variation over time), they are not explained by differences in the molar absorption coefficients values. Data found regarding catechin-quinone suggests its absorption coefficient (< 1300 M^{-1} cm^{-1}) [47] is lower than that of oxidized form of catechol (*o*-benzoquinone, *ca.* 1400 M^{-1} cm^{-1}) [48] and other simple *o*-quinones [49]. The higher formation ratio of catechin products is then better attributed to a more efficient catalysis of this flavonoid compared to the simpler phenols tested. In fact, a more efficient oxidation of catechin by laccases from plants and bacteria is reported in comparative studies against catechol [45] and sinapic acid [50], respectively. In summary, the hereby presented catalytic profile of LacMG reveals that catechin and gallic acid are suitable phenolic candidates as analytes to be detected by a LacMG-based biosensing interface.

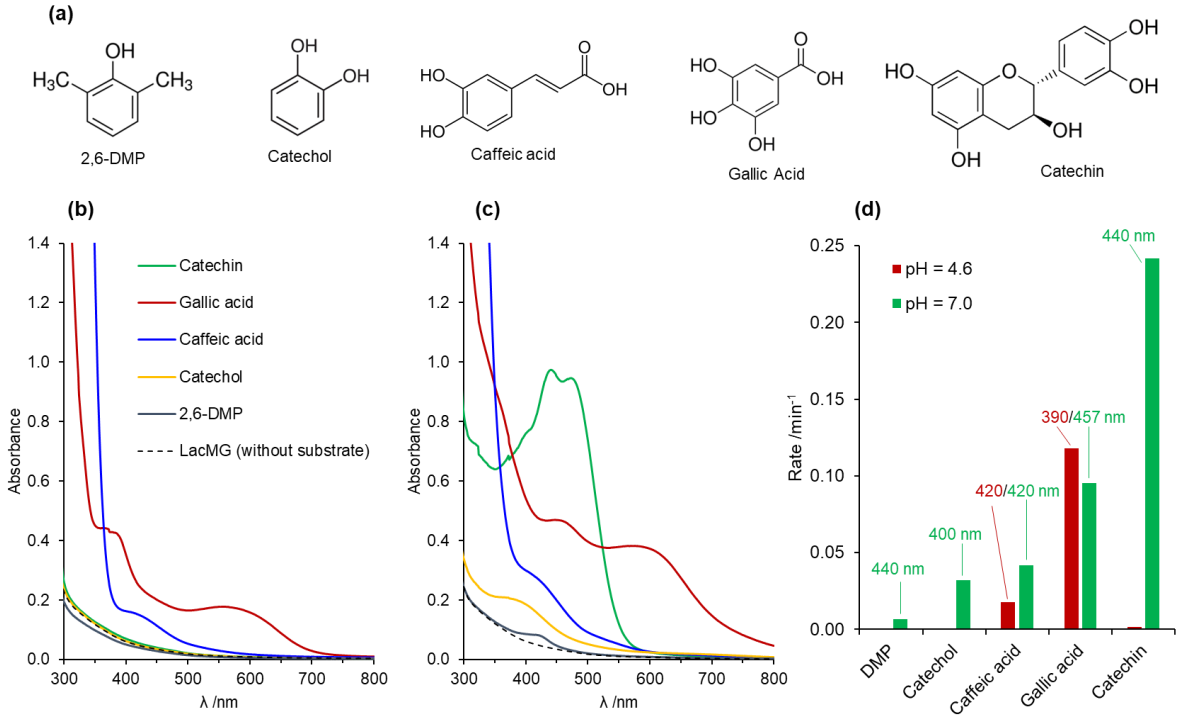

Figure 6.9: Chemical structurers of 2,6-DMP, catechol, caffeic acid, gallic acid and catechin **(a)**; UV-Vis spectra of 0.5 mM of phenolic compound at pH 4.6 **(b)** and 7.0 **(c)** in the presence of LacMG (1:2×10^4) after 3 min and 10 s; Initial product formation rate of the several phenolic compounds at pH 4.6 and 7.0 followed at the indicated wavelengths **(d)**.

6.2.2. One-step *versus* two-step immobilization methods

The one-step deposition method developed in this work (section 6.1) was proven to be robust, being able to prepare a phenolic biosensor in fast and reproducible manner from an industrial laccase cocktail of fungal origin (LacNZ). It was then interesting to test the viability of this one-step electrochemical method to immobilize other industrial laccase cocktails, namely, the bacterial laccase cocktail provided by MetGen (LacMG). The potentiostatic polymerization of catechol was then carried out at 0.3 V for 200 s using different dilutions of LacMG (1:10, 1:50 and 1:200). Firstly, to assess the catalytic activity of the immobilized enzyme, the modified graphite electrodes were submitted to 0.4 V in the presence of different concentrations of ABTS, as presented in **Figure 6.10**. It was clear that the use of more diluted solutions of LacMG (1:200 and 1:50) did not result in measurable catalytic activity of the modified electrodes, since there was no increase in the reduction current upon additions of ABTS (**Figure 6.10a**). This result proves that no active enzyme was efficiently immobilized at the electrode surface, although the amount of enzyme used to modify the electrodes in these cases is *ca.* 0.25 and 1 U mL^{-1} (*cf.* calculations in section 3.3, chapter III). The immobilization was also tested using dopamine instead of catechol as starting monomer, however there was also no evidence of active laccase attached to the electrode. Using a much more concentrated solution of LacMG (1:10), it is possible to effectively modify the graphite electrode with a polycatechol film that encompasses active laccase (Graph/ePCA-LacMG, blue curve in **Figure 6.10b**). The catalytic response of this electrode follows a Michaelis-Menten curve (*cf.* **Equation 3.1**, chapter III) with a K_M apparent constant of 502 μM and a maximum current density of 18.5 μA cm^{-2} (blue circles in **Figure 6.10c**). Since the dilution 1:10 represents a quite concentrated solution of laccase (*ca.* 5 U mL^{-1}), a control assay was performed to evaluate the contribution of physically adsorb laccase on the bare graphite electrode. After 3 hours of incubation of the pristine graphite electrode (Graph/LacMG, black squares in **Figure 6.10c**), there is in fact some adsorbed laccase that remains attached to the surface, however, the catalytic activity of this electrode towards ABTS is lower than the one modified in one step in just 200 s (Graph/ePCA-LacMG, blue circles in **Figure 6.10c**), proving that LacMG can be actively immobilized during the electropolymerization of catechol.

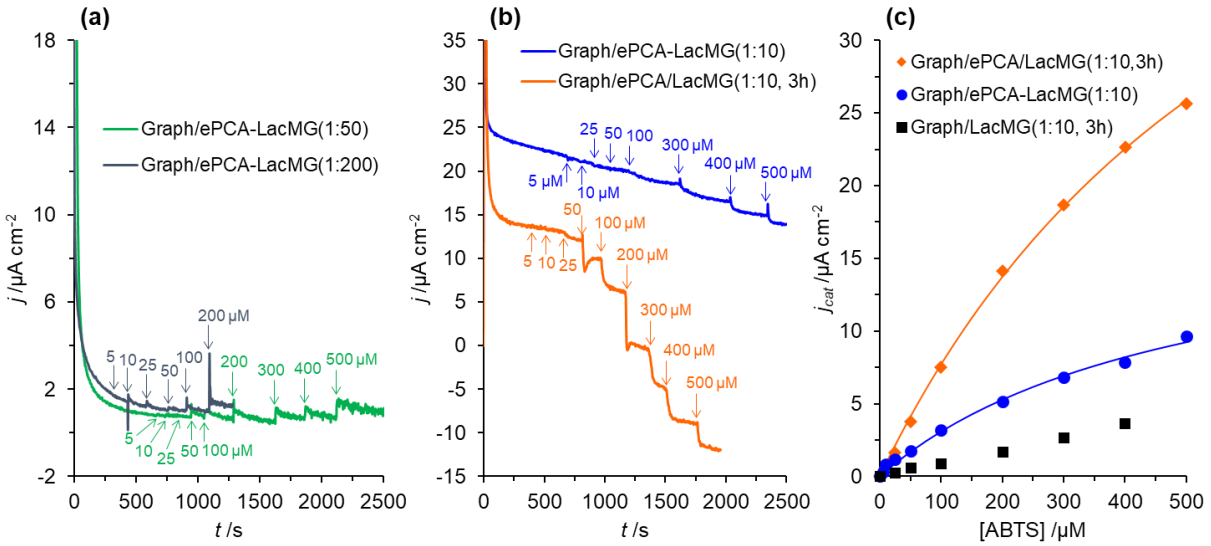

Figure 6.10: Chronoamperometric response of graphite electrodes towards ABTS (5 – 500 µM) after potentiostatic growth of polycatechol in the presence of LacMG in the dilution ratios of 1:50 and 1:200 **(a)**; Chronoamperometric response of modified graphite electrodes with using a one-step (graph/ePCA-LacMG) or two-step (graph/ePCA/LacMG) method, using a LacMG dilution ratio of 1:10 **(b)**; Catalytic current densities ($j_{cat} = |j – j_b|$) *versus* ABTS concentration, obtained by chronoamperometric assays of the modified graphite electrodes and respective Michaelis-Menten fitted curves **(c)**; The assays were performed at an applied potential of 0.4 V in oxygenated CPB pH 4.6 buffer.

A two-step method to immobilize the bacterial laccase from the industrial cocktail was also tested as follows: i) potentiostatic deposition of the polycatechol film in the absence of laccase; ii) incubation of the modified electrode in a laccase solution (1:10) for 3 hours. As it is possible to observe by the chronoamperometric response in **Figure 6.10b**, the two-step modified electrode (graph/ePCA/LacMG, orange curve) displays higher catalytic currents in the presence of ABTS compared to the one-step modified electrode. The Michaelis-Menten response of graph/ePCA/LacMG electrode is characterized by a K_M apparent constant of 717 µM and a maximum current density of 62.9 µA cm^{-2} (orange diamonds in **Figure 6.9c**), which is indicative of an improvement in the amount of immobilized active enzyme. In this particular case, the one-step electrochemical method seems to be limited by the amount of laccase that is immobilized by co-precipitation with the polymer. The impaired immobilization process carried out with LacMG contrasts with the successful one-step procedure applied to LacNZ, and might be explained by the presence of some unknown component in the industrial cocktail of MetGen enzymes. From this point on, the study of graphitic electrodes modified with LacMG is carried out using only the two-step method using a dilution ratio of 1:50 (*ca.* 1 U mL^{-1}).

6.2.3. Catalytic properties of polycatecholamines/laccase electrodes towards phenolic compounds

The modification of graphite electrodes with LacMG by the successful two-step method described above was extended to more relevant substrates than ABTS (*e.g.* phenolic compounds: 2,6-DMP, gallic acid and catechin) and two promising immobilization matrices, polydopamine and polynorepinephrine. To carry out a comparative study of the performance of the two polycatecholamines, the potentiostatic growth duration was adjusted to yield ePNE and ePDA films with the same thickness. The chronoamperograms corresponding to their potentiostatic growths on glassy carbon are presented in **Figure 6.11a**. As shown in chapter V, the microgravimetric studies revealed a faster potentiodynamic polymerization rate for ePDA than for ePNE during the initial 10 potential cycles. For this reason, the applied potential pulse for ePNE formation must be longer than that of ePDA (200 *vs.* 120 s) to attain similar thicknesses. The currents shown in **Figure 6.11a** decrease over time, revealing that both polymers have low conductivity when compared to conventional conducting polymers (*e.g.* PEDOT, polyaniline), where the current rises after a nucleation step, due to a 3D growth of a conducting phase under diffusion control [10,51]. In catecholamines case, rather than a diffusional regulation of their growth, polymerization is limited by the increasing resistance of the layer as it thickens, which inevitably leads to a continuous decrease of the rate of charge transfer. Thus, although ePNE and ePDA display similar current profiles, the decrease in current observed for ePNE is less accentuated, suggesting the presence of a less insulating polymer layer. The cyclic voltammograms obtained for both polymers in CPB pH 7.0 (**Figure 6.11b**), reveal the typical two-electron two-proton redox processes of polycatecholamines, as thoroughly discussed in chapters IV and V. Both films display very similar oxidation and reduction charge proving that identical amounts of electroactive material are deposited on the glassy carbon surface.

The main process (I) in **Figure 6.11b**, occurring at higher potentials, corresponds to *o*-quinone/*o*-diphenolic moieties conversion, the intermediate process (II) can be assigned to the presence of indole-type species and the more negative process (III) is attributed to the indolinequinone/dihydroxyindoline groups. Indolinic species result from a chemical step involving an intramolecular cyclization of catecholamines, upon oxidation to *o*-quinones, due to nucleophilic attack of the nitrogen atoms to the catechol rings, whereas the indolic species, arise from an isomerization process of the indolinic species. Despite their similarities (**Figures 6.11c** and **6.11d**), the redox properties of ePNE are better-defined than those of ePDA, and the

presence of indolic moieties is clearly denoted. The insets of **Figures 6.11c** and **6.11d** show the linear relationship between the oxidation and reduction peak currents of the process I against the potential sweep rate for ePNE and ePDA, respectively, revealing that electrochemical conversions of the immobilized redox active groups for both polymers are not determined by mass-transfer phenomena.

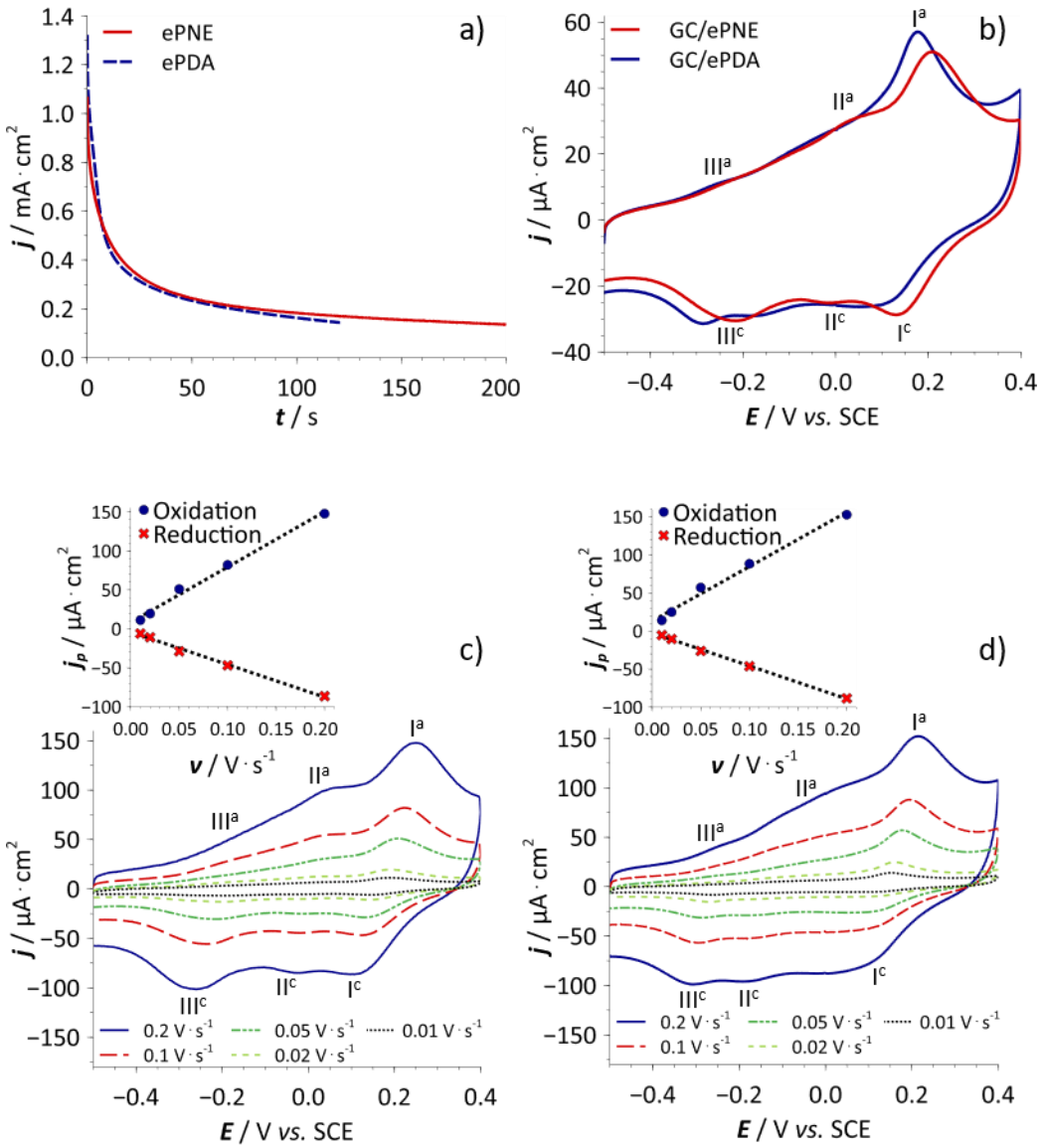

Figure 6.11: Potentiostatic synthesis (0.3 V) of ePNE (200 s) and ePDA (120 s) films from 5 mM DA and NE in CPB pH 7.0 solutions, respectively **(a)**; Cyclic voltammograms of ePNE and ePDA in CPB pH 7.0, recorded at 50 mV s^{-1} **(b)**; Cyclic voltammograms at different potential scan rates for ePNE **(c)** and ePDA **(d)** modified electrodes in CPB pH 7.0, respectively. The insets show the representations of the peak current density (process I) *versus* potential scan rate of ePNE (R^2 oxidation = 0.9925; R^2 reduction = 0.9943), and ePDA films (R^2 oxidation = 0.9890; R^2 reduction = 0.9984).

AFM topographic images were taken on modified HOPG electrodes with ePNE and ePDA thin films before (**Figures 6.12a** and **6.12b**, respectively) and after (**Figures 6.12c** and

6.12d, respectively) LacMG incubation (1:50, 3 h). HOPG was employed in the topographic analysis of the polycatecholamines, since it is an atomically flat surface, allowing to perfectly distinguish the deposited thin polymeric films from the underlying carbon electrode, in contrast with previous polydopamine topographic studies on GC, where the roughness of the coatings was highly associated to the polished GC surfaces (*cf.* section 4.1). The morphologies of the ePDA and ePNE are consistent with those observed before for these polycatecholamines, revealing very uniform films with a regular granular morphology. Root mean-square roughness values of 0.80 nm and 0.88 nm are obtained for ePNE and ePDA, respectively (**Figures 6.12a** and **6.12b**, respectively). After intentional scratching, the images of exposed HOPG surface show the typical atomically flat terraces (**Figures 6.12e** and **6.12f**), with a height variation of 0.33 nm or multiples of that, corresponding to a single or multilayers of carbon atoms [52]. Through the height profiles taken, it can be concluded that the thickness of both films is very similar of *ca.* 5 nm (**Figure 6.11g**), perfectly agreeing with the thickness value obtained previously for ePDA grown at glassy carbon using the same conditions (5.2 ± 0.7 nm, *cf.* Table 6.1). Similarly, the GC/ePNE interface was also analyzed by *ex situ* ellipsometry outputting a complex refractive index of 1.80(±0.01) – 0.52(±0.02)*i* and a thickness of 5.3(±0.5) nm. The calculated refractive index of polycatecholamines is high when compared to well-known conducting polymers, such as polypyrrole [53], or PEDOT [54], confirming the presence of an optically dense film. Nevertheless, ePNE presents a slightly lower refractive index than ePDA, indicative of a less dense film. On the other hand, the value of the extinction coefficient, that is related to the electronic π-π* transitions, is higher for ePNE than for ePDA, suggesting that the former may have a larger amount of double bonds in polymer backbone, whether they are conjugated or not [55]. In fact, when comparing the cyclic voltammograms of **Figure 6.11b**, the redox processes assigned to the indolic form (II), are better defined for ePNE than for the ePDA coating.

As mentioned, **Figures 6.12c** and **6.12d** show the polycatecholamines upon incubation in a laccase solution followed by thorough rinsing. Since the size of enzyme molecules, imaged by AFM, are similar to those of polymer clusters, it is difficult to clearly discriminate between individual laccase and polymer globules. Besides, their mechanical properties are also alike, also precluding distinguishing them by phase imaging. However, the presence of enzyme can still be depicted by the globular features distributed on top of the polymer layers, especially for ePNE, as pinpointed by the white circles. The images suggest a good enzyme distribution on the surface, since no large agglomerates could be depicted upon laccase immobilization. The fact that the modified electrodes are thoroughly washed after enzyme adsorption step ensures a

robust interaction between the enzyme and the polymer. Further confirmation of enzyme immobilization is provided by water contact angle measurements at glassy carbon. The WCA for ePNE (25° ± 2°) is lower than that of ePDA (35° ± 2°), revealing that, as observed for the potentiodynamic electrosynthesis on gold surfaces (*cf.* **Table 5.1**), the extra hydroxyl group is kept upon potentiostatic polymerization NE, yielding a more hydrophilic film. After laccase incubation, the WCA values increase to 65° ± 1° (ePNE/LacMG) and 63° ± 1° (ePDA/LacMG), confirming laccase presence on the polymeric films.

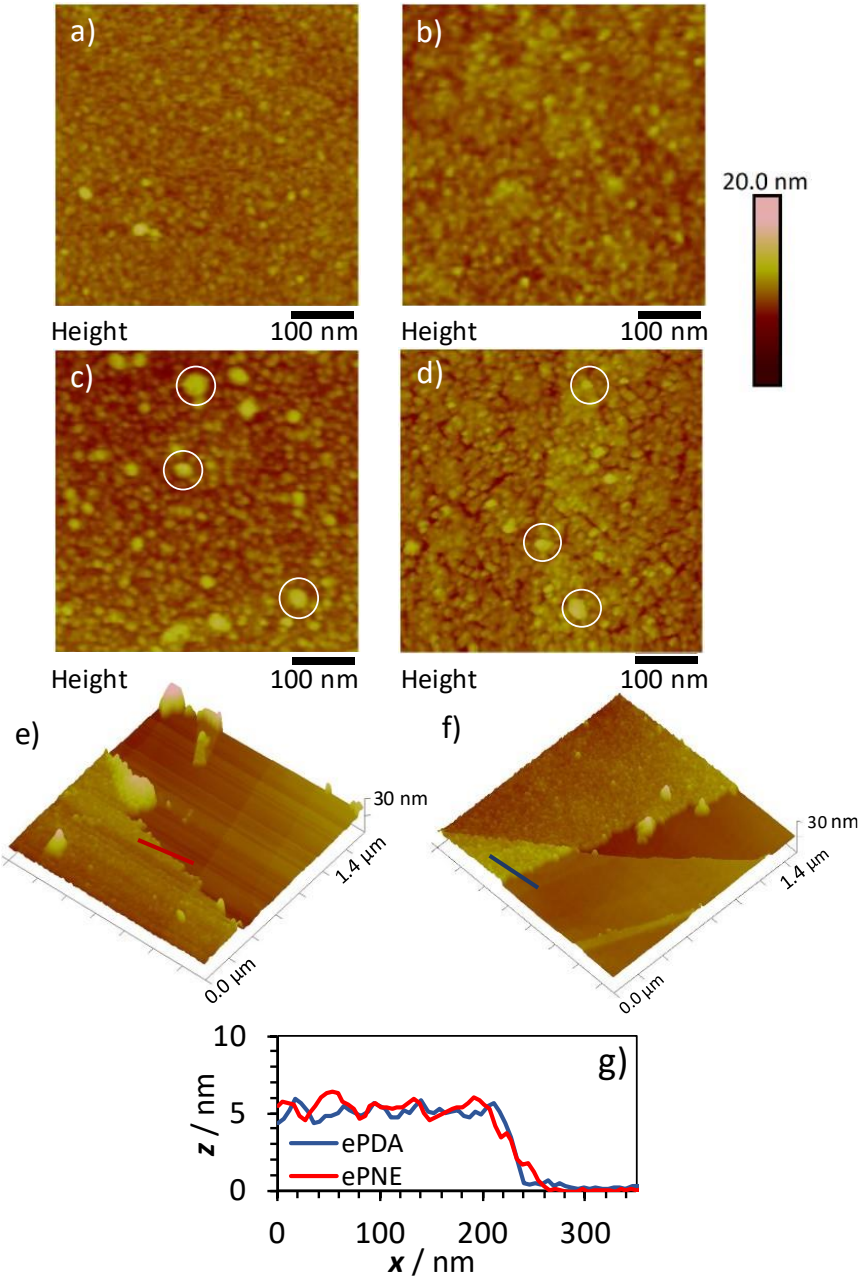

Figure 6.12: AFM topographic images of ePNE **(a)** and ePDA **(b)** films, grown potentiostatically on HOPG electrodes, from 5 mM NE and DA in CPB pH 7.0, at 0.3 V for 200 and 120 s, respectively, and after their incubation in LacMG (1:50) solution for 3 hours: ePNE/LacMG **(c)** and ePDA/LacMG **(d)**. The 3D images of ePNE **(e)** and ePDA **(f)** coatings also exhibit clean HOPG areas after intentional scratching; the corresponding cross section analysis are shown in panel **(g)**.

When preparing an amperometric biosensor interface, it is important to evaluate the ability of the polymer modified electrode for the electrochemical conversion of positively and negatively charged soluble ionic species, at the working pH of the enzyme. **Figure 6.13** illustrates the redox behavior of 1 mM $[Fe(CN)_6]^{4-/3-}$ or $[Ru(NH_3)_6]^{2+/3+}$ species, at CPB pH 5.0 and 7.0, on ePNE and ePDA films. The electrochemical response of a bare GC electrode is also included for comparison. It is observed that ePNE does not hinder the oxidation or reduction of either the anionic or the cationic species, at any of the solutions studied. In contrast, on ePDA modified GC electrode, there is a decrease in the anodic and cathodic peak currents at pH 5.0, for the $[Ru(NH_3)_6]^{2+/3+}$ redox conversion, and at pH 7.0 for the negatively charged $[Fe(CN)_6]^{4-/3-}$ redox probe. This behavior suggests that ePDA polymer charge changes according to the solution pH, affecting its transduction properties. In fact, both ePDA and ePNE are expected to change their net charge, at distinct pH values, being positive at pH below 4 – 5 and negatively charged above this value, as discussed for potentiodynamic grown films at gold electrodes (*cf.* **Figure 5.6**). Thus, despite of having very similar thickness, ePNE interface allows a better electrochemical conversion than ePDA, revealing either a more porous layer or a less insulating polymer.

After establishing the growth conditions for the polycatecholamine immobilization matrices, the applicability of the two-step modified graphite electrode was firstly evalutated using 2,6-dimethylphenol (DMP) as phenolic analyte. DMP is an important xylenol, classified as a xenobiotic, since it is extract from coal, petroleum, or produced by chemical synthesis, thus not usually found in nature. It is the precursor used in the synthesis of the thermoplastic poly(2,6-dimethyl-1,4-phenyleneoxide) (PPO), resins, and other compounds such as pesticides, dyes, and antioxidants [56,57]. Although toxic [58], DMP can be biodegraded and do not persist in the environment [59–61]. Large-scale industries that produce or apply DMP [62] are then obliged to carefully monitor their wastewaters, in order to avoid serious environmental pollution problems and the implementation of bioremediation processes. Due to the resemblance of the chemical structure of DMP and syringic compounds, this xenobiotic can be enzymatically oxidized by laccases and it is used to characterize the catalytic behaviors of such enzymes. For instance, several bacterial laccases from *Bacillus* and *Streptomyces sp.* exhibit an optimal pH for the catalytic oxidation of DMP near pH 7, differently from eukaryotic laccases which are most active at acidic media [42]. The LacMG provided by MetGen is even more alkaliphilic, since the optimal pH for the oxidation of a hydrogen donating substrate, such as DMP, is near 10, as reported elsewhere [36]. Although the optimal pH for the homogeneous enzymatic catalysis is a crucial factor for the performance of a biosensor, the stability of the

analyte and immobilization matrix are also important factors, affected by pH, that must be consider when envisaging a working biosensing interface. Firstly, the electrochemical behavior of DMP was briefly analyzed in neutral media using a glassy carbon electrode (**Figure 6.14a**). The most intense anodic peak occurring at 0.53 V is a characteristic irreversible oxidation of a monophenol to its corresponding phenoxy radical, involving the loss of one electron and one proton [13,63]. Due to the instability of this radical, oxidation products are rapidly formed during the first anodic scan that are observed in the following scans as a reversible redox process centered at *ca.* 0.09 V (**Figure 6.14a**). The increase in intensity as potential scan progresses, suggests some accumulation of the oxidation product that was not originally present. One possible attribution to this redox process is the electrochemical conversion of a *p*-benzoquinone, as the result of DMP hydroxylation in the meta position – a reaction pathway known to occur during phenol electrochemical oxidation [13,63]. It is worth noting that a similar reversible redox process, observed in organic media, was previously attributed to the DMP dimer formed by C-C coupling at the meta position of two radicals [64–66]. Although the chemical oxidation is known to originate the aforementioned dimer, or even polymer segments [56], these species were not consensually identified by electrochemical methods. Furthermore, it was not possible to attribute the irreversible oxidation peak at 0.23 V to any particular species derived from DMP. Since this oxidation process appears in the first anodic scan, it might suggest the presence of some unidentified impurity. Nonetheless, the performed cyclic voltammograms allow to conclude that a low potential value (for instance, -0.1 V at pH 7) would be adequate for the reductive detection of any oxidation products generated by laccase enzymatic activity.

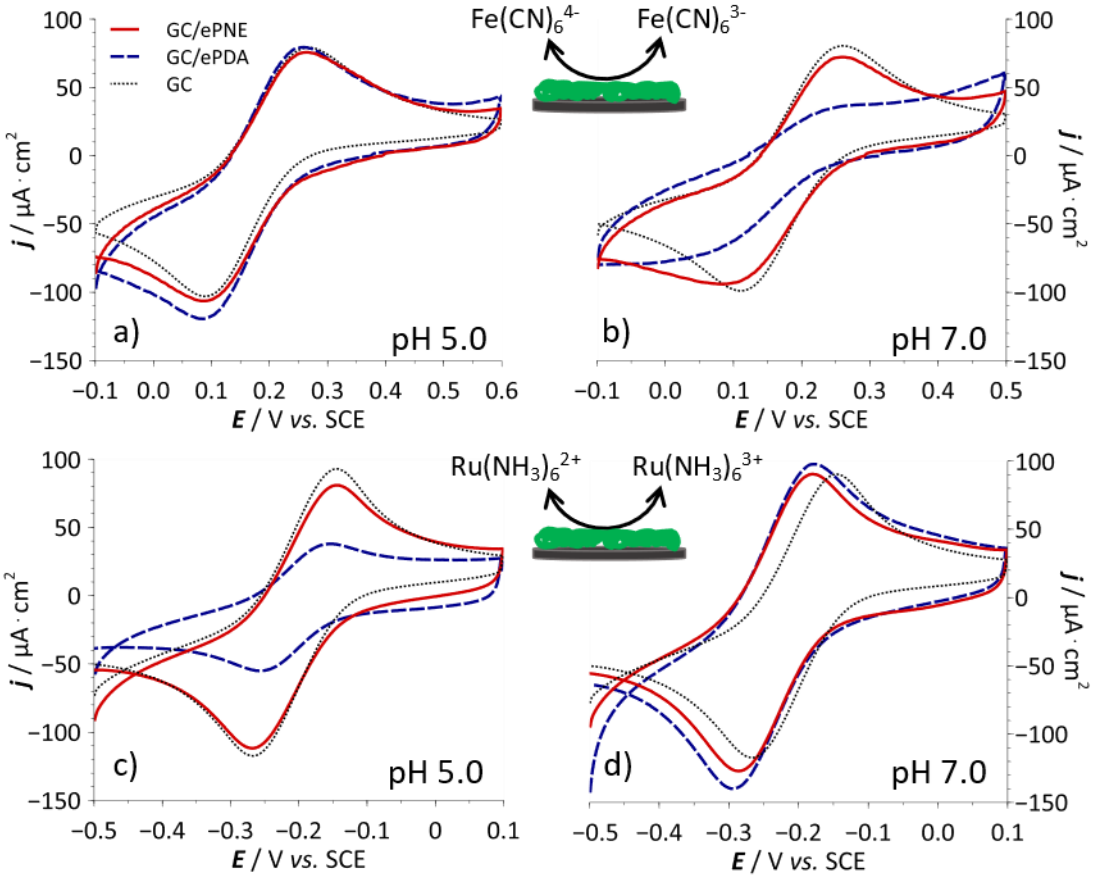

Figure 6.13: Cyclic voltammograms, recorded at 50 mV s^{-1} of bare GC and GC modified with ePDA, ePNE, grown potentiostatically at 0.3 V for 120 and 200 seconds, respectively. 1 mM $K_3[Fe(CN)_6]$ in CPB pH 5.0 **(a)** and pH 7.0 **(b)**; 1 mM $[Ru(NH_3)_6]Cl_3$ in CPB pH 5.0 **(c)** and pH 7.0 **(d)**.

Having the electrochemical behavior of DMP in consideration, a graphite electrode modified with polydopamine and LacMG by the two-step method was tested as biosensing interface for the amperometric detection of DMP (**Figure 6.14b**). No catalytic current was observed at -0.1 V at pH 7, although a wide concentration range of analyte was used (10 to 600 µM), which indicates a negligible catalytic activity of the immobilized enzyme. This result is consistent with the homogeneous catalysis data obtained by UV-Vis spectroscopy (**Figure 6.9**), where the enzymatic oxidation of DMP stands out as the slowest at neutral pH. The same biosensing interface was tested in alkaline pH, 9, closer to the optimal working pH of LacMG, as shown in **Figure 6.14c**. One inherent problem of using an alkaline media concerns the stability of polydopamine films. As the solution pH gets closer to the first macroscopic pK_a of catecholamines (*ca.* 9 [67]), deprotonation of amine and catechol groups is expected, disrupting important electrostatic interactions within the polymeric structure and causing its partial delamination [68]. In fact, the cathodic current of the graphite electrode modified with polydopamine (**Figure 6.14c**), registered at pH 9, decreases over time, suggesting the gradual

loss of polymeric material. The observed decrease in current is not affected by the addition of DMP to the electrolytic solution, as expected in the absence of laccase. In contrast, after the immobilization of LacMG, the modified electrode exhibits a catalytic response to DMP, displaying a sensitivity of 7.7 μA cm^{-2} mM^{-1} in a linear range of 25 – 400 μM (**Figure 6.14d**). Compared to other developed sensing interfaces, capable of detecting methylated phenols through electrochemical transduction [69–71], the biosensing platform here presented stands out by its particular wide linear range. Although further work is needed to ensure the stability of the polymeric matrix, a single-use biosensor can be constructed for the detection of DMP. In addition, the non-catalytic response observed for this biosensing interface at neutral or acidic media represents a possible analytical strategy to discard the presence of other phenolic compounds in a real sample.

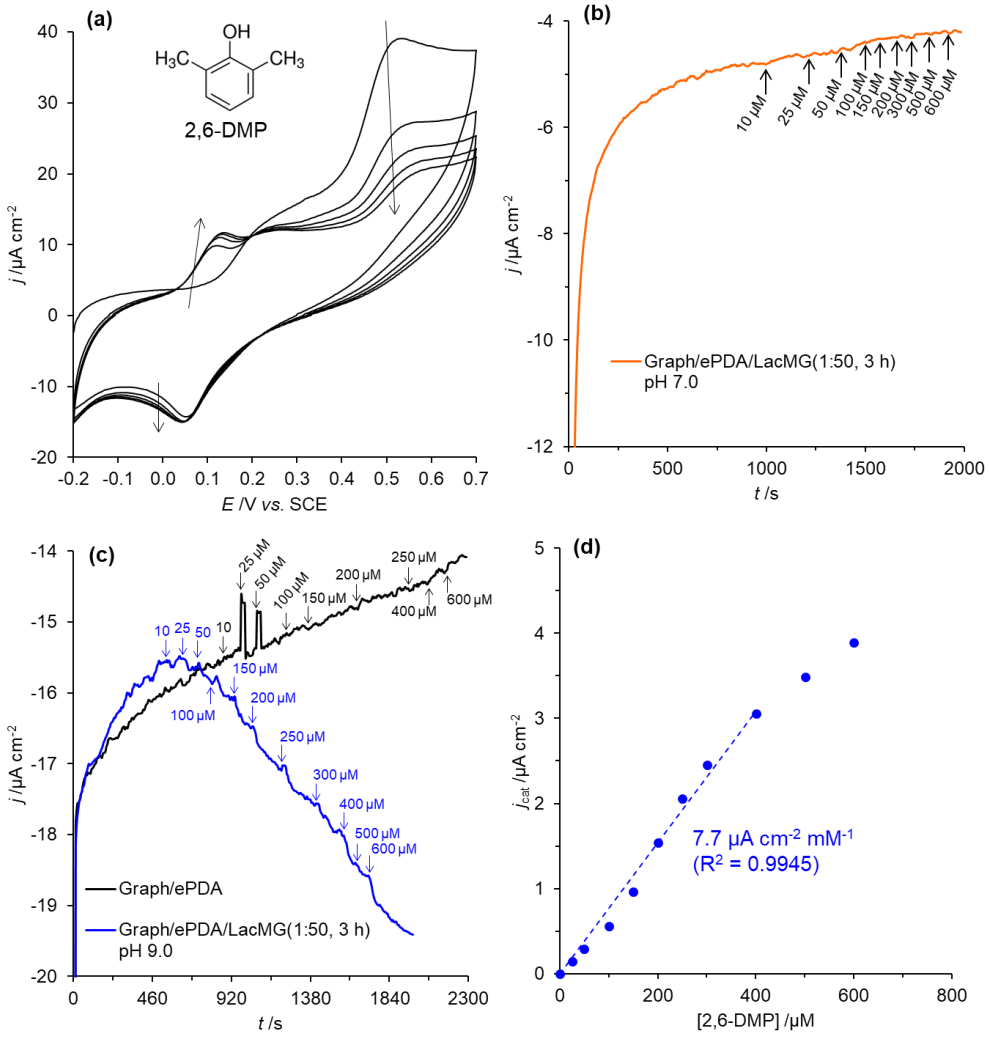

Figure 6.14: Consecutive cyclic voltammograms of bare GC electrode in 0.1 mM 2,6-DMP deoxygenated solution buffered at pH 7, recorded at 50 mV s^{-1} **(a)**; The molecular structure of 2,6-DMP is included; Chronoamperometric response of the modified electrode graph/ePDA/LacMG(1:50, 3 h) at pH 7 **(b)** and pH 9 **(c)** to successive additions of 2,6-DMP (10 – 600 μM), applying

a constant potential of -0.1 V and -0.2 V respectively; The response of the modified electrode without LacMG (graph/ePDA) is also included in panel (c); Catalytic current densities ($j_{cat} = |j - j_b|$) *versus* 2,6-DMP concentration **(d)**, obtained by chronoamperometric assay at pH 9 – panel (c).

The simple phenolic acid, gallic acid, was selected to perform a comparative study of the catalytic performance of graphite electrodes modified with polydopamine and polynorepinephrine at pH 5.0 and 7.0 (**Figure 6.15**). The electrochemical conversion of gallic acid at pH 7.0 can be depicted in **Figure 6.15a**, revealing an irreversible two-electron two-proton oxidation process, at 0.23 V, corresponding to the formation of 3-hydroxy-1,2-benzoquinone as the oxidation product [23,24]. It is known that the quinone species generated upon oxidation go through further chemical processes, thus not being reduced on the reverse cycle, for low sweep rates. Besides, consecutive cycling leads to a film deposition at the electrode surface, especially at neutral or basic pH values. As stated before, to avoid the undesired passivation of the electrode, the chronoamperometric detection of gallic acid products is performed at 0.0 V and -0.1 V for pH 5.0 and 7.0, respectively (**Figure 6.15b** and **6.15c**). A pulse of 200 s was chosen to ensure that the current obtained was stabilized for each concentration of analyte studied. The chronoamperometric assays performed at such conditions reveal that the graph/ePNE/LacMG electrodes exhibits catalytic responses to gallic acid at both pH values, as seen by the decrease of currents with the substrate concentration increments, confirming the presence of active immobilized enzyme within the ePNE matrix. Great current decreases are observed at pH 7.0 (**Figure 6.15b**), whereas smaller current variations are observed at pH 5.0 (**Figure 6.15c**). The differences between the assays performed at pH 5.0 and 7.0 can be better depicted in **Figure 6.15d**, where the average of catalytic currents at the same pH is plotted against the gallic acid concentration. The steeper slope of graph/ePNE/LacMG catalytic curve at neutral pH clearly reveals that the electrochemical reduction of gallic acid oxidation products is more extensive than in acidic medium (*ca.* 5 times stepper than the pH 5.0 slope). According to the spectroscopic assays performed in homogeneous conditions, the catalytic rate of conversion by laccase is similar at both pH values (*cf.* **Figure 6.9c**); likewise, the electrochemical sensitivities of the biosensing interface is expected to be similar at those pH values considering that the enzymatic activity should be the dominant factor to control the surface concentration of oxidation products. As so, the differences observed in the electrochemical data strongly indicate that other factors besides the catalytic activity of laccase are influencing the charge transfer between the gallic acid oxidation product (or products) and the electrode. An important fact to consider is the presence of an

ePNE/LacMG film covering the electrode surface, which may display pH-depending charge transfer properties. The behavior of pristine ePNE films covering glassy carbon (**Figure 6.13**) and gold electrodes (**Figure 5.6**, chapter V) is already evaluated against redox probes, revealing that this type of film allows a better charge transfer of negatively charged probes at acidic pH values than neutral, independently of the underlying electrode material. It is also clear that the ePNE film prepared potentiostatically at glassy carbon is much less sensitive to the pH compared to the ePNE film prepared potentiodynamically on gold. As different factors may be playing a role in determining the charge transfer properties of ePNE (*e.g.* electrode material, and electrosynthesis mode), it is difficult to predict the behavior of the ePNE/Lac film prepared potentiostatically on graphite. Further studies of ePNE/Lac charge transfer properties should be conducted to fully explain the current data.

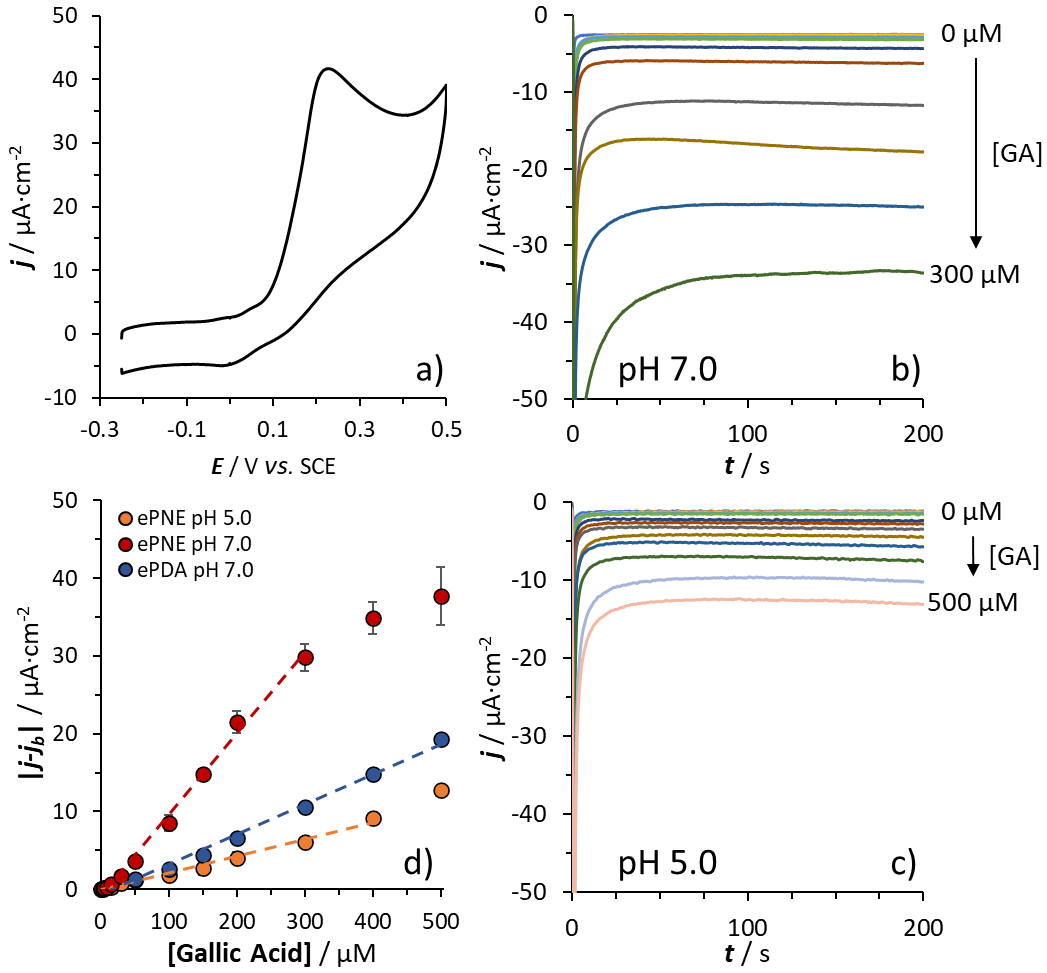

Figure 6.15: Cyclic voltammogram of bare GC electrode in deaerated 0.1 mM gallic acid solution in CPB pH 7.0, recorded at 50 mV s^{-1} **(a)**; Chronoamperometric responses of graphite/ePNE/LacMG electrode at pH 7.0 **(b)** and 5.0 **(c)**, with successive additions of gallic acid (1, 3, 5, 10, 15, 30, 50, 100, 150, 200, 300, 400, 500 µM) by applying a potential pulse of 0.0 V (pH 5.0) or -0.1 V (pH 7.0) for 200 s; Average catalytic current densities ($|j–j_b|$, j_b is the background current density) *versus* gallic acid concentration **(c)**, obtained from three chronoamperometric assays of graphite/ePNE/LacMG and graphite/ePDA/LacMG electrodes.

The analytical parameters withdrawn from the chronoamperometric assays (**Figure 6.15**) are compiled in **Table 6.4**. At pH 7.0, the sensitivity of the ePNE/LacMG interface towards gallic acid is exceptionally enhanced (104 μA cm^{-2} mM^{-1}), compared to that obtained by the one-step potentiostatic polydopamine-LacNZ deposition (19.3 μA cm^{-2} mM^{-1}, *cf.* **Table 6.2**), at pH 4.6 (the optimal pH value for the fungal laccase used). Furthermore, even using a non-optimal pH value of 5.0 for LacMG, the achieved sensitivity of ePNE/LacMG (21.58 μA cm^{-2} mM^{-1}) is slightly higher than that obtained for LacNZ, at pH 4.6. In addition, much wider linear ranges (3 – 300 or 3 – 400 μM) are achieved for the present bacterial laccase at both pH values, compared to that obtained previously (1 – 150 μM). Moreover, the modified electrode that displayed the best performance at pH 7.0 was ePNE, with a considerably higher sensitivity than that achieved with ePDA (19.3 μA cm^{-2} mM^{-1}, **Table 6.4**), grown under the conditions that indicate similar thicknesses for both polymers, highlighting the use of norepinephrine as an alternative monomer to dopamine. This result agrees with the higher electroactivity and with the better electrochemical transducing properties disclosed for ePNE regarding ePDA, which can be tentatively explained by ePNE higher organization/porosity. In addition, AFM images (**Figures 6.12c,d**) suggest more enzyme adsorbed onto polynorepinephrine than on polydopamine films.

Table 6.4: Analytical parameters for gallic acid detection by the graphite/ePDA/LacMG and graphite/ePNE/LacMG modified graphite electrodes at acidic and neutral pH medium: limit of detection (LOD), linear range, sensitivity, and corresponding coefficient of determination (R^2).

Interface	pH	LOD* /μM	Linear range /μM	Sensitivity /μA cm^{-2} mM^{-1}	R^2
ePNE/LacMG	5.0	2.2	3 – 400	21.58 ± 0.05	0.9902
	7.0	0.7	3 – 300	104 ± 6	0.9950
ePDA/LacMG	7.0	5.4	5 – 500	39 ± 2	0.9945

*LOD values were estimated using the expression 3σ/s, where σ is the standard deviation of the background current and s is the sensitivity of the sensor.

As mentioned before, apart from DMP and gallic acid, catechin was also selected as analyte to test the modified graphite electrodes with LacMG. Catechin is a simple flavonoid, representing a class of compounds with health benefits that are found in plants, their products and industrial wastes [72]. The detection and quantification of catechin, gallate derivatives, and their epimers, is of special relevance in the characterization and nutritional quality assessment

of green teas [73,74], and chocolate products [75], since these flavanols are the major polyphenols found in *Camellia sp.* extracts and *Theobroma sp.* beans, respectively. Contrasting with the xenobiotic DMP, catechin is a secondary metabolite that participates in natural browning of seeds coating – a multi-enzymatic process involving laccase [76]. In fact, as discussed above, laccases were found to efficiently oxidize catechin compared to other phenolic compounds, positioning catechin as a desirable testing analyte.

Figure 6.16a shows the electrochemical behavior of catechin in CPB pH 7.0 using a glassy carbon electrode. As major process, a typical quasi-reversible redox conversion of an *ortho*-quinone/hydroquinone group is identified, centered at *ca.* 0.18 V. Since catechin-quinone is the expected enzymatic oxidation product [77], the potential selected for its amperometric detection was -0.1 V at pH 7.0, and 0.0 V at pH 5.0, as a result of potential shift due the pH change [51]. The imposed potential will prevent any phenolic compound oxidation reaction at the electrode surface, so that the detected cathodic current during the assay only comes from the enzymatic activity.

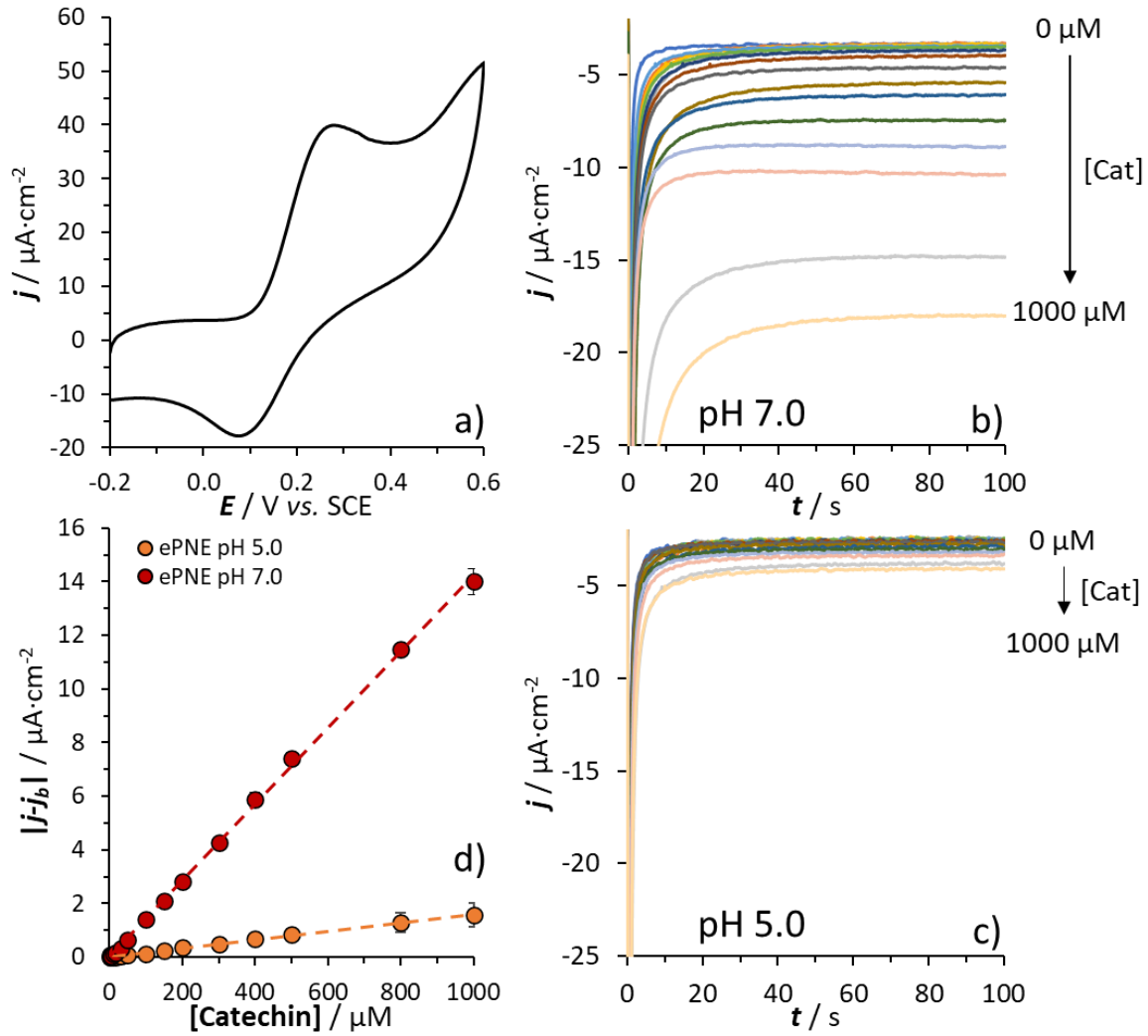

Figure 6.16: Cyclic voltammogram of bare GC electrode in deaerated 0.1 mM catechin solution in CPB pH 7.0, recorded at 50 mV s^{-1} **(a)**; Chronoamperometric responses of graphite/ePNE/LacMG electrode at pH 7.0 **(b)** and 5.0 **(c)**, with successive additions of catechin (1, 3, 5, 10, 15, 30,50, 100, 150, 200, 300, 400, 500, 800, 1000 µM) by applying a potential pulse of 0.0 V (pH 5.0) or -0.1 V (pH 7.0) for 200 s; Average catalytic current densities ($|j - j_b|$, j_b is the background current density) *versus* catechin concentration **(d)**, obtained from three chronoamperometric assays for different modified electrodes.

After incubating graphite/ePNE electrodes with LacMG, catalytic responses to catechin at pH 7.0 and 5.0 were observed, as seen by the increase of cathodic current at each increment of catechin concentration from 1 to 1000 µM (**Figure 6.16b** and **6.16c**, respectively). The analytical parameters of the electrodes at both pH values are compile in **Table 6.5** for a clear analysis. In agreement with the UV-Vis absorption spectra (*cf.* **Figure 6.9**), considerably more intense amperometric responses were observed at neutral media compared to the acidic conditions, confirming the pH-dependent catalytic behavior of the immobilized bacterial laccase. As a consequence of the low catechin oxidation rate at pH 5.0, a low sensitivity is observed at this pH for ePNE/Lac modified electrodes (1.2 µA cm^{-2} mM^{-1}), whereas at pH 7.0 this parameter is more than 10 times greater (14.4 µA cm^{-2} mM^{-1}), as better depicted in **Figure**

6.16c. This feature distinguishes this biosensing interface from those constructed using fungal laccases (from *Coriolus versicolor* [78] and *Cerrena unicolor* [79]) that display an optimal working pH in the acidic domain. A plant laccase from *Rhus vernicifera* was also used before to build a complex biosensing interface on a glassy carbon surface, displaying an optimal pH of 6.5, however, a much lower linear range of catechin detection is reported (0.1–10 μM) [80]. In fact, the observed wide linear range of graphite/ePNE/LacMG is unusual considering the ranges of other enzymatic sensors with amperometric transduction [81]. The characteristics found for the developed interface may be attributed to the bacterial laccase LacMG used, with distinct catalytic properties as those more commonly found in the literature.

Table 6.5: Analytical parameters for catechin detection by the graphite/ePNE/LacMG modified electrode: limit of detection (LOD), linear range, sensitivity, and corresponding coefficient of determination (R^2).

Interface	pH	LOD* /μM	Linear range /μM	Sensitivity /μA cm^{-2} mM^{-1}	R^2
ePNE/LacMG	5.0	11.2	10 – 1000	1.2 ± 0.3	0.9944
	7.0	1.3	1 – 1000	14.4 ± 0.3	0.9999

*LOD values were estimated using the expression 3σ/s, where σ is the standard deviation of the background current and s is the sensitivity of the sensor.

The validation of the graphite modified electrodes as reproducible electrodes for single use purposes is portrayed in the catalytic responses of **Figures 6.15** and **6.16**, and their respective analytical informations reported in **Tables 6.4** and **6.5**. To verify the robustness of the immobilization, consecutive assays of phenols detection were performed after the first use of the graphite/ePNE/LacMG electrode (**Figure 6.17**). The deviation in amperometric responses between the first and the second assay are minimal and lie on the reproducibility error found for multiple single uses of the same electrode (*cf.* **Figures 6.15d** and **6.16d**). The repeatability tests thus confirm the absence of enzyme leakage during the first and second assays, and in-between washing steps, supporting the robustness of the interface to be used multiple times.

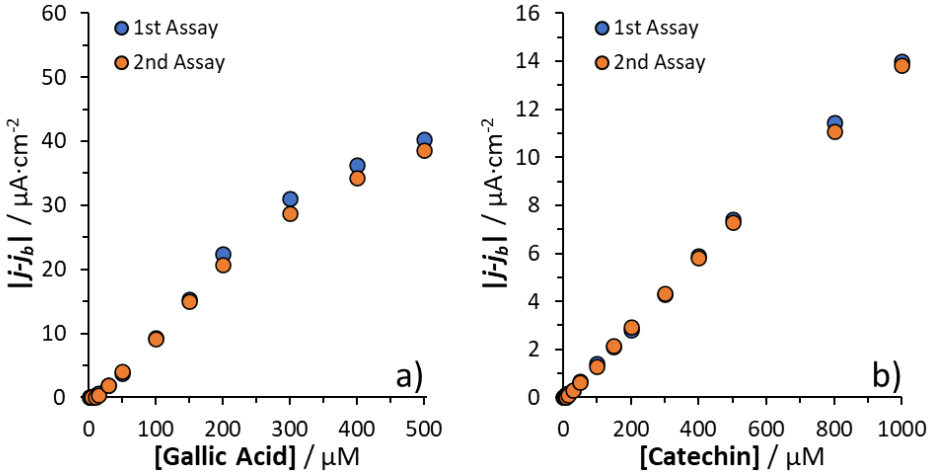

Figure 6.17: Current densities ($|j - j_b|$, j_b is the background current density) vs. substrate concentration obtained for two consecutive chronoamperometric responses of graphite/ePNE/LacMG at pH 7.0 by applying potential pulses of -0.1 V of 200 s for gallic acid **(a)** and 100 s for catechin **(b)**.

The facile association of polycatecholamine matrices, especially ePNE, with a bacterial laccase with alkaliphilic nature, has the great potential to allow the direct monitoring of polyphenols in samples that are neutral or slightly basic, without the need to work in acidic medium as it is usual for laccase-based biosensors.

6.3. Conclusions

The success of laccase immobilization on electrode surface is found to be strongly dependent on enzyme origin and used strategy. When using Novozymes laccase (LacNZ), a robust immobilization is achieved through the one-step potentiostatic method using different catechol derivatives, being particularly efficient when dopamine or norepinephrine are used, which highlights the important role of the amine group in the electrochemical co-deposition of polymer and laccase. The extensive characterization of ePDA-LacNZ films reveals that the incorporation of enzyme does not greatly affect the redox behavior, optical properties, and morphology of a pristine polydopamine film, suggesting the existence of physical interactions between the entrapped enzyme and polymer matrix, as well as a good enzyme surface distribution. Furthermore, the proposed one-step biofunctionalization method is easily transposed to cheap and disposable graphite electrodes, as demonstrated by the very reproducible and highly catalytic responses to several phenolic compounds: caffeic, rosmarinic and gallic acid. In addition, the biosensor was used to measure the gallic acid content on an aqueous extract of chestnut shell waste, yielding a value close to that obtained by HPLC quantification.

In the case of MetGen laccase (LacMG), the two-step immobilization strategy proved to be a much more efficient immobilization method than the one-step potentiostatic strategy, although a longer procedure is required. This fact suggests that the two-step method is more adaptable to different immobilization conditions, namely, solution components or laccase composition, whereas the one-step method requires a fast formation of interactions between the target enzyme and polymer segments for an efficient co-deposition; that may not happen ambiguously with all laccases. Despite the selected modification method, the suitability of catechol derivatives (dopamine and norepinephrine) as immobilization agents is clearly demonstrated by the amperometric responses to dimethylphenol, gallic acid and catechin obtained at different pH values. The amperometric responses of the modified surfaces are related to the catalytic behavior of the bacterial laccase in homogenous conditions assessed by UV-Vis spectroscopy. Due to the alkaliphilic properties of the MetGen laccase, the prepared biosensing interfaces may be used in the monitoring of monophenols (*e.g.* DMP) in alkaline conditions, after the instability of polydopamine matrix at pH 9 is solved, namely by substituting dopamine by other catechol derivatives less susceptible to delamination. The constructed phenolic biosensor is found to efficiently operate at neutral pH for the detection of gallic acid and catechin. Graphite electrodes modified with polynorepinephrine and MetGen laccase are particularly promising due to the sensitivity enhancements regarding the use of polydopamine, highlighting promising implementation of such biosensing interfaces in gallic acid and catechin quantification in diverse food products, natural extracts or valuable industrial wastes.

6.4. References

[1] P.O. Saboe, E. Conte, M. Farell, G.C. Bazan, M. Kumar, Biomimetic and bioinspired approaches for wiring enzymes to electrode interfaces, Energy and Environmental Science. 10 (2017) 14–42. doi:10.1039/c6ee02801b.

[2] M. Li, C. Deng, Q. Xie, Y. Yang, S. Yao, Electrochemical quartz crystal impedance study on immobilization of glucose oxidase in a polymer grown from dopamine oxidation at an Au electrode for glucose sensing, Electrochimica Acta. 51 (2006) 5478–5486. doi:10.1016/j.electacta.2006.02.023.

[3] H. He, Q. Xie, S. Yao, An electrochemical quartz crystal impedance study on anti-human immunoglobulin G immobilization in the polymer grown during dopamine oxidation at

an Au electrode, Journal of Colloid and Interface Science. 289 (2005) 446–454. doi:10.1016/j.jcis.2005.03.085.

[4] J. Liebscher, Chemistry of Polydopamine – Scope, Variation, and Limitation, European Journal of Organic Chemistry. 2019 (2019) 4976–4994. doi:10.1002/ejoc.201900445.

[5] L.C. Almeida, J.P. Correia, A.S. Viana, Electrochemical and optical characterization of thin polydopamine films on carbon surfaces for enzymatic sensors, Electrochimica Acta. 263 (2018) 480–489. doi:10.1016/j.electacta.2018.01.077.

[6] Y. Li, M. Liu, C. Xiang, Q. Xie, S. Yao, Electrochemical quartz crystal microbalance study on growth and property of the polymer deposit at gold electrodes during oxidation of dopamine in aqueous solutions, Thin Solid Films. 497 (2006) 270–278. doi:10.1016/j.tsf.2005.10.048.

[7] L.C. Almeida, R.D. Correia, A. Marta, G. Squillaci, A. Morana, F. La Cara, J.P. Correia, A.S. Viana, Electrosynthesis of polydopamine films - tailored matrices for laccase-based biosensors, Applied Surface Science. 480 (2019) 979–989. doi:10.1016/j.apsusc.2019.03.015.

[8] D. Li, L. Luo, Z. Pang, L. Ding, Q. Wang, H. Ke, F. Huang, Q. Wei, Novel Phenolic Biosensor Based on a Magnetic Polydopamine-Laccase-Nickel Nanoparticle Loaded Carbon Nanofiber Composite, ACS Applied Materials & Interfaces. 6 (2014) 5144–5151. doi:10.1021/am500375n.

[9] J.H. Ryu, P.B. Messersmith, H. Lee, Polydopamine surface chemistry: a decade of discovery, ACS Applied Materials and Interfaces. 10 (2018) 7523–7540. doi:10.1021/acsami.7b19865.

[10] D. Sazou, M. Kourouzidou, E. Pavlidou, Potentiodynamic and potentiostatic deposition of polyaniline on stainless steel: Electrochemical and structural studies for a potential application to corrosion control, Electrochimica Acta. 52 (2007) 4385–4397. doi:10.1016/j.electacta.2006.12.020.

[11] A.I. Melato, A.S. Viana, L.M. Abrantes, Different steps in the electrosynthesis of poly(3,4-ethylenedioxythiophene) on platinum, Electrochimica Acta. 54 (2008) 590–597. doi:10.1016/j.electacta.2008.07.030.

[12] M. Sugumaran, Reactivities of quinone methides versus o-Quinones in catecholamine metabolism and eumelanin biosynthesis, International Journal of Molecular Sciences. 17 (2016) 1–23. doi:10.3390/ijms17091576.

[13] T.A. Enache, A.M. Oliveira-Brett, Phenol and para-substituted phenols electrochemical oxidation pathways, Journal of Electroanalytical Chemistry. 655 (2011) 9–16. doi:10.1016/j.jelechem.2011.02.022.

[14] M.M. Rodríguez-Delgado, G.S. Alemán-Nava, J.M. Rodríguez-Delgado, G. Dieck-Assad, S.O. Martínez-Chapa, D. Barceló, R. Parra, Laccase-based biosensors for detection of phenolic compounds, TrAC - Trends in Analytical Chemistry. 74 (2015) 21–45. doi:10.1016/j.trac.2015.05.008.

[15] M.Y. Arica, B. Salih, O. Celikbicak, G. Bayramoglu, Immobilization of laccase on the fibrous polymer-grafted film and study of textile dye degradation by MALDI–ToF-MS, Chemical Engineering Research and Design. 128 (2017) 107–119. doi:10.1016/J.CHERD.2017.09.023.

[16] I. Almeida, A.C. Cascalheira, A.S. Viana, One step gold (bio)functionalisation based on CS2-amine reaction, Electrochimica Acta. 55 (2010) 8686–8695. doi:10.1016/j.electacta.2010.07.084.

[17] I. Almeida, F. Henriques, M.D. Carvalho, A.S. Viana, Carbon disulfide mediated self-assembly of Laccase and iron oxide nanoparticles on gold surfaces for biosensing applications, Journal of Colloid and Interface Science. 485 (2017) 242–250. doi:10.1016/j.jcis.2016.09.042.

[18] M. Fernández-Fernández, M.Á. Sanromán, D. Moldes, Recent developments and applications of immobilized laccase, Biotechnology Advances. 31 (2013) 1808–1825. doi:10.1016/j.biotechadv.2012.02.013.

[19] E. de Souza Gil, T. Adrian Enache, A. Maria Oliveira-Brett, Redox Behaviour of Verbascoside and Rosmarinic Acid, Combinatorial Chemistry & High Throughput Screening. 16 (2013) 92–97. doi:10.2174/138620713804806337.

[20] D.M.A. Gil, M.J.F. Rebelo, Gallic acid interference on polyphenolic amperometric biosensing using Trametes versicolor laccase, Journal of Molecular Catalysis B: Enzymatic. 72 (2011) 193–198. doi:10.1016/j.molcatb.2011.06.005.

[21] H.A.L. Filipe, C. Sousa, J.T. Marquês, D. Vila-Viçosa, A. de Granada-Flor, A.S. Viana, M.S.C.S. Santos, M. Machuqueiro, R.F.M. de Almeida, Differential targeting of membrane lipid domains by caffeic acid and its ester derivatives, Free Radical Biology and Medicine. 115 (2018) 232–245. doi:10.1016/J.FREERADBIOMED.2017.12.002.

[22] J. Teixeira, A. Gaspar, E.M. Garrido, J. Garrido, F. Borges, Hydroxycinnamic Acid Antioxidants: An Electrochemical Overview, BioMed Research International. 2013 (2013) 1–11. doi:10.1155/2013/251754.

[23] R. Abdel-Hamid, E.F. Newair, Electrochemical behavior of antioxidants: I. Mechanistic study on electrochemical oxidation of gallic acid in aqueous solutions at glassy-carbon electrode, Journal of Electroanalytical Chemistry. 657 (2011) 107–112. doi:10.1016/j.jelechem.2011.03.030.

[24] C.H. Hung, W.T. Chang, W.Y. Su, S.H. Cheng, Electrochemical determination of pyrogallol at conducting poly(3,4-ethylenedioxythiophene) film-modified screen-printed carbon electrodes, Electroanalysis. 26 (2014) 2237–2243. doi:10.1002/elan.201400296.

[25] H.R. Zare, S.M. Golabi, Caffeic acid modified glassy carbon electrode for electrocatalytic oxidation of reduced nicotinamide adenine dinucleotide (NADH), Journal of Solid State Electrochemistry. 4 (2000) 87–89. doi:10.1007/s100080050006.

[26] M. Bilgi, E.M. Sahin, E. Ayranci, Sensor and biosensor application of a new redox mediator: Rosmarinic acid modified screen-printed carbon electrode for electrochemical determination of NADH and ethanol, Journal of Electroanalytical Chemistry. 813 (2018) 67–74. doi:10.1016/j.jelechem.2018.02.012.

[27] B. Haghighi, L. Gorton, T. Ruzgas, L.J. Jönsson, Characterization of graphite electrodes modified with laccase from Trametes versicolor and their use for bioelectrochemical monitoring of phenolic compounds in flow injection analysis, Analytica Chimica Acta. 487 (2003) 3–14. doi:10.1016/S0003-2670(03)00077-1.

[28] M. Diaconu, S.C. Litescu, G.L. Radu, Laccase-MWCNT-chitosan biosensor-A new tool for total polyphenolic content evaluation from in vitro cultivated plants, Sensors and Actuators, B: Chemical. 145 (2010) 800–806. doi:10.1016/j.snb.2010.01.064.

[29] C. Tortolini, M. Di Fusco, M. Frasconi, G. Favero, F. Mazzei, Laccase-polyazetidine prepolymer-MWCNT integrated system: Biochemical properties and application to analytical determinations in real samples, Microchemical Journal. 96 (2010) 301–307. doi:10.1016/j.microc.2010.05.004.

[30] S.C. Litescu, S.A. V. Eremia, A. Bertoli, L. Pistelli, G.-L. Radu, Laccase-Nafion Based Biosensor for the Determination of Polyphenolic Secondary Metabolites, Analytical Letters. 43 (2010) 1089–1099. doi:10.1080/00032710903518518.

[31] M. Di Fusco, C. Tortolini, D. Deriu, F. Mazzei, Laccase-based biosensor for the determination of polyphenol index in wine, Talanta. 81 (2010) 235–240. doi:10.1016/j.talanta.2009.11.063.

[32] A. Jarosz-Wilkołazka, T. Ruzgas, L. Gorton, Amperometric detection of mono- and diphenols at Cerrena unicolor laccase-modified graphite electrode: Correlation between

sensitivity and substrate structure, Talanta. 66 (2005) 1219–1224. doi:10.1016/j.talanta.2005.01.026.

[33] P. Ibarra-Escutia, J.J. Gómez, C. Calas-Blanchard, J.L. Marty, M.T. Ramírez-Silva, Amperometric biosensor based on a high resolution photopolymer deposited onto a screen-printed electrode for phenolic compounds monitoring in tea infusions, Talanta. 81 (2010) 1636–1642. doi:10.1016/j.talanta.2010.03.017.

[34] G. Squillaci, F. Apone, L.M. Sena, A. Carola, A. Tito, M. Bimonte, A. De Lucia, G. Colucci, F. La Cara, A. Morana, Chestnut (Castanea sativa Mill.) industrial wastes as a valued bioresource for the production of active ingredients, Process Biochemistry. 64 (2018) 228–236. doi:10.1016/j.procbio.2017.09.017.

[35] Z.B. Guan, Y. Shui, C.M. Song, N. Zhang, Y.J. Cai, X.R. Liao, Efficient secretory production of CotA-laccase and its application in the decolorization and detoxification of industrial textile wastewater, Environmental Science and Pollution Research. 22 (2015) 9515–9523. doi:10.1007/s11356-015-4426-6.

[36] V. Hämäläinen, T. Grönroos, A. Suonpää, M.W. Heikkilä, B. Romein, P. Ihalainen, S. Malandra, K.R. Birikh, Enzymatic Processes to Unlock the Lignin Value, Frontiers in Bioengineering and Biotechnology. 6 (2018) 1–10. doi:10.3389/fbioe.2018.00020.

[37] Y. Yang, W.Y. Song, H.G. Hur, T.Y. Kim, S. Ghatge, Thermoalkaliphilic laccase treatment for enhanced production of high-value benzaldehyde chemicals from lignin, International Journal of Biological Macromolecules. 124 (2019) 200–208. doi:10.1016/j.ijbiomac.2018.11.144.

[38] P.S. Chauhan, B. Goradia, A. Saxena, Bacterial laccase: recent update on production, properties and industrial applications, 3 Biotech. 7 (2017) 1–20. doi:10.1007/s13205-017-0955-7.

[39] Y. Zhang, Z. Lv, J. Zhou, F. Xin, J. Ma, H. Wu, Y. Fang, M. Jiang, W. Dong, Application of eukaryotic and prokaryotic laccases in biosensor and biofuel cells: recent advances and electrochemical aspects, Applied Microbiology and Biotechnology. 102 (2018) 10409–10423. doi:10.1007/s00253-018-9421-7.

[40] L.O. Martins, P. Durão, V. Brissos, P.F. Lindley, Laccases of prokaryotic origin: Enzymes at the interface of protein science and protein technology, Cellular and Molecular Life Sciences. 72 (2015) 911–922. doi:10.1007/s00018-014-1822-x.

[41] Y. Zhang, Z. Lv, J. Zhou, Y. Fang, H. Wu, F. Xin, W. Zhang, J. Ma, N. Xu, A. He, W. Dong, M. Jiang, Amperometric Biosensors Based on Recombinant Bacterial Laccase

CotA for Hydroquinone Determination, Electroanalysis. 32 (2020) 142–148. doi:10.1002/elan.201900395.

[42] R. Reiss, J. Ihssen, M. Richter, E. Eichhorn, B. Schilling, L. Thöny-Meyer, Laccase versus Laccase-Like Multi-Copper Oxidase: A Comparative Study of Similar Enzymes with Diverse Substrate Spectra, PLoS ONE. 8 (2013). doi:10.1371/journal.pone.0065633.

[43] S. Brander, J.D. Mikkelsen, K.P. Kepp, Characterization of an alkali- and halide-resistant laccase expressed in E. coli: CotA from Bacillus clausii, PLoS ONE. 9 (2014). doi:10.1371/journal.pone.0099402.

[44] J. Ihssen, R. Reiss, R. Luchsinger, L. Thöny-Meyer, M. Richter, Biochemical properties and yields of diverse bacterial laccase-like multicopper oxidases expressed in Escherichia coli, Scientific Reports. 5 (2015) 1–13. doi:10.1038/srep10465.

[45] H.L. Ma, S. Kermasha, J.M. Gao, R.M. Borges, X. zhu Yu, Laccase-catalyzed oxidation of phenolic compounds in organic media, Journal of Molecular Catalysis B: Enzymatic. 57 (2009) 89–95. doi:10.1016/j.molcatb.2008.07.006.

[46] S. Kim, A. Cavaco-Paulo, Laccase-catalysed protein-flavonoid conjugates for flax fibre modification, Applied Microbiology and Biotechnology. 93 (2012) 585–600. doi:10.1007/s00253-011-3524-8.

[47] M.A. Rouet-Mayer, J. Ralambosoa, J. Philippon, Roles of o-quinones and their polymers in the enzymic browning of apples, Phytochemistry. 29 (1990) 435–440. doi:10.1016/0031-9422(90)85092-T.

[48] G. Albarran, W. Boggess, V. Rassolov, R.H. Schuler, Absorption Spectrum, Mass Spectrometric Properties, and Electronic Structure of 1,2-Benzoquinone, The Journal of Physical Chemistry A. 114 (2010) 7470–7478. doi:10.1021/jp101723s.

[49] J.H. Waite, Calculating extinction coefficients for enzymatically produced o-quinones, Analytical Biochemistry. 75 (1976) 211–218. doi:10.1016/0003-2697(76)90072-5.

[50] S. Sheng, E.T. Farinas, Laccase and its mutant displayed on the Bacillus subtilis spore coat for oxidation of phenolic compounds in organic solvents, Catalysts. 11 (2021) 1–13. doi:10.3390/catal11050606.

[51] S. Patra, K. Barai, N. Munichandraiah, Scanning electron microscopy studies of PEDOT prepared by various electrochemical routes, Synthetic Metals. 158 (2008) 430–435. doi:10.1016/j.synthmet.2008.03.002.

[52] W. Han, P.T. Mathew, S. Kolagatla, B.J. Rodriguez, F. Fang, Toward Single-Atomic-Layer Lithography on Highly Oriented Pyrolytic Graphite Surfaces Using AFM-Based

Electrochemical Etching, Nanomanufacturing and Metrology. 5 (2022) 32–38. doi:10.1007/s41871-022-00127-9.

[53] S.J. Higgins, A. Hamnett, In situ ellipsometric study of the growth and electrochemical cycling of polypyrrole films on platinum, Electrochimica Acta. 36 (1991) 2123–2134. doi:10.1016/0013-4686(91)85220-2.

[54] L.M. Abrantes, J.P. Correia, A.I. Melato, An ellipsometric study of poly(3,4-ethylenedioxythiophene) electrosynthesis - From the initial stages to thick layers formation, Journal of Electroanalytical Chemistry. 646 (2010) 75–84. doi:10.1016/j.jelechem.2010.02.025.

[55] M. Łapkowski, A. Proń, Electrochemical oxidation of poly(3,4-ethylenedioxythiophene) — "in situ" conductivity and spectroscopic investigations, Synthetic Metals. 110 (2000) 79–83. doi:10.1016/S0379-6779(99)00271-4.

[56] P. Gamez, C. Simons, R. Steensma, W.L. Driessen, G. Challa, J. Reedijk, A spectacular increase in the polymerisation rate of 2,6-dimethylphenol induced by acetonitrile, European Polymer Journal. 37 (2001) 1293–1296. doi:10.1016/S0014-3057(00)00259-7.

[57] K. Saito, T. Tago, T. Masuyama, H. Nishide, Oxidative Polymerization of 2,6-Dimethylphenol To Form Poly(2,6-dimethyl-1,4-phenyleneoxide) in Water, Angewandte Chemie. 116 (2004) 748–751. doi:10.1002/ange.200352764.

[58] M. Brinkmann, A. Schneider, K. Bluhm, S. Schiwy, G. Lehmann, B. Deutschmann, A. Müller, A. Tiehm, H. Hollert, Ecotoxicity of Nitrogen, Sulfur, or Oxygen Heterocycles and Short-Chained Alkyl Phenols Commonly Detected in Contaminated Groundwater, Environmental Toxicology and Chemistry. 38 (2019) 1343–1355. doi:10.1002/etc.4423.

[59] J. Ji, Y. Zhang, Y. Liu, P. Zhu, X. Yan, Biodegradation of plastic monomer 2,6-dimethylphenol by Mycobacterium neoaurum B5-4, Environmental Pollution. 258 (2020) 113793. doi:10.1016/j.envpol.2019.113793.

[60] H. Fiege, Cresols and Xylenols, Ullmann's Encyclopedia of Industrial Chemistry, Electronic Release. 10 (2012) 419–461. doi:10.1002/14356007.a08_025.

[61] S. Ray, S. Panjikar, R. Anand, Structure Guided Design of Protein Biosensors for Phenolic Pollutants, ACS Sensors. 2 (2017) 411–418. doi:10.1021/acssensors.6b00843.

[62] A. Kahru, L. Põllumaa, R. Reiman, A. Rätsep, M. Liiders, A. Maloveryan, The toxicity and biodegradability of eight main phenolic compounds characteristic to the oil-shale industry wastewaters: A test battery approach, Environmental Toxicology. 15 (2000) 431–442. doi:10.1002/1522-7278(2000)15:5<431::AID-TOX11>3.0.CO;2-T.

[63] M. Ferreira, H. Varela, R.M. Torresi, G. Tremiliosi-Filho, Electrode passivation caused by polymerization of different phenolic compounds, Electrochimica Acta. 52 (2006) 434–442. doi:10.1016/j.electacta.2006.05.025.

[64] N. Oyama, T. Ohsaka, Y. Ohnuki, T. Suzuki, Anodic Oxidation of 2,6-Dimethylphenol in Various Electrolytic Solutions, Journal of The Electrochemical Society. 134 (1987) 3068–3073. doi:10.1149/1.2100341.

[65] K. Yamamoto, H. Nishide, E. Tsuchida, Electro-oxidative polymerization of 2,6-dimethylphenol in the presence of methanol, Die Makromolekulare Chemie, Rapid Communications. 8 (1987) 11–15. doi:10.1002/marc.1987.030080103.

[66] E. Tsuchida, H. Nishide, T. Maekawa, Synthesis of Oligo (Phenyleneoxide) by Electro-Oxidative Polymerization, Journal of Macromolecular Science: Part A - Chemistry. 21 (1984) 1081–1096. doi:10.1080/00222338408056593.

[67] M.T.I.W. Schüsler-Van Hees, G.M.J.B. Van Henegouwen, M.F.J. Driever, Ionization constants of catechols and catecholamines, Pharmaceutisch Weekblad Scientific Edition. 5 (1983) 102–108. doi:10.1007/BF01960985.

[68] S. Hong, Y. Wang, S.Y. Park, H. Lee, Progressive fuzzy cation-π assembly of biological catecholamines, Science Advances. 4 (2018) eaat7457. doi:10.1126/sciadv.aat7457.

[69] Q. Li, Electrochemical sensitive detection of 2, 6-dimethylphenol in petrochemical wastewater based on ferroporphyrin modified glassy carbon electrode, International Journal of Electrochemical Science. 17 (2022) 220739. doi:10.20964/2022.07.43.

[70] S. Campuzano, B. Serra, M. Pedrero, F.J.M. De Villena, J.M. Pingarrón, Amperometric flow-injection determination of phenolic compounds at self-assembled monolayer-based tyrosinase biosensors, Analytica Chimica Acta. 494 (2003) 187–197. doi:10.1016/S0003-2670(03)00919-X.

[71] S.K. Ozoner, E. Erhan, F. Yilmaz, A. Celik, B. Keskinler, Newly synthesized poly(glycidyl methacrylate-co-3-thienylmethylmethacrylate)-based electrode designs for phenol biosensors, Talanta. 81 (2010) 82–87. doi:10.1016/j.talanta.2009.11.040.

[72] M. Abbas, F. Saeed, F.M. Anjum, M. Afzaal, T. Tufail, M.S. Bashir, A. Ishtiaq, S. Hussain, H.A.R. Suleria, Natural polyphenols: An overview, International Journal of Food Properties. 20 (2017) 1689–1699. doi:10.1080/10942912.2016.1220393.

[73] J.J. Dalluge, B.C. Nelson, Determination of tea catechins, Journal of Chromatography A. 881 (2000) 411–424. doi:10.1016/S0021-9673(00)00062-5.

[74] L. Peng, X. Song, X. Shi, J. Li, C. Ye, An improved HPLC method for simultaneous determination of phenolic compounds, purine alkaloids and theanine in Camellia species,

Journal of Food Composition and Analysis. 21 (2008) 559–563. doi:10.1016/j.jfca.2008.05.002.

[75] M. Rusconi, A. Conti, Theobroma cacao L., the Food of the Gods: A scientific approach beyond myths and claims, Pharmacological Research. 61 (2010) 5–13. doi:10.1016/j.phrs.2009.08.008.

[76] L. Pourcel, J.M. Routaboul, V. Cheynier, L. Lepiniec, I. Debeaujon, Flavonoid oxidation in plants: from biochemical properties to physiological functions, Trends in Plant Science. 12 (2007) 29–36. doi:10.1016/j.tplants.2006.11.006.

[77] P. Janeiro, A.M. Oliveira Brett, Catechin electrochemical oxidation mechanisms, Analytica Chimica Acta. 518 (2004) 109–115. doi:10.1016/j.aca.2004.05.038.

[78] S.A.S.S. Gomes, M.J.F. Rebelo, A new laccase biosensor for polyphenols determination, Sensors. 3 (2003) 166–175. doi:10.3390/s30600166.

[79] A. Jarosz-Wilkołazka, T. Ruzgas, L. Gorton, Use of laccase-modified electrode for amperometric detection of plant flavonoids, Enzyme and Microbial Technology. 35 (2004) 238–241. doi:10.1016/j.enzmictec.2004.04.016.

[80] M.A. Rahman, H.B. Noh, Y.B. Shim, Direct electrochemistry of laccase immobilized on Au nanoparticles encapsulated-dendrimer bonded conducting polymer: Application for a catechin sensor, Analytical Chemistry. 80 (2008) 8020–8027. doi:10.1021/ac801033s.

[81] S. Singh, D.V.S. Jain, M.L. Singla, One step electrochemical synthesis of gold-nanoparticles-polypyrrole composite for application in catechin electrochemical biosensor, Analytical Methods. 5 (2013) 1024–1032. doi:10.1039/c2ay26201k.

Chapter VII

Development of immunosensing platforms

A part of the content found in this chapter is published in:

- L.C. Almeida, T. Frade, R.D. Correia, Y. Niu, G. Jin, J.P. Correia, A.S. Viana, Electrosynthesis of polydopamine-ethanolamine films for the development of immunosensing interfaces, Scientific Reports. 11 (2021) 1–12, doi:10.1038/s41598-021-81816-1.

7. Development of immunosensing platforms

Immunosensors, based on the affinity reactions between an immobilized antibody and a target antigen, are extremely powerful and sensitive tools for disease control, environmental screening, and food quality monitoring [1]. There are, however, major challenges that must be overcome to achieve an efficient transduction interface in biosensors. These include a proper linkage of the biorecognition element to the surface, biomolecule-compatibility to avoid protein denaturation upon adsorption, and ability to prevent non-specific interactions with interferent proteins, during affinity assays [2]. The latter challenge is crucial for further development of labeled or label-free immunosensors and immunoassays technologies, and it is not deeply investigated when catechol-based surface modification strategies are concerned.

Section 7.1 of this chapter starts by exploring the chemical and electrochemical modification of polydopamine films with ethanolamine (ETA), evaluating possible aways to control the non-specific adsorption in a polycatecholamine-based interfaces. ETA has been used before to react with the active surface groups that remain after other surface modifications with capture anti-bodies (*e.g.* carbodiimide activated COOH groups in SAMs [3,4]), populating the surface with hydroxyl groups which are known to prevent non-specific protein adsorption. As so, a simple incubation of a polydopamine film in ETA solution might provide a simple strategy to block latent reactive sites of its surface. In addition to this strategy, the electrochemical incorporation of ETA during polymer synthesis in potentiodynamic mode is also explored. Spectroscopic and morphological characterization of the new thin films is provided in order to explain their optical performance in the detection of standard human immunoglobulins affinity reaction.

To address the challenge of binding and orientation of immunoglobulin G, surfaces modified with electrosynthesized polynorepinephrine, polyDOPA and polycatechol are also tested in section 7.2, since they provide different chemical environments, morphologies, porosities and hydrophilicities, as carefully discussed in chapter V. These different physicochemical properties of films originate, fundamentally, from the molecular interactions within their polymeric structure, which can be traced down to their different chemical groups. As so, an opportunity to evaluate and discuss the effect of catechol, amine, hydroxyl and carboxyl groups in the adsorption of immunoglobulin G and subsequent specific bonding of anti-immunoglobulin G is given. Section 7.3 presents a complementary way to tune the interactions between protein molecules and the surface, with the prospect of improving the immobilization robustness and molecular orientation, concerning the polarization of the

interface – a complex topic since it requires consideration of all intervenient intermolecular forces, namely, electrostatic, hydrogen bonds and Van der Waals interactions [5,6]. Attempts to generalize adsorption phenomena of proteins under the influence of an applied electrical potential have not been successful [7–9]. Thus, it is a scientifically interesting topic to explore that may offer, not only new insights into the main responsible molecular interactions between proteins and polycatecholamines, but also, introduce versatility in the application of polycatecholamines as immunosensing platforms.

7.1. Polydopamine-ethanolamine films for immunosensing

7.1.1. Electropolymerization of dopamine in the presence of ethanolamine

The incorporation of ethanolamine into polydopamine matrices, as mentioned, is envisaged as a strategy to inhibit the non-specific adsorption that occurs at the adhesive polydopamine surface, upon the immobilization of the biorecognition protein. To achieve such purpose, the electropolymerization of dopamine was performed in the presence of several concentrations of ethanolamine (10, 50 and 100 mM). Polydopamine films were potentiodynamically synthesized using a fast scan rate (200 mV s^{-1}) and a low number of potential cycles (6 cycles) to obtain a thin, uniform and reproducible polymeric layer that is suited for post-modification with proteins and appropriate for electrochemical and optical detection of affinity biosensor recognition events. **Figure 7.1** shows the cyclic voltammograms of dopamine electropolymerization in the absence of ethanolamine, and in the presence of the highest concentration of ethanolamine studied (100 mM), where the effect of this additive can be clearly depicted. As discussed in Chapters IV and V, two redox processes are attributed to quinone/hydroquinone (Q/HQ) species in solution and can be observed during dopamine electropolymerization in the absence of ethanolamine (**Figure 7.1a** and **7.1c**). Redox process I, occurring at $E_{1/2}$ = 0.20 V, corresponds to the oxidation of dopamine to dopaminoquinone, and its respective reduction, as represented in the scheme of **Figure 7.2**. These redox peaks decrease upon cycling which proves the formation of a low conducting polydopamine layer (**Figure 7.1a**). As seen by the first anodic scan, process II is not present at the beginning of the electropolymerization. It is known that only after electrogeneration of dopaminoquinone, this reactive quinone undergoes a chemical step (intramolecular cyclization) originating an indoline bicyclic species, leucodopaminochrome (**Figure 7.2**), that is not present in the initial monomer solution. Due to the electrodonating effect of the nitrogen atom attached to the catechol ring in the position 5, the oxidation of leucodopaminochrome (II_a) and the reduction of its

corresponding redox pair, dopaminochrome (II_c), occur at significantly lower potential values than the process I. These two indoline-type species accumulate in solution during polymerization, which justifies the increase in peak currents II_a and II_c in the first three potential cycles (**Figure 7.1c**). From the third to the last potential cycle, the intensity of process II decreases due to polymer thickening that hinders charge transfer across the film.

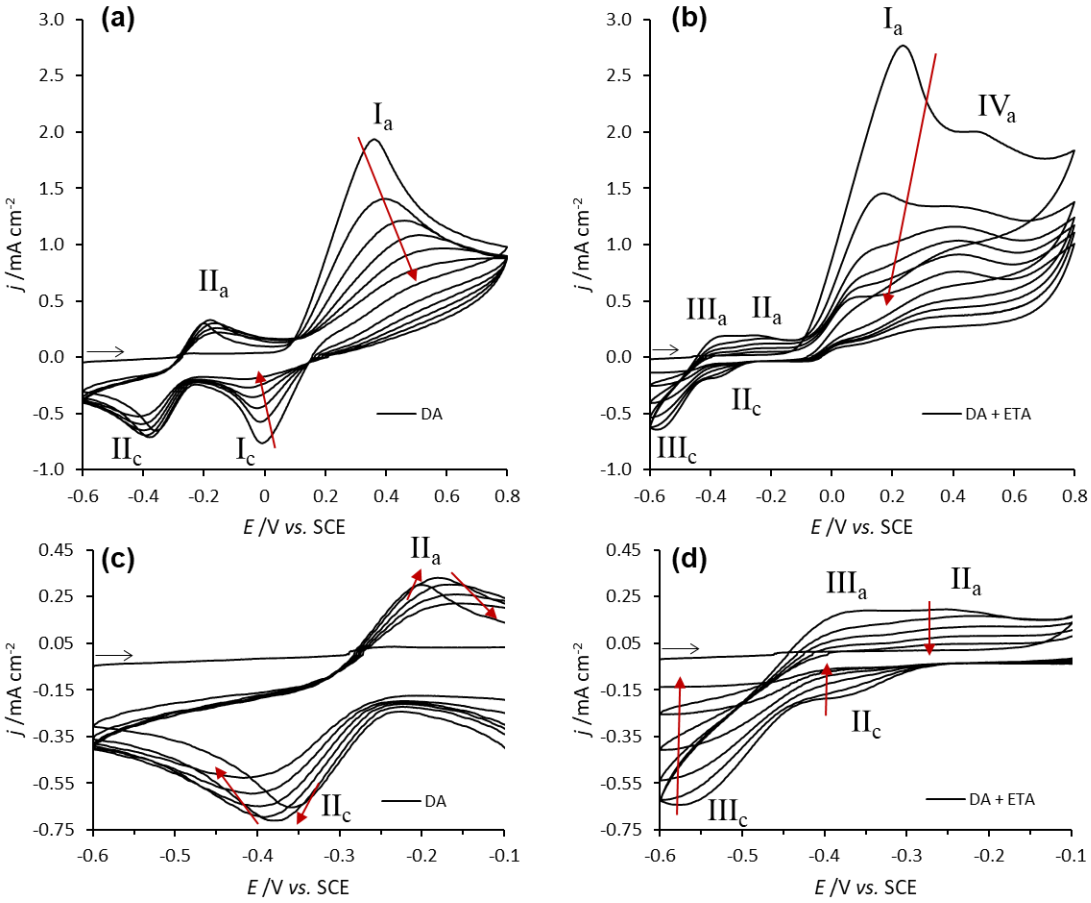

Figure 7.1: Potentiodynamic polymerization of 5 mM dopamine in the absence **(a)** and presence **(b)** of 100 mM ethanolamine, carried out at 200 mV s^{-1} for 6 potential cycles in deoxygenated CPB. Cyclic voltammograms **(c)** and **(d)** are amplifications of **(a)** and **(b)** respectively.

The presence of ethanolamine in the electrolyte solution causes a drastic effect on the original cyclic voltammograms of dopamine electropolymerization, as depicted in **Figure 7.1b** and **2d**. The previously identified Q/HQ redox processes I and II are shifted towards lower potential values due to the increase of pH, caused by the basic behavior of ethanolamine in solution (pH =10.2). In the presence of this compound, process I_a occurs at E_{pa} = 0.23 V (1st potential cycle), whereas process II occurs at $E_{1/2}$ = -0.29 V. In fact, an identical shift is observed when dopamine is electropolymerized in alkaline media (**Figure A6**, Annex), where redox process I occurs at $E_{1/2}$ = 0.23 V and process II at $E_{1/2}$ = -0.33 V. Besides the potential shifts in

the Q/HQ conversions, the process I became completely irreversible in the presence of ethanolamine (**Figure 7.1b**), which indicates a very fast consumption of the electrogenerated dopaminoquinone into aminocatecholic species (N-substituted catecholic species). This is expected in alkaline medium since the deprotonation of amines and their subsequent nucleophilic attack to the quinone molecules is more favorable compared to the neutral medium [10,11]. This is true for the nucleophilic reaction of ethanolamine to the catechol ring, as well as to the intramolecular cyclization of dopamine. The nucleophilic attack of ethanolamine may occur through Michael addition (position 5 of catechol ring) or Schiff-base reaction to the carbonyl groups (position 1 or 2) [12]. In the latter case, an iminoquinone is formed and its redox potential is expected to be overlapped with Process I [13], therefore difficult to distinguish by cyclic voltammetry. In contrast, the redox processes of aminocatecholic species during electropolymerization are ascribed to processes II and III (**Figure 7.2**). Redox process II occurring at $E_{1/2}$ = -0.33 V, is attributed to monoaminocatechols, namely, the indoline-type species originated from intramolecular cyclization of dopamine and also to the hydroxyethylamino-dopamine species, arising from ethanolamine nucleophilic attack at the position 5 of the catechol ring [14]. Redox process III, occurring at $E_{1/2}$ = -0.47 V, is assigned to Q/HQ species that must have been further attacked by ethanolamine in the available positions of the quinone ring, which justifies the low redox potential value. **Figure 7.2** shows possible structures of diaminocatechols, namely, the adduct of DAC with ethanolamine and the adduct of dopamine with two ethanolamine molecules. In fact, the new redox process III is not observed when dopamine is electropolymerized in alkaline medium in the absence of ethanolamine (**Figure A6**, Annex). Only when using a high concentration of ethanolamine (100 mM), multiple attacks to the quinone rings should become more frequent and thus observable during electrochemical growth. The formation of aminophenolic adducts reflects an effective covalent bond between ethanolamine and the monomeric species that contribute to the building of the hybrid polymer. Besides, an irreversible oxidation process, at *ca.* 0.5 V (IV_a), is depicted during the electropolymerization process only in the presence of ethanolamine (**Figure 7.1b**). A control assay was performed only in the presence of 100 mM ethanolamine (in the absence of dopamine) (**Figure A7**, Annex), confirming the presence of process IV_a. This was assigned to the irreversible oxidation of ethanolamine to its radical cation [15,16]. Due to its reactive nature, it is expected that this radical may participate in the formation of hybrid oligomers of dopamine and ethanolamine, resulting in new ePDA-ETA polymers. Therefore, these polymers should contain additional alkyl hydroxyl groups with anti-fouling properties, required to avoid the non-specific adsorption of interferent proteins.

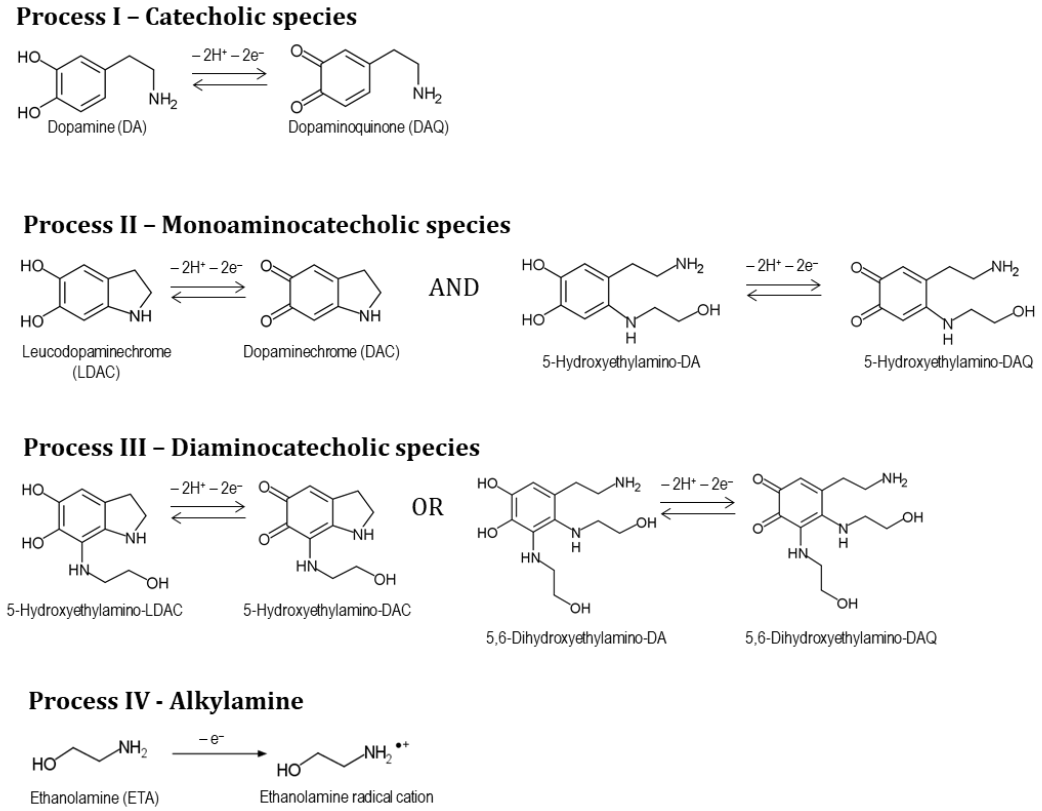

Figure 7.2: Electrochemical processes of catecholic (I), monoaminocatecholic (II), diaminocatecholic (III), and alkylamine (IV) species possibly occurring in the electropolymerization of dopamine in the presence of ethanolamine.

The formation of electroactive polymers on the surface of the gold was confirmed by cyclic voltammetry, performed in monomer-free electrolyte solution (**Figure 7.3a**). The pristine ePDA film cyclic voltammogram displays a well-defined redox process at $E_{1/2}$ = 0.14 V attributed to Q/HQ conversions of the polymeric chains of dopamine, as extensively discussed in Chapters IV and V. However, as mentioned above this process may also account for iminoquinones/aminophenols redox conversion, as a result of Schiff base reactions [13]. This main redox process is found to be greatly affected when ethanolamine is added to the electrosynthesis solution (one-step, ePDA-ETA) or when the electrosynthesized polymer is incubated in an ethanolamine solution (two-step, ePDA/ETA), as it can be depicted by the current decrease of such process in both cyclic voltammograms of ePDA-ETA and ePDA/ETA (**Figure 7.3a**). A lower electroactivity of the ethanolamine modified polymers strongly suggests that the nucleophilic attack of ethanolamine to the polydopamine affects the Q/HQ redox process.

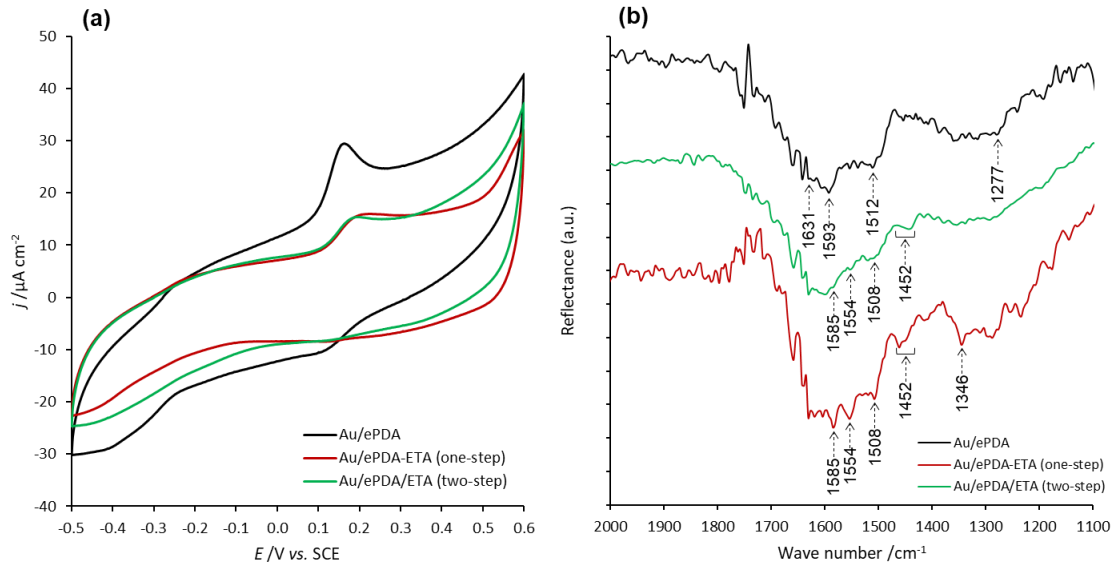

Figure 7.3: Cyclic voltammograms **(a)** and FTIR spectra **(b)** of gold electrodes modified with polydopamine (Au/ePDA), poly(dopamine-ethanolamine) (Au/ePDA-ETA) and polydopamine film after incubation in ethanolamine solution (Au/ePDA/ETA), recorded at 50 mV s^{-1} in CPB pH = 7.0.

Pristine and ethanolamine-modified films were characterized by FTIR (**Figure 7.3b**), confirming the incorporation of ethanolamine in ePDA using either a one-step or a post-modification approach. ePDA spectra displays bands at 1631, 1593, 1512 and 1277 cm^{-1}, as already discussed for a thicker film presented in **Figure 4.7** of Chapter IV. The two most intense peaks, at 1631 and 1593 cm^{-1}, correspond to aromatic asymmetric C=C stretching modes of the dihydroxyphenol ring, while less intense aromatic symmetric C=C stretching (1512 cm^{-1}) and phenolic C-OH stretching (1277 cm^{-1}) modes can also be depicted. The band at 1593 cm^{-1} may also have the contribution of NH_2 scissoring mode [17]. After incubation of ePDA film with ethanolamine, new features appear in the ePDA/ETA spectra suggesting the presence of a small amount of ethanolamine on the polymer film. The modification is more evident when a one-step electrochemical approach is used, indicating the incorporation of a larger amount of ethanolamine during electropolymerization, that leads to better-defined peaks at frequencies typical of ethanolamine. The three characteristic IR peaks reported for free [18,19] and surface-adsorbed [20,21] ethanolamine, can be identified in both ethanolamine-modified films spectra (**Figure 7.3b**), namely, the coupled deformation modes of NH_2 with CNH (1585 cm^{-1}), CH_2 with NCH (1442-1462 cm^{-1}) and OCH with CCH (1340-1346 cm^{-1}). Moreover, the peaks appearing at 1554 and 1508 cm^{-1} indicate the presence of *p*-quinoid and *p*-benzenoid rings, respectively, similar to those reported for polyaniline [22], poly(N-ethylaniline) [23] and

poly(*o*-aminophenol) [24], which corroborates the covalent linkage of ethanolamine to the dihydroxyphenol rings of the pristine ePDA.

X-ray photoelectron spectroscopy (XPS) analysis was carried out on ePDA and ePDA-ETA films aiming at characterizing the bonds established during the one-step modification and to further confirm the presence of ethanolamine in ePDA polymer. The atomic ratios N/C: 0.11 (ePDA) and 0.13 (ePDA-ETA), and O/C: 0.28 (ePDA) and 0.26 (ePDA-ETA), are identical for both films, and are in agreement within the expected values for polydopamine films [25,26], since N/C and O/C atomic ratios for dopamine are 0.125 and 0.250, respectively. The main differences between the two polymers arise from C1s spectral region shown in **Figure 7.4** (N 1s and O 1s spectral regions are provided on Annex, **Figure A8**). The C 1s spectra have been fitted into four main components attributed to C-C, C-H_x (284.9 eV), C-O, C-N (286.3 eV), C=O, C=N (287.9 eV) and $\pi \rightarrow \pi^*$ (291.4 eV) [26,27]. It is possible to observe a significant increase of the C-O, C-N component in ePDA-ETA spectrum (**Figure 7.4b**) relatively to pristine ePDA spectrum (**Figure 7.4a**). The (C-O, C-N)/(C-C, C-H_x) ratios for ePDA-ETA and ePDA are 0.85 and 0.67, respectively, accounting for a higher number of C-N and C-OH bonds, arising from the successful attachment of aliphatic ethanolamine molecules.

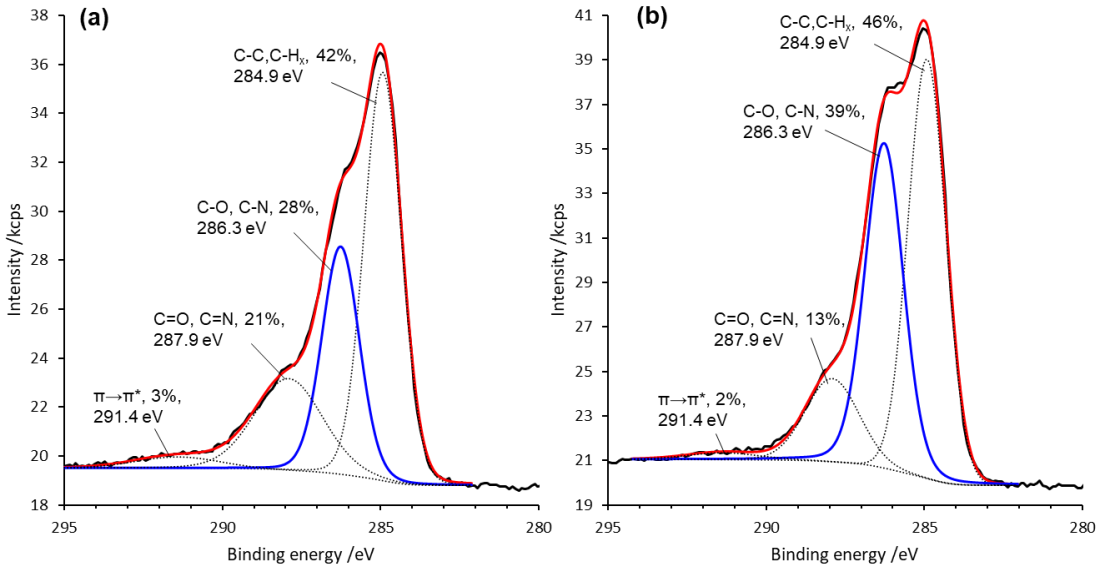

Figure 7.4: XPS spectra of C 1s region of pristine polydopamine (ePDA) **(a)** and one-step modified polydopamine (ePDA-ETA) **(b)**.

7.1.2. IgG adsorption on ePDA and ethanolamine-modified films

The polymers were incubated in IgG solution and analyzed by ellipsometry (**Figure 7.5**) and AFM (**Figure 7.6**), to evaluate the optical thickness increase and morphological changes occurring at the ePDA interface upon the adsorption of this protein.

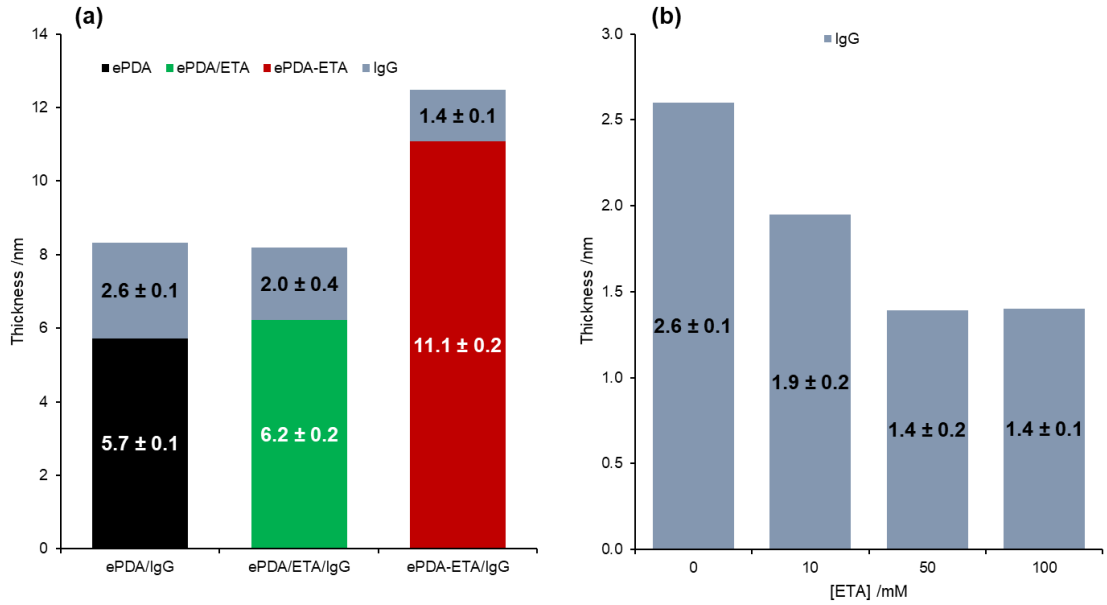

Figure 7.5: Optical thicknesses of pristine polydopamine (ePDA), two-step modified polydopamine (ePDA/ETA) and one-step modified polydopamine (ePDA-ETA), before and after IgG incubation on the several polymers **(a)**; Effect of ethanolamine concentration during ePDA-ETA electrosynthesis on the IgG layer thickness **(b)**; Ellipsometry is performed *ex situ* at an incident angle of 70°.

The estimated thickness for ePDA film, *ca.* 5.7 nm (**Figure 7.5a**), confirms the formation of a thin polymeric coating on gold, in agreement with order of magnitude already estimated using glassy carbon (*cf.* **Table 4.1**) and gold electrodes (*cf.* **Table 5.1**). The AFM morphological image of ePDA (**Figure 7.6a**) shows a granular and uniform polymer with a slightly higher root-mean-square roughness (R_q) than that of bare gold (R_q = 0.5 nm [28]). After incubation with ethanolamine, there is a very small, yet consistent, thickness increase relative to the ePDA layer (**Figure 7.5a**), which corroborates the modification of the polymer surface with this molecule using the two-step strategy (ePDA/ETA). As suggested by FTIR data, only a small amount of ethanolamine is foreseen to be present at ePDA/ETA modified film, and indeed the roughness of this interface is very similar to the ePDA film before modification (**Figure 7.6**). Even so, it is possible to observe a less uniform surface of ePDA/ETA (**Figure 7.6b**), when compared to ePDA film topography (**Figure 7.6a**). The electrochemically synthesized film by the one-step strategy (ePDA-ETA) is considerably thicker (11.1 nm, **Figure 7.5a**) in

comparison with ePDA, due to the faster electropolymerization growth in a more alkaline media provided by ethanolamine, as discussed above. Consequently, ePDA-ETA (**Figure 7.6c**) is considerably rougher than ePDA or ePDA/ETA.

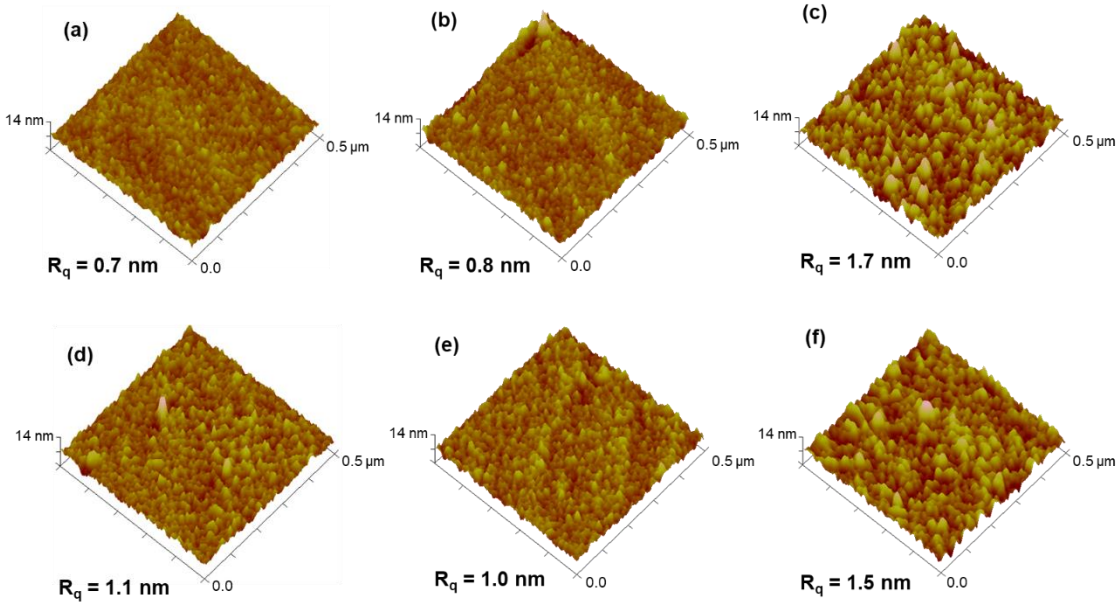

Figure 7.6: AFM 3D images of modified gold with ePDA **(a)**, ePDA/ETA **(b)**, ePDA-ETA **(c)**, ePDA/IgG **(d)**, ePDA/ETA/IgG **(e)** and ePDA-ETA/IgG **(f)**.

Polydopamine films were incubated in IgG solution and thoroughly washed to remove the protein molecules that did not robustly attach at pristine and ethanolamine-modified polymeric surfaces. It is expected that IgG molecules, which contain amine groups, may also establish covalent bonds with oxidized catechol moieties in the polymer, similarly to ethanolamine. Due to the complexity and richness of protein surface functionalities, it is also conceivable that intermolecular interactions may also contribute to the robust protein immobilization [29]. One can depict a small increase in the number of large features on ePDA/IgG (**Figure 7.6d**) and ePDA/ETA/IgG (**Figure 7.6e**), when compared to the same surfaces before IgG incubation, with a consequence increase in roughness. These small changes reflect the presence of well-distributed IgG over polymers following the granular film morphology. The similarity between the size of polymer grains and proteins, imaged by AFM, precludes the clear visualization of individual protein molecules. Nevertheless, the increase in thickness upon IgG incubation on ePDA and ePDA/ETA, retrieved by ellipsometry (**Figure 7.5a**), confirms the great ability of the film to immobilize proteins, without the need of any chemical activation step. The thickness variation is higher for ePDA/IgG (2.6 nm) than for ePDA/ETA/IgG (2.0 nm) interface, proving that the two-step strategy diminishes the number of available binding sites for IgG, still allowing a significant protein coverage that is required

for the following biorecognition event. We have also observed that ePDA films incubated in 5 or 100 mM ethanolamine solutions (**Figure A9**, Annex) yield very similar protein thicknesses. Thus, the lowest ethanolamine concentration was used for the biorecognition reactions using the two-step ePDA/ETA interfaces.

In the case of the ePDA-ETA interface, the surface morphology was kept after IgG adsorption, with a slight decrease of R_q values (**Figure 7.6f**). In fact, the increase in thickness for the protein layer on ePDA-ETA is only 1.4 nm, which is inferior than the previous polymer/IgG interfaces. This lower IgG coverage indicates that the amount of incorporated ethanolamine, using the one-step strategy, is more effective in reducing the number of sites for IgG adsorption in the polymer surface, certainly providing a better distribution and more spaced molecules at the biorecognition interface [30]. Besides, as shown in **Figure 7.5b**, the concentration of ethanolamine was changed from 10 to 100 mM during the potentiodynamic polymerization of dopamine, clearly affecting the inhibition of protein adsorption on ePDA/ETA films. These observations demonstrate the suitability of the one-step electrochemical process for polymer functionalization, that promotes the nucleophilic attack of ethanolamine molecules to the generated quinones during the potential application.

7.1.3. Evaluation of the immunosensing performance

After evaluating the effect of ethanolamine on the interaction of proteins with the surface of the modified polydopamine films, these interfaces were tested in real-time SPR assays to access their performance as immunosensors (**Figure 7.7**). As shown previously by the *ex situ* ellipsometric results (**Figure 7.5a**), the pristine polydopamine layer is able to capture IgG and preserve a stable bond even after extensive rinsing with buffer. This is also clear in the SPR curves (**Figure 7.7**), since the decrease of optical signal is minimal after rising the surface that is exposed to IgG. This is crucial to ensure the lowest leaking of the capture antibody during the following steps of modification or detection. After interacting with Anti-IgG, the ePDA/IgG interface yields an Anti-IgG/IgG ratio of 1.6 (**Figure 7.7b**), most probably due to the contribution of specific and non-specific protein interactions, the latter arising from the adhesive properties of the polydopamine films. Hence, upon the immobilization of IgG there might be still some polymer binding sites that can interact with Anti-IgG, accounting for a number of protein non-specific linkages. The *ex situ* ellipsometric measurements, presented in **Figure 7.8**, indicate that for the pristine ePDA film, the Anti-IgG layer is *ca.* 1.5 times thicker than the IgG layer, corroborating the real-time SPR data.

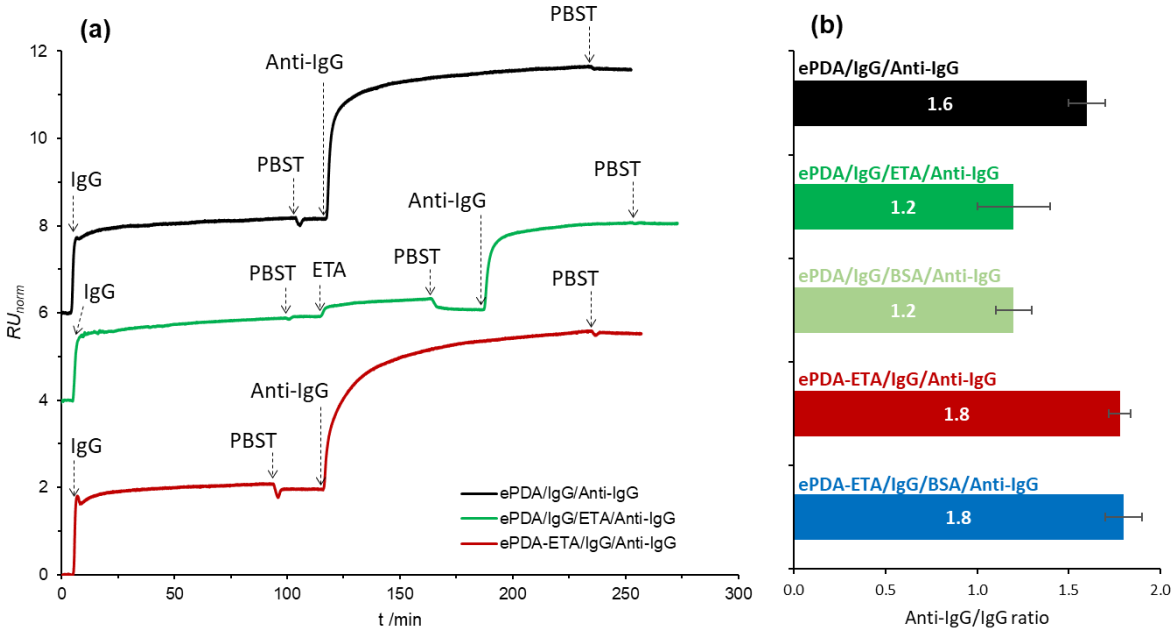

Figure 7.7: Representative real-time SPR curves showing the IgG and Anti-IgG interaction on gold surfaces modified with ePDA, in the absence and presence of a blocking step using either ETA or BSA; and with ePDA-ETA film, in the absence and presence of a blocking step using BSA **(a)**; Anti-IgG/IgG ratios obtained from three independent SPR assays **(b)**. The normalized response units were calculated by the following equation: $RU_{norm} = RU/(RU_{PBS}–RU_{water})$.

When a blocking step with ethanolamine is used, after IgG immobilization on ePDA (**Figure 7.7a**, middle curve), there is no visible removal of IgG. Indeed, as expected for a small molecule, the SPR signal does not change significantly after the introduction of ethanolamine, as it is also corroborated by the estimated optical thicknesses for IgG and IgG/ETA layers, 2.6 and 2.9 nm, respectively (**Figure 7.8**). The blocking of the polymer binding sites with ethanolamine can be inferred by the much lower variation of the optical signal caused by the capture of Anti-IgG, which causes a decrease of Anti-IgG/IgG ratio from 1.6 to 1.2 (**Figure 7.7**). Thus, the Anti-IgG that is captured in this case must be specifically bonded to IgG. To confirm this result, a common blocking agent, BSA [31], was also used to block the polymer binding sites that remain after IgG incubation. The same low ratio of 1.2 is observed (**Figure 7.7b**), proving that ethanolamine can effectively replace protein-based blocking buffers.

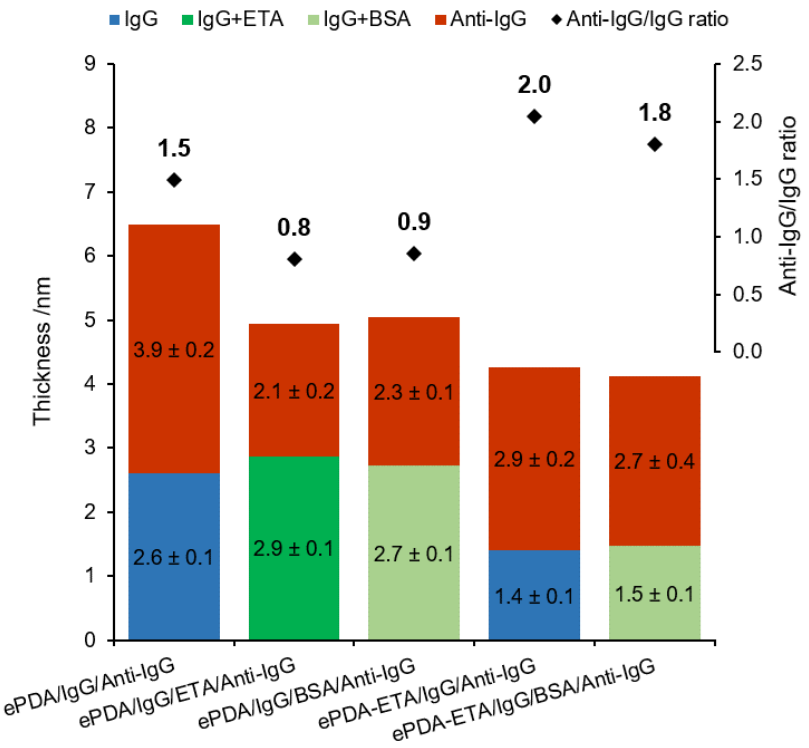

Figure 7.8: Optical thicknesses of IgG and Anti-IgG interaction on gold surfaces modified with ePDA, in the absence and presence of a blocking step using either ETA and BSA; and with ePDA-ETA film, in the absence and presence of a blocking step using BSA. Anti-IgG/IgG ratios, obtained from three independent ellipsometric assays, are also presented. Ellipsometry is performed *ex situ* at an incident angle of 70°.

The performance of the one-step synthetized ePDA-ETA film was also investigated as a biosensor interface, displaying an Anti-IgG/IgG ratio of 1.8 (**Figure 7.7b**), which is considerably higher than the ratio obtained when using a pristine ePDA film in the absence or presence of a blocking step. This is a great improvement revealing that the incorporation of ethanolamine during the electrosynthesis improves the IgG spacing, allowing a better accommodation of the bonded Anti-IgG. Ellipsometric data agrees with this result, showing an Anti-IgG layer two times thicker than the IgG layer (**Figure 7.8**). More importantly, this interaction is specific since the introduction of a blocking step with BSA did not affect (within the experimental error) the Anti-IgG/IgG ratio (**Figure 7.7b** and **7.8**). The electrosynthesis of a polydopamine film in the presence of a simple blocking agent is then an efficient strategy to be used in the reproducible preparation of ready-to-use platforms as immunosensing interfaces.

7.2. Polycatecholamines as platforms for optical immunosensing

The use of other bio-inspired polycatecholamines in the preparation of immunosensing platforms, besides the most studied polydopamine, is also an envisaged task of this doctoral work. Before starting with a comparative study between the different polymers, there is the need to establish a working polymer thickness. SPR gold slides were then modified with potentiodynamically synthesized polydopamine using 6 or 20 potential cycles, yielding thicknesses of 4.2 and 11.9 nm, respectively, as measured by *ex situ* ellipsometry (**Table 7.1**). The two gold/polydopamine interfaces were then submitted to IgG/Anti-IgG optical assays, as shown in **Figure 7.9**, allowing the evaluation of the thickness effect on the sensing performance.

Table 7.1: Refractive index (*n*), extinction coefficient (*k*) and thickness (*L*), of polydopamine (ePDA), polynorepinephrine (ePNE), polyDOPA (ePDOPA) and polycatechol (ePCA) films grown on gold SPR slides under 200 mV s^{-1} for different number of potential cycles. Multiangle ellipsometry is carried out *ex situ* at incident angles 60° 65°, and 70°.

Film	***n***	***k***	***L* /nm**
ePDA(6 c)	1.78 ± 0.09	0.02 ± 0.03	4.2 ± 0.3
ePDA(20 c)	1.69 ± 0.01	0.04 ± 0.02	11.9 ± 0.5
ePNE(20 c)	1.62 ± 0.07	0.07 ± 0.007	12.2 ± 0.8
ePDOPA(70 c)	1.90 ± 0.04	0.04 ± 0.02	11.5 ± 0.4
ePCA(50 c)	1.74 ± 0.02	0.000 + 0.008	12.0 ± 0.2

As clearly depicted in **Figure 7.9a** and **7.9b**, the normalized optical response of the thicker polymer is enhanced regarding the thinner film, especially during the detection of Anti-IgG. As mentioned before, the IgG/Anti-IgG specific interaction ratio using the thin polydopamine film is 1.2 (*cf.* **Figure 7.7b**), contrasting with the ratio obtained using a thicker polydopamine film: 2.0. Since the amount of adsorbed IgG in the two polymers is identical, it is reasonable to assume that IgG is better oriented on the thicker polymer, allowing the interaction with a higher number of Anti-IgG molecules. This result suggests that the IgG orientation is extremely sensitive to slight changes in the morphology or surface chemistry of identical materials. It is worth noting that the so obtained detection ratio is in the same order of magnitude as the ratio obtained when using the one-step synthetized ePDA-ETA film (1.8, *cf.* **Figure 7.7b**), which validates the use of both interfaces in designing efficient immunosensing platforms. The selection of one interface over the other will depend on the desired promptness and sensitivity of the analysis.

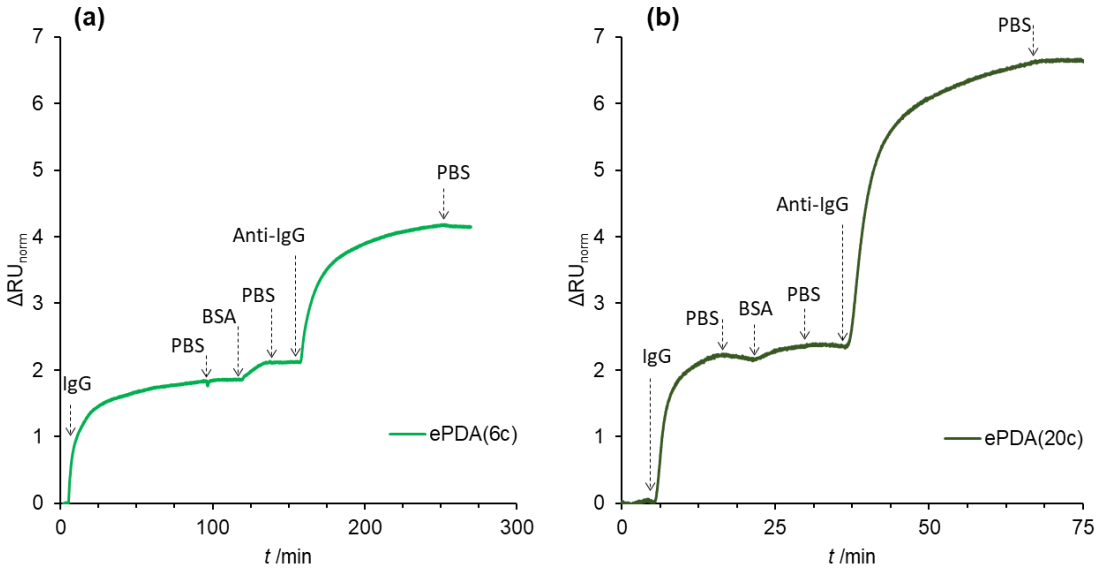

Figure 7.9: Real-time SPR curve showing IgG, BSA and Anti-IgG interactions on a gold surface modified with potentiodynamically synthesized ePDA for 6 cycles **(a)** or for 20 cycles **(b)**, at a flow rate of 25 µL min^{-1}; The normalized response units were calculated by the following equation: $\Delta RU_{norm} = \Delta RU/(RU_{PBS}–RU_{water})$.

After observing the good performance of polydopamine with a thickness close to 12 nm, the number of potential cycles in the potentiodynamic synthesis of polynorepinephrine, polyDOPA and polycatechol was adjusted in order to achieve an identical thickness and to carried out a comparative study between the different polymers. As seen in the *ex situ* ellipsometric results of **Table 7.1**, the potentiodynamic synthesis offers great control in the film thicknesses, allowing to prepare different polycatecholamines that differ less than 1 nm. Polynorepinephrine is prepared with the same number of potential cycles as polydopamine (20 cycles), polyDOPA is prepared with the highest number of potential cycles due to its slow thickening (70 cycles); and polycatechol required an intermediate number (50 cycles). The real-time sensorgrams of the SPR assays associated with polynorepinephrine, polyDOPA and polycatechol are presented in **Figures 7.10a–c**. Identically to polydopamine, all other polymers displayed high optical responses to the flow of IgG (> 2 RU_{norm}) and Anti-IgG (> 4 RU_{norm}), demonstrating the adequate affinity of polycatecholamines for immunologic assays. Furthermore, the absence, or very low decrease, of optical signal during the PBS washing steps, reveals very robust protein-polymer interactions. In the case of polyDOPA and polycatechol assays, a small unexpected increase of optical signal is observed during the washing step after Anti-IgG interaction (**Figures 7.10b** and **7.10c**). Commonly, this increase in the refractive index next to the surface is commonly associated to the adsorption of protein or to the exchange for a

solution with higher refractive index. A contamination of the PBS solution is a possible explanation for this unexpected behaviour.

The optical responses of the different polymers to IgG interaction reveal that the amount of adsorbed IgG is much lower on polycatecholamines compared to polycatechol (**Figure 7.10d**). Considering the extensive physicochemical characterization of these type of polymers presented in Chapter V, the main property that can be successfully correlated with the amount of adsorbed IgG is the chemical composition of the polymers, since no correlation is found with respect to polymers charge, porosity, wettability or roughness. Thus, the results suggest that the presence of amine groups in the surface of polycatecholamines lowers the amount of adsorbed IgG compared to the polycatechol surface. Nonetheless, the IgG adsorbed on polycatecholamines should be better distributed and/or better oriented allowing a more efficient detection of Anti-IgG compared to polycatechol interface. As a result, Anti-IgG/IgG ratios for ePDA, ePNE and ePDOPA are higher (2.0, 2.1, 1.4, respectively) than the ratio obtained with ePCA (1.1). Although the affinities of IgG towards ePDOPA surface and the other two polycatecholamines are similar (**Figure 7.10d**), a more disorganized capture layer is expected in the first case, as suggested by its lower Anti-IgG/IgG ratio of 1.4, which may be caused by the presence of carboxyl groups in ePDOPA. In what concerns the sensitivity during Anti-IgG detection, ePNE displayed the best performance (5.7 RU), followed by ePCA (5.1 RU), although the IgG layers of the two cases should exhibit distinct protein packing and orientation. Both polymers are very promising to construct very sensitive immunosensors with low limits of detection.

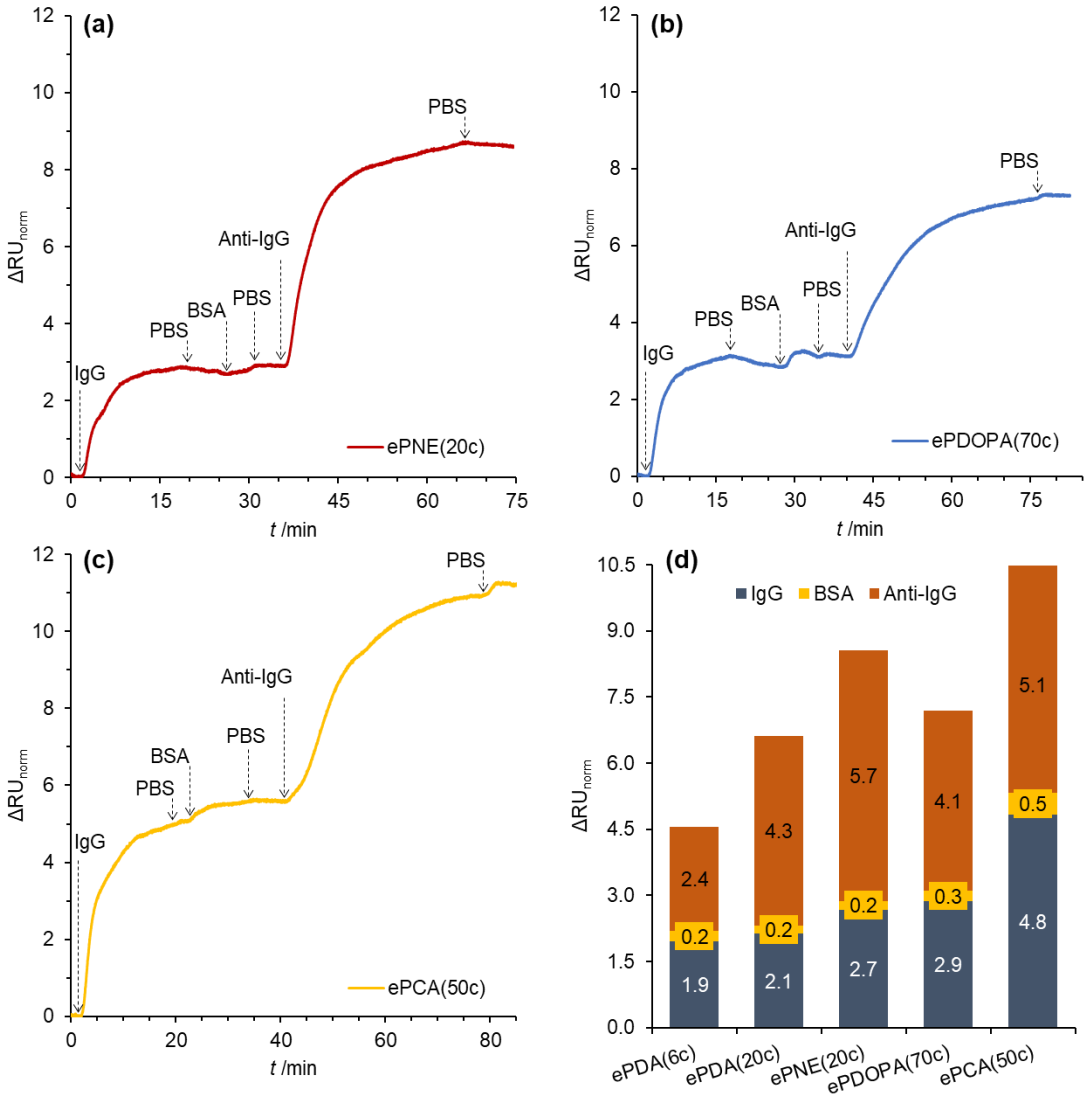

Figure 7.10: (a) Real-time SPR curve showing IgG, BSA and Anti-IgG interactions on a gold surface modified with potentiodynamically synthesized ePNE for 20 cycles **(a)**, ePDOPA for 70 cycles **(b)**, and ePCA for 50 cycles **(c)**, at a flow rate of 25 μL min^{-1}; **(d)** Variation of normalized response units ($\Delta RU_{norm} = \Delta RU/(RU_{PBS}–RU_{water})$) of gold modified surfaces with ePDA (6 and 20 cycles), ePNE (20 cycles), ePDOPA (70 cycles) and ePCA (50 cycles) upon interaction with IgG, BSA and Anti-IgG (0.1 mg mL^{-1}).

To further compare the performance polycatechol against a polycatecholamine, lower concentrations of Anti-IgG were also used, as presented in **Figure 7.11**. Although the use of polycatechol resulted in the lowest Anti-IgG/IgG ratio, the great amount of adsorbed IgG at polycatechol surface allowed a much more intense response towards low concentrations of Anti-IgG compared to polydopamine (**Figure 7.11a**). This contrast is clearly evidenced in **Figure 7.11b**, showing that polycatechol signal is 2 to 5 times more intense compared to that of protein recognition on polydopamine films. More assays are necessary to determine the limit

of detection, nonetheless this analytical parameter should be between 1 and 5 μg mL^{-1}, which is in the same order of magnitude as previous studies using self-assembled monolayers [2,32].

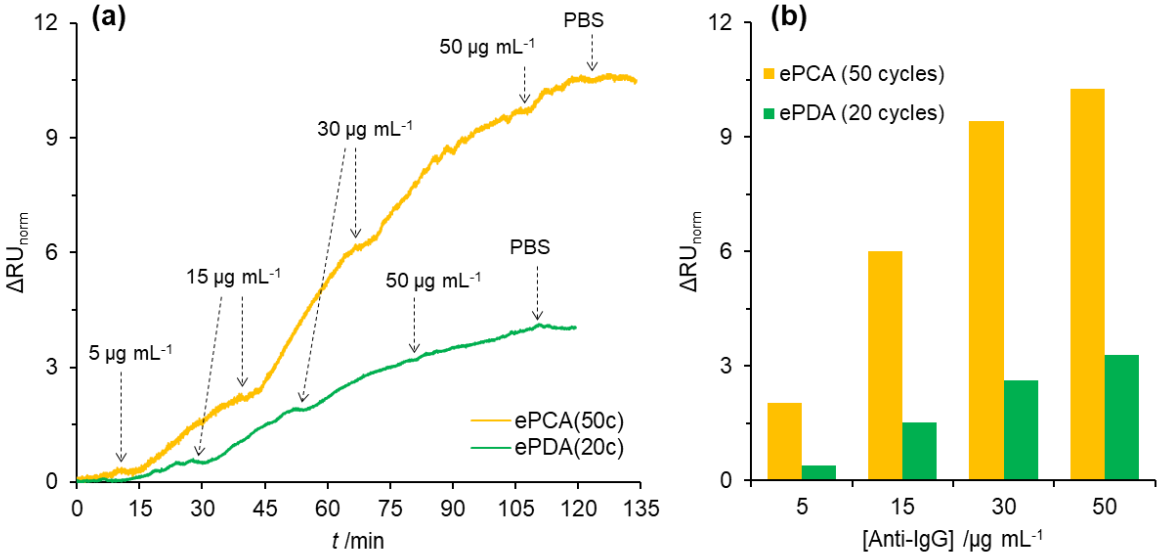

Figure 7.11: (a) Real-time SPR curves showing the Anti-IgG interaction with ePDA(20 cycles)/IgG/BSA and ePCA(50 cycles)/IgG/BSA interfaces at different concentration values (5, 15, 30 and 50 μg mL^{-1}), using a flow rate of 25 μL min^{-1}. **(b)** Variation of normalized response units obtained from (a). The normalization of response units followed the expression: $\Delta RU_{norm} = \Delta RU/(RU_{PBS}–RU_{water})$.

7.3. Effect of electric potential on immunoassays performed at ePDA surface

So far the modulation of the amount and orientation of the immobilized IgG molecules at the surface, as well as, the control of the non-specific adsorption were pursued by chemical and electrochemical alterations of the surface with different polymeric coatings, namely, polydopamine modified with ethanolamine (*cf.* section 7.1) and different electrosynthesized polycatecholamines (*cf.* section 7.2). These successful modification strategies are free of labeled antibodies and orientation proteins, relying on the simple and spontaneous linkage of the capture antibody and blocking components, which greatly outperformed random adsorption. An alternative strategy that can allow the control of antibodies orientation and immobilized amount is the application of an electric potential to the solid-liquid interface during the interaction event with the polymeric coating. To study the effect of potential, several electrochemical SPR assays are performed on gold slides modified with ePDA(20c) applying a constant potential during all the time length of the assay. The selection of −0.15, 0.2 and 0.4 V (*vs.* Ag) as working potential values is based on the redox activity of polydopamine at neutral pH (*cf.* **Figure 7.3a**). The potential difference between the Ag wire and a SCE was measured

to be +34 mV. The lower potential (−0.15 V) reduces the main hydroquinone groups of the polymer; the higher potential (+0.4 V) provides the surface with quinone groups; while the intermediate potential (+0.2 V) should provide a mixture of the two chemical groups.

Figures 7.12a to **7.12c** show SPR sensorgrams of ePDA(20c) during the interaction with IgG, BSA and Anti-IgG at different applied potentials. The normalized optical signal variation corresponding to formation of an IgG capture layer can be easily compared using **Figure 7.12d** (dark blue bars). Comparative to the OCP condition (2.1 units), the amount of IgG increases significantly (+19%) when a lower potential is used (−0.15 V), whereas the higher potentials values of 0.2 V (−5%) and 0.4 V(+5%) did not seem to enhance the adsorbed amount. Although exhaustive studies of IgG adsorption under the influence of potential are not found in the current literature, S. E. Moulton [33] and T. E. Benavidez [9] do report enhancements of IgG adsorption amount under 0.7 V (+72%) and 0.8 V (+48%) on unmodified gold and transparent carbon surfaces, respectively, both against Ag/AgCl reference electrode. In the reported cases, the great enhancement in the adsorbed amount is indicative of the formation of a multilayer or a very dense layer of horizontally adsorbed molecules, which does not correspond to the results presented in this work. Hereby, the used lower overpotentials regarding OCP leads to smaller variations in bonded IgG in respect to Moulton and Benavidez works, indicating the formation of monolayer or submonolayers that are suitable for immunosensing. Therefore, the main driving force of IgG adsorption phenomena at the applied potential values seems to be the interactions with the ePDA chemical groups (either electrostatic, hydrogen bonds, Van der Waals, or covalent), identically to OCP, while the charging of the double layer interface is responsible for slight changes in availability of the interacting chemical groups towards IgG. At −0.15 V, the overall interaction forces between ePDA and IgG molecules had to increase in order to explain the observed increase in optical signal regarding OCP. Hydrogen bonds from the hydroquinone groups and Van der Waals interactions should be the promoting IgG adsorption, since covalent and electrostatic interactions are not expected to increase at this low potential. One most consider that at the neutral working pH, IgG net charge is neutral to slightly negative (p*I* from 5.8 to 7.0) [9,34] and the negative charge of the surface increases at lower potential values, thus repulsion is the foreseen effect. Clearly, this is an oversimplified rational that contradicts the experiment of **Figure 7.12**. As already stated in a protein adsorption study using ITO as sorbent surface [8], although electrostatic interactions may be important, the hydrogen bonds and Van der Waals interactions may be equally or more important to explain the adsorption phenomena at polarized interfaces.

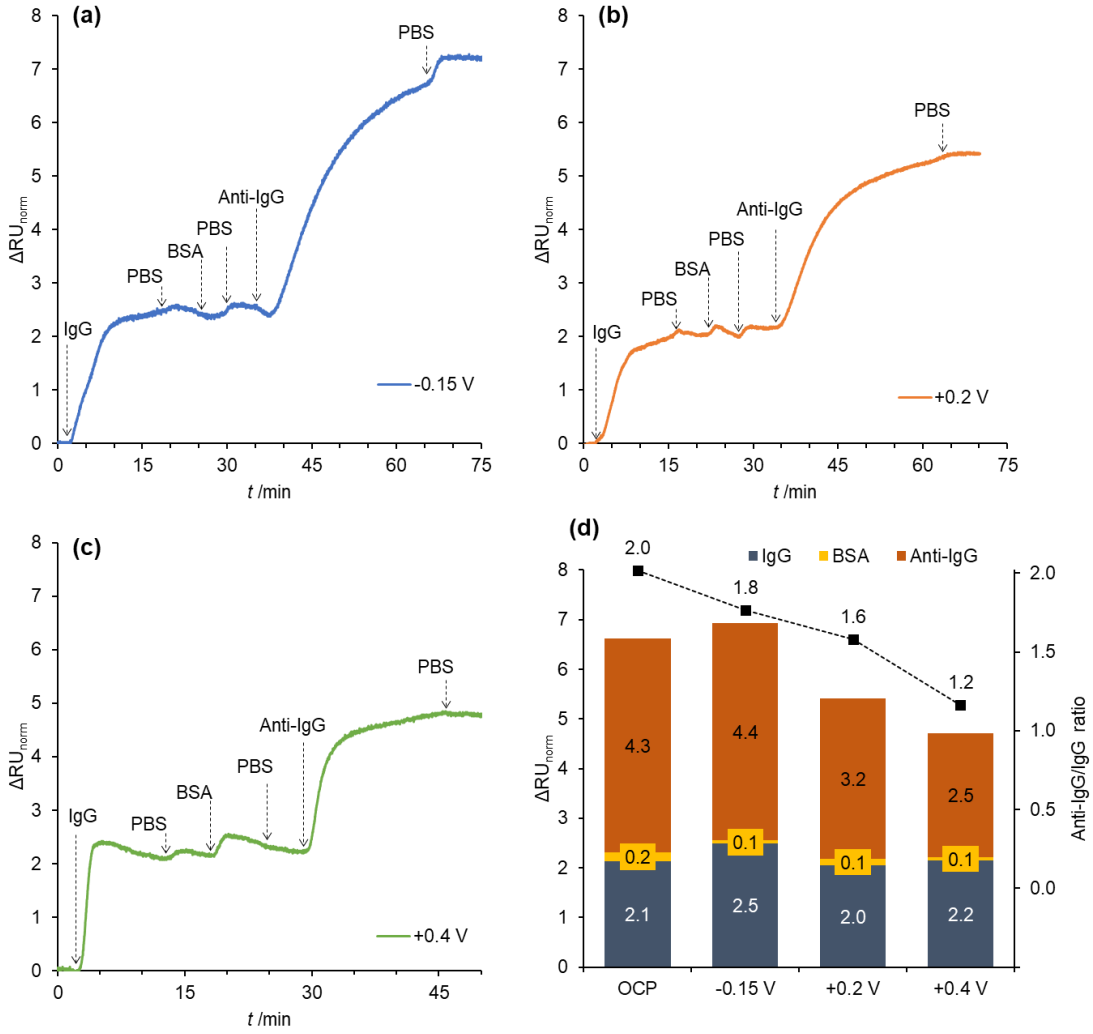

Figure 7.12: Real-time SPR curve showing IgG, BSA and Anti-IgG interactions on a gold surface modified with potentiodynamically synthesized ePDA for 20 cycles at an applied potential of -0.15 V **(a)**, 0.2 V **(b)** and 0.4 V **(c)** *versus* Ag, at a flow rate of 25 μL min^{-1}; **(d)** Variation of normalized response units ($\Delta RU_{norm} = \Delta RU/(RU_{PBS}–RU_{water})$) of gold modified surfaces with ePDA (20 cycles) at OCP and at the potentials of figures (a),(b), and (c). Anti-IgG/IgG ratios are also presented.

Comparative to −0.15 V, at 0.2 and 0.4 V, as hydroquinones are converted to quinones, hydrogen bonds should decrease in number, but covalent bonds are more probable through the reactive quinone groups, while the effect of Van der Waals is difficult to predict. At the same time, the more positive potential could favor the electrostatic attraction of the slight negatively charged IgG molecules. Albeit there are multiple possible changes in the number and strength of the polymer-protein interactions, the overall effect do not contribute to the increase of the adsorbed amount regarding OCP conditions. Independently of the applied potential it is also important to state that the IgG is robustly bonded to the ePDA surface, as indicated by the very small or absent decreases in optical signal during washing steps (*cf.* **Figures 7.9b** and **7.12**).

Regarding the formation of the detection layer of Anti-IgG, there is a much clearer influence of the applied potential (**Figure 7.12**). The highest potential value tested (0.4 V) lead to the lowest amount of bonded Anti-IgG (2.5 units), 0.2 V lead to the an intermediate amount (3.2 units), and the lowest potential value (−0.15 V) lead to a high amount of bonded Anti-IgG of 4.4 units. Trivially, the Anti-IgG to IgG ratio follows the same trend (**Figure 7.12d**). One possible explanation to rationalize the observed effect of potential is that a lower potential value promotes the correct orientation of IgG binding sites towards the solution, which lead to a sensitive detection of Anti-IgG, while higher potentials promote an incorrect orientation or deformation of IgG. This hypothesis is not in line with the work of P. Ghisellini [35] that claims exactly the opposite: lower potential values cause deformation of vertically oriented IgG molecules, while higher potentials promote the right orientation of binding sites, which in turn greatly affect the amount of bonded antigen. P. Ghisellini used a gold surface modified with the well-known protein A (from *Staphylococcus aureus*), rendering a completely different surface chemistry of the ePDA film used hereby. Thus, the hypothesis that the potential modulation influences ePDA interactions with IgG molecules still holds. Although operating the immunosensing interface at −0.15 V did not improve its sensitivity regarding the OCP condition, the potential modulation offers a new way to partially control the interaction with an antigen.

7.4. Conclusions

The electrochemical coating of gold surfaces with bio-inspired polymers is a fast, versatile and reproducible strategy for the construction of high-performance immunosensing platforms. A successful one-step modification strategy with ethanolamine allowed the synthesis of a ready-to-use polydopamine-based platform that prevents the non-specific adsorption without the need for additional chemical coupling reactions or blocking steps throughout protein affinity interactions. New redox reactions during polydopamine electrosynthesis in the presence of ethanolamine were assigned to species originated from the covalent coupling of ethanolamine to monomer or oligomers, resulting in the efficient incorporation of ethanolamine in the polymeric film. Real-time immunosensing assays by SPR show that incubation of ethanolamine, after protein immobilization, causes a similar blocking effect as standard BSA, however this two-step strategy does not achieve the high detection ratio of the one-step strategy (1.2 *vs.* 1.8).

In alternative to the hybrid polydopamine-ethanolamine films, the surface of thick films of polydopamine and polynorepinephrine films (*ca.* 12 nm) was also verified to promote a correct orientation of adsorbed IgG molecules, leading to high Anti-IgG detection ratios (*ca.* 2.0). The use of this pristine polycatecholamines requires, nonetheless, the use of an additional blocking step to prevent non-specific adsorption. Furthermore, the introduction of carboxyl groups in the polycatecholamine matrix was found to contribute to a more disorganized IgG layer, as seen by the worse performance of polyDOPA. Due to the absence of amine groups, polycatechol has performed distinctly from polycatecholamines, displaying the highest protein adsorption which highlights its promising use in the construction of sensitive immunosensors with low limits of detection.

Finally, modulation of the potential of a polydopamine modified surface during the interaction with proteins of an immunoassay revealed significant effects over the affinity reaction between IgG and Anti-IgG molecules. Even with the potential modulation of the ePDA interface, the adsorption phenomena of IgG seem to be dictated by the molecular interactions that ePDA surface provides, resulting in robust immobilizations at low and high potential values, similarly to OCP condition. The affinity reaction is, nonetheless, greatly affected by the working potential suggesting that the IgG is better oriented at lower potential values leading to more sensitive detection of the Anti-IgG. Altought, the low potential did not improve the immunosensor sensitivity regarding OCP, the results clearly show that sensitivity can be tuned, opening the possibility to improve the immunosensing performance of other platforms/systems based on polymeric coatings.

7.5. References

[1] F.S. Felix, L. Angnes, Electrochemical immunosensors – A powerful tool for analytical applications, Biosensors and Bioelectronics. 102 (2018) 470–478. doi:10.1016/j.bios.2017.11.029.

[2] T.O. Paiva, I. Almeida, J.T. Marquês, W. Liu, Y. Niu, G. Jin, A.S. Viana, Nanostructured interfaces with site-specific bioreceptors for immunosensing, Applied Surface Science. 412 (2017) 455–463. doi:10.1016/j.apsusc.2017.03.180.

[3] F. Frederix, K. Bonroy, G. Reekmans, W. Laureyn, A. Campitelli, M.A. Abramov, W. Dehaen, G. Maes, Reduced nonspecific adsorption on covalently immobilized protein surfaces using poly(ethylene oxide) containing blocking agents, Journal of Biochemical and Biophysical Methods. 58 (2004) 67–74. doi:10.1016/S0165-022X(03)00150-7.

[4] C. Wu, X. Li, S. Song, Y. Pei, L. Guo, Z. Pei, QCM Biosensor Based on Polydopamine Surface for Real-Time Analysis of the Binding Kinetics of Protein-Protein Interactions, Polymers. 9 (2017) 482. doi:10.3390/polym9100482.

[5] M.G.E.G. Bremer, J. Duval, W. Norde, J. Lyklema, Electrostatic interactions between immunoglobulin (IgG) molecules and a charged sorbent, Colloids and Surfaces A: Physicochemical and Engineering Aspects. 250 (2004) 29–42. doi:10.1016/j.colsurfa.2004.05.026.

[6] R.A. Hartvig, M. van de Weert, J. Østergaard, L. Jorgensen, H. Jensen, Protein Adsorption at Charged Surfaces: The Role of Electrostatic Interactions and Interfacial Charge Regulation, Langmuir. 27 (2011) 2634–2643. doi:10.1021/la104720n.

[7] J.M. Kleijn, D. Barten, M.A. Cohen Stuart, Adsorption of Charged Macromolecules at a Gold Electrode, Langmuir. 20 (2004) 9703–9713. doi:10.1021/la049656m.

[8] M.A. Bos, Z. Shervani, A.C.I. Anusiem, M. Giesbers, W. Norde, J.M. Kleijn, Influence of the electric potential of the interface on the adsorption of proteins, Colloids and Surfaces B: Biointerfaces. 3 (1994) 91–100. doi:10.1016/0927-7765(93)01109-5.

[9] T.E. Benavidez, D. Torrente, M. Marucho, C.D. Garcia, Adsorption of Soft and Hard Proteins onto OTCEs under the Influence of an External Electric Field, Langmuir. 31 (2015) 2455–2462. doi:10.1021/la504890v.

[10] H. Lee, J. Rho, P.B. Messersmith, Facile conjugation of biomolecules onto surfaces via mussel adhesive protein inspired coatings, Advanced Materials. 21 (2009) 431–434. doi:10.1002/adma.200801222.

[11] I. Ismail, T. Okajima, S. Kawauchi, T. Ohsaka, Studies on the early oxidation process of dopamine by electrochemical measurements and quantum chemical calculations, Electrochimica Acta. 211 (2016) 777–786. doi:10.1016/j.electacta.2016.05.056.

[12] C.-Y. Liu, C.-J. Huang, Functionalization of Polydopamine via the Aza-Michael Reaction for Antimicrobial Interfaces, Langmuir. 32 (2016) 5019–5028. doi:10.1021/acs.langmuir.6b00990.

[13] H. Beiginejad, D. Nematollahi, F. Varmaghani, Electrochemical Oxidation of Some Aminophenols in Various pHs, Journal of The Electrochemical Society. 160 (2013) H41–H46. doi:10.1149/2.043301jes.

[14] B. Kalyanaraman, C.C. Felix, R.C. Sealy, Semiquinone anion radicals of catechol(amine)s, catechol estrogens, and their metal ion complexes., Environmental Health Perspectives. 64 (1985) 185–198. doi:10.1289/ehp.8564185.

[15] J. Niedbała, A. Budniok, P. Matyja, Electro-oxidation of ethanolamine on modified layers of Cu-Ni alloys in alkaline environment, Thin Solid Films. 237 (1994) 148–154. doi:10.1016/0040-6090(94)90252-6.

[16] L.A. Hull, G.T. Davis, D.H. Rosenblatt, C.K. Mann, Oxidations of amines. VII. Chemical and electrochemical correlations, Journal of Physical Chemistry. 73 (1969) 2142–2146. doi:10.1021/j100727a007.

[17] T. Yadav, V. Mukherjee, Interpretation of IR and Raman spectra of dopamine neurotransmitter and effect of hydrogen bond in HCl, Journal of Molecular Structure. 1160 (2018) 256–270. doi:10.1016/j.molstruc.2018.01.066.

[18] M. V. Korolevich, V. V. Sivchik, N.A. Matveeva, R.G. Zhbankov, V.A. Lastochkina, M.L. Frenkel', A.I. Ladut'ko, A. V. Pavlov, E.P. Petryaev, A study of the vibrational spectrum of monoethanolamine, Journal of Applied Spectroscopy. 46 (1987) 400–403. doi:10.1007/BF00660054.

[19] W. Yang, C. Liu, Z. Zhang, Y. Liu, S. Nie, One step synthesis of uniform organic silver ink drawing directly on paper substrates, Journal of Materials Chemistry. 22 (2012) 23012. doi:10.1039/c2jm34264b.

[20] C.L. Tseng, Y.K. Chen, S.H. Wang, Z.W. Peng, J.L. Lin, 2-Ethanolamine on TiO2 investigated by in situ infrared spectroscopy. Adsorption, photochemistry, and its interaction with CO 2, Journal of Physical Chemistry C. 114 (2010) 11835–11843. doi:10.1021/jp9117166.

[21] S. Ahn, Y.J. Choi, K. Kim, Y.J. Eo, A. Cho, J. Gwak, J.H. Yun, K. Shin, S.K. Ahn, K. Yoon, Amorphous Cu-In-S nanoparticles as precursors for CuInSe2 thin-film solar cells with a high efficiency, ChemSusChem. 6 (2013) 1282–1287. doi:10.1002/cssc.201200894.

[22] P. Bober, J. Stejskal, M. Trchová, J. Prokeš, The preparation of conducting polyaniline-silver and poly(p-phenylenediamine)-silver nanocomposites in liquid and frozen reaction mixtures, Journal of Solid State Electrochemistry. 15 (2011) 2361–2368. doi:10.1007/s10008-011-1414-8.

[23] V. Chabukswar, A. Horne, S. Bhavsar, A. Bhise, K. Mohite, V. Gaikwad, Synthesis of nano conducting poly(N-ethylaniline) and its function as reusable catalyst for bis-benzpyrrole synthesis, Journal of Macromolecular Science, Part A: Pure and Applied Chemistry. 49 (2012) 1035–1040. doi:10.1080/10601325.2012.728465.

[24] H.J. Salavagione, J. Arias-Pardilla, J.M. Pérez, J.L. Vázquez, E. Morallón, M.C. Miras, C. Barbero, Study of redox mechanism of poly(o-aminophenol) using in situ techniques:

Evidence of two redox processes, Journal of Electroanalytical Chemistry. (2005). doi:10.1016/j.jelechem.2004.10.013.

[25] F. Ponzio, J. Barthès, J. Bour, M. Michel, P. Bertani, J. Hemmerlé, M. D'Ischia, V. Ball, Oxidant Control of Polydopamine Surface Chemistry in Acids: A Mechanism-Based Entry to Superhydrophilic-Superoleophobic Coatings, Chemistry of Materials. 28 (2016) 4697–4705. doi:10.1021/acs.chemmater.6b01587.

[26] S. Rella, E. Mazzotta, A. Caroli, M. De Luca, C. Bucci, C. Malitesta, Investigation of polydopamine coatings by X-ray Photoelectron Spectroscopy as an effective tool for improving biomolecule conjugation, Applied Surface Science. 447 (2018) 31–39. doi:10.1016/j.apsusc.2018.03.057.

[27] R.A. Zangmeister, T.A. Morris, M.J. Tarlov, Characterization of polydopamine thin films deposited at short times by autoxidation of dopamine, Langmuir. 29 (2013) 8619–8628. doi:10.1021/la400587j.

[28] J.T. Marquês, A.S. Viana, R.F.M. De Almeida, A biomimetic platform to study the interactions of bioelectroactive molecules with lipid nanodomains, Langmuir. 30 (2014) 12627–12637. doi:10.1021/la503086a.

[29] H. He, Q. Xie, S. Yao, An electrochemical quartz crystal impedance study on anti-human immunoglobulin G immobilization in the polymer grown during dopamine oxidation at an Au electrode, Journal of Colloid and Interface Science. 289 (2005) 446–454. doi:10.1016/j.jcis.2005.03.085.

[30] Z.H. Wang, A.S. Viana, G. Jin, L.M. Abrantes, Immunosensor interface based on physical and chemical immunoglobulin G adsorption onto mixed self-assembled monolayers, Bioelectrochemistry. 69 (2006) 180–186. doi:10.1016/j.bioelechem.2006.02.001.

[31] I. Almeida, J.T. Marquês, W. Liu, Y. Niu, R.F.M. de Almeida, G. Jin, A.S. Viana, Phospholipid/cholesterol/decanethiol mixtures for direct assembly of immunosensing interfaces, Colloids and Surfaces B: Biointerfaces. 136 (2015) 997–1003. doi:10.1016/j.colsurfb.2015.10.048.

[32] Y. Niu, A.I. Matos, L.M. Abrantes, A.S. Viana, G. Jin, Antibody oriented immobilization on gold using the reaction between carbon disulfide and amine groups and its application in immunosensing, Langmuir. 28 (2012) 17718–17725. doi:10.1021/la303032f.

[33] S.. Moulton, J.. Barisci, A. Bath, R. Stella, G.. Wallace, Investigation of protein adsorption and electrochemical behavior at a gold electrode, Journal of Colloid and Interface Science. 261 (2003) 312–319. doi:10.1016/S0021-9797(03)00073-0.

[34] Y. Shu, X.W. Chen, J.H. Wang, Ionic liquid-polyvinyl chloride ionomer for highly selective isolation of basic proteins, Talanta. 81 (2010) 637–642. doi:10.1016/j.talanta.2009.12.059.

[35] P. Ghisellini, M. Caiazzo, A. Alessandrini, R. Eggenhöffner, M. Vassalli, P. Facci, Direct electrical control of IgG conformation and functional activity at surfaces, Scientific Reports. 6 (2016) 37779. doi:10.1038/srep37779.

Chapter VIII

Final conclusion

8. Final conclusion

This final section aims at summarizing the main results and conclusions achieved throughout the doctoral work, and how they contribute to the global scientific knowledge.

As its scientific nature implies, the present thesis emerges from a specific unsolved challenge with potential beneficial implications for contemporary or future society. In particular, it tackles the multidisciplinary problem of biomolecule surface immobilization in the context of biosensor development – powerful devices that provide critical analytical information on food quality, disease diagnostics, and pollution control. Biomolecules immobilization is not a straightforward task since it implies confining them to insoluble supports, usually leading to partial or complete loss of their biological activities (catalytic or affinity reactions). Focused on the material science required to achieve successful biomolecule immobilization, the main objective of the present doctoral thesis is inspired by the adhesive role of catechol and amine groups, previously found on natural adhesives. Inspiration acts only as a starting point to build knowledge around a complex problem, and thus it is fair to state that the catechol and amine groups are by themselves responsible for part of the successful results achieved in this work, however, without "intelligent tuning" of their chemical behaviors the preparation of working biosensing interfaces would not be possible at all. The multitude of possible reactions brought by the simple combination of a catechol group and an aliphatic amine in a single catecholamine molecule still preclude the complete understanding of their molecular aggregation process, subsequent supramolecular deposition at solid surfaces, and consequent adhesive behavior and biomolecule-compatibility of the resulting polycatecholamine coating. Nonetheless, as exposed throughout this doctoral thesis, electrochemical techniques offered new insightful explanations for this complicated process, as well as, the "intelligent tuning" necessary to prepare useful biomolecule-compatible coatings from catechol-containing molecules. Furthermore, the next paragraphs aim to state the role of catechol chemistry in the several experimental chapters.

Chapter IV starts by disclosing the relevance of electrochemical techniques in the work progress. For instance, straightforward electrochemical characterizations by cyclic voltammetry of polydopamine coatings allow for direct evaluation of their chemical variability and structural order – a tremendously difficult task to perform by spectroscopic characterization of the surface and almost impossible for analytical tools due to the insolubility and scarcity of the deposited material. This easy access to structure-property relationships of coatings boosted the work progress in a way that may not be possible otherwise. In fact, the first important

scientific breakthrough is the recognition of electrosynthesized polydopamine as a material with better structural order than its chemically synthesized counterpart – fundamental to explain its improved performance in electrochemical biosensing, justifying the continuation of the scientific work displayed in subsequent chapters. Polydopamine is not only adaptable to different substrate materials (as already known), but it is also compatible with electrosynthetic methods that favor a more ordered assembly and beneficial changes in its chemical structure, in particular, the preferable incorporation of non-cyclized over cyclized species. To rationalize the observed differences in the electrochemical and spectroscopic characterizations of chemically and electrochemically prepared polydopamine, a rethinking of the proposed polymerization process was necessary. The linear reactional pathway repeatedly proposed in the literature that assumes a homopolymer of dihydroxyindole units conflicts with the plurality of redox processes found for the polydopamine coating. Indeed, the existence of parallel pathways is a better description for the polymerization of dopamine and the Raper-Manson scheme is a pathway that leads to chemical heterogeneity. A co-polymeric model is therefore much more convenient to explain the formation of a coating from the several electroactive species present in solution during electrosynthesis, to explain the several surface-confined quinone-hydroquinone redox processes of polydopamine, and also to explain the variations of coatings hydrophilicity, morphology, and biomolecule-compatibility. During the electropolymerization of dopamine, oxidation conversions are accelerated and chemical equilibria are shifted, favoring a faster incorporation of uncyclized repeating units compared to an oxygen-driven polymerization. As so, electrochemical techniques were crucial to characterize the fine structure of polydopamine, identify monomeric species in solution, increase coating growth rate with thickness control, and to deliver a biomolecule-compatible surface with better performance compared to the one prepared by the standard chemical dip coating method.

Further molecular mechanistic insights of coatings formation from dopamine and other catechol-containing molecules are achieved in Chapter V, thanks to the combined use of electrochemical, gravimetric, and spectroscopic techniques during electrosynthesis, and thanks to the extensive characterization of thin films. In analogy with dopamine, the electrosynthesis of coatings from norepinephrine and DOPA can also be conveniently explained by the existence of parallel reactional pathways, namely, the Raper-Manson scheme that starts with the intramolecular cyclization of the initial molecule, and the C-C coupling of the several catechol containing species. The assumption of an oligomerization pathway based on C-C coupling was again necessary to explain the preservation of the chemical groups of the initial molecules, as

evidenced by the polymers redox properties, hydrophilicity, and spectroscopic characterizations.

In a broad sense, coating formation from the several catecholamines studied are identical processes since they lead to poorly conducting nanometric films with thickness-dependent properties. In a narrow sense, the variations within coatings formation caused by the presence of hydroxyl or carboxyl groups lead to distinct surface hydrophilicities, electroactivities, porosities, and charge transfer properties, that are of utmost importance due to the implications on their biosensing performance. A fundamental insight is then provided in this doctoral work: having dopamine as a reference, the addition of an hydroxyl group affects the oligomerization pathway but not the supramolecular aggregation or deposition; whereas, the extra carboxyl group affects both oligomerization and material deposition. As a consequence, polynorepinephrine displays a similar, yet more invariable, deposition rate to polydopamine; while polyDOPA barely grows. A more in-depth explanation would require a detailed understanding of the dimerization of catecholamines and what factors may affect its kinetics – a current gap in scientific knowledge. For instance, *in silico* studies that compare the energies involved in radical and molecular adduct formation are still necessary. The provided scientific discussion contributes to closing such a gap by comparing the electropolymerization of catecholamines with catechol-containing molecules without amine groups: catechol and caffeic acid. It became very clear that alkylamine substitution on the ring position 4 is not strictly necessary for electropolymerization of catechol-containing molecules to occur, however, this substitution affects oligomerization and seems to provide improved deposition rates regarding catechol and caffeic acid. Beyond the complicated oligomerization process brought by Raper-Manson conversions in polycatecholamines formation, the oligomerization of caffeic acid appears as a simpler process that should follow only the proposed C-C coupling route, rendering a monotonous structure, as corroborated by the simpler redox response produced by the corresponding coating. Further electropolymerization studies may be interesting to conduct using caffeic acid and other substituted catechols in the ring position 4 with a non-nucleophilic group since they have a good chance to provide the necessary data to formulate a general polymerization model based on C-C coupling as the primary route. This particular type of mono-substituted catechols is hereby suggested as a potential model to deliver insightful information about the separated influences of chemical groups in the oligomerization and deposition processes. The existence of intramolecular cyclization in the studied catecholamines precludes this type of fundamental clairvoyance.

Catechol is the simpler molecule submitted to electropolymerization in this doctoral study, yet the absence of alkylation in position 4 leads to a coating material with multiple redox processes alike polycatecholamines. The complicated redox responses may therefore be attributed to the variable quinone/hydroquinone structures derived from intermolecular or intramolecular nucleophilic attacks in the case of catechol or catecholamines, respectively. Again, parallel reactional pathways can explain the presence of multiple and discrete redox processes in polycatechol coatings, analogously to polycatecholamines. Both types of starting monomers, catechol and catecholamines, may follow a C-C coupling oligomerization, whereas catechol seems to additionally follow a C-O-C coupling route. From all the molecular mechanistic reasoning, it becomes clear that further insights will be achievable with the continuation of electropolymerization studies of more molecules with chemical structures that resemble catecholamines.

In addition to the molecular insight of films formation, Chapter V also demonstrates that the use of electrochemical techniques, in particular, to grow polydopamine, goes beyond the kinetic control of film deposition. Although the non-conducting properties of polydopamine impose a thickness limit in potentiodynamic and potentiostatic growths, this limit can be surpassed by using higher anodic limits – an unseen phenomenon not reported elsewhere at the date of the experiments. Polydopamine films grown potentiodynamically until 1.1 V (*vs.* SCE) are thicker, more electroactive, more porous towards hexaammineruthenium cation and display similar composition, yet a completely different surface morphology, compared to lower anodic limit films (0.8 V *vs.* SCE). Although the immobilization of laccase on this promising film was not successful, it is important to note that future exploration of electrosynthetic conditions may uncover polycatecholamine films with new unobserved properties.

As mentioned, the scientific endeavor of constructing a working biosensing interface requires good compatibility between biomolecules and the electrosynthesized polycatecholamines matrix. The nature of protein-film interactions is continuously pursued throughout the several chapters, and, although they are not undoubtedly identified, the robust immobilization of biologically active laccases and human immunoglobulins clearly proves the existence of favorable interactions between those proteins and electrosynthesized polycatecholamines – a remarkable finding given the complexity of the possible interactions. Polycatecholamines do strongly adhere to amine-modified AFM tips, and they can incorporate aminoferrocene in their matrices, however, this information is not enough to distinguish covalent or non-covalent interactions. In addition, the electrosynthesis and spectroscopic characterization of the hybrid polydopamine-ethanolamine films provided confirmation of

amino-quinone adducts formation, and thus, covalent modification with amine-containing molecules occurs. There are other pieces of evidence against the formation of covalent bonds between proteins and polydopamine: i) in chapter VI, the hybrid polydopamine-laccase film produced by the one-setup method displays a very similar cyclic voltammogram to be pristine polydopamine film; ii) in chapter VII, potential modulation of the polydopamine film decreased the amount of adsorbed immunoglobulin G, disproving the pivotal role of quinone/hydroquinone states on protein-film interaction. Further investigations about the reactivity of the chemical groups present in the surface of polycatecholamines films, as well as, the reaction medium during their electrosynthesis are still necessary to accept or dismiss the idea that covalent links with nucleophilic groups of proteins are significantly important to explain the success of proteins immobilization, as repeatedly stated in the literature. At the moment, it is recommended to consider both covalent and non-covalent interactions when debating protein-films interactions.

In chapter VI, the success of the one-step and two-step modification methods used to modify electrode surfaces with fungal and bacterial laccases demonstrates the great adaptability of the catecholamines to different methods and enzymes. Dopamine and norepinephrine were extremely suitable molecules for the immobilization of the fungal laccase by the one-step potentiostatic deposition, in contrast to catechol which did not allow the achievement of the same electrocatalytic performances. Amine groups are thus important to provide favorable interactions (or reactions) between the enzyme and the monomers or oligomers during co-deposition. Despite delivering very fast and reproducible modifications, this method proved ineffective in immobilizing a bacterial laccase, underscoring the significant influence of enzyme origin on the immobilization process on the electrode surface.

Chapter VII shows the success of the two-step method by demonstrating the straightforward adsorption of yet another protein (human immunoglobulin G) in all the investigated polycatecholamine films. Interestingly, the variations in the chemical groups of dopamine, norepinephrine, DOPA, and catechol seem to have a causal relationship with the adsorption phenomena onto the respective thin films, highlighting the importance of chemical manipulation of these molecules to provide optimal interactions with specific proteins. Regardless of the exact nature of the favorable interactions that allowed the immobilization during adsorption, the multitude of possibilities have granted its success – an advantage brought by the inspiration in mussels catechol chemistry.

The electrosynthetic methods employed in this thesis provided adequate polycatecholamine coatings for the amperometric and optical biosensing platforms, matching

or surpassing the performance of previously developed laccase-based electrodes and immunosensing surfaces. In addition to their electrochemical modulation, polycatecholamine films display operational stability in acidic and neutral conditions, without signs of passivation when detecting phenolic compounds on their surfaces or loss of material coating. The proposed one-step potentiostatic method for the co-immobilization of fungal laccase and polydopamine on cost-effective disposable graphite electrodes resulted in highly reproducible and sensitive catalytic responses towards various phenolic compounds, such as caffeic, rosmarinic, and gallic acid at pH 4.6. The graphite/ePDA-Lac electrodes enabled the quantification of the phenol content of a chestnut shell extract derived from agro-industrial wastes. Furthermore, successful immobilization of bacterial laccase is demonstrated on graphite/polynorepinephrine modified electrodes, yielding superior catalytic responses compared to polydopamine modified electrodes. This modification also results in a shift of the optimal working pH to neutral values, as demonstrated by the sensitive responses to catechin and gallic acid.

In immunosensing, polydopamine demonstrated the additional feature of being extremely versatile to be chemically or electrochemically modified with ethanolamine in order to control non-specific adsorption. The performance of the constructed biosensing platforms critically changes with the used monomer: in general terms, polydopamine and polynorepinephrine are better suited for amperometric biosensing, while polycatechol and polynorepinephrine performed better in optical sensing. Signal sensitivity is a complex result of the favorable interactions during immobilization and the transduction capabilities of each thin polymeric layer. Polynorepinephrine should be highlighted by its structural organization that resulted in better amperometric transduction and better protein immobilization, as ultimately transpired by the highly sensitive phenolic electrodes based on bacterial laccase and the highly sensitive immunologic surfaces based on human immunoglobulins.

Electrosynthesized polycatecholamines thin films demonstrated to be powerful materials to tackle the challenging task of constructing optimal biosensing surfaces, and the scientific understanding of how the simple catechol and catecholamine molecules can form a biomolecule-compatible substrate is now ameliorated thanks to the structure-property relationships hereby provided. A longer history has yet to be written, but I am confident that even superior material designs can be reached in an amazingly shorter time scale than the time it took mussels to develop their adhesive proteins.

Annex

Annex

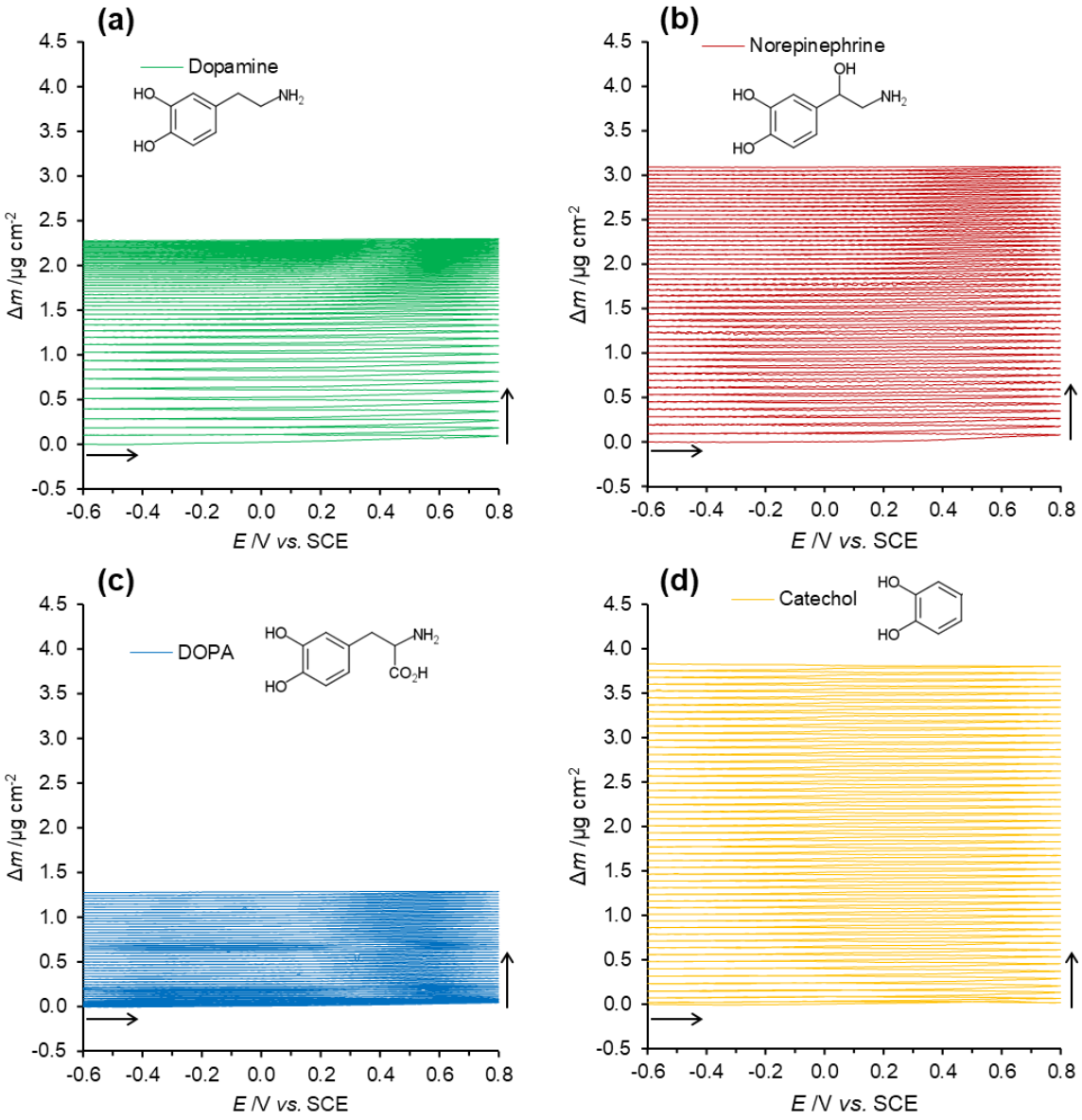

\

Figure A1: EQCM mass variation during the potentiodynamic growth of polydopamine **(a)**, polynorepinephrine **(b)**, polyDOPA **(c)**, and polycatechol **(d)** at 200 mV s^{-1} for 50 potential cycles in a deoxygenated CPB pH=7.0 solution containing 5 mM of monomer.

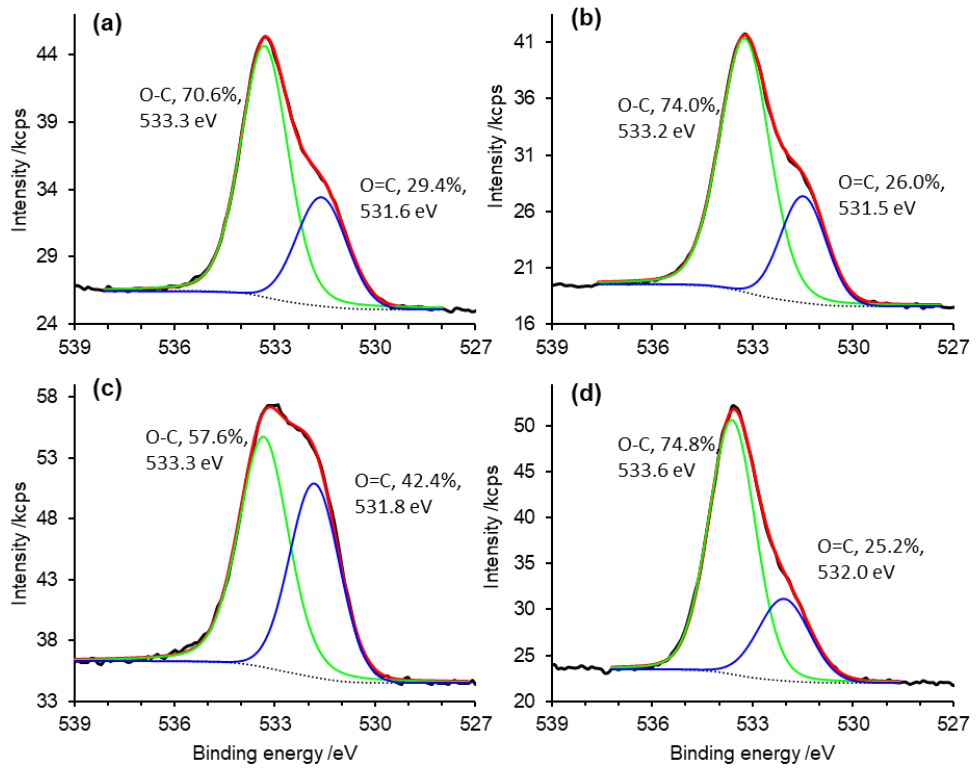

Figure A2: XPS spectra of O 1s region of modified gold electrodes with polydopamine **(a)**, polynorepinephrine **(b)**, polyDOPA **(c),** and polycatechol **(d)**, electropolymerized at 200 mV s^{-1} for 50 potential cycles.

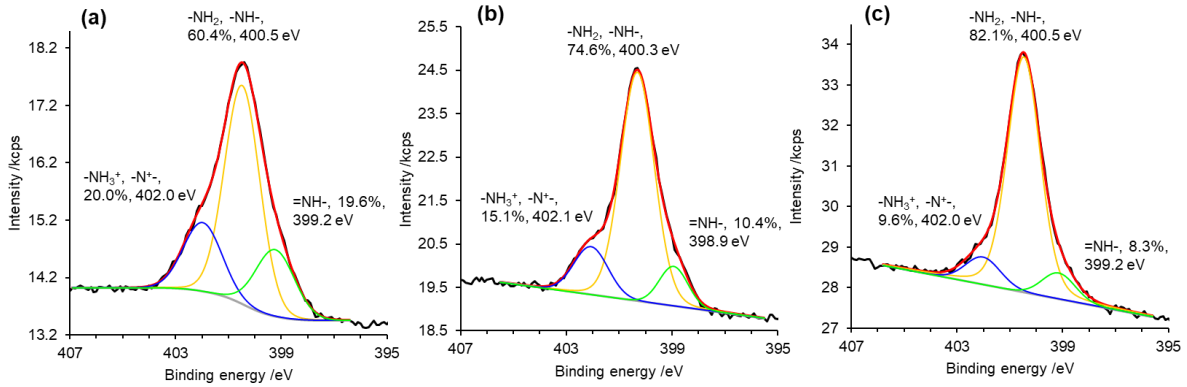

Figure A3: XPS spectra of N 1s region of modified gold electrodes with polydopamine **(a)**, polynorepinephrine **(b),** and polyDOPA **(c)**, electropolymerized at 200 mV s^{-1} for 50 potential cycles.

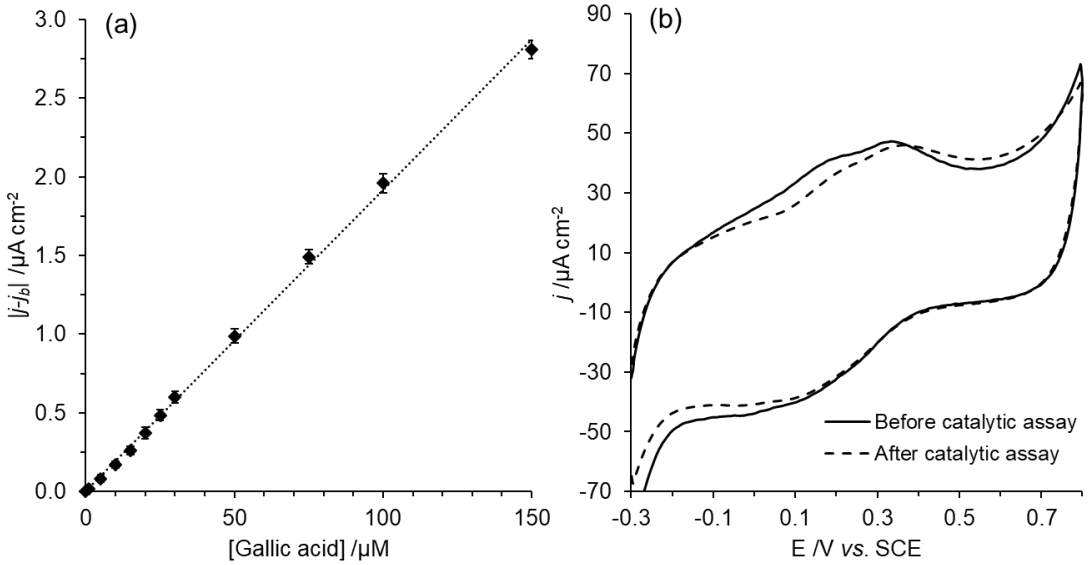

Figure A4: (a) Current responses of the graphite/ePDA-Lac modified electrode to gallic acid from 1 to 150 µM, acquired from chronoamperometric measurements performed at an applied potential of 0.0 V – error bars represent the standard deviation of 3 independent assays. **(b)** Cyclic voltammograms, recorded at 50 mV s^{-1}, of the graphite/ePDA-Lac electrode before and after the catalytic assay performed at (a). All the assays were performed in oxygenated CPB pH 4.6 buffer.

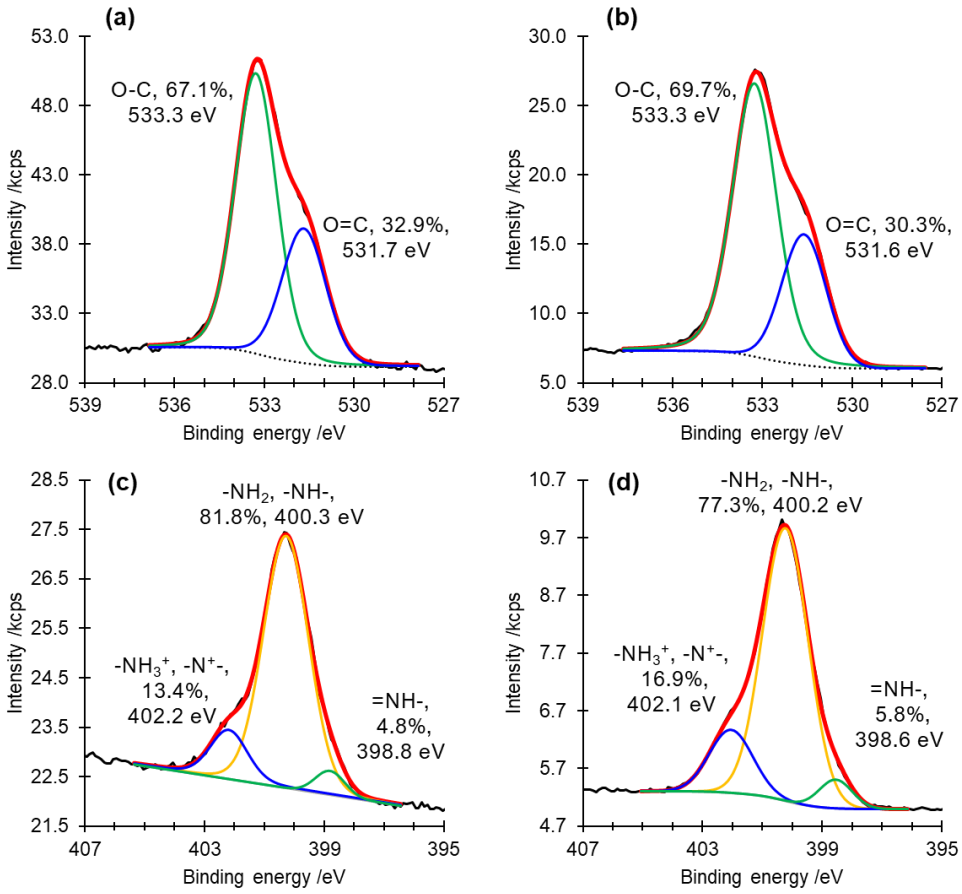

Figure A5: XPS spectra of O 1s and N 1s regions of gold electrodes modified with polydopamine electrosynthesized at 200 mV s^{-1}, from -0.8 to 1.1 V (*vs.* SCE), using 20 **(a,c)** and 100 **(b,d)** potential cycles.

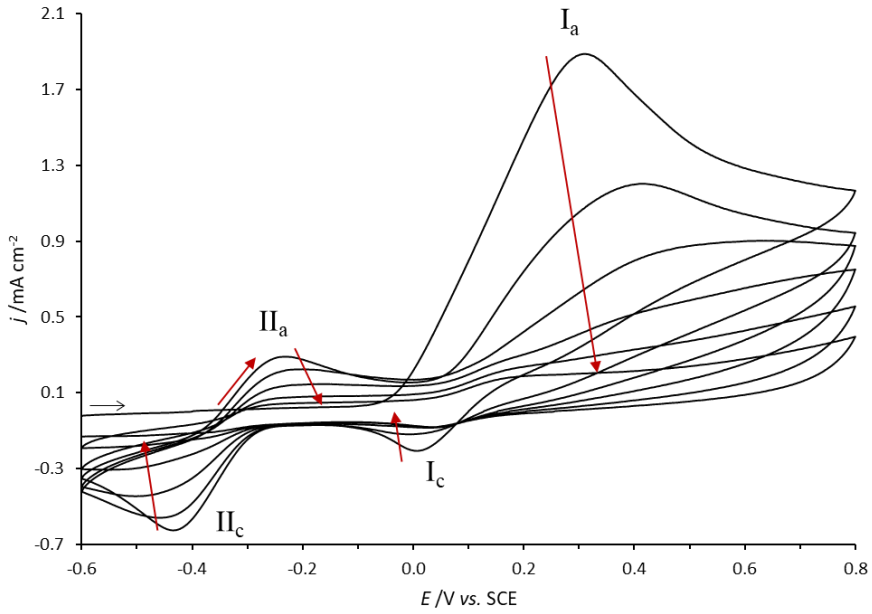

Figure A6: Potentiodynamic polymerization of 5 mM dopamine, performed at 200 mV s^{-1} for 6 potential cycles in deoxygenated CPB (pH = 10.2).

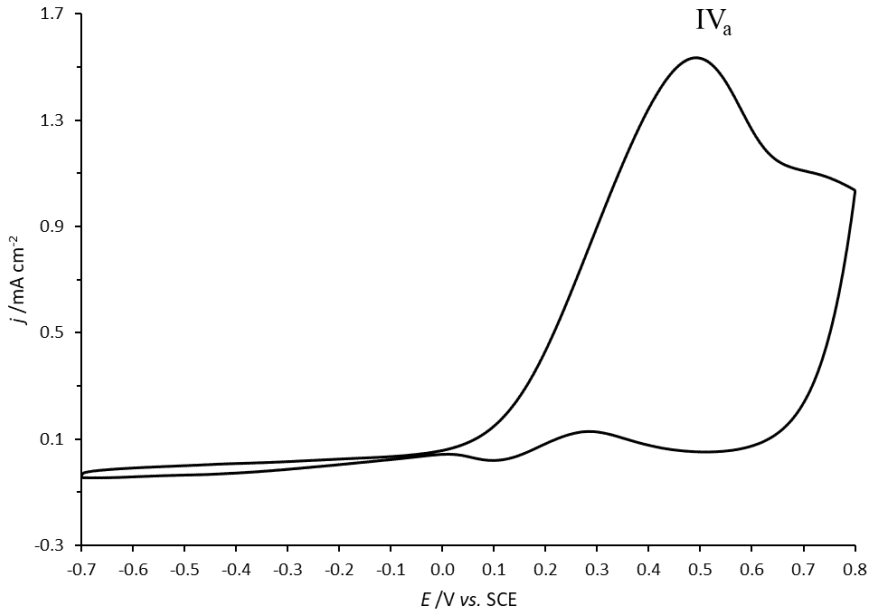

Figure A7: Cyclic voltammetry of gold electrode, recorded at 200 mV s^{-1} in 100 mM ethanolamine solution (deoxygenated CPB).

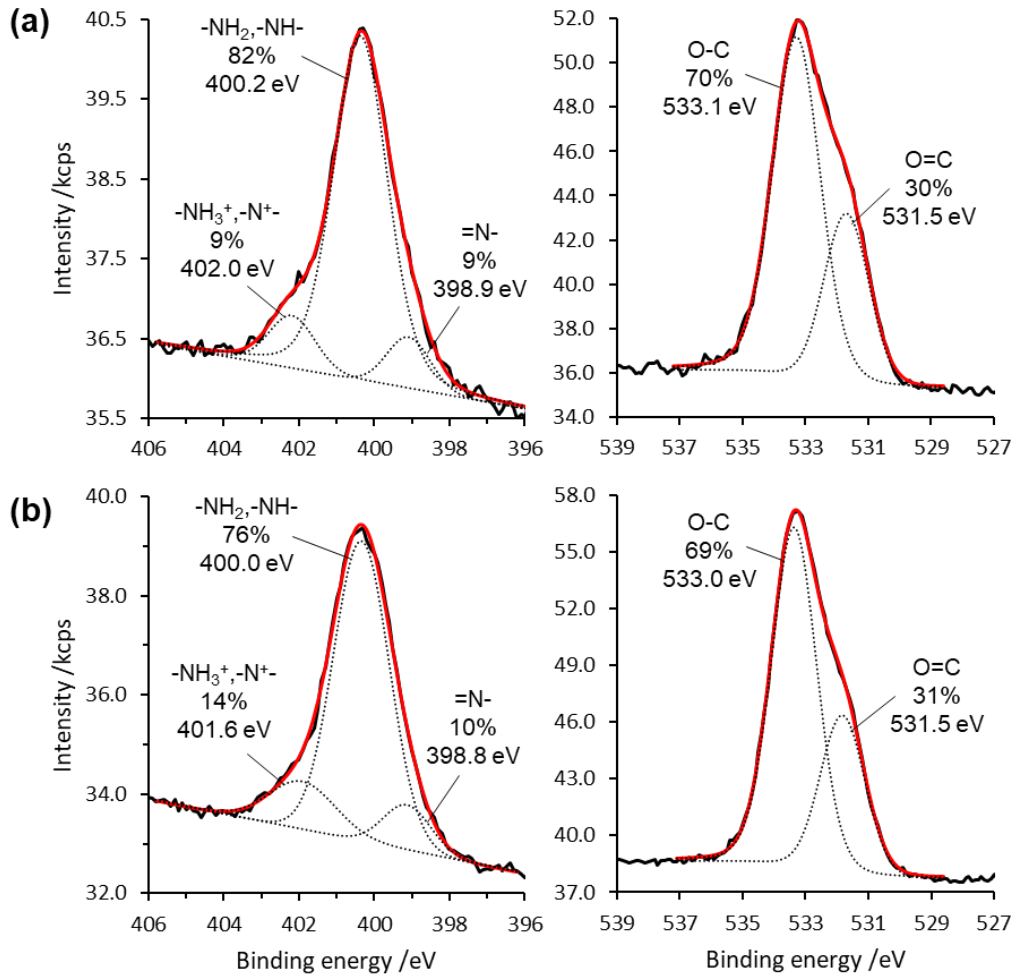

Figure A8: XPS spectra of N 1s and O 1s regions of Au/ePDA **(a)** and Au/ePDA-ETA **(b)** modified electrodes.

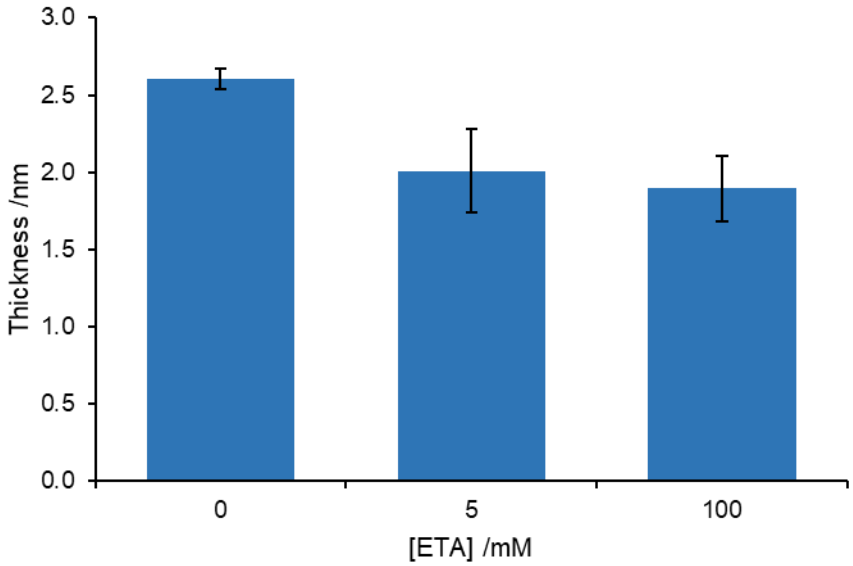

Figure A9: Optical thickness of IgG layer deposited on gold modified with pristine polydopamine film (ePDA) and incubated polydopamine films in 5 and 100 mM of ethanolamine (ePDA/ETA).

Table A1: *Ex situ* ellipsometric data of GC modified electrodes with ePCA films prepared by potentiostatic deposition for 120, 300 and 600 s: the table contains average experimental angles (Ψ_{exp}, Δ_{exp}) at several incident angles (φ_0), and calculated ellipsometric angles (Ψ_{calc}, Δ_{calc}) for an isotropic and finite ePCA layer characterized by its refractive index (n), extinction coefficient (k) and thickness (L). The semi-finite substrate layer of GC is considered isotropic with a refractive index of 1.818 ± 0.006 and an extinction coefficient of 0.771 ± 0.009.

Time /s	φ_0 /°	Ψ_{exp} /°	Δ_{exp} /°	Ψ_{calc} /°	Δ_{calc} /°	n	k	L /nm
	70	16.59 ± 0.06	52.6 ± 0.2	16.5329	52.5721			
120	65	13.65 ± 0.06	82.7 ± 0.3	13.5410	82.9769	2.20 ± 0.05	0.743 ± 0.003	1.4 ± 0.3
	60	14.64 ± 0.06	115.6 ± 0.3	14.4012	115.3629			
	70	16.80 ± 0.06	51.8 ± 0.2	16.8197	51.7574			
300	65	13.76 ± 0.04	81.0 ± 0.2	13.7044	81.4552	2.12 ± 0.06	0.62 ± 0.02	2.8 ± 0.5
	60	14.50 ± 0.03	114.0 ± 0.2	14.3710	113.8041			
	70	17.31 ± 0.04	51.0 ± 0.2	17.3456	51.3905			
600	65	14.11 ± 0.02	79.5 ± 0.2	14.1615	80.0019	1.97 ± 0.04	0.36 ± 0.06	4.1 ± 0.8
	60	14.65 ± 0.04	112.0 ± 0.4	14.6034	111.6996			